VNIVERSITAT DE VALÈNCIA

Application of physiologically based pharmacokinetic-pharmacodynamic modelling strategies in the preclinical and clinical setting

Tesi Doctoral_ Programa de Doctorat en Biomedicina i Farmàcia

València, Abril 2023

Departament de Farmàcia i
Tecnologia Farmacèutica i Parasitologia

Javier Reig López

Directors | Dra. Matilde Merino Sanjuán
Dr. Víctor Mangas Sanjuán

VNIVERSITAT DE VALÈNCIA

Application of physiologically based pharmacokinetic-pharmacodynamic modelling strategies in the preclinical and clinical setting

Tesi Doctoral

Programa de Doctorat en Biomedicina i Farmàcia

Javier Reig López

Directors:

Dra. Matilde Merino Sanjuán

Dr. Víctor Mangas Sanjuán

Universitat de València

Departament de Farmàcia i Tecnología Farmacèutica i Parasitologia

València - Maig 2023

Cover page designed by Elena Reig (embolic Studio)

To Cris

Dra. Matilde Merino Sanjuán, Catedràtica del Departament de Farmàcia i Tecnologia Farmacèutica i Parasitologia de la Universitat de València, i Dr. Víctor Mangas Sanjuán, Professor Titular del Departament de Farmàcia i Tecnologia Farmacèutica i Parasitologia de la Universitat de València, ambdós per igual en condició de directors,

CERTIFIQUEN

Que la Memòria realitzada per D. Javier Reig López per a optar al grau de Doctor titolada *Application of physiologically based pharmacokinetic-pharmacodynamic modelling strategies in the preclinical and clinical setting*, s'ha desenvolupat baix la seua direcció i supervisió, i reuneix tots els requisits necessaris per al seu judici i qualificació.

El que subscriuen en Burjassot a 2 de maig de 2023.

MARIA MATILDE\| MERINO\| SANJUAN

Firmado digitalmente por MARIA MATILDE\| MERINO\|SANJUAN
Fecha: 2023.05.02 11:09:52 +02'00'

Dra. Matilde Merino Sanjuán

MANGAS SANJUAN VICTOR - 48575410P

Firmado digitalmente por MANGAS SANJUAN VICTOR - 48575410P
Fecha: 2023.05.02 10:29:31 +02'00'

Dr. Víctor Mangas Sanjuán

Table of Contents

Overview

Modelling and simulation strategies are a powerful resource to increase the efficiency in the drug discovery and development process. Able to differentiate system- and drug-related parameters, physiologically based pharmacokinetics (PBPK) allows to "easily" develop mechanistic models to check untested or untestable scenarios and to answer "what-if" questions in the safest possible way. Open software and designed modelling software tools do exist to develop PBPK models, being the latter necessarily qualified for its purpose. Because of its algorithmic nature, these software need systems of ordinary differential equations defining local processes and relation among the tissues/organs that ultimately constitute the system/organism. And these equations must be defined from scratch by the modeller or by the designer.

The present Thesis will start with the validation of a multilevel object-oriented and acausal (non-algorithmic) modelling methodology and will be proposed as an alternative to algorithmic methodologies because of its re-usability (object-oriented) and comfort (no need to define ordinary differential equations systems) for the modeller.

In the second part of the Thesis, preclinical utility of PBPK modelling will be highlighted through the development of a PBPK/pharmacodynamic model for the small molecule MBQ-167 to predict tumour growth inhibition for two breast cancer cell lines (i.e., HER2 positive and triple negative) in mice. Additionally, model simulations will be performed to explore the effect of more intensive dosing regimens in tumour size reduction.

After an extensive review of the pharmacokinetic parameters driving atorvastatin absorption, distribution, metabolism and excretion processes, the development of a PBPK model for atorvastatin and its metabolites to *in silico* assess the drug-gene interaction with *SLCO1B1* polymorphisms will be presented, moving the application of PBPK modelling and simulations to the clinical setting. Finally, the last part of the present Thesis will focus on the PBPK modelling of large molecules in oncology by means of the development of PBPK models for the monoclonal antibodies directed to EGFR family membrane receptors pertuzumab, trastuzumab, and cetuximab.

Acknowledgments / Agraïments

I perfectly remember the first email I wrote to and the first meeting I had with Prof. Matilde Merino Sanjuán and Dr. Víctor Mangas Sanjuán. This was five years ago now, and after a lot of analyses, reports, conferences, and papers here I am, writing probably the most difficult part of the Thesis, as to summarise all the feelings, memories and experiences lived during the last years is more than challenging.

I want to start these acknowledgements lines expressing my most sincere gratitude to my thesis directors, Víctor and Mati.

Mati, thanks for the opportunity of joining your team and for putting your trust on me. Thanks for all the time we have spent talking about not only pharmacokinetics, but also about other topics I have really enjoyed. Thanks for being there all the time.

Víctor, my *master*, thanks for all the moments we have shared and all you have done. Because without you I would never have discovered the amazing and field of pharmacometrics. Because you have made that something previously unknown becomes a passion.

It has been a privilege learning from you and a pleasure working with you. Thank you very, very much.

Also, I want to express my gratitude to three brilliant people for the time they spent working with me.

Firstly, I want to thank Dr. Manuel Prado Velasco all the time we shared talking about acausal modelling. Manolo, thanks for making easy such difficult concepts.

To Alfredo García Arieta, my preferred reviewer, whose comments, and suggestions, as well as positive and constructive discussions, had always been very appreciated.

Last, but not the least, I want to express my gratitude to Dr. Pradeep Sharma, my friend and supervisor at AstraZeneca during my research stay, for sharing with me a bit of his huge knowledge in PBPK modelling.

Many thanks to you three.

I am also very thankful to Dr. Jorge Duconge Soler, Dr. María del Mar Maldonado Montalbán and Dr. Suranganie Dharmawardhane, from the University of Puerto Rico (USA), for the opportunity of working with them in the MBQ-167 project. Many thanks.

To my *UVmetriX* group mates Kike, Aymara, Karine, and Marina: thanks for all the moments we have lived around the world. An incredible future is waiting for you.

To my friends and colleagues from *CB2 group*: many thanks for the coffees, laughs and good moments we shared during my stay in Cambridge (UK). So, Carlos T., Unai, Itziar, and Lucía, thank you very much.

A special acknowledgment deserve Dr. Ignacio González García and Dr. Carlos Fernández Teruel.

Nacho, many thanks for being always willing and Ready to help.

Carlos, thank you so much for an opportunity I will never forget.

Als meus pares, Elodia i Aurelio, els que sempre han estat al meu costat: GRÀCIES, no soles per tot el suport aquests últims anys (reconec que el alguns moments he estat insuportable), sinó per tot el que sempre heu fet per mi.

Gràcies també a tu, Elisa, per tots els moments que hem passat parlant de les coses que ens apassionen.

A Juani i Eduardo vull agrair l'ajuda, sempre incondicional, que en tot moment ens han proporcionat.

A Anna i Edu: moltes gràcies per totes les "guàrdies" que vos ha tocat fer. I especialment a tu, "Dr. E. Duard", exemple de constància, perseverança i, també, cabuderia (ves preparant-te que a partir d'ara ja podrem parlar de "tu a tu"). De veritat, Edu, gràcies per creure en mi.

Als quatre: gràcies per estar ahí.

Per supost, als meus menuts Ada, Gauss, Tesla, i també a Euler (qui va veure escomençar aquest projecte però no l'ha pogut veure acabar). Gràcies per totes les hores compartides.

Arribat aquest punt, hi haurà dues persones que estaran pensant "i nosaltres què?". Vosaltres aneu a part.

Al meu germà, "Dr. ***Mario****": gràcies per estar al meu costat en els bons moments però, sobretot, gràcies, moltíssimes gràcies per ajudar-me a superar eixos moments no tant bons que hem viscut; i també per tots eixos "fish and chips". Mariet: has sigut i eres una font d'inspiració i motivació.*

I a tu, ***Cris****, la meua millor amiga i companya en la vida: em quede curt donant-te les gràcies amb paraules però, que anem a fer, el llenguatge és així. Aquests últims anys hem passat molt bons moments però, també altres durs i difícils. Moments que podrien haver causat que aquest treball no veguera la llum, però sempre has mantingut la meua motivació i il·lusió perquè continuara endavant.*

Així que açò és per tu i per a tu. Tres mil gràcies.

List of publications

The present Thesis is based on the following manuscripts:

1. **A multilevel object-oriented modelling methodology for physiologically-based pharmacokinetics (PBPK): Evaluation with a semi-mechanistic pharmacokinetic model.**
   J. Reig-Lopez, M. Merino-Sanjuan, V. Mangas-Sanjuan, M. Prado-Velasco
   Comput Methods Programs Biomed. 2020 Jun;189:105322
   Journal statistics: IF 5.428, Q1 (Computer Science, Theory and Methods)

2. **Physiologically-Based Pharmacokinetic/Pharmacodynamic Model of MBQ-167 to Predict Tumor Growth Inhibition in Mice.**
   J. Reig-López, MDM Maldonado, M. Merino-Sanjuan, AM. Cruz-Collazo,JF. Ruiz-Calderón, V. Mangas-Sanjuán, S. Dharmawardhane, J. Duconge
   Pharmaceutics. 2020 Oct 15;12(10):975
   Journal statistics: IF 6.321, Q1 (Pharmacology & Pharmacy)

3. **Current Evidence, Challenges, and Opportunities of Physiologically Based Pharmacokinetic Models of Atorvastatin for Decision Making.**
   J. Reig-López, A. García-Arieta, M. Merino-Sanjuan and V. Mangas-Sanjuan
   Pharmaceutics. 2021 May 13;13(5):709
   Journal statistics: IF 6.525, Q1 (Pharmacology & Pharmacy)

4. **A physiologically based pharmacokinetic model for open acid and lactone forms of atorvastatin and metabolites to assess the drug-gene interaction with SLCO1B1 polymorphisms.**
   J. Reig-López, A. García-Arieta, M. Merino-Sanjuan and V. Mangas-Sanjuan
   Biomed Pharmacother. 2022 Dec;156:113914
   Journal statistics: IF 7.419, Q1 (Pharmacology & Pharmacy)

5. **Application of population physiologically based pharmacokinetic modelling to optimize target expression and clearance mechanisms of therapeutic monoclonal antibodies**
   J. Reig-Lopez, W. Tang, C. Fernandez-Teruel, M. Merino-Sanjuan, V. Mangas-Sanjuan, D. W. Boulton and P. Sharma
   British Journal of Clinical Pharmacology. 2023;1-12
   Journal statistics: IF 3.716, Q2 (Pharmacology & Pharmacy)

List of abbreviations

2OH-ATS: 2-hydroxy-atorvastatin
2OH-ATS-L: 2-hydroxy-atorvastatin lactone
4OH-ATS: 4-hydroxy-atorvastatin
4OH-ATS-L: 4-hydroxy-atorvastatin lactone
AAFE: absolute average fold error
ADME: absorption, distribution, metabolism and excretion
AFE: average fold error
ATS: atorvastatin
ATS-Ca: atorvastatin calcium salt
ATS-L: atorvastatin lactone
B/P: blood-to-plasma concentration ratio
BC: breast cancer
CL_{int}: intrinsic clearance
CTX: cetuximab
CYP450: cytochrome P450
DDI: drug-drug interaction
DGI: drug-gene interaction
ET: extensive transporter
FIH: first in human
f_u: fraction unbound in plasma
GI: gastrointestinal
GUI: graphical user interface
IP: intraperitoneal
IT: intermediate transporter
IVIVE: *in vitro-in vivo* extrapolation
k_{deg}: first order degradation rate constant of receptor (receptor turnover)
K_{pt}: tissue-to-plasma concentration ratio
M&S: modelling and simulation
mAb: monoclonal antibody
MAE: mean absolute error
MID3: model-informed drug discovery and development
NTCP: sodium-taurocholate transporting polypeptide

OATP: organic anion transporting polypeptide

ODE: ordinary differential equation

PBPK: physiologically based pharmacokinetics

PD: parent drug

PE: prediction error

$P_{eff,man}$: human jejunum effective permeability

P-gp: P glycoprotein

PhysPK: PhysPK Biosimulation Software

PK: pharmacokinetics

PM: primary metabolite

popPBPK: population physiologically based pharmacokinetics

PPE: percent prediction error

PT: poor transporter

PTZ: pertuzumab

RE: relative error

R_{max}: receptor abundance

RMSE: root mean squared error

SM: secondary metabolite

TGI: tumour growth inhibition

TMDD: target-mediated drug disposition

TTZ: trastuzumab

UGT: UDP-glucuronosyltransferase

UT: ultra-rapid transporter

vNM: semi-mechanistic version of the theoretical model with extraction-based metabolism of parent drug. Ordinary Differential Equations (ODEs) were implemented and solved in NONMEM

vPPK: physiological multilevel version of the theoretical model implemented in PhysPK. vPPK uses an acausal object-oriented modelling approach

vPSEM: model version with the same mathematical approximation that vNM but implemented in PhysPK.

vPSIM: semi-mechanistic version of the theoretical model with intrinsic clearance-based metabolism of parent drug implemented in PhysPK

Resum de la tesi

Introducció

Quan parlem de models farmacocinètics basats en la fisiologia (PBPK per les seues sigles en anglès) parlem d'estructures matemàtiques definint un organisme (el sistema) i construïdes amb una sèrie de compartiments diferenciats que representen òrgans i teixits, tots ells connectats per fluxos sanguinis arterials i venosos. Aquest tipus de models contenen tota una representació directa dels òrgans més rellevants per als processos d'Absorció, Distribució, Metabolisme i Excreció (ADME) d'un fàrmac, essent els més habituals pulmons, cervell, cor, fetge, tracte gastrointestinal (GI), pàncrees, melsa, gònades, ronyons, pròstata, músculs, teixit adipós, tim, ossos i pell.

Cadascun d'aquests teixits i òrgans està caracteritzat pel seu volum, flux sanguini i composició (volums fraccionals d'aigua, fosfolípids, i lípids neutres i la fracció intersticial), amb diferent estructures internes que van des de la més simple (el teixit com a un tot) a altres més complexes amb espais vascular, intersticial i intracel·lular o també arribant a tenir en compte l'espai endosomal (molt apropiat quan es treballa amb fàrmacs biològics). A més a més, informació addicional com abundàncies enzimàtiques i de transportadors de membrana, hematòcrit, pH i temps de buidat gàstrics, filtració glomerular, hepatocel·lularitat (milions de cèl·lules hepàtiques per gram de teixit hepàtic), pH plasmàtic, dimensions del tracte GI (radi i llargària) s'han de tenir en compte per a poder definir de la millor manera possible la fisiologia d'aquests òrgans. A banda d'aquestes característiques fisiològiques, informació demogràfica com l'edat, el pes, l'alçada i el gènere és afegida al model PBPK per tal de completar la parametrització de l'organisme. Cas que la variabilitat interindividual en tots aquests paràmetres siga coneguda i estiga quantificada es pot arribar a generar una població virtual per tal de representar escenaris més realistes, passant a parlar-se de PBPK poblacional o popPBPK.

Afegits al bloc del sistema, es necessiten dos blocs més per a generar l'entramat que constituirà el model PBPK. El primer és el fàrmac. La incorporació de propietats fisicoquímiques com el pes molecular, estructura química, caràcter àcid o bàsic i la lipofília, així com la fracció lliure en plasma (f_u), coeficients de partició

sang/plasma (B/P) i teixit/plasma (K_{pt}), aclariments intrínsecs (CL_{int}) per a processos metabòlics i de transport actiu, i excreció renal i/o biliar com a paràmetres de l'ADME constitueixen els paràmetres del model PBPK relacionats amb el fàrmac. Per últim, la forma farmacèutica a estudiar (comprimit, solució oral, etc.), el disseny de l'estudi (dosi i esquema d'administració, duració, etc.) així com esdeveniments particulars (ingesta d'aliments, per exemple) defineixen el bloc de paràmetres relacionats amb l'assaig clínic o preclínic. Aquesta diferenciació per blocs és necessària per a poder desenvolupar models genèrics i independents i utilitzar-los en una àmplia varietat d'escenaris. És a dir, el fàrmac X (amb la seua parametrització) podrà ser avaluat en la població Y (amb les seues característiques) amb un disseny experimental (dosi i freqüència d'administració) particular però, sobretot, flexible. O expressat d'altra manera: poder arribar a respondre preguntes de l'estil "què passaria si...?".

L'ús del modelat PBPK en el procés de descobriment i desenvolupament de medicaments ha estat limitat en el passat degut a la complexitat d'aquests models i la gran quantitat de dades que són necessàries per a desenvolupar-los. La disponibilitat de determinades tècniques experimentals i sistemes *in vitro* que permeten la determinació indirecta d'alguns processos de l'ADME, així com la millora de les tècniques d'extrapolació *in vitro-in vivo* (IVIVE) i de mètodes de predicció dels coeficients de partició B/P i K_{pt} o de la permeabilitat intestinal efectiva en humans ($P_{eff,man}$) ha fet possible la combinació de tots aquests paràmetres que venen de fonts diferents (prediccions *in silico*, experiments *in vitro* o determinacions *in vivo*) en models fisiològics per tal de predir perfils de concentració en funció del temps en plasma sanguini o determinats teixits d'una manera mecanística, també conegut baix el terme anglosaxó aproximació "bottom-up".

Aquesta metodologia mecanística de modelat difereix de les tècniques més convencionals d'anàlisi de dades o aproximacions "top-down", amb les quals els models farmacocinètics es desenvolupen un cop els valors de concentració en funció del temps estan disponibles. Un avantatge de les aproximacions "bottom-up" (i per tant dels models PBPK) que es pot deduir ràpidament és que el treball de modelat i simulació (M&S) pot començar ben prompte en el procés de desenvolupament de medicaments, quan aquests valors de concentració encara no hi estan disponibles. No obstant això, no es pretén que ambdues tècniques siguen incompatibles, ja que la informació que proporcionen es pot utilitzar per reforçar-se mútuament. Aquesta simbiosi és el que es coneix baix el terme d'aproximacions "middle-out".

El modelat i simulació fisiològic és una tècnica potent (i sobretot, eficient) per tal d'accelerar la transició entre les diferents fases del procés de desenvolupament

de medicaments i avaluar l'efecte de factors intrínsecs (insuficiències orgàniques, edat, embaràs, etc.) i extrínsecs (interaccions entre fàrmacs o DDIs, tabaquisme, etc.), aïllades o en combinació, sobre l'exposició al fàrmac en qüestió. El modelat i simulació en PBPK pot ajudar en el disseny d'un assaig clínic i reduir els temps de decisió interna, així com també rebaixar la incertesa de les agències reguladores de medicaments. L'increment en l'ús del modelat PBPK per la indústria farmacèutica en els darrers anys i la inclusió cada vegada més freqüent de resultats derivats d'aquestes aproximacions a les sol·licituds d'autorització per a la comercialització de medicaments ha ocasionat el reconeixement i l'acceptació per part de les principals agències reguladores (*European Medicines Agency* [UE], *Food and Drug Administration* [EEUU], *Pharmaceuticals and Medicals Devices Agency* [Japó]) i la publicació de guies de bones pràctiques en modelat PBPK per tal d'estandarditzar els informes presentats, traslladant el modelat i la simulació PBPK de la curiositat acadèmica a la pràctica habitual per la indústria farmacèutica i l'acceptació a nivell regulador. Tant és així, que aquest tipus de simulacions han servit no sols per informar fitxes tècniques de medicaments (posologia, risc de DDIs, ús en poblacions específiques com malaltia renal o insuficiència hepàtica), sinó que han arribat a substituir la realització de determinats assajos clínics; situacions que d'altra manera hagueren ocasionat un buit terapèutic en una situació específica.

El desenvolupament de programes informàtics sofisticats i potents que són capaços d'integrar i combinar d'una manera eficient l'estructura fisiològica d'un organisme, les propietats fisicoquímiques i de l'ADME del fàrmac i el disseny de l'estudi ha suposat un punt d'inflexió per a la difusió i acceptació dels models PBPK. Ajudant-se d'una interfície gràfica i col·leccions de poblacions i fàrmacs, el principal avantatge d'aquestes eines informàtiques és que poden ser utilitzats per professionals que dominen els principis fisiològics i farmacocinètics però, que manquen de l'experiència necessària per a la codificació d'aquestes estructures matemàtiques des de zero. Entre els programes informàtics més àmpliament utilitzats en aquest sector cal destacar SimCYP® (Certara), PK-Sim® (Open Systems Pharmacology) i GastroPlus® (Simulation Plus). En aquests programes, l'estructura bàsica del model PBPK està prèviament definida pels seus desenvolupadors i per tant, no és accessible per a l'usuari final. Açò no vol dir que aquests programes no siguen transparents, ja que habitualment se'ls anomena "caixes negres" per aquest "blindatge" que porten per defecte. En realitat, totes les assumpcions en què es basen estan clarament definides i disponibles per a l'usuari. És per això que, el terme "caixes de cristall" recentment definit, potser encaixa millor en la definició d'aquests programes. És més, aquesta inaccessibilitat ha de ser interpretada en termes de qualitat, ja que tan sols uns pocs especialistes (i experts) poden obrir aquesta "caixa", accedir a l'estructura

del model, fer els canvis i millores que corresponguen i requalificar el programa per mantenir la confiança en els resultats que proporciona.

Tots aquests programes es basen en sistemes d'equacions diferencials ordinàries (ODE) que bé siga l'usuari final o el desenvolupador ha de definir per a poder descriure els processos locals i les relacions entre compartiments (o teixits/òrgans en el nostre cas). No obstant això, altres metodologies hi existeixen, com programes basats en sistemes d'equacions diferencials algebraiques i tecnologia de "machine learning" acausal. El principal avantatge d'aquests llenguatges de simulació és que la descripció matemàtica dels components de simulació no és algorítmica (acausal) i per tant, les variables d'entrada i eixida no tenen per què definir-se en la fase inicial de construcció del model.

Hipòtesi i objectius

Més enllà de la necessitat constant d'avançar en la millora de les tècniques d'extrapolació *in vitro-in vivo* i en la recopilació de dades fisiològiques per perfeccionar la caracterització virtual dels essers vius, existeix també una necessitat de perfeccionar i refinar la utilització del modelat farmacocinètic fisiològic en el procés de desenvolupament de medicaments informat per models.

A més a més, els treballs d'investigació que han analitzat els principals programes informàtics de modelat farmacocinètic fisiològic han estat centrats en els mecanismes fisiològics integrats, les característiques de modelat que satisfan els requeriments dels usuaris i de les agències reguladores de medicaments, així com la capacitat d'abordar poblacions especials o avaluar interaccions entre fàrmacs, però no en els aspectes metodològics en què es basen.

Per tot el descrit anteriorment, l'**objectiu principal** de la present Tesi doctoral és:

Desenvolupar, validar i aplicar models farmacocinètics fisiològics des d'un punt de vista metodològic i de presa de decisions i enfocat a optimitzar el procés de descobriment i desenvolupament de medicaments informat per models.

En particular, els **objectius específics** són:

1. Avaluar la capacitat predictiva del programa per a modelat i simulació fisiològiques PhysPK front al software de referència més emprat en farmacocinètica poblacional NONMEM.

2. Comparar les metodologies de modelat causal i acausal en un model farmacocinètic semimecanístic.
3. Caracteritzar la dinàmica de creixement tumoral de dos línies humanes de càncer de pit (HER2+ i Triple Negativa).
4. Desenvolupar un model PBPK/farmacodinàmic per al fàrmac MBQ-167 administrat per via intraperitoneal en ratolins.
5. Desenvolupar un model PBPK per a l'atorvastatina i els seus principals metabòlits en forma àcida i lactonitzada.
6. Avaluar quantitativament l'impacte dels polimorfismes genètics al gen *SLCO1B1* en la farmacocinètica de l'atorvastatina.
7. Proposar una estratègia general per al modelat PBPK d'anticossos monoclonals i la seua aplicació en l'àmbit de la farmacologia clínica per a optimitzar l'expressió de la diana terapèutica al lloc d'acció i també mecanismes d'eliminació d'aquests fàrmacs biològics.

Resultats i discussió

Part 1: aspectes metodològics dels programes informàtics per a modelat farmacocinètic fisiològic

En aquesta part es resolen els obejctius específics 1 i 2. Agafant com a referència un model teòric semimecanístic que incorporava un procés d'absorció complex per administració oral d'una forma farmacèutica sòlida, trànsit intestinal, dissolució del fàrmac limitada per la seua solubilitat, transportadors de secreció intestinal activa amb expressió variable al llarg del tracte GI, metabolisme intestinal i hepàtic, tres versions del fàrmac administrat per via oral (primera generació o PD i dos metabòlits, PM i SM), i excreció renal dels metabòlits, es van generar quatre versions o aproximacions a aquesta estructura bàsica teòrica:

- **vNM**: versió semimecanística descrita amb un sistema d'ODEs al programa NONMEM i definint el metabolisme de PD amb taxes d'extracció.
- **vPSEM**: versió idèntica a vNM però, definida al programa PhysPK.
- **vPSIM**: versió semimecanística descrita amb un sistema d'ODEs al programa PhysPK i definint el metabolisme de PD amb aclariments intrínsecs.
- **vPPK**: versió fisiològica i multinivell del model teòric definida a PhysPK. Aquesta versió fa ús de la metodologia de modelat acausal i orientat a objectes.

Finalment, es va generar un set de 32 escenaris incloent fàrmacs de classe BCS II i IV, dos nivells de dosi, i metabolisme (intestinal i hepàtic) i activitat de la glicoproteïna P (P-gp) lineal i no lineal. Aquesta bateria d'escenaris es va sotmetre a una avaluació per mitjà de diferents comparacions de les versions del model teòric descrites anteriorment.

Validació del programa PhysPK: vNM *vs* vPSEM

L'avaluació gràfica dels perfils concentració plasmàtica en funció del temps (Cp-t) generats amb PhysPK són pràcticament idèntics als obtinguts amb NONMEM per a PD en tots els escenaris considerats. La correspondència entre programes per a PM i SM és bona per a valors baixos-mitjos de concentració, i lleugerament diferent per a valors alts de concentració (prop de la concentració plasmàtica màxima o C_{max}) als escenaris corresponents a una baixa permeabilitat intestinal i una activitat lineal de la P-gp. No obstant, el coeficient de correlació lineal (R^2) va resultar superior a 0.96 en tots els casos i amb errors relatius (RE) mitjos inferiors al 7% per a l'àrea baix la corba Cp-t (AUC) i inferiors al 3% per a C_{max}.

Avaluació del metabolisme: vPSEM *vs* vPSIM

En aquesta fase es va dur a terme la comparació de dues versions del model teòric, ambdues definides al programa PhysPK, diferenciant-se únicament en l'abordatge del metabolisme de PD (taxes d'extracció *vs* aclariment intrínsec). De la manera com s'esperava, PD va resultar la versió del fàrmac més sensible als canvis en el metabolisme. La saturació del metabolisme hepàtic comporta una disminució en la velocitat d'eliminació, fent més gran la diferència en AUC i C_{max} entre versions degut a la manera com està parametritzat el metabolisme en ambdues versions.

Comparació de metodologies: vPSIM *vs* vPPK

Els resultats de la comparació de les versions PSIM i PPK van revelar una correspondència excel·lent entre ambdues aproximacions en la predicció de l'exposició a PD, sense cap tendència d'infrapredicció o sobrepredicció en cap escenari, i amb RE mitjos en la predicció d'AUC i C_{max} del -0.02% i -0.04%, respectivament. Quant als metabòlits PM i SM, la determinació de diferències significatives entre ambdues versions és deguda a la falta de perfusió sanguínia en la vPSIM, en la que PM i SM són disposats immediatament als seus compartiments un cop formats. A la vPPK, més fisiològica, les prediccions de la concentració plasmàtica de PM i SM van resultar superiors a les obtingudes amb la vPSIM perquè tant PM com SM circulen pel torrent sanguini abans de ser

excretats amb la orina, fenòmen que ocorre immediatament a la versió PSIM tan prompte com s'han format, predient-se una exposició menor a la que fisiològicament té lloc.

Part 2: modelat farmacocinètic fisiològic al context preclínic

Aquesta part dóna resposta als objectius específics 3 i 4. La molècula de síntesi MBQ-167 és una candidata a fàrmac anticancerós que inhibeix la metàstasi de cèl·lules malignes de càncer de mama *in vivo* i ha sigut caracteritzada com un inhibidor potent de les Rho GTPases Rac i Cdc42. Aquests enzims presenten una activitat molt incrementada en diferents tipus de càncer i promouen la migració cel·lular, invasió, proliferació i transformació oncogènica. MBQ-167 inhibeix ambdues GTPases, amb una concentració responsable del 50% de la capacitat inhibitòria màxima (IC50) de 0.1 i 0.08 μM per a Rac i Cdc42, respectivament. Diferents assajos preclínics han demostrat que MBQ-167 inhibeix la migració cel·lular de cèl·lules malignes de càncer de mama, la seua viabilitat, el creixement del tumor (un 91% de reducció en la mida del tumor s'aconsegueix ja amb dos mesos de tractament) i la metàstasi *in vivo* sense una aparent toxicitat.

Seguint una aproximació de modelat "middle-out", els resultats del model PBPK després de la simulació de l'administració intraperitoneal (IP) de 10 mg/kg van posar de manifest la capacitat predictiva del model fisiològic no sols en la predicció dels paràmetres d'exposició AUC, C_{max} i el temps en què s'arriba a la C_{max} (T_{max}) en plasma, sinó també en altres òrgans com cor, pulmons, fetge, melsa i ronyons, amb errors de predicció ($Param_{pred}/Param_{obs}$) molt pròxims a la unitat i RE, en general, inferiors al 20%.

El model de creixement tumoral (no pertorbat pel fàrmac) desenvolupat seguint l'estructura d'un model de Simeoni, descriu perfectament les dades experimentals de les dos línies cel·lulars estudiades (HER2+ i Triple Negativa), ja que el perfil simulat cau dins de l'interval de confiança al 95% (95CI) en tots els temps d'observació. Quan s'incorpora l'efecte d'MBQ-167 per a pertorbar el creixement tumoral, el model PBPK/PD també descriu les dades observades d'inhibició del creixement tumoral (TGI) en les dos línies cel·lulars. Concretament per a les cèl·lules HER2+, les simulacions del model prediuen amb una bona exactitud (RE<20%) la reducció del volum tumoral observat tant amb l'administració IP d'1 com de 10 mg/kg tres vegades per setmana durant 65 dies, amb una reducció del 94.3% amb el nivell de dosi més alt. En el cas de les cèl·lules Triple Negatives, el model desenvolupat va predir satisfactòriament la reducció en el creixement tumoral per al nivell de dosi d'1 mg/kg, mentre que les prediccions per al nivell de dosi més alt van resultar en un volum final lleugerament inferior a l'observat

després d'administrar MBQ-167 tres vegades per setmana durant 108 dies. No obstant, la capacitat predictiva del model va estar confirmada ja que la dinàmica de creixement tumoral simulada va caure dins el 95CI de les observacions en els dos nivells de dosi i la predicció de la reducció del volum tumoral amb 10 mg/kg (89.6%) és molt pròxima a l'observada *in vivo* (87.0%).

Verificada la capacitat predictiva del model PBPK/PD, es van realitzar una sèrie de simulacions per tal de respondre a les preguntes "Què passaria si MBQ-167 s'administrara una o dues vegades al dia en lloc de tres vegades per setmana? S'incrementaria la reducció de la mida del tumor amb pautes posològiques més intensives?" Els resultats d'aquestes simulacions va revelar que la reducció de la mida del tumor (era major quan MBQ-167 s'administra una o dues vegades al dia, especialment per a la línia cel·lular HER2+, on l'erradicació del tumor podria anticipar-se administrant 1 mg/kg dues vegades al dia o 10 mg/kg una o dues vegades al dia. Per a la línia cel·lular Triple Negativa, l'efecte màxim s'aconsegueix ja amb 1 mg/kg, anticipant-se una estabilització del creixement tumoral quan MBQ-167 s'administra una o dues vegades al dia.

Part 3: modelat farmacocinètic fisiològic al context clinic

Avaluant interaccions entre fàrmacs i gens: el cas particular de l'ATS

En aquesta part es dóna resposta als objectius específics 5 i 6 de la present tesi doctoral. L'atorvastatina (ATS) és una estatina sintètica de segona generació que s'administra en la forma àcida i farmacològicament activa de la salt càlcica (ATS-Ca). L'ATS és una de les estatines més utilitzades a nivell global per al tractament de la hipercolesterolèmia i conseqüent reducció del risc cardiovascular. La posologia d'ATS és l'administració diària d'un comprimit d'entre 10-80 mg en qualsevol moment del dia. Precisament, aquest és un dels principals avantatges d'aquesta estatina ja que, tant per la seua prolongada semivida biològica ($t_{1/2}$) (14 h) com per l'existència de metabòlits actius (als quals s'atribueix un 70% de l'activitat inhibidora de l'enzim 3-hidroxi-3-metilglutaril coenzim A reductasa o HMG-CoA) no és necessari que l'administració d'aquest fàrmac tinga lloc de vesprada-nit, quan l'activitat d'aquest enzim responsable de la síntesi endògena de colesterol té una major activitat. A més a més, parlem d'un fàrmac ben tolerat i segur, essent l'efecte advers més freqüent (5-10%) la presència de miopaties o molèsties musculars.

L'acumulació hepàtica de les estatines en general i de l'atorvastatina en particular, està mediada per estructures proteiques localitzades a les membranes

basolaterals i canaliculars dels hepatòcits i que pertanyen a les famílies de polipèptids transportadors d'anions orgànics (OATP), polipèptids cotransportadors de taurocolat depenent de sodi (NTCP), i per transportadors de secreció activa depenent d'ATP (ABC). Estudis *in vitro* sobre la captació hepàtica d'ATS han demostrat que els transportadors OATP1B1 i OATP1B3 són els més rellevants, mentre que la contribució del transportador NTCP ha resultat minoritària per als processos de disposició d'aquesta estatina. Estudis en humans han posat de manifest que tant ATS com els seus metabòlits àcids són sensibles a polimorfismes en el gen *SLCO1B1*, ja que la concentració plasmàtica d'aquests va resultar ser superior en individus portadors de la variant al·lèlica *SLCO1B1* 521C (genotip T/C) al comparar-se amb la variant típica o "salvatge" 521 T/T.

El metabolisme de l'ATS és un procés complex en el qual intervenen reaccions enzimàtiques de glucuronidació, lactonització, i oxidació. Tant ATS com els seus metabòlits àcids directes, 2-hidroxi-ATS (2OH-ATS) i 4-hidroxi-ATS (4OH-ATS), estan en equilibri amb les corresponents formes neutres lactonitzades (ATS-L, 2OH-ATS-L i 4OH-ATS-L). Aquest procés de lactonització (o formació d'un éster cíclic) pot tindre lloc espontàniament a un medi amb pH<6, o catalitzat per enzims pertanyents a la família d'UDP-glucuronosiltranferases (UGTs). El mecanisme de reacció proposat per aquesta lactonització enzimàtica és la formació d'un acil-β-D-glucurònid d'ATS, el qual experimenta un procés de ciclació espontània prèvia pèrdua del grup glucurònid. El procés contrari, és a dir, la hidròlisi de la lactona per obrir la molècula i tornar a donar la forma àcida i farmacològicament activa, té lloc espontàniament en medis amb pH>6 o pot estar catalitzada per esterases i paraoxonases plasmàtiques. És per això que ambdós processos (lactonització i hidròlisi) han de tenir-se en compte a l'hora de desenvolupar models farmacocinètics fisiològics per a l'ATS. El procés d'oxidació a través del citocrom P450 (CYP450) està considerat com la ruta majoritària per a la biotransformació d'estatines en la espècie humana, essent l'isoenzim CYP3A4 el més rellevant en el cas de l'ATS. Amb diferents afinitats i velocitats de reacció, aquests processos enzimàtics mediats pel CYP450 estan clarament polaritzats cap a les formes lactonitzades, essent més eficient l'oxidació d'ATS-L que la d'ATS. És a dir, el procés de lactonització d'ATS canvia la preferència del CYP450, essent molt més actiu sobre les formes neutres lactonitzades que sobre les formes àcides.

El model PBPK desenvolupat a la plataforma Simcyp® V19 va descriure adequadament l'exposició a ATS, ATS-L, 2OH-ATS-L i 4OH-ATS-L després de la simulació d'una dosi única per via oral d'un comprimit d'ATS-Ca de 20, 40 o 80 mg i després de la simulació de l'administració diària de 10 mg d'ATS-Ca durant una setmana. Un aspecte important a tindre en compte és que, degut a limitacions intrínseques a la plataforma Simcyp® V19, únicament es va considerar el procés

de lactonització enzimàtica mediada per UGTs. La lactonització presistèmica pel baix pH de l'estómac no es va poder implementar com a via paral·lela de l'actonització per limitacions estructurals de la plataforma Simcyp. És per això, que el model desenvolupat no contempla processos d'absorció d'ATS-L, ja que la seua formació és, en tot moment, sistèmica.

De la manera com s'ha descrit en altres treballs d'investigació, el mecanisme principal per a la formació dels metabòlits hidroxilats 2OH-ATS i 4OH-ATS és la lactonització d'ATS, hidroxilació d'ATS-L pel CYP450 i hidròlisi final dels metabòlits lactonitzats. No obstant això, la hidroxilació directa d'ATS pel CYP450 també està activa i funciona de manera paral·lela a aquesta ruta principal, encara que contribuint de manera minoritària al procés global d'eliminació d'aquesta estatina. És per això que la simulació de l'exposició a 2OH-ATS no va poder ser reproduïda adequadament pel model desenvolupat, amb errors de predicció de 0.57 per a AUC i 0.33 per a C_{max}, a l'agarrar els factors d'extrapolació entre sistemes validats per al sistema *in vitro* en el que es van determinar les cinètiques de metabolisme per a cada isoforma del CYP450.

La capacitat predictiva del model desenvolupat es va verificar mitjançant la simulació de les DDIs observades en el context clínic amb inhibidors del CYP450 (itraconazol i claritromicina) i d'OATPs (rifampicina). Com que en tots els escenaris considerats l'error de predicció en la variació d'AUC i C_{max} com a conseqüència de la interacció farmacocinètica resultaren entre 0.66 i 1.45, tant l'estructura de les reaccions metabòliques proposada com la contribució relativa de cadascun dels transportadors de captació activa a l'interior dels hepatòcits (OATP1B1 (53.2%) > OATP1B3 (37.8%) >> OATP2B1 (9%)) va estar confirmada.

Analitzant l'impacte de l'activitat de l'OATP1B1 sobre l'aclariment, AUC i C_{max} d'ATS, les simulacions dutes a terme van revelar que aquells individus portadors d'una variant d'aquest transportador poc activa (PT), codificada pel polimorfisme *SLCO1B1*5*, presentaven una disminució en l'aclariment d'ATS del 30% ($p<0.01$) respecte a individus amb la variant típica o "salvatge" (ET). Com a conseqüència, l'AUC i la C_{max} en aquests individus estava incrementada en un 40% ($p<0.05$) i un 33% ($p<0.05$), respectivament. A més a més, les prediccions del model PBPK revelaren que un 34.8% dels individus simulats tindrien un aclariment aparent d'ATS inferior a 414.67 L/h, valor que s'ha determinat com a mínim per baix del qual s'incrementa el risc de patir efectes adversos a nivell muscular. Entre aquests individus, els més afectats serien els PT, ja que el 63% estaria en risc de patir miopaties; com era d'esperar, el nombre d'individus en risc va disminuir de manera inversa a l'activitat del transportador OATP1B1 (transportadors intermitjos (IT), 42%; ET, 32%; transportadors ultraràpids (UT), 21%).

Quantitativament, els individus amb un major risc de patir molèsties musculars per presentar un aclariment aparent d'ATS inferior a 414.67 L/h tindrien una exposició major tant a ATS (220%, $p<0.0001$) com a ATS-L (176%, $p<0.0001$). Aquests resultats estan en consonància amb l'increment en el risc de patir miopaties que s'ha observat en el context de la pràctica clínica diària per a pacients portadors de la variant *SLCO1B1*5* d'1.4 (95CI: 1.1-1.7, $p=0.02$) i que és causa d'interrupcions en el tractament hipolipemiant amb ATS. És més, les prediccions són coherents també amb l'increment observat en l'exposició a ATS-L ($p<0.01$) i la prolongació en la $t_{1/2}$ per a ATS ($p<0.01$) que presenten els pacients amb miopaties respecte els que no refereixen molèsties musculars. D'aquesta manera, el model PBPK desenvolupat per a ATS i els seus metabòlits anticipa i quantifica una relació exposició-seguretat entre ATS i ATS-L i efectes adversos a nivell muscular.

Optimització de l'expressió i la cinètica de receptors i processos d'eliminació d'anticossos monoclonals terapèutics utilitzats en oncologia.

Aquesta part inclou la resolució de l'objectiu específic 7 d'aquesta tesi doctoral. L'activació de receptors tirosina quinasa transmembrana és clau en la patogènesi de molts trastorns neoplàsics. La família de receptors del factor de creixement epidèrmic (EGFR) està constituïda per un grup de quatre receptors transmembrana involucrats en processos de transducció de senyals que regulen la diferenciació i el creixement cel·lular. Aquests receptors (EGFR/HER1/ErbB-1, HER2/ErbB-2/neu, HER3/ErbB-3 i HER4/ErbB-4) presenten un domini extracel·lular (ECD) voluminós que constitueix una oportunitat terapèutica excel·lent per a dirigir fàrmacs biològics racionalment dissenyats per a alterar els canvis estructurals desencadenats per la unió natural (encara que en aquest cas, patològica) de lligands interns i/o processos de dimerització, fent possible el concepte de "magic bullet" proposat per Paul Ehrlich ja al segle 19.

Modelat farmacocinètic fisiològic d'anticossos monoclonals dirigits a HER2

La sobreexpressió del receptor HER2 al teixit tumoral va ser incorporada als paràmetres del sistema del model PBPK aplicant un factor de 25 vegades l'abundància d'aquest als teixits sans (normals), ja que la concentració mitjana del receptor HER2 ha estat determinada en 1293.8 i 31656 pg/mg en teixits normals i tumorals, respectivament. El model de disposició del fàrmac mediada per la unió a la diana terapèutica o TMDD va estar caracteritzat per una concentració del receptor (R_{max}) no alterada per la unió del fàrmac biològic, ja que

ni pertuzumab (PTZ) ni trastuzumab (TTZ), els dos anticossos monoclonals (mAbs) escollits per a desenvolupar els corresponents models PBPK, indueixen la internalització del receptor com a conseqüència de la interacció farmacodinàmica. Degut a la falta de consens en l'impacte dels nivells circulants del domini extracel·lular d'aquest receptor (cHER2-ECD) sobre la farmacocinètica d'aquests mAbs, no es va incorporar cap procés de "shedding" (pèrdua del ECD) en el model PBPK.

L'optimització de la constant de degradació (k_{deg}) del receptor HER2 en teixits i òrgans normals a un valor de 0.398 h^{-1} va proporcionar una parametrització correcta del model TMDD en particular, i del PBPK en general, per descriure amb exactitud i precisió la farmacocinètica de PTZ en diferents nivells de dosi, pautes posològiques i trastorns neoplàsics. Aquest procés de degradació accelerada del receptor HER2 en teixits normals quan es compara amb el teixit tumoral, és coherent amb treballs d'investigació previs on s'ha caracteritzat l'impacte que la sobreexpressió del receptor HER2 en un trastorn neoplàsic té sobre la maquinària d'endocitosi i transport intracel·lular implicada en la seua degradació i reciclatge, aparentment degut a una quantitat limitada d'aquests recursos cel·lulars. El nostre model prediu que la constant de velocitat de degradació al teixit tumoral és molt probablement 5 vegades inferior (0.079 h^{-1}) que la que presenten els teixits sans. Aquests resultats, van també de la mà amb models matemàtics que han caracteritzat les rutes intracel·lulars d'aquest receptor i han suggerit que, la sobreexpressió del receptor HER2 desviaria el curs fisiològic d'entrada a l'endosoma per a la seua degradació cap a rutes de reciclatge i retorn a la membrana cel·lular a les cèl·lules tumorals.

L'avaluació numèrica de la capacitat predictiva del model PBPK desenvolupat per a PTZ amb l'optimització de l'expressió i la cinètica del receptor HER2 va resultar satisfactòria, amb errors de predicció percentuals (PPE) inferiors al 15%. La parametrització del receptor HER2 va estar verificada amb el model PBPK per a TTZ, obtenint-se PPEs del 16% per AUC i del 7% per a C_{max}.

Modelat farmacocinètic fisiològic d'anticossos monoclonals dirigits a EGFR

En el cas del receptor HER1 o EGFR, es va desenvolupar un model PBPK per a cetuximab (CTX) amb la finalitat d'optimitzar i avaluar processos d'eliminació de fàrmacs biològics. Després d'afegir un aclariment sistèmic addicional de 0.033 L/h als processos de catabolisme proteic i als processos d'eliminació pel model TMDD, el model PBPK desenvolupat va descriure satisfactòriament l'evolució temporal de la concentració plasmàtica de CTX en una àmplia varietat d'esquemes de dosificació amb PPEs del 13% i del 10% per a AUC i C_{max}, respectivament. El

model va ser capaç també de predir adequadament la concentració vall o mínima en la majoria dels escenaris simulats, la que ha estat reconeguda com un paràmetre d'exposició important en la resposta al tractament. Aquest aclariment addicional afegit als processos d'eliminació de CTX pot ser degut a: 1) la unió al receptor FcγRIIIA, 2) la unió al subcomponent C1q, i/o 3) als processos d'escissió proteolítica de la regió frontissa baixa per metaloproteinasses presents en la matriu tumoral.

L'estratègia de modelat PBPK seguida, tindria dues aplicacions majoritàries en el context de la farmacologia clínica d'un programa de desenvolupament d'anticossos monoclonals terapèutics. En primer lloc, permet verificar i validar l'expressió i la cinètica del receptor (paràmetre del sistema i depenent de la malaltia), molt important en el desenvolupament de models prospectius de mAbs dirigits a la mateixa diana terapèutica. En segon lloc, verificada la capacitat predictiva del model PBPK, aquest es podria aplicar per a respondre preguntes de l'estil "què passaria si...?" i predir 1) la farmacocinètica en un escenari concret no avaluat, com ara diferents esquemes de dosificació per minimitzar efectes adversos, 2) la concentració local en un determinat teixit o òrgan, i 3) l'ocupació del receptor aconseguida amb un esquema de dosificació concret.

Conclusions

1. El programa PhysPK Biosimulation Software ha sigut validat satisfactòriament prenent NONMEM com a referència per avaluar l'exactitud i la precisió dels resultats.
2. Els models PBPK amb una aproximació acausal, multinivell i orientada a objectes permeten descriure l'evolució temporal de l'exposició sistèmica a un fàrmac considerant de manera independent els components de simulació i les funcions matemàtiques del sistema fisiològic.
3. El comportament farmacocinètic i l'activitat antitumoral sobre les línies cel·lulars de càncer de mama HER2+ i Triple Negativa de la molècula candidata a fàrmac anticancerós MBQ-167 han sigut descrites i adequadament caracteritzades desenvolupant un model PBPK/PD.
4. La simulació de l'administració intraperitoneal de 10 mg/kg una o dues vegades al dia anticipa l'eradicació del tumor HER2+ i l'estabilització del creixement per a la línia cel·lular Triple Negativa.
5. El model PBPK de l'atorvastatina descriu l'evolució temporal d'aquest fàrmac i els seus metabòlits tant en forma àcida com lactonitzada. L'avaluació de la capacitat predictiva del model mitjançant la simulació de

les interaccions farmacocinètiques observades en clínica verifica l'esquema metabòlic i de transport actiu proposat.

6. L'avaluació quantitativa de la interacció amb polimorfismes al gen *SLCO1B1* ha posat de manifest que el 63% de pacients portadors de la variant *SLCO1B1*5* tindrien un risc elevat de patir efectes adversos musculars.
7. L'optimitzacio de l'abundància i la cinètica de dianes terapèutiques, així com dels processos d'eliminació de fàrmacs biològics mitjançant el modelat PBPK, ha posat de manifest el potencial d'aquesta tècnica en el procés de descobriment i desenvolupament de fàrmacs orientat per models

Introduction

Pharmacometrics: optimizing the drug discovery and development process

Almost $1000 million [1] and 10 years [2] are the estimated economic and time cost of bringing to the market a new drug, highlighting how much expensive and time consuming the drug development process is. Because of this, new approaches and technologies have been (are being) applied to increase the efficiency of the drug development process and among them, model informed drug discovery and development (MID3) has positioned itself as more than a valuable methodology to achieve such a goal. The basis of MID3 relies on three elemental pillars [3]:

1. A thorough and mechanistic understanding of the disease and the drug.
2. The development of mathematical models able to integrate information from different sources (e.g., preclinical, clinical, *in vitro*, *in silico*).
3. The ability to apply these strategies to address issues during the drug development process, regulatory revision, and clinical use.

Modelling and simulation (M&S) strategies represent an efficient tool since they allow to integrate large, complex, and heterogeneous information datasets with the aim of establishing quantitative and predictive relationships for a more efficient and optimal model-informed dose selection in the drug discovery and development process. In this context, pharmacometrics can be defined as “the science of developing and applying mathematical and statistical methods to characterize, understand, and predict a drug’s pharmacokinetic, pharmacodynamic, and biomarker–outcomes behaviour” [4]. Combining elements from disciplines such as pharmacology and statistics, pharmacometrics allows to quantitatively characterize the variability associated with drug exposure and effect to provide a temporal description of the pharmacological response. Consequently, the contribution of the individual characteristics to the response can be differentiated from confounding factors that would otherwise limit data interpretation, thus allowing the individualization of drug administration. This feature represents the main application of pharmacometrics and an opportunity for implementing the MID3 paradigm.

Under the umbrella of pharmacometrics, one of the disciplines with the greatest recognition and growth in recent years has been physiologically based pharmacokinetic (PBPK) modelling.

Physiologically based pharmacokinetics

It was 1937 when Torsten Teorell[1], "the father of pharmacokinetics" [5], proposed for the first time a physiological structure for drug absorption, distribution, metabolism and excretion (ADME) to derive "general mathematical relations from which it is possible, at least for practical purposes, to describe the kinetics of distribution of substances in the body" in order to reveal what the body does to the drug [6]. To achieve such a challenging work in that time, Teorell developed a simplified model of an organism that comprised the site of drug administration, eliminating organs (liver and kidneys) and other tissues, all of them with their corresponding volumes. Finally, the blood circulation connected all the constituting parts of the model and permeability coefficients described drug diffusion from the bloodstream to organs and tissues (Figure 1). The analogy with present day physiologically based pharmacokinetic (PBPK) models is more than evident.

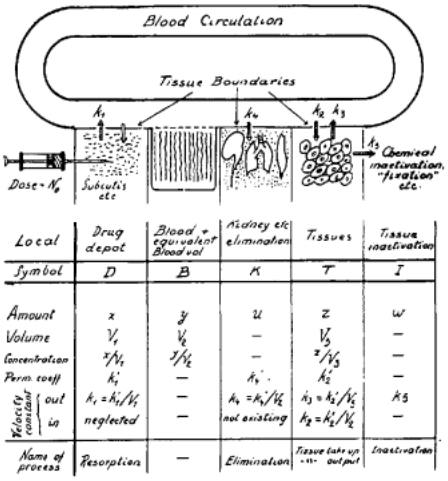

Figure 1. Distribution model for extravascular administered drugs proposed by Torsten Teorell in 1937. Adapted from [5]

[1] One cannot begin to talk about physiologically based pharmacokinetics (PBPK) without honouring which is probably the first PBPK model in the history.

A whole-body PBPK model is a mathematical structure defining an organism (the system) and build-up with anatomically differentiated compartments representing organs and tissues, all of them connected through the cardiovascular system by means of arterial and venous blood flows. This kind of models contain an explicit representation of the most relevant organs to the ADME of a drug and typically are lungs, brain, heart, liver, gastrointestinal (GI) tract (stomach, small and large intestine), pancreas, spleen, kidneys, gonads, prostate, muscles, adipose tissue, thymus, bone and skin (Figure 2).

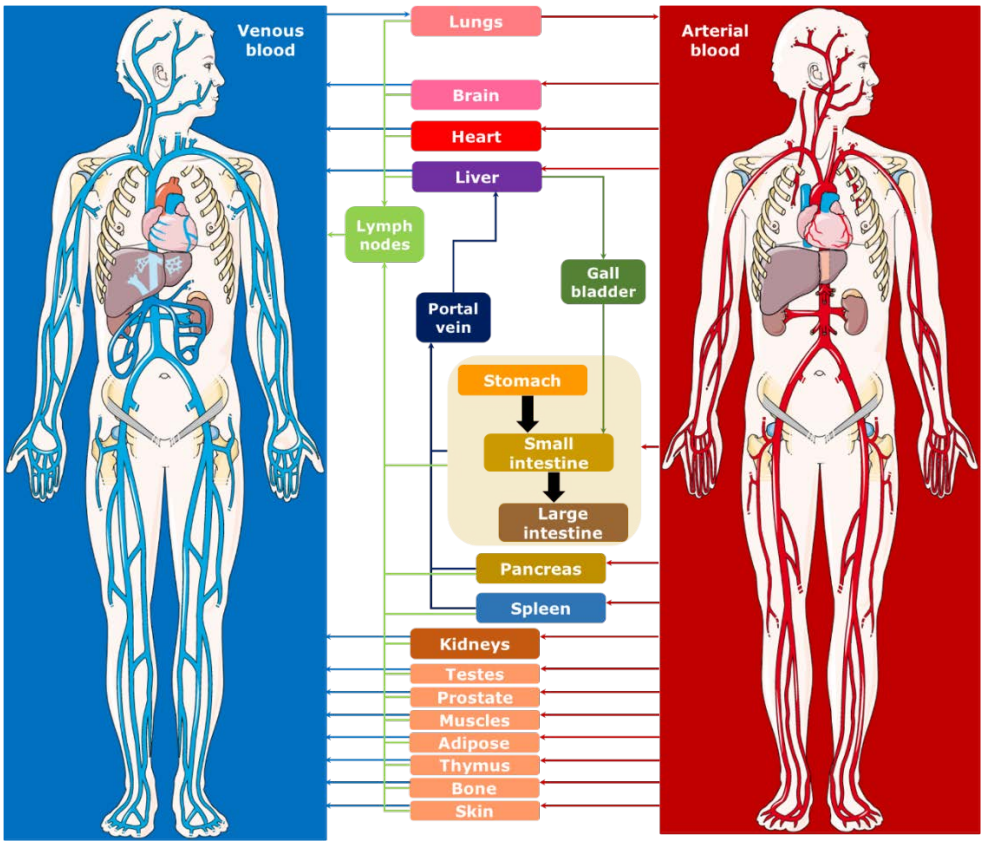

Figure 2. Illustration of a generic whole-body physiologically based pharmacokinetic (PBPK) model.

Each tissue is characterized by its volume, density, blood flow and composition (fractional volumes of water, phospholipids, neutral lipids, and interstitial fraction), with different structural organizations ranging from a simple whole tissue (Figure 3A) to a more complex structure that comprises vascular (Figure 3B), interstitial and intracellular spaces (Figure 3C) or also considering the

endosomal space (Figure 3D) to better account for disposition processes of biologic drugs.

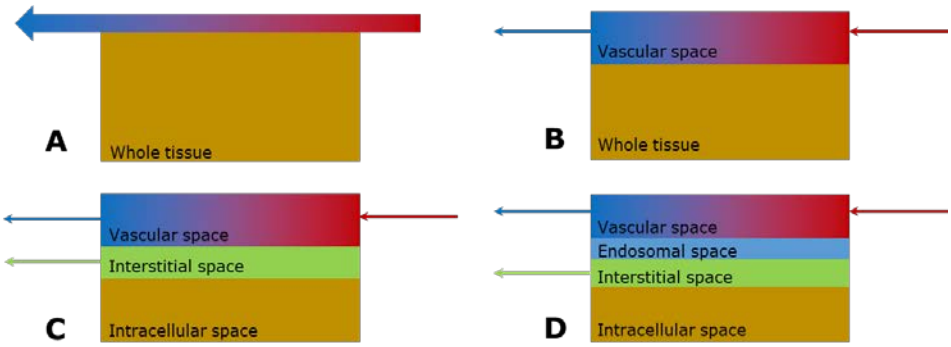

Figure 3. Different structural organizations of tissues in a PBPK model. Red-to-blue colour degradation represents the sense of the blood perfusing the tissue (i.e., arterial and venous blood). Green arrow represents lymph flow.

Additional information such as enzyme and transporters abundances, haematocrit, gastric pH and emptying time, glomerular filtration rate, hepatocellularity (as million hepatocytes per gram of liver or HPGL), plasma pH, GI tract dimensions (radius and length) are also taken into account to best describe the physiology of each tissue of the organism. Thus, an important feature of PBPK modelling is the availability of a comprehensive and mechanistic representation of the physiology of an organism [7]. Apart from the physiological information provided by the system-related parameters previously mentioned, demographic and genetic factors (e.g., age, weight, height, sex) are also added to the PBPK model to finish with the parameterisation of this building block. Adding the known variability of demographic, anatomic, physiological, genetic and tissue-specific characteristics as well as covariates or correlations between different specifications of the population, allows to generate virtual subjects and populations (population PBPK or popPBPK) that are more representative of the real world [8].

Two additional building blocks are needed to ultimately parameterise the PBPK model. The first one is the drug itself. Molecular weight (MW), chemical structure (number of hydrogen bond donors and/or polar surface area), acidic character (neutral, monoprotic acid, monoprotic base, etc…), pK_a and lipophilicity (logP) as physicochemical properties, and intestinal permeability, fraction unbound in plasma (f_u), blood-to-plasma ratio (B/P), tissue-to-plasma ratios (K_{pt}), intrinsic clearances (CL_{int}) for metabolic and trasporter-mediated processes, and excretion pathways (renal (CL_R) or biliary (CL_{bile}) clearances) as ADME parameters will define the drug-related parameters of the PBPK model. Finally, study protocol

(dose, frequency and route of administration and study duration), formulation characteristics (e.g., capsule, oral solution, tablet, etc.) and special events (e.g., food intake) will constitute the trial-related parameters and will close the parameterisation of the PBPK model. This differentiation is necessary to allow the development of general and drug-independent models to be used in a wide range of scenarios [9].

The use of PBPK modelling in MID3 has been limited in the past because of the mathematical complexity of these models and the large amount of *in vivo* data of drug tissue concentrations needed [10]. However, the availability of *in vitro* systems that act as surrogates of *in vivo* ADME processes (e.g., Caco-2, MDCK, Hep, rCYPs) and the development and refinement of *in vitro-in vivo* (IVIVE) extrapolations techniques [11] and *in silico* methods to predict K_{pt} [12-15], B/P [16,17] and human jejunum effective permeability ($P_{eff,man}$) [18] have significantly influenced the feasibility to combine input parameters from different sources (*in silico* predictions, *in vitro* experiments or *in vivo* measurements) [9] in order to quantitatively predict plasma and tissues concentration-time profiles, which is commonly known as “bottom-up” approach.

This mechanistic modelling methodology clearly differs from the more classical and data-driven “top-down” approach, with which PK models are developed once data are generated and are analysed using different approaches including population PK (popPK) data analysis. A clear advantage of “bottom-up” approaches (and thus of PBPK) is that modelling and simulation work can start at early stages of drug development when drug concentrations are not yet available. Notwithstanding, there should not be any incompatibility between both approaches as they can borrow strengths from each other [19]. This symbiosis starts in the middle grey zone and constitutes what is known as “middle-out” approaches [20]. As Professor Amin Rostami-Hodjegan states in a brilliant state of the art paper [21], “they are not just restricted to explaining the observed data but they intend to go backwards (in explaining the clinical observations) in order to go forwards beyond the perimeters of the initial clinical study using the prior *in vitro* and system information. This provides the necessary “qualification” for the model to be used with confidence for *pre*-dictions”.

A general workflow to develop PBPK models is depicted in Figure 4. After characterising the ADME processes and pharmacodynamic (PD) properties of the drug candidate and elaborating a parameters database, the physiological parameters of the system are added, the model structure is defined and the PBPK model is build. Simulations of concentration-time profiles are then performed and compared with *in vivo* data. Model refinement is performed to best describe the observed PK following an iterative process that can involve multiple cycles of

"predict, learn, and confirm" [22] (Step 1). Following is the model verification, a process in which the model is tested to predict the PK in a different scenario such as drug-drug interactions (DDIs) (Step 2). Now, the model can be used to explore untested scenarios and to answer "what if" questions (Step 3). The validation of the model (Step 4) comes at much later stages (if at all), when the data from the clinical studies the model was intended to anticipate (the question of interest in a particular context of use) are available, thus constituting a post-application step [19].

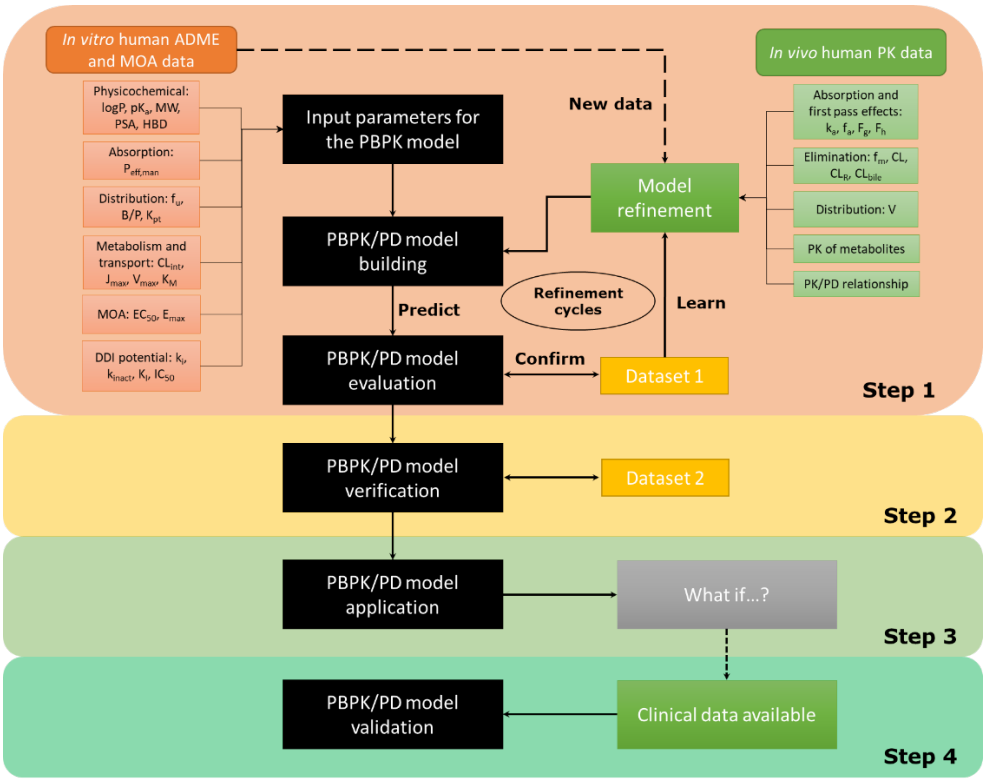

Figure 4. A general workflow to develop PBPK models. ADME: absorption, distribution, metabolism and excretion; MOA: mechanism of action; logP: logarithm of the octanol:water partition coefficient; pK_a: minus logarithm of the acidity constant; MW: molecular weight; PSA: polar surface area; HBD: hydrogen-bond donnors; $P_{eff,man}$: jejunum effective permeability in humans; f_u: fraction unbound in plasma; B/P: blood-to-plasma concentration ratio; K_{pt}: tissue-to-plasma concentration ratio; CL_{int}: intrinsic clearance; J_{max}: maximum rate of transporter-mediated efflux or uptake; V_{max}: maximum rate; K_M: concentration at half-V_{max}; EC_{50}: unbound drug concentration at half-E_{max} (sensitivity); E_{max}: maximum drug effect (intrinsic activity); k_i: absolute inhibition constant; k_{inact}: maximum inactivation rate; K_I: concentration at half-maximal k_{inact}; IC_{50}: inhibitor concentration required to inhibit 50% of a metabolic pathway; k_a: absorption rate constant; f_a: fraction of dose absorbed; F_g: fraction of absorbed drug scaping gut wall metabolism; F_h: fraction of absorbed drug scaping hepatic first pass effect; f_m: fraction metabolised; CL: clearance; CL_R: renal clearance; CL_{bile}: biliary clearance; V: volume of distribution.

Relevance and applications of PBPK models

Physiologically based pharmacokinetic M&S can answer "what-if" questions, assess untested or untestable scenarios and make predictions of high pharmacological relevance simulating drug concentration not only in plasma, but also at the site of drug action, which may be extremely difficult or impossible to determine experimentally. It constitutes a powerful technique to advance the understanding and transition of data from phase to phase of the drug development process [23], and to assess the effect of intrinsic (e.g., organ dysfunction, age, pregnancy, genetics) and extrinsic factors (e.g., DDIs), alone or in combination, on drug exposure [24]. This pharmacometrics methodology can inform study design, guide internal decisions on the timing of different studies and reduce regulatory uncertainty [25]. Another important feature of PBPK models is that, as they are based on physiology, it is easier to professionals not belonging to the clinical pharmacology field to understand model outcomes and results and incorporate them in drug development decisions [26].

An overview of the main applications of PBPK along the value chain of MID3 is detailed below[2]:

1. **Drug discovery**
    - *Lead optimization:*
        - Data integration for hypothesis testing to identify PK mechanisms.
        - Assessment of relevance to humans.
2. **Preclinical drug development:**
    - Translation of efficacy and toxicity through PBPK/PD and PBPK/safety modelling, respectively.
    - Prediction of starting dose for *first in human* (FIH) trials.
    - Data integration for human ADME prediction.
    - Assessment of solubility to decide on the need for formulation development.
3. **Clinical development**
    - *Phase I:*
        - Update/refine models with first clinical data to allow for prospective predictions of absorption, DDIs or extrapolation to different populations.
        - Prediction of food and acid reducing agent (ARA) effects*

[2] Asterisks indicate PBPK applications with regulatory interest. Adapted from [25].

- Simulation of untested scenarios: for example, modified release formulations. *

- *Phase II/III:*
  - Incorporation of variability in physiological parameters and enzymology to look for extreme individuals (non responders or at high risk for toxicity).
  - PK prediction of target population by incorporating all known disease-driven changes in physiological parameters and enzymology.
  - Virtual bioequivalence. *
  - *What-if* testing to optimise dosing strategy in DDI studies*
  - Assessment of exposure in vulnerable populations to justify their inclusion/exclusion in clinical trials.
  - Supplement clinical data in difficult to recruit subgroups (paediatrics, pregnancy). *
  - Assessment of untested scenarios to inform drug labels or waive studies. *

Regulatory acceptance of PBPK models

The increased utilization of PBPK M&S by the pharmaceutical industry and the inclusion of results derived from these approaches in regulatory submissions have been recognised by the main authorities (European Medicines Agency (EMA) [EU], Food and Drugs Administration (FDA) [USA], Pharmaceuticals and Medical Devices Agency (PMDA) [Japan]) and have prompted the publication of specific guidelines on PBPK [27-29], thus moving PBPK M&S from academic curiosity to industrial routine and, ultimately, to regulatory acceptance [30]. Consequently, PBPK simulations have been used in lieu of conducting clinical trials or have informed the prescribing information of many drugs that otherwise would have result in a gap on some specific situations [30,31]. For example, the FDA granted a waiver to the sponsor of voxelotor, a haemoglobin S polymerization inhibitor indicated for the treatment of sickle cell disease, avoiding the *in vivo* assessment of its PK as a victim drug of cytochrome P450 (CYP450) 3A family-mediated DDI. Extensive PBPK analyses using a range of fractions metabolised through CYP3A in conjunction with the PK/PD analysis was considered sufficient to inform dose adjustment when concomitantly administered with inhibitors or inducers of CYP3A without the need of providing any clinical data of the effect of CYP3A modulation on the PK of voxelotor. Another example comes from the EMA, who proposed that, for very rare diseases or high medical need, paediatric clinical study waiver could be allowed based on PopPK and/or PBPK simulations without any clinical PK data

in children [32]. More case-studies and lists of drugs with PBPK model-informed labelling can be found elsewhere [22,30,31,33].

A recent analysis performed by the FDA's Office of Clinical Pharmacology has revealed that the highest number of submissions containing PBPK-related information is in oncology, followed by haematology, neurology and psychiatry [31]. The distribution of PBPK modelling in regulatory submissions to the FDA between 2018 and 2019 by various application areas is shown in Figure 5.

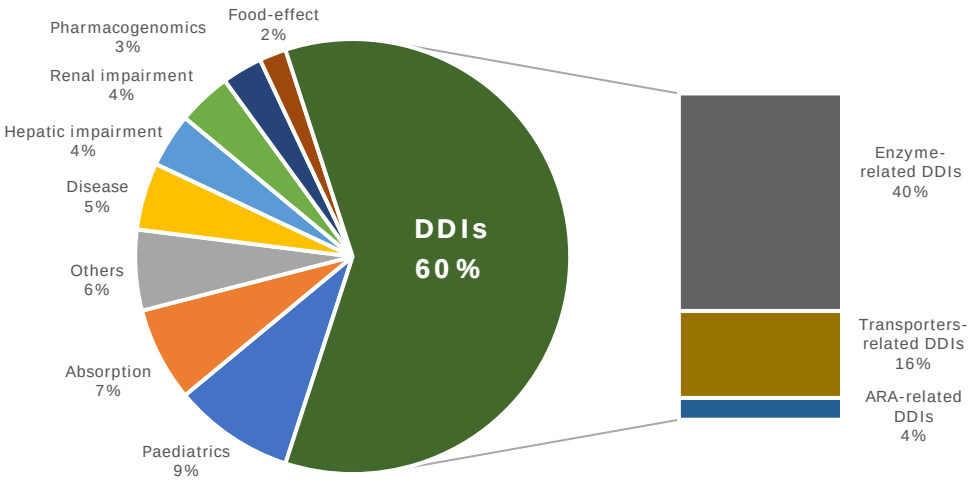

Figure 5. Distribution of PBPK M&S application areas in regulatory submissions to FDA between 2018 and 2019. Others: prediction of FIH and/or tissue specific PK; DDI: drug-drug interaction; ARA: acid-reducing agent.

DDIs assessment ranks position #1 among applications of PBPK models in regulatory submissions, with the enzyme-related DDI evaluation covering the 40% of total applications and is followed by extrapolation to paediatrics (9%) and absorption-related assessments (7%). The low presence of PBPK absorption modelling in marketing authorisation applications could be attributed to the low regulatory acceptance of PBPK analyses for biopharmaceutics and oral drug absorption, also called physiologically based biopharmaceutics modelling (PBBM), as the lack of a complete understanding of the physiology of the GI tract, the frequent overparameterization, and/or the insufficient model validation and/or platform qualification compromise their translatability and predictive performance [34]. Nonetheless, the regulatory recognition of PBPK modelling and simulation is the reason that a great part of the quantitative information contained in the

Clinical Pharmacology dedicated section of the United States Prescribing Information comes from PBPK assessment [31].

Software tools for PBPK modelling and simulation

The development of powerful and sophisticated platforms (PBPK platforms) that efficiently allow to merge and integrate the physiological structure, the biochemical mechanisms and the drug-related properties and facilitate the building and use of PBPK models has been an inflexion point in their spread and acceptance. A definition of PBPK platform has already been provided [22]: "a PBPK platform is an integrated software environment that allows building and running PBPK models that may or may not provide compound or population-specific databases. From a software perspective, a platform includes various components such as graphical user interface (GUI), data structures, collections of various models, computational engine, as well as interfaces for presenting the simulation results".

Before the advent of such sophisticated PBPK platforms, open-source software tools originally developed for engineering and mathematical disciplines were used by PBPK modellers. The users were thus conditioned to write from scratch their own models, codifying the whole system and the ADME processes, as well as the trial design. This work required to have not only an expertise in the fields of physiology and pharmacokinetics, but also to learn the specific coding language used by the software. Nowadays, software like Matlab-Simulink®, ADAPT5®, Berkeley-Madonna® and SAAM II® have specific modules for PBPK modelling, with equation libraries and a GUI that allows a rapid generation of standard PBPK model templates. This open software PBPK platforms give complete control of model structure, equations and development process, so the modeller can adapt the framework to include new findings related to the system and/or the drug [35]. Notwithstanding, with such power comes great responsibility, as the modeller must clearly state the scientific reasons of any change and there is an inherent risk of making incorrect assumptions or mathematical errors. Additionally, they are time consuming and the databases of physiological parameters must be continuously updated by the modeller.

On the other hand, designed software require less programming skills as they do provide a friendly GUI to facilitate the development of the PBPK model. In this case, the modeller does not need to learn the programming language to build the model: the model structure is already built in the PBPK platform. So, the main advantage of these software tools is that they can be used by scientists that have the physiological and pharmacokinetic knowledge but lack of the computer

programming expertise or time to create their own models [35]. These designed PBPK platforms are also provided with libraries of validated populations and compounds, allowing the modeller to efficiently response “what if” questions. The most used designed PBPK platforms (open source or commercial) are SimCYP® (Certara), PK-Sim® (Open Systems Pharmacology) and GastroPlus® (Simulation Plus)[3]. As previously said, the model structure, i.e., the backbone of the PBPK model, is already implemented into the software, but it is not accessible to the end user. This does not mean these software are not transparent, as they are usually called “black boxes”, when in fact all the assumptions they are based on are transparently stated and provided to the end user. So, the more appropriate term “glass boxes” recently suggested fits better [36]. Moreover, this inaccessibility has to be interpreted in terms of quality and confidence, as only a few specialists can open the “box”, access to the model structure, make the changes and improvements properly and re-qualify the PBPK platform. Extensive reviews about quality aspects and credibility of PBPK M&S can be found elsewhere [19,22,37].

All these software (either open or designed) are based on systems of ordinary differential equations (ODE) that the end user or the designer must develop, by defining the local processes and the relationships among compartments. However, other modelling methodologies do exist, such as software based on differential algebraic equations (DAE) and acausal machine learning technology. The main advantage of models based on acausal simulation languages is that the mathematical formulation of simulation components is not algorithmic (i.e., acausal), and therefore output and input variables do not need to be defined at the stage of model definition.

[3]A detailed comparison of the main features of these PBPK platforms is provided in Table 2 of [35]. However, it must be noted that, as a consequence of new software releases since the date of the referred publication, some features have, most probably, changed to improve the software features.

Hypothesis and objectives

Physiologically based pharmacokinetic modelling and simulation has positioned itself as a valuable tool in the MID3 paradigm in the last years. The development of M&S software that facilitate the building or use of PBPK models has been a key issue in their emergence and acceptance. It constitutes a powerful technique to advance the understanding and transition of data from phase to phase of the drug development process [23], early on the preclinical setting anticipating drug efficacy through PBPK/PD modelling and suggesting initial doses for FIH clinical trials, as well as assessing the effect of intrinsic (e.g., organ dysfunction, age, pregnancy, genetics) and extrinsic factors (e.g., DDIs), alone or in combination, on drug exposure [24] later on the clinical phases of drug development.

Besides the continuous need to bridge the knowledge gaps in both system-related (developmental, disease and organ dysfunction-related) and drug-related (ADME assumptions and IVIVE) components, there is also a necessity for continued research in order to formulate and refine best practices in the use of PBPK approaches during drug development and regulatory review [26].

Moreover, studies that analyse the most common software tools are mainly focused on the modelling features that cope with user and regulatory requirements, like the physiological mechanisms supported, type of mathematical techniques implemented and the ability to address special populations (e.g., paediatrics) and situations (e.g., DDIs) instead of the methodological aspects they are based on. In this regard, and to the best of our knowledge, none of the current well-known PBPK software tools (open software such as Matlab-Simulink®, ADAPT5®, Berkeley-Madonna® and SAAM II® or designed software such as PK-Sim®, Simcyp®, GastroPlus®) are based on the multilevel object-oriented acausal modelling language approach.

Therefore, the **general objective** of the present thesis is:

To develop, validate and apply physiologically based pharmacokinetic models from a methodological and decision-making perspectives focused on optimising model-informed drug discovery and development processes

The **specific objectives** to achieve such a goal are:

1. To assess the predictive reliability of the physiologically based software PhysPK Biosimulation Software *versus* the well-known population approach software NONMEM.
2. To compare acausal with algorithmic modelling approaches in the framework of semi-mechanistic PK models.
3. To characterize tumour growth dynamics in two human breast cancer cell lines (HER2+ and Triple Negative).
4. To develop a PBPK/PD model of MBQ-167 after intraperitoneal administration in mice.
5. To develop a full PBPK model for atorvastatin and its metabolites in both, open acid and lactone forms.
6. To quantitatively assess the impact of polymorphisms in *SLCO1B1* on atorvastatin pharmacokinetics.
7. To propose a general workflow for PBPK modelling of therapeutic monoclonal antibodies and its application in clinical pharmacology to optimise target expression and clearance mechanisms

Chapter 1

A Multilevel Object-Oriented Modelling Methodology for Physiologically-Based Pharmacokinetics (PBPK): Evaluation with a Semi-Mechanistic Pharmacokinetic Model

J. Reig-Lopez[1,2], M. Merino-Sanjuan[1,2], V. Mangas-Sanjuan[1,2], M. Prado-Velasco[3]

Authors Affiliation:[1] Department of Pharmacy and Pharmaceutical Technology and Parasitology, University of Valencia, Valencia, Spain; [2] Interuniversity Research Institute for Molecular Recognition and Technological Development, Polytechnic University of Valencia-University of Valencia, Valencia, Spain; [3] Multiscale Modeling in Bioengineering Research Group and Department of Graphic Engineering. University of Seville, Seville, Spain.

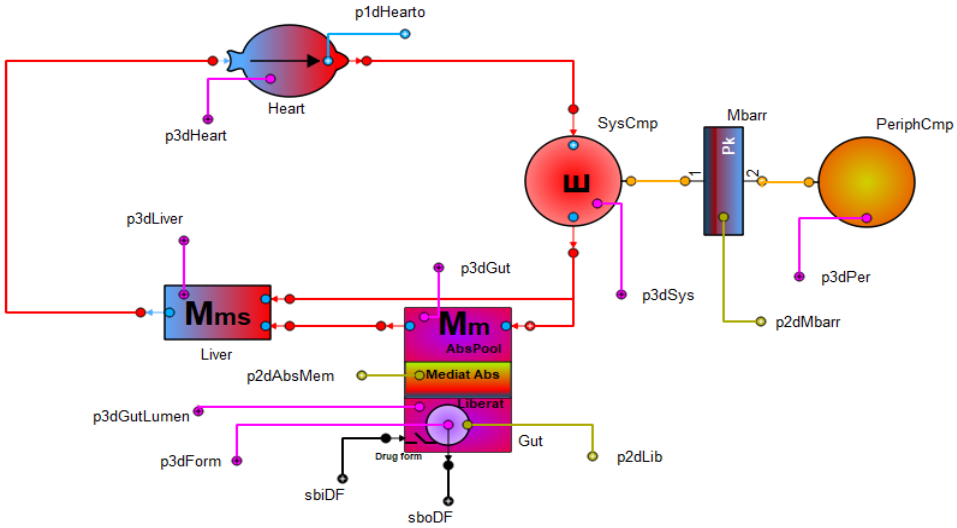

Computer Methods and Programs in Biomedicine, 2020 Jun;189:105322

INTRODUCTION

Physiologically based pharmacokinetic (PBPK) modelling has emerged in the last decade as a valuable tool during model-informed drug discovery and development process, gaining recognition by the main regulatory authorities for drug approval[1]. Briefly, PBPK models are mathematical representations that incorporate drug-related and biological/physiological (system-related) parameters able to simulate the behaviour of a drug over time in tissues and blood. This "bottom-up" approach contains the knowledge of the anatomical characteristics of the body and the mechanisms that are involved[1,2]. This key feature of PBPK models expands the spectrum of modelling and simulation from the early drug discovery to beyond phase III clinical trials[3]. Despite their evolution in last decades, there are still important gaps regarding system-related parameters that need filling in order to generate adequate PBPK models[1,3].

The development of modelling software tools that facilitate the building or use of PBPK models has been a key issue in their emergence and acceptance. Studies that analyse the most common software tools are mainly focused on the modelling features that cope with user and regulatory requirements, like the physiological mechanisms supported, type of mathematical techniques implemented and the ability to address with special populations (paediatrics) and situations (drug-drug interactions)[4]. However, to the best of our knowledge none of the current well-known PBPK software tools is based on the acausal modelling language approach[5]. The main advantage of models based on acausal simulation languages is that mathematical formulation of simulation components is not algorithmic, and therefore output and input variables do not need to be defined at that stage of model definition. In this sense, a simulation component is closer to the physiological entity that tries to describe. Modelica standard defines one of the most known simulation languages based on the acausal paradigm[6], although other proprietary languages exist. This is the case of EcosimPro language (EL)[7].

Semi-mechanistic models have been largely applied to account for the concentration-time course profile of a drug within the body. These types of models are partially empirically based, as their structure is based on the fitting of observed data ("top-down" approach). However, their ability to predict longitudinal pharmacokinetic (PK) data have been questioned as they cannot deal with the complex physiological and pathophysiological processes that may affect the time-course of the drug in the body. In the last years, several semi-mechanistic models[8-12] have evaluated the most sensitive analyte to changes in drug product performance for bioequivalence studies after single or multiple administration schedules, assuming one- or two-compartment PK model, with

pre-systemic metabolism (intestinal and/or liver) and intestinal efflux transporters.

We have developed a PBPK version of the semi-mechanistic model presented in[11] based on the EL acausal simulation language by means of the PhysPK Biosimulation Software (PhysPK). The aims of this work are (i) to assess the predictive reliability of the physiologically based software PhysPK *versus* the well-known population approach software NONMEM for the cited semi-mechanistic PK model, (ii) to determine whether both modelling approaches are interchangeable and (iii) to compare acausal with causal modelling approaches in the framework of semi-mechanistic PK models.

MATERIAL AND METHODS

Pharmacokinetic model

The theoretical description of the PK model presented in this work was previously published elsewhere[11]. In order to reflect complex absorption processes, the model incorporates intestinal transit, dissolution limited by solubility, variable efflux transporter expression along the gut and linear and non-linear metabolism in gut and liver. Table 1 summarizes the value of each parameter of the model. Inter-individual random effects were considered in all PK parameters (CV = 20%).

In order to achieve the aims mentioned above, different approximations to the theoretical model were developed:

- **vNM**: semi-mechanistic version of the theoretical model with extraction-based metabolism of parent drug (PD). Ordinary Differential Equations (ODEs) were implemented in NONMEM[13].
- **vPSEM**: model version with the same mathematical approximation that vNM but implemented in PhysPK. Accordingly, it was based on the same ODEs system that vNM.
- **vPSIM**: semi-mechanistic version of the theoretical model with intrinsic clearance-based metabolism of PD implemented in PhysPK. This model version substitutes extraction based metabolic equations by intrinsic clearance functions. The full mathematical formulation of vPSIM appears at Supplementary Material B, where it can be compared with the mathematical approximation of the vNM (and vPSEM) developed by Mangas-Sanjuan et al.[11].
- **vPPK**: physiologic multilevel version of the theoretical model implemented in PhysPK. vPPK uses an acausal object-oriented modelling approach. This approach is based on two complementary types of

descriptions: multilevel diagrams with relationships among simulation components and mathematical equations of physiological mechanisms. A full definition of vPPK according to this approach appears at Supplementary Material B. The parameterization of vPPK agrees with that of the others model versions (vNM, vPSEM and vPSIM).

Table 1. Population parameters used in simulations.

Parameter	Units	Value
Operative absorption time of passive diffusion (OAT1)	h	7
Operative absorption time of efflux transporter (OAT2)	h	3
Degradation rate constant in intestinal lumen	h^{-1}	0
Dissolution rate coefficient	$h^{-1} \cdot mg^{-1}$	4
Maximum soluble amount	mg	Dose x 0.1
Intrinsic absorption rate constant of the drug	h^{-1}	0.2 2
Primary intestinal intrinsic clearance	L/h	60
Secondary intestinal intrinsic clearance	L/h	6
Primary hepatic intrinsic clearance	L/h	300
Secondary hepatic intrinsic clearance	L/h	30
K_M intestinal efflux transporter	mg	1 10000
K_M intestinal intrinsic clearance	mg/L	1 10000
K_M hepatic intrinsic clearance	mg/L	1 10000
Renal clearance of primary metabolite	L/h	20
Renal clearance of secondary metabolite	L/h	30
Intestinal blood flow	L/h	72
Hepatic blood flow	L/h	18
Gut volume	L	1
Liver volume	L	1
Systemic compartment volume	L	40
Peripheral compartment volume	L	60
Primary metabolite compartment volume	L	40
Secondary metabolite compartment volume	L	40

Study design

Selection of scenarios was based on drug BCS characteristics, efflux, intestinal and hepatic metabolism and dose level. As dissolution was limited by the intrinsic solubility of the drug (10% of the dose administered), only 2 different BCS drugs

were proposed: class II (low solubility, high permeability) and IV (low solubility, low permeability). Both BCS drugs, were analysed at high or low dosing regimens in order to achieve non-linear or linear kinetics of the efflux transporters at the gut wall and/or non-linear or linear gut/liver metabolism. Supplementary Material B contains a detailed description of the conditions. A set of 32 different scenarios were analysed (BCS drug types II and IV, 2 levels of $K_{M,Pgp}$, in 4 metabolic scenarios and 2 dose levels). Each scenario considered 24 healthy volunteers and sample collection for the single dose regimen was stablished at 0.1, 0.2, 0.4, 0.8, 1, 2, 4, 6, 8, 10, 12, 14, 16, 18, 20, 24, and 48 h after oral administration of the drug form. The individual parameters used were obtained from the theoretical model presented above in NONMEM 7.3.

Comparison Strategy

The comparison strategy followed in this analysis is illustrated in Figure 1. First stage involved the validation of PhysPK predictions using a replica model of the vNM implemented in PhysPK as a modelling element constructed with the same ODEs system (vPSEM). In this stage, 32 scenarios at single dose administration regimen were assessed. At second stage, we developed in PhysPK a new version of the theoretical model (vPSIM) which incorporated intrinsic gut and liver clearance functions for PD metabolism in order to evaluate its predictive capacity versus the semi-mechanistic approximation based on extraction ratios (vPSEM) using the 32 scenarios at single dose administration regimen. Last stage concerned the development of a multilevel physiologic version of the theoretical model (vPPK) through an acausal and object-oriented modelling language approach (EL language) with the aim of assessing its predictive capability compared to previous model versions: vPPK *vs* vPSEM and vPPK *vs* vPSIM. Single and multiple dose administration regimen of the 32 scenarios were assessed. A final comparison between classical modelling approaches of models vNM, vPSEM and vPSIM against the multilevel and object-oriented approach of vPPK was performed.

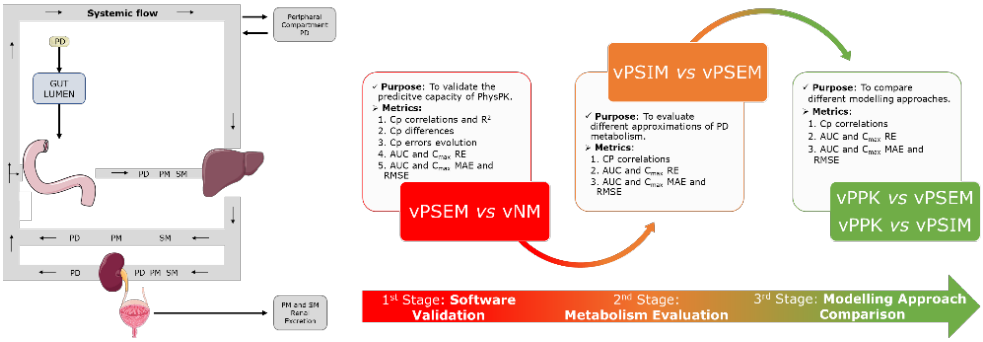

Figure 1. PBPK model (left) and workflow followed in the analysis (right). PD: Parent Drug; PM: Primary Metabolite; SM: Secondary Metabolite; RE: Relative Error; MAE: Mean Absolute Error; RMSE: Root Mean Squared Error; vNM: NONMEM implemented semi-mechanistic version of the theoretical model with extraction-based metabolism of PD; vPSEM: PhysPK implemented semi-mechanistic version of the theoretical model with extraction-based metabolism of PD; vPSIM: PhysPK implemented semi-mechanistic version of the theoretical model with intrinsic clearance-based metabolism of PD; vPPK: physiologic version of the theoretical model developed in PhysPK.

Numerical and graphical evaluation

The workflow included graphical correlation of plasmatic concentrations at each scenario and numerical analysis through the estimation of the Relative Error (RE), Mean Absolute Error (MAE) and Root Mean Squared Error (RMSE) of $AUC_{0\text{-}48}$ (calculated by trapezoidal rule) and C_{max}. Metrics used for data analysis are described as follows:

$$RE = \frac{p_i - a_i}{a_i} \qquad \text{Equation 1,}$$

$$RMSE = \sqrt{\frac{\sum_{i=1}^{n}(p_i - a_i)^2}{n}} \qquad \text{Equation 2}$$

and

$$MAE = \frac{\sum_{i=1}^{n}|p_i - a_i|}{n} \qquad \text{Equation 3,}$$

where p_i is the predicted value, a_i is the reference value and n the number of individuals in each scenario. For graphical and numerical analysis, the 64 bits R software (http://cran.r-project.org, version 3.5.1) was used.

RESULTS

Numerical analysis of RE, MAE and RMSE for all analytes and all comparisons are summarized in Table 2. Individual $AUC_{0\text{-}48}$ and C_{max} for all analytes, scenarios and model versions after single dose administration regimen are presented in Supplementary Material A Figure 1.

Software validation

Correlations of plasma concentration levels of each analyte (PD, PM, and SM) derived from the vPSEM *vs* vNM comparison after single dose administration for each scenario are shown in Figure 2. Graphical analysis demonstrates the ability of PhysPK to simulate almost equivalent concentration levels of PD, irrespective of the scenario considered (Figure 2a). PM and SM levels (Figure 2b) are in good agreement between both software at low-medium concentration values, but small discrepancies were observed in scenarios 10, 12, 14, 16, 26, 28, 30, and 32 at high concentrations (C_{max}). These scenarios are characterized by low k_a values and linear kinetics of P-gp-mediated intestinal efflux process in both dose levels but combine linear and non-linear kinetics for gut and liver metabolism of PD. As low drug permeability and linear kinetics of the efflux transporter are the most restrictive scenarios in terms of drug absorption, small changes in the predicted concentration due to integration errors may dramatically affect the correlation between both software, especially at high concentrations.

Table 2. Numerical analysis for all versions comparison results.

Model Versions Comparison	Parent Drug			Primary Metabolite			Secondary Metabolite		
	Mean RE (%) (Range)	MAE (Range)	RMSE (Range)	Mean RE (Range)	MAE (Range)	RMSE (Range)	Mean RE (Range)	MAE (Range)	RMSE (Range)
Single Dose Administration Regimen									
				AUC_{0-48} (mg·h/L)					
vPSEM *vs* vNM	3.96 (-1.45, 9.61)	$2.41 \cdot 10^{-2}$ ($7.90 \cdot 10^{-4}$, $1.74 \cdot 10^{-1}$)	$3.28 \cdot 10^{-2}$ ($8.63 \cdot 10^{-4}$, $2.77 \cdot 10^{-1}$)	6.61 (0.93, 13.81)	$3.98 \cdot 10^{-1}$ ($3.76 \cdot 10^{-2}$, $9.36 \cdot 10^{-1}$)	$6.26 \cdot 10^{-1}$ ($4.10 \cdot 10^{-2}$, 1.74)	5.81 (0.30, 12.51)	$2.76 \cdot 10^{-2}$ ($2.46 \cdot 10^{-3}$, $7.11 \cdot 10^{-2}$)	$4.02 \cdot 10^{-2}$ ($2.78 \cdot 10^{-3}$, $1.15 \cdot 10^{-1}$)
vPPK *vs* vPSEM	-4.82 (-51.57, 13.72)	$2.97 \cdot 10^{-1}$ ($1.36 \cdot 10^{-6}$, 4.08)	$3.20 \cdot 10^{-1}$ ($1.53 \cdot 10^{-6}$, 4.33)	15.86 (11.30, 26.83)	2.91 ($1.35 \cdot 10^{-1}$, 9.36)	3.51 ($1.67 \cdot 10^{-1}$, 11.22)	11.73 (7.23, 22.27)	$1.71 \cdot 10^{-1}$ ($8.25 \cdot 10^{-3}$, $5.60 \cdot 10^{-1}$)	$2.20 \cdot 10^{-1}$ ($1.02 \cdot 10^{-2}$, $7.22 \cdot 10^{-1}$)
vPSIM *vs* vPSEM	-4.80 (-51.53, 13.72)	$2.97 \cdot 10^{-1}$ ($1.11 \cdot 10^{-6}$, 4.08)	$3.20 \cdot 10^{-1}$ ($1.52 \cdot 10^{-6}$, 4.32)	3.81 (-0.16, 13.64)	$1.49 \cdot 10^{-1}$ ($3.48 \cdot 10^{-5}$, $5.62 \cdot 10^{-1}$)	$2.14 \cdot 10^{-1}$ ($4.15 \cdot 10^{-5}$, $9.37 \cdot 10^{-1}$)	3.85 (-0.21, 13.67)	$1.44 \cdot 10^{-2}$ ($3.99 \cdot 10^{-6}$, $5.17 \cdot 10^{-2}$)	$1.96 \cdot 10^{-2}$ ($4.57 \cdot 10^{-6}$, $7.33 \cdot 10^{-2}$)
vPPK *vs* vPSIM	-0.02 (-0.10, 0)	$3.83 \cdot 10^{-4}$ ($6.28 \cdot 10^{-7}$, $4.39 \cdot 10^{-3}$)	$5.04 \cdot 10^{-4}$ ($7.76 \cdot 10^{-7}$, $5.69 \cdot 10^{-3}$)	11.52 (11.48, 11.55)	2.84 ($1.14 \cdot 10^{-1}$, 9.12)	3.45 ($1.40 \cdot 10^{-4}$, 11.04)	7.52 (7.48, 7.55)	$1.65 \cdot 10^{-4}$ ($6.30 \cdot 10^{-3}$, $5.43 \cdot 10^{-1}$)	$2.13 \cdot 10^{-1}$ ($7.78 \cdot 10^{-3}$, $7.06 \cdot 10^{-1}$)
				C_{max} (mg/L)					
vPSEM *vs* vNM	0.16 (-2.68, 3.79)	$5.76 \cdot 10^{-3}$ ($5.67 \cdot 10^{-5}$, $6.52 \cdot 10^{-2}$)	$8.10 \cdot 10^{-3}$ ($7.57 \cdot 10^{-5}$, $9.53 \cdot 10^{-2}$)	2.92 (0.41, 5.72)	$6.26 \cdot 10^{-2}$ ($1.85 \cdot 10^{-3}$, $2.25 \cdot 10^{-1}$)	$8.12 \cdot 10^{-2}$ ($2.29 \cdot 10^{-3}$, $2.94 \cdot 10^{-1}$	1.53 (-1.16, 4.09)	$4.52 \cdot 10^{-3}$ ($1.42 \cdot 10^{-4}$, $1.83 \cdot 10^{-2}$)	$5.83 \cdot 10^{-3}$ ($1.74 \cdot 10^{-4}$, $2.16 \cdot 10^{-2}$)
vPPK *vs* vPSEM	-5.39 (-52.28, 11.59)	$5.90 \cdot 10^{-2}$ ($1.32 \cdot 10^{-6}$, $8.24 \cdot 10^{-1}$)	$6.58 \cdot 10^{-2}$ ($1.68 \cdot 10^{-6}$, $8.89 \cdot 10^{-1}$)	14.99 (9.68, 23.01)	$4.29 \cdot 10^{-1}$ ($1.42 \cdot 10^{-2}$, 1.48)	$5.11 \cdot 10^{-1}$ ($1.72 \cdot 10^{-2}$, 1.79)	11.42 (6.52, 18.42)	$2.80 \cdot 10^{-2}$ ($9.51 \cdot 10^{-4}$, $9.96 \cdot 10^{-2}$)	$3.45 \cdot 10^{-2}$ ($1.16 \cdot 10^{-3}$, $1.21 \cdot 10^{-1}$)
vPSIM *vs* vPSEM	-5.36 (-52.22, 11.61)	$5.89 \cdot 10^{-2}$ ($1.52 \cdot 10^{-6}$, $8.23 \cdot 10^{-1}$)	$6.57 \cdot 10^{-2}$ ($1.95 \cdot 10^{-6}$, $8.87 \cdot 10^{-1}$)	4.55 (0.01, 11.62)	$6.89 \cdot 10^{-2}$ ($4.46 \cdot 10^{-5}$, $5.55 \cdot 10^{-1}$)	$8.13 \cdot 10^{-2}$ ($5.58 \cdot 10^{-5}$, $6.65 \cdot 10^{-1}$)	4.46 (-0.02, 10.92)	$5.47 \cdot 10^{-3}$ ($2.64 \cdot 10^{-6}$, $4.17 \cdot 10^{-2}$)	$6.80 \cdot 10^{-3}$ ($3.31 \cdot 10^{-6}$, $5.03 \cdot 10^{-2}$)
vPPK *vs* vPSIM	-0.04 (-0.11, -0.01)	$1.42 \cdot 10^{-4}$ ($2.67 \cdot 10^{-7}$, $1.39 \cdot 10^{-3}$)	$2.04 \cdot 10^{-4}$ ($3.44 \cdot 10^{-7}$, $2.18 \cdot 10^{-3}$)	10.01 (9.59, 10.26)	$4.13 \cdot 10^{-1}$ ($1.25 \cdot 10^{-2}$ 1.47)	$4.93 \cdot 10^{-1}$ ($1.51 \cdot 10^{-2}$, 1.75)	6.64 (6.36, 6.80)	$2.60 \cdot 10^{-2}$ ($7.56 \cdot 10^{-4}$, $9.51 \cdot 10^{-2}$)	$3.22 \cdot 10^{-2}$ ($9.08 \cdot 10^{-4}$, $1.19 \cdot 10^{-1}$)
Multiple Doses Administration Regimen									
				AUC_{last} (mg·h/L)					
vPPK *vs* vPSIM	-0.05 (-0.27, 0.03)	$1.23 \cdot 10^{-3}$ ($3.66 \cdot 10^{-6}$, $1.11 \cdot 10^{-2}$)	$1.44 \cdot 10^{-3}$ ($4.26 \cdot 10^{-6}$, $1.41 \cdot 10^{-2}$)	11.47 (11.45, 11.51)	2.85 ($1.09 \cdot 10^{-1}$, 9.23)	3.45 ($1.33 \cdot 10^{-1}$, 11.15)	7.54 (7.52, 7.58)	$1.66 \cdot 10^{-1}$ ($6.07 \cdot 10^{-3}$, $5.49 \cdot 10^{-1}$)	$2.14 \cdot 10^{-1}$ ($7.46 \cdot 10^{-3}$, $7.14 \cdot 10^{-1}$)
				C_{max} (mg/L)					
vPPK *vs* vPSIM	-0.07 (-0.33, 0.03)	$3.11 \cdot 10^{-4}$ ($5.79 \cdot 10^{-7}$, $3.05 \cdot 10^{-3}$)	$3.90 \cdot 10^{-4}$ ($6.81 \cdot 10^{-7}$, $4.23 \cdot 10^{-3}$)	10.34 (10.01, 10.59)	4.39·10^-1 (1.31·10-2, 1.55)	$5.26 \cdot 10^{-1}$ (1.59·10-2, 1.86)	6.73 (6.53, 6.89)	$2.69 \cdot 10^{-2}$ ($7.81 \cdot 10^{-4}$, $9.84 \cdot 10^{-2}$)	$3.35 \cdot 10^{-2}$ ($9.49 \cdot 10^{-4}$, $1.24 \cdot 10^{-1}$)

MAE and RMSE represents the average of this metrics for all scenarios.

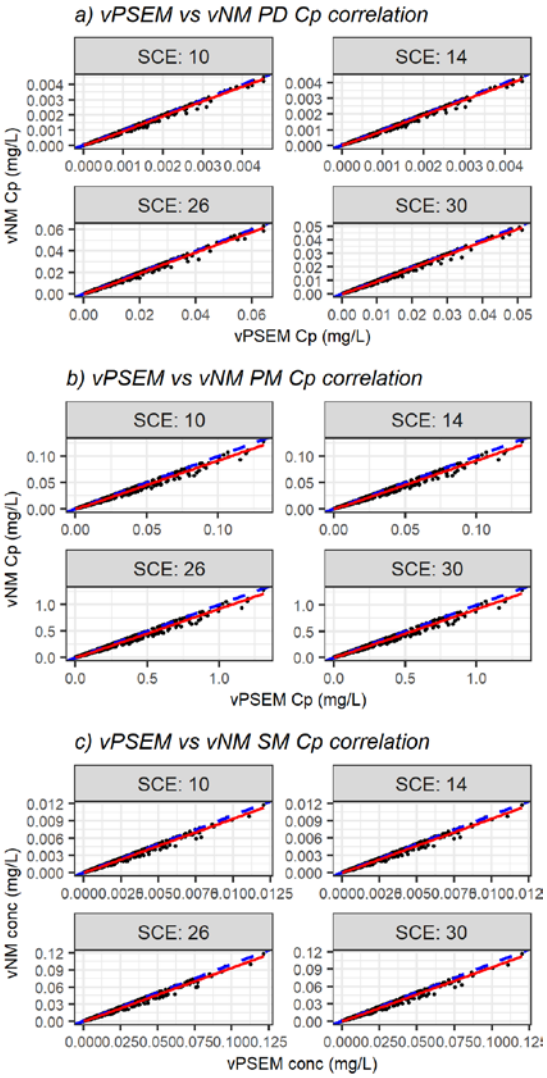

Figure 2. Semi-mechanistic vNM concentration results (y-axis) versus semi-mechanistic vPSEM concentration results (x-axis). a) Parent Drug; b) Primary Metabolite; c) Secondary Metabolite. Blue dashed line represents identity line; red continuous line represents the correlation between both versions.

Mean RE for AUC_{0-48} and C_{max} of vPSEM and vNM comparison were 3.96, 6.61 and 5.81% and 0.16, 2.92 and 1.53% for PD, PM, and SM (Table 2), respectively. Based on the results from Figure 3, good agreement between both approaches can be observed for compounds with high k_a value in terms of AUC_{0-48} for PD, but higher individual RE (>10%) are observed for PM and SM in scenarios 5 and 21, where non-linear kinetics in both gut and liver metabolism are present. For low k_a

compounds, differences in AUC_{0-48} based on individual RE greater than 10 % for PM and SM were predicted in most of scenarios (except scenarios 9, 15, 25, and 31, combining non-linear kinetics for P-gp-mediated intestinal efflux of PD with linear and non-linear kinetics of PD Gut and Liver metabolism). C_{max} individual RE (Figure 3) were within the ±10% threshold for all analytes and scenarios. MAE and RMSE values, as negatively oriented scores (lower the values better the prediction), demonstrate the accuracy of PhysPK in the estimation of C_{max} and AUC_{0-48} (Table 2).

Although the good agreement between vPSEM and vNM (Supplementary Material A Table 1), where vPSEM is a replica of vNM but implemented in PhysPK, supports the validation of PhysPK as a simulation software, the above results do not clarify the underlying reasons for those small numerical differences. This key issue is addressed in discussion section of this paper.

Metabolism Evaluation

AUC_{0-48} and C_{max} individual RE for all analytes in single dose administration regimen scenarios are shown in Figure 4. PD is the most sensitive analyte in this comparison as is expected to change due to differences in equations describing metabolism. In fact, individual RE for both PD AUC_{0-48} and C_{max} reached up to -50% in scenarios 17 and 18, corresponding to non-linear kinetics metabolism of PD in gut and liver. P-gp-mediated intestinal efflux process works under non-linear kinetics in scenario 17 and under linear kinetics in scenario 18, showing here a negligible effect. For scenarios with linear kinetics in P-gp activity and gut and liver metabolism (8, 16, 24 and 32) individual RE for all analytes in both AUC_{0-48} and C_{max} are roughly zero, in contrast with scenarios with non-linear kinetics in all of these processes (1, 9, 17 and 25), where greatest individual RE in all analytes are detected. Scenarios 5, 13, 21 and 29 showed high individual RE in both PK parameters (AUC_{0-48} and C_{max}), which describe linear kinetics in gut metabolism and non-linear kinetics in P-gp activity and liver metabolism. Mean RE for AUC_{0-48} and C_{max} for all scenarios were -4.80, 3.81 and 3.85% and -5.36, 4.55 and 4.46% for PD, PM and SM (Table 2), respectively. Correlations of plasmatic concentrations for PD, PM and SM in this model versions comparison are shown in Figures 2-3 of the Supplementary Material A.

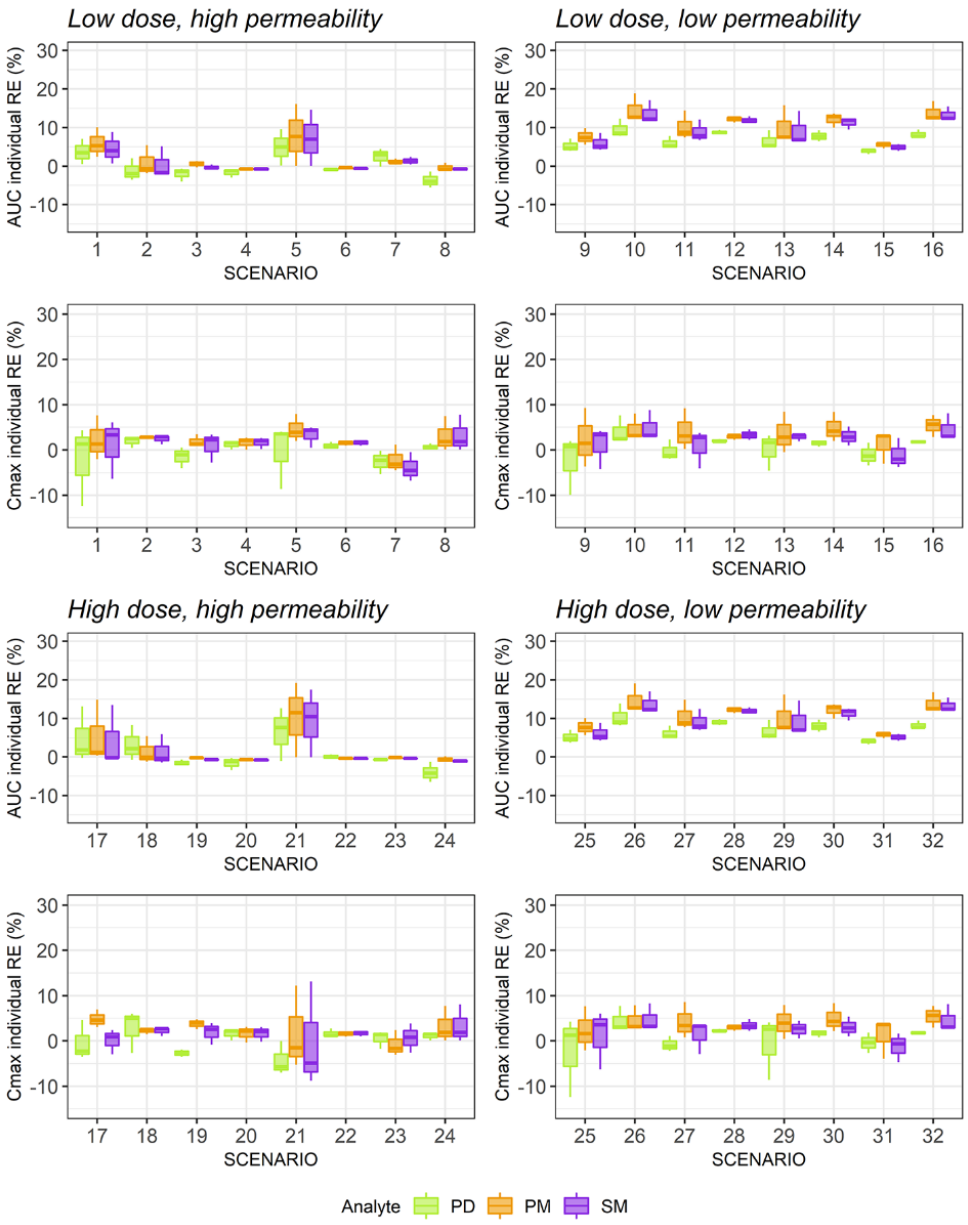

Figure 3. Relative Error for each analyte in each scenario in the estimation of individual $AUC_{0\text{-}48}$ and C_{max} for the semi-mechanistic vPSEM version taking vNM as reference. Boxplots represents 50% of the data including the median (horizontal line) and the range (whiskers).

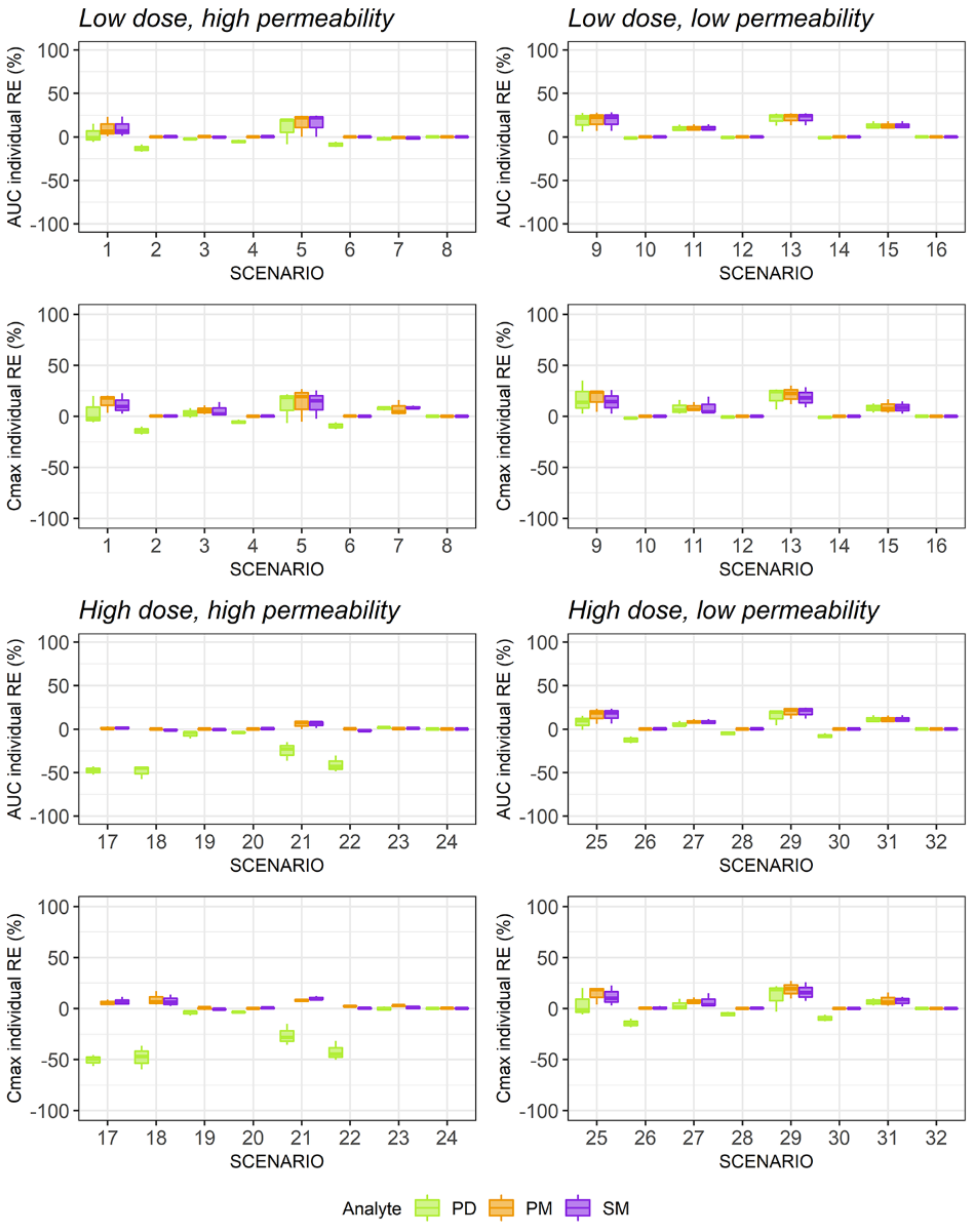

Figure 4. Relative Error for each analyte in each scenario in the estimation of individual $AUC_{0\text{-}48}$ and C_{max} for the semi-mechanistic vPSIM version taking vPSEM one as reference. Boxplots represents 50% of the data including the median (horizontal line) and the range (whiskers).

Modelling Approach Comparison

Figure 5 shows AUC_{0-48} and C_{max} individual RE for PD, PM and SM in the 32 single dose administration regimen scenarios for the multilevel and physiologic (vPPK) *vs* semi-mechanistic (vPSEM) versions comparison, where greater RE (>10%) were obtained in all scenarios for AUC_{0-48} and C_{max} as expected. PD AUC_{0-48} and C_{max} individual RE were roughly identical in all scenarios than those of the vPSEM *vs* vPSIM comparison, with almost equal MAE and RMSE values for PD AUC_{0-48} and C_{max} (Table 2). In fact, mean RE of PD AUC_{0-48} and C_{max} were -4.82 and -5.39%, respectively, in agreement with PD AUC_{0-48} and C_{max} mean RE for the vPSEM *vs* vPSIM comparison (-4.80 and -5.36%, respectively). However, individual RE for both exposure metrics (AUC_{0-48} and C_{max}) of PM and SM were more pronounced in this case, where mean RE of AUC_{0-48} and C_{max} for PM and SM were 15.86 and 11.73%, and 14.99 and 11.42%, respectively. Correlation of plasmatic concentrations for all three analytes is shown in Supplementary Material A Figures 4-5.

Results from comparison between vPPK *vs* vPSIM after single dose administration regimen are shown in Figure 6. Individual AUC_{0-48} and C_{max} successfully matched between vPPK and vPSIM for PD, with mean RE for AUC_{0-48} and C_{max} of -0.02 and -0.04%, respectively. This outcome was independent of the absorption properties, dose level, and P-gp, gut and/or liver metabolic kinetics. MAE and RMSE of PD AUC_{0-48} and C_{max} also improved in this comparison (Table 2) and agreed with the negligible RE detected. Individual RE for AUC_{0-48} and C_{max} of PM and SM were greater than 10 % in some scenarios, with mean RE for PM and SM for AUC_{0-48} and C_{max} of 11.52 and 7.52%, and 10.01 and 6.64%, respectively. However, a significant improvement in the estimation of exposure metrics of metabolites can be observed with this new metabolism approximation compared to the extraction-based metabolism (vPSEM) semi-mechanistic version (Table 2). Correlations of plasmatic concentrations of PD, PM and SM for this model versions comparison are shown in Supplementary Material A Figure 6.

Comparison between vPPK *vs* vPSIM after multiple doses administration regimen in the 32 scenarios are shown in Supplementary Material A Figure 9. PD shows a perfect matching between both modelling approaches, with mean RE of -0.05% for AUC_{0-48} and -0.07% for C_{max}. MAE and RMSE agreed with this observation with values of 10^{-3} and 10^{-4} for AUC_{0-48} and C_{max}, respectively. However, as after single dose administration regimen, AUC_{0-48} and C_{max} mean RE of PM (11.47% and 10.34%) and SM (7.54% and 6.73%), respectively, were higher compared to PD (Supplementary Material A Figures 7 and 8). However, no significant differences were found in MAE and RMSE for both exposure metrics of both metabolites regarding to the single dose administration regimen (Table 2).

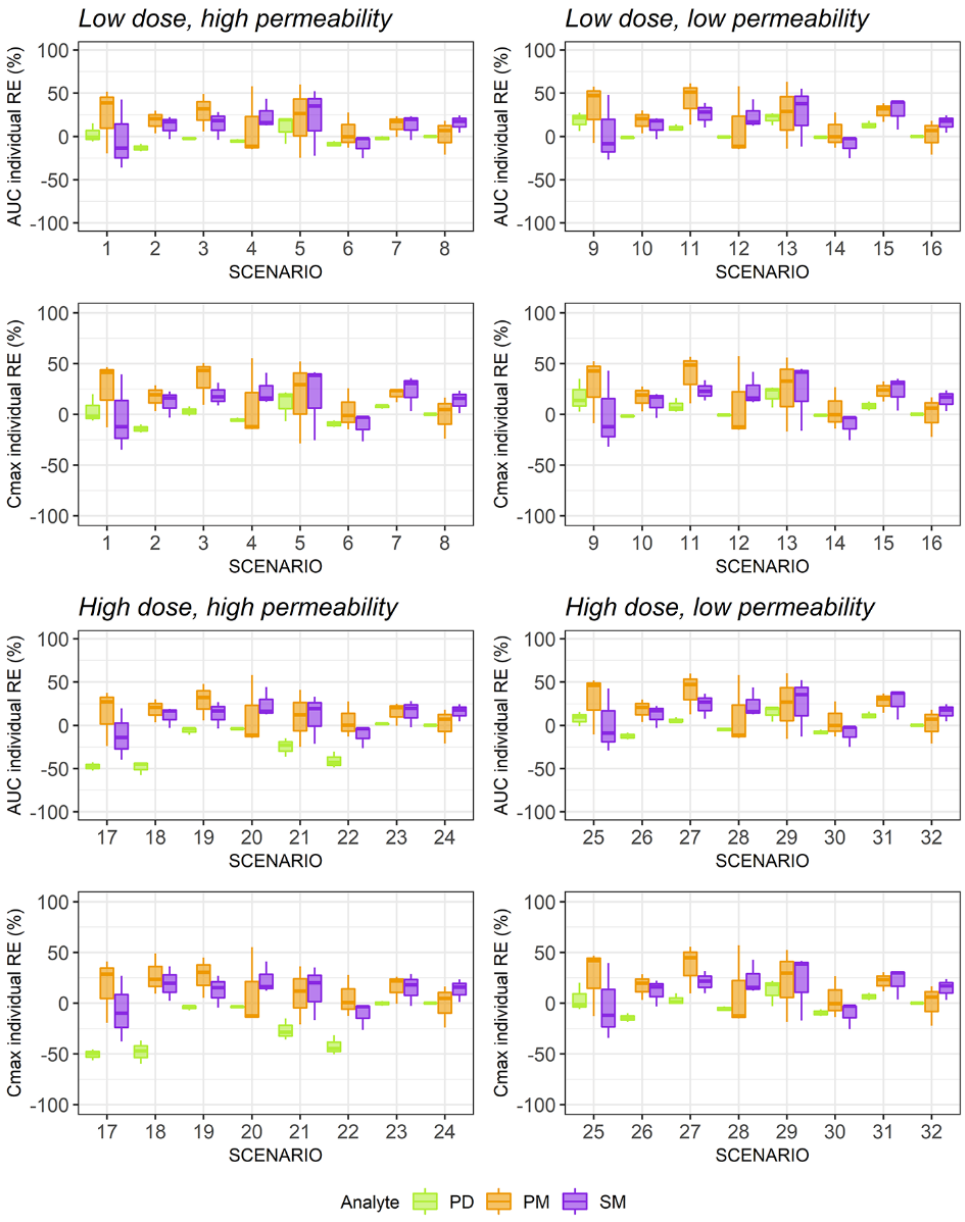

Figure 5. Relative Error for each analyte in each scenario in the estimation of individual $AUC_{0\text{-}48}$ and C_{max} for the physiologic PPK version taking semi-mechanistic PSEM version as reference. Boxplots represents 50% of the data including the median (horizontal line) and the range (whiskers).

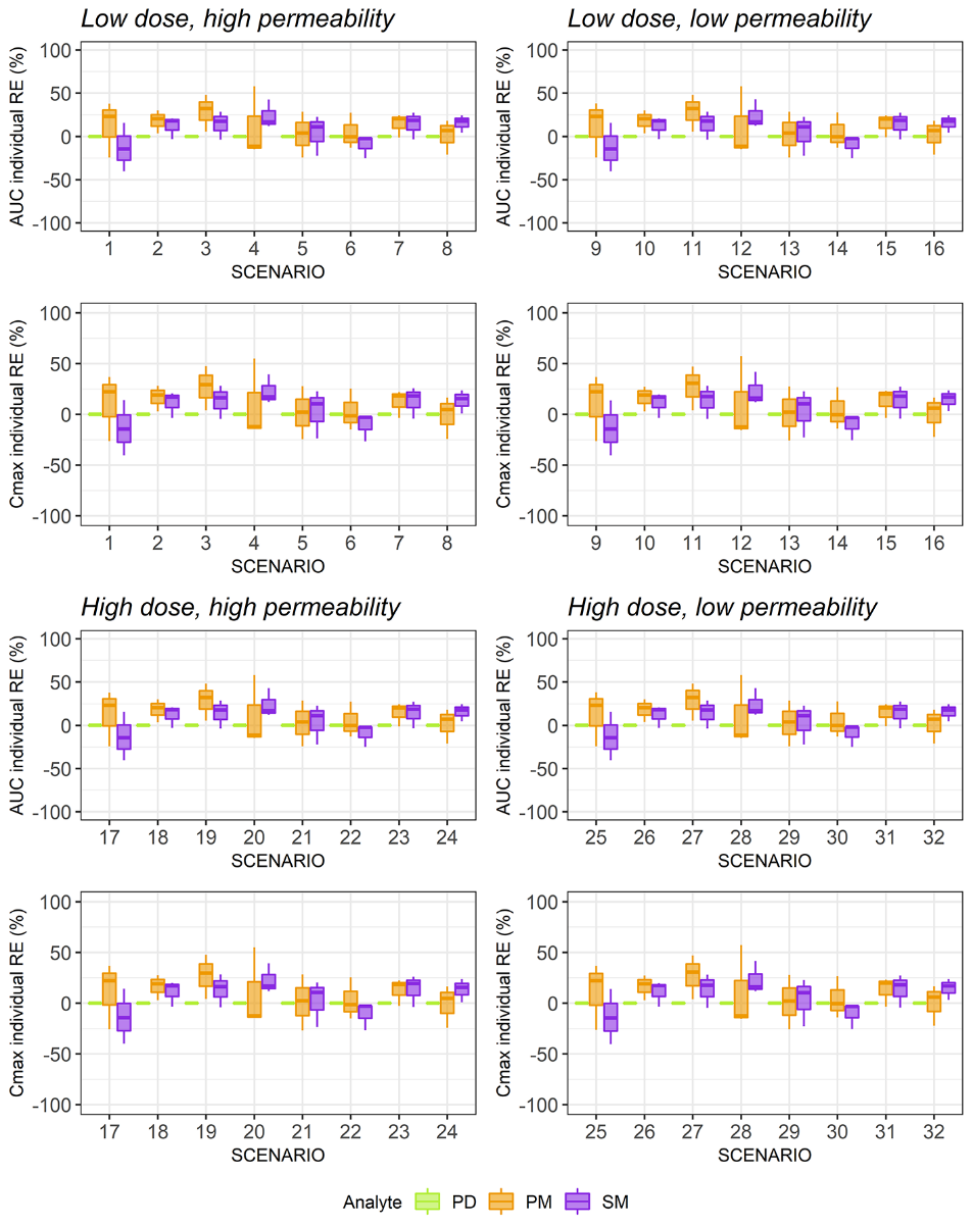

Figure 6. Relative Error for each analyte in each scenario in the estimation of individual $AUC_{0\text{-}48}$ and C_{max} for the physiologic vPPK version taking semi-mechanistic vPSIM version as reference. Boxplots represents 50% of the data including the median (horizontal line) and the range (whiskers).

DISCUSSION

In this work, a semi-mechanistic reference model was used to validate the reliability and accuracy of numerical results obtained using a new biosimulation software (PhysPK). Secondly several mathematical and modelling approaches to the physiological mechanisms were compared using PhysPK. The software validation cases included the parent drug and two metabolites (primary and secondary) after oral administration. The comparisons among mathematical approximations and modelling approaches were conducted with single and multiple dosing regimen.

Software validation

Every case in which all the pharmacokinetic processes (e.g., absorption, intestinal efflux, metabolism, distribution and metabolites excretion) were linear and not saturated (i.e. during the first 5 hours of the simulation), resulted in plasma concentration RE less than 10% (Supplementary Material A Figure 10-12). A relevant feature of numerical errors associated with numerical solutions of dynamic systems is their accumulative character[14]. That is, difference between simulation predictions by vPSEM (PhysPK) and vNM (NONMEM) should increase with time, starting at the softwares' local error precision of 10^{-6} for both simulation software and climbing toward an upper limit of the absolute value of the numerical predictions. The latter is valid because both versions of the theoretical model employ the same ODEs system. As such, differences between simulated results from the NONMEM and PhysPK softwares should only be due to the numerical precision of integrators and solvers. This postulate was confirmed through the computation of absolute differences between plasmatic concentrations of PD, PM and SM from vPSEM versus vNM. Supplementary Material A Figures 13-15 show that, for all analytes and scenarios, the absolute error was lower than 10^{-5} mg/L during the first hour, and that it increased to a maximum value within the range 10^{-3} -10^{-1} mg/L around C_{max} (t_{max}), after which it decreased in agreement with the reduction in concentration values. These results attest to the precision and reliability of PhysPK Biosimulation Software.

Metabolism Evaluation

This stage involved the comparison of two mathematical approximations of the theoretical model that can be selected in the PhysPK software (vPSIM *vs* vPSEM), which only differed from each other in their parametrization of metabolism. The aim was to visualize how the different mathematical approaches for PD metabolism may impact the time-course of analytes, thus providing more than strictly a software validation. As expected, results revealed PD to be the most

sensitive analyte to changes in metabolism. Low permeability drugs (BCS IV class) at both dose levels (scenarios 9-16 and 25-32) show a clear pattern (see Table 3) regarding kinetics of P-gp activity: scenarios with non-linear P-gp kinetics of PD show greater AUC_{0-48} and C_{max} RE for all analytes, with higher values when hepatic metabolism is saturated. On the other hand, scenarios with linear P-gp kinetics show negligible differences in AUC_{0-48} and C_{max}, irrespective of the kinetics of both gut and liver metabolic processes. For high permeability drugs (BCS II class) at both dose levels (scenarios 1-8 and 17-24) this pattern is not so obvious, but a tendency is observed for PM and SM with lower AUC_{0-48} and C_{max} RE than PD. Further, when non-linear hepatic metabolism appears, the greatest AUC_{0-48} and/or C_{max} RE are observed (-50%). The saturation of liver metabolism leads to a reduction in the rate of the metabolic process, increasing the differences in AUC_{0-48} and C_{max} due to the different parametrization between the two approaches (hepatic blood flow).

Modelling Approach Comparison

When comparing vPPK *vs* vPSEM, differences in AUC_{0-48} and C_{max} show an interesting result: vPPK underestimates PK parameters for PD (-4.82 % in AUC_{0-48} and -5.39% in C_{max}), while metabolites are overestimated by approximately 15% for PM and 12% for SM. A detailed revision of vPSEM mathematical approximation (Equations 2,3,5,8 and 9 of Mangas-Sanjuan et al.[11]) showed that PD results are in agreement with the extraction-based metabolism simplification applied in enterocytes and hepatocytes of that model version. Metabolites' differences between the two model versions are due in part to the fact that in vPSEM metabolites are immediately distributed to their compartments once they are formed and independently of the route of formation (gut or liver). In vPPK, on the other hand, metabolites formed in gut passes through the liver before reaching systemic circulation, according to a physiological blood perfusion.

The equivalence of the mathematical approximations in vPSIM and vPPK for PD compound was confirmed by comparing the vPPK *vs* vPSIM mean RE of AUC_{0-48} and C_{max}. Those values diminished dramatically and MAE and RMSE average significantly improved. In the case of metabolites, the existence of differences between vPPK and vPSIM point to the lack of a physiological blood perfusion in vPSIM, since metabolites in the later are immediately distributed to their compartments. This explains the higher mean plasmatic concentrations in vPPK (Supplementary Material A Figures 9 and 10) as they are incorporated into the systemic circulation before being excreted by kidneys, in contrast of what happens in vPSIM where, as mentioned above, they immediately start to be excreted once they are formed.

A numerical comparison between results from vPPK vs vPSEM/vPSIM agrees with expectations, given the mathematical expressions that the respective model versions implement. However, there are important differences in the modelling methodology that underlies their mathematical approximations. Both vPSEM and vPSIM require development of the ODEs that define the temporal variation of each analyte in each compartment. These equations include input and output mass flow rates associated with different types of physiological mechanisms, together with the relationship among the related compartments. Equation B.4 (PD variation in liver) clarifies this concept. Variation of A_3 (PD mass in liver) over time depends on PD concentrations in other compartments (systemic and gut) and liver metabolism.

The mathematical model that underlies the vPPK separates the two types of terms that define the ODEs: local mechanisms and relationships among entities. The relationships among physiological entities are defined by simulation components diagrams (interconnected components networks) from the top description level to the lowest one. These diagrams define the behavior of complex physiological entities. In summary, the modeler does not need to develop the cited ODEs system. The final differential equations system of vPPK is built by the simulation software tool[7]. The vPPK definition can be accessed in the Supplementary Material B and the methodology is referred as multilevel acausal object-oriented modelling approach. The ability to build new physiological models from scratch or from previous models, without the need to develop the entire ODEs system, is an important advantage of the vPPK multilevel and object-oriented methodology over the vPSEM-vPSIM methodology.

The main limitations of the current work are the use of simulated data generated from individual parameters and the lack of a proper comparison using experimental observations. Further studies are encouraged to validate and confirm the conclusion obtained. Additionally, the theoretical model taken into consideration is not directly related to any specific drug, so some scenarios might not be physiologically/biopharmaceutically plausible.

Table 3. Dose level, permeability, gut and liver metabolism and P-gp activity characteristics of the different scenarios studied.

Scenario	Dose level	Permeability	Gut Metabolism	Liver Metabolism	Pgp activity
1	Low	High	Non linear	Non linear	Non linear
2	Low	High	Non linear	Non linear	Linear
3	Low	High	Non linear	Linear	Non linear
4	Low	High	Non linear	Linear	Linear
5	Low	High	Linear	Non linear	Non linear
6	Low	High	Linear	Non linear	Linear
7	Low	High	Linear	Linear	Non linear
8	Low	High	Linear	Linear	Linear
9	Low	Low	Non linear	Non linear	Non linear
10	Low	Low	Non linear	Non linear	Linear
11	Low	Low	Non linear	Linear	Non linear
12	Low	Low	Non linear	Linear	Linear
13	Low	Low	Linear	Non linear	Non linear
14	Low	Low	Linear	Non linear	Linear
15	Low	Low	Linear	Linear	Non linear
16	Low	Low	Linear	Linear	Linear
17	High	High	Non linear	Non linear	Non linear
18	High	High	Non linear	Non linear	Linear
19	High	High	Non linear	Linear	Non linear
20	High	High	Non linear	Linear	Linear
21	High	High	Linear	Non linear	Non linear
22	High	High	Linear	Non linear	Linear
23	High	High	Linear	Linear	Non linear
24	High	High	Linear	Linear	Linear
25	High	Low	Non linear	Non linear	Non linear
26	High	Low	Non linear	Non linear	Linear
27	High	Low	Non linear	Linear	Non linear
28	High	Low	Non linear	Linear	Linear
29	High	Low	Linear	Non linear	Non linear
30	High	Low	Linear	Non linear	Linear
31	High	Low	Linear	Linear	Non linear
32	High	Low	Linear	Linear	Linear

CONCLUSION

Successful validation of PhysPK Biosimulation Software was achieved using NONMEM as the control basis for judging accuracy and precision of the results. Considering that the extraction-based mathematical formulation for saturable

metabolisms used in vPSEM is a simplified version of the mathematical description used in vPSIM, it is recommended that the vPSEM approximation be limited to semi-mechanistic PK studies that deal with BCS class IV drugs in which P-gp-mediated intestinal efflux may be considered linear. Under other conditions, vPSEM's AUC_{0-48} and C_{max} absolute predictions could be inaccurate. Semi-mechanistic models that include intrinsic-clearance metabolism may serve as an adequate approximation of the physiological system only for parent drug. PBPK models with multilevel and acausal object-oriented modelling approaches allow for precise description of the time-course of the drug as they differentiate simulation components from mathematical functions of the biological system.

Declaration of competing interest: Research partly supported by the collaboration agreement (2018) with Empresarios Agrupados Internacional.

Supplementary Materials: Supplementary material associated with this article can be found, in the online version, at doi: 10.1016/j.cmpb.2020.105322.

References

[1] M. Rowland, L.J. Lesko, A. Rostami-Hodjegan, Physiologically Based Pharmacokinetics Is Impacting Drug Development and Regulatory Decision Making, CPT Pharmacometrics Syst Pharmacol, 4 (2015) 313-315.

[2] A.S. Darwich, K. Ogungbenro, A.A. Vinks, J.R. Powell, J.L. Reny, N. Marsousi, Y. Daali, D. Fairman, J. Cook, L.J. Lesko, J.S. McCune, C. Knibbe, S.N. de Wildt, J.S. Leeder, M. Neely, A.F. Zuppa, P. Vicini, L. Aarons, T.N. Johnson, J. Boiani, A. Rostami-Hodjegan, Why has model-informed precision dosing not yet become common clinical reality? lessons from the past and a roadmap for the future, Clin Pharmacol Ther, 101 (2017) 646-656.

[3] M. Jamei, Recent Advances in Development and Application of Physiologically-Based Pharmacokinetic (PBPK) Models: a Transition from Academic Curiosity to Regulatory Acceptance, Curr Pharmacol Rep, 2 (2016) 161-169.

[4] F. Bouzom, K. Ball, N. Perdaems, B. Walther, Physiologically based pharmacokinetic (PBPK) modelling tools: how to fit with our needs?, Biopharm Drug Dispos, 33 (2012) 55-71.

[5] L.P. Roa, M., Simulation Languages, in: M. Akay (Ed.) Wiley Encyclopedia of Biomedical Engineering, John Wiley and Sons, Inc2006, pp. 3186-3198.

[6] Modelica-Association, A Unified Object-Oriented Language for Physical Systems Modeling, Language Specification, ModelicaTM2017.

[7] E.A. Internacional, EcosimPro 6.0 User Manual, 2019.

[8] A. Cuesta-Gragera, C. Navarro-Fontestad, V. Mangas-Sanjuan, I. Gonzalez-Alvarez, A. Garcia-Arieta, I.F. Troconiz, V.G. Casabo, M. Bermejo, Semi-physiologic model validation and bioequivalence trials simulation to select the best analyte for acetylsalicylic acid, Eur J Pharm Sci, 74 (2015) 86-94.

[9] C. Fernandez-Teruel, I. Gonzalez-Alvarez, C. Navarro-Fontestad, A. Garcia-Arieta, M. Bermejo, V.G. Casabo, Computer simulations of bioequivalence trials: selection of design and analyte in BCS drugs with first-pass hepatic metabolism: Part II. Non-linear kinetics, Eur J Pharm Sci, 36 (2009) 147-156.

[10] C. Fernandez-Teruel, R. Nalda Molina, I. Gonzalez-Alvarez, C. Navarro-Fontestad, A. Garcia-Arieta, V.G. Casabo, M. Bermejo, Computer simulations of bioequivalence trials: selection of design and analyte in BCS drugs with first-pass hepatic metabolism: linear kinetics (I), Eur J Pharm Sci, 36 (2009) 137-146.

[11] V. Mangas-Sanjuan, C. Navarro-Fontestad, A. Garcia-Arieta, I.F. Troconiz, M. Bermejo, Computer simulations for bioequivalence trials: Selection of analyte in BCS class II and IV drugs with first-pass metabolism, two metabolic pathways and intestinal efflux transporter, Eur J Pharm Sci, 117 (2018) 193-203.

[12] C. Navarro-Fontestad, I. Gonzalez-Alvarez, C. Fernandez-Teruel, A. Garcia-Arieta, M. Bermejo, V.G. Casabo, Computer simulations for bioequivalence trials: selection of analyte in BCS drugs with first-pass metabolism and two metabolic pathways, Eur J Pharm Sci, 41 (2010) 716-728.

[13] S.L.S. Beal, I.B.; Boeckmann A.; Bauer R.J., NONMEM Users Guides, Icon Development Solutions, Ellicott City, Maryland, USA, 2015.

[14] P.E. Zadunaisky, On the Estimation of Errors Propagated in the Numerical Integration of Ordinary Differential Equations, Numerische Mathematik, 27 (1976).

Chapter 2

Physiologically-based Pharmacokinetic/Pharmacodynamic model of MBQ-167 to predict tumor growth inhibition in mice

Javier Reig-López[1*], María del Mar Maldonado[2*], Matilde Merino-Sanjuan[1,3], Ailed M. Cruz-Collazo[2], Jean F. Ruiz-Calderón[2], Victor Mangas-Sanjuán[1,3¶], Suranganie Dharmawardhane[2¶], Jorge Duconge[4]

Affiliation: [1]Department of Pharmacy and Pharmaceutical Technology and Parasitology, University of Valencia. Valencia, Spain. [2]Department of Biochemistry, University of Puerto Rico Medical Sciences Campus. San Juan, Puerto Rico. [3]Interuniversity Research Institute for Molecular Recognition and Technological Development. Valencia, Spain. [4]School of Pharmacy, University of Puerto Rico Medical Sciences Campus. San Juan, Puerto Rico. *Contributed equally. ¶Author jointly supervised work

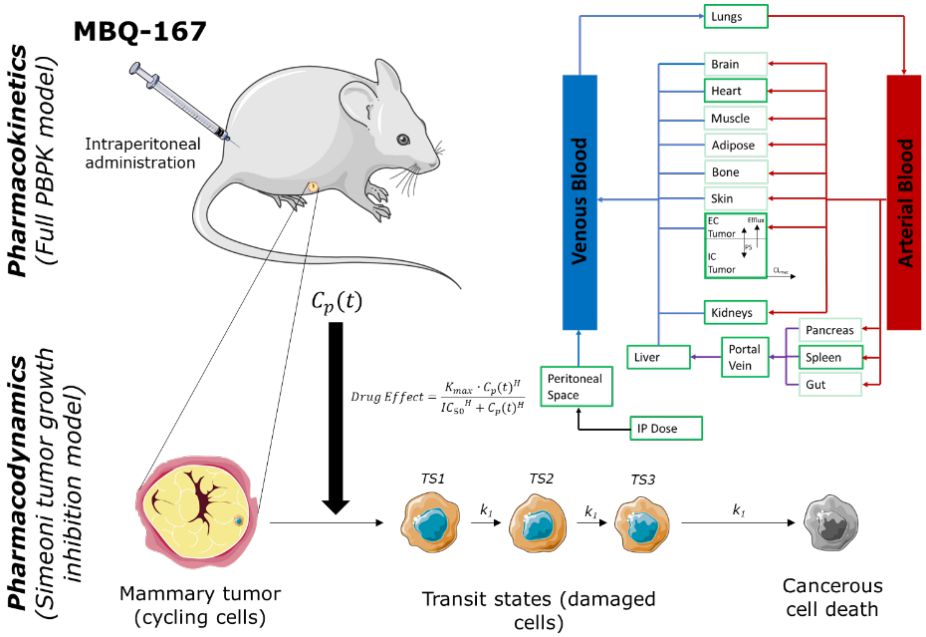

Pharmaceutics, 2020 Oct 15;12(10):975

INTRODUCTION

Drug discovery and development represents an increasing economic and temporal cost for the pharmaceutical industry, which does not translate into significant increases in the number of approved active ingredients, especially in the oncology area.[1,2] One alternative is to develop mathematical models at the preclinical stages of the drug development process capable of better predicting efficacy or safety outcomes in order to efficiently design clinical trials.[3] Physiologically based pharmacokinetic (PBPK) modelling represents a mathematical framework that integrates physicochemical, physiological, and biochemical information to predict the concentration-time course at target tissues for a wide range of exposure conditions in animals or humans. [4] In recent years, the use of PBPK models has clearly improved the model-informed drug discovery and development process of several drugs [5–7], which has facilitated its recognition by the main regulatory agencies (FDA and EMA). [8,9] Currently, the main purposes of PBPK models are to qualitatively and quantitatively predict drug-drug interactions and to support initial dose selection in pediatric and first-in-human trials. [8]

The tumor growth inhibition (TGI) model [10] constitutes a highly valuable preclinical methodology in oncology for the selection of therapeutic candidates and the design of optimal clinical evaluation strategies for the *in vivo* evaluation of anti-tumor effect. [11–16] The Simeoni TGI model has been widely implemented to characterize the pharmacological response of drug candidates in single-agent and combination experiments by linking drug concentration in the target tissue to the inhibition of tumor growth. [17]

The small molecule MBQ-167 is an anticancer therapeutic candidate that inhibits breast cancer metastasis *in vivo* and has been characterized as a potent inhibitor of the Rho GTPases Rac and Cdc42 [18]. These GTPases are overactive in different cancer types [19–23] and promote cancer cell migration, invasion, proliferation, and oncogenic transformation. MBQ-167 dually inhibits the activation of both GTPases, with half-maximal inhibitory concentrations (IC_{50}) of 0.1 μM and 0.08 μM for Rac and Cdc42, respectively. Preclinical studies have shown that MBQ-167 inhibits breast cancer cell migration, viability, tumor growth, and metastasis *in vivo* without apparent toxicity. [18,24] Currently, this compound is being developed for clinical applications as a potential anti-metastatic therapeutic. Nonetheless, further studies are needed to characterize the tumoral pharmacokinetics (PK) of MBQ-167, which is essential to improve therapy efficacy and success rate further. [25]

Therefore, the aims of this work are (i) to develop a PBPK model of MBQ-167 after intraperitoneal (IP) administration in mice, and (ii) to characterize tumor growth dynamics in two human breast cancer cell lines (Her2+ and Triple Negative).

MATERIALS AND METHODS

Materials

MBQ-167 and EHop-0036 (internal standard) were synthesized as previously described [18,26]. Purity (>98%) was verified by thin-layer chromatography (TLC), nuclear magnetic resonance (NMR), and gas chromatography/mass spectrometry. Sodium chloride, ethyl acetate, heptane, acetonitrile, methanol, and all materials required for compound synthesis were also purchased from Sigma-Aldrich (Saint Louis, MO, USA). Formic acid was purchased from Fisher (Fair Lawn, NJ, USA).

Animal protocol

All animal studies were conducted under approved animal protocols (#A8180117, #A8180112) by the University of Puerto Rico Medical Sciences Campus Institutional Animal Care and Use Committee, in accordance with the principles and procedures outlined in the *NIH Guideline for the Care and Use of Laboratory Animals* [27]. Four to five-week-old female BALB/c mice (Charles River Laboratories, Inc. Wilmington, MA) were housed under pathogen-free conditions in HEPA-filtered cages and kept on a 12 h light/dark cycle, and controlled temperature (22-24°C), and humidity (25%). Food and water were given *ad libitum*. MBQ-167 was prepared as a stock solution of 2 mg/mL in cremophor:ethanol:PBS (12.5:12.5:75) solution. Each mouse was administered a single 0.1 mL dose of MBQ-167 (in 12.5% ethanol, 12.5% Cremophor, 75% Phosphate Buffered Saline, pH 7.4) that corresponded to 10 mg/kg body weight (BW) by IP injection.

Tumor pharmacokinetics

Thirty-five BALB/c mice were injected with $2.5 \cdot 10^5$ 4T1 murine metastatic breast cancer cells at the mammary fat pad under isoflurane inhalation (1%–3% in oxygen using an inhalation chamber at 2 L/min) to produce primary tumors, as described [28]. Following IP treatment with a single dose of MBQ-167 (10 mg/kg), five mice/group were sacrificed by cervical dislocation at 0.5, 1, 3, 6, 9,12, and 24 hours. Following sacrifice, tumors were collected and flushed with normal saline, individually wrapped in aluminum foil, snap-frozen in liquid nitrogen, and stored frozen at −80°C until use.

Tumor sample preparation

Tumor samples were extracted by liquid-liquid extraction method, as previously described by [26]. Briefly, frozen tumors were thawed, weighed (100 mg), and

homogenized using the Polytron PT 2100 instrument in pH 7.4 saline (1:4 w/v). Tumor homogenate (100 μL) was then transferred to another tube, and the internal standard EHop-0036 (10 μL from 4,500 ng/mL stock) was added to the samples followed by vortex (30 secs). A hundred microliters (100 μL) of sodium hydroxide 0.5 M were then added to the mixture, and samples were mixed by vortex for 5 minutes. Afterwards, 790 μL of heptane: ethyl acetate mixture (1:1) were added, and samples were vortexed again for 10 minutes. The upper layer was recovered following centrifugation (5 minutes at 510 x g), and the solvent was evaporated for one hour in a Labconco Centrivap console at room temperature. Samples were then reconstituted with 100 μL of methanol, vortexed for ten minutes, and centrifuged at 1000 x g for 1 minute.

Instrumentation

We used a validated bioanalytical method using supercritical fluid chromatography coupled with tandem mass spectrometry to quantify MBQ-167 in tumors and tissues, as previously described [26]. The analysis was performed on an Acquity UPC^2 system (Waters Corp., Milford, MA, USA) coupled to a triple quadrupole tandem mass spectrometer (MS/MS). An Acquity UPC^2 BEH (3.0x100 mm^2, 1.7 μm) column was used for separation purposes.

Her2/Triple-negative tumor growth study

As published elsewhere [18], female athymic nude (nu/nu) mice, 4 to 5 weeks old (Charles River Laboratories, Inc., Wilmington, MA) were maintained under pathogen-free conditions in HEPA-filtered cages (5 mice per cage) under controlled light (12 h light and dark cycle), temperature (22-24°C), and humidity (25%).

Mammary fat pad tumors were established using green fluorescent protein (GFP)-tagged MDA-MB-435 (HER2+) cells in Matrigel (BD Biosciences, San Jose, CA) or GFP-MDA-MB-231 (TNBC) cells by injecting at the fourth right mammary fat pad under isofluorane inhalation (1-3% in oxygen using an inhalation chamber at 2 L/min) to produce orthotopic primary tumors. After tumor establishment (1-week post-inoculation), the animals from the same litter with similar weight and tumor size were randomly divided into experimental treatment groups (n=10 per treatment group).

Mice were treated with vehicle (12.5% ethanol, 12.5% Cremophor (Sigma-Aldrich, St. Louis, MO), and 75% 1X PBS pH 7.4), or 1, 5, or 10 mg/kg BW MBQ-167 by IP injection in a 100 μL volume every other day, three times a week.

Treatments continued until sacrifice at day 65 for the HER2+ tumors and day 108 for the Triple Negative cell line.

Whole body fluorescence image analysis

Mammary tumor growth was quantified as changes in the integrated density of green fluorescent protein (GFP) fluorescence. Mice were imaged one week following breast cancer cell inoculation (on day 1 of treatment administration) and once a week thereafter. The FluorVivo small animal *in vivo* imaging system (INDEC Systems, Inc., Santa Clara, CA) was used for whole body imaging of GFP fluorescence. Tumor fluorescence intensities were analyzed using Image J software (National Institutes of Health, Bethesda, MD). Relative tumor growth was calculated as the integrated density of fluorescence of each tumor on each day of imaging relative to the integrated density of fluorescence of the same tumor on day 1 of treatment administration, relative to vehicle controls.

Physiologically based Pharmacokinetic model

Modelling strategy

The PBPK model of MBQ-167 in mice after IP administration (Figure 1) was developed in Simcyp V19 Animal Simulator. Physicochemical properties and both *in vitro* and *in vivo* ADME data were incorporated into the software for evaluating the drug's exposure and response dynamics. The modelling strategy ("middle-out" approach) is briefly described as follows and fully depicted in **Supplementary Material Figure 1**.

Parameter estimation (PE) was performed using the PE Module of the Simcyp Animal V19 using the Nelder-Mead method, Weighted Least Squares by the reciprocal of Square of Maximum observed value as the objective function and the termination criteria defined as the improvement of less than 1% of the objective function value. Optimization was manually performed to best fit the observed data.

The physiological parameters of the typical mouse were modified to reproduce the mice population used in the experimental procedure. Initial parameter estimation of the fraction unbound in plasma (f_u) and blood-to-plasma (B/P) ratio was performed based on the reported systemic plasma clearance and volume of distribution of MBQ-167 [26], assuming an intravenous bolus injection of 30 seconds, since no IP route of administration is explicitly implemented in Simcyp V19 Animal Simulator. After defining the kinetics of the IP absorption process, systemic plasma clearance was predicted by scaling the intrinsic clearance from

in vitro hepatocytes. Optimization of the tissue-to-plasma partition coefficients (Kp_t) led to improve predictions of the base PBPK model and extrapolate them to other tissues such as the lungs, liver, kidneys, heart, and spleen (advanced PBPK model). Finally, modeling of the tumor disposition provided the final MBQ-167 PBPK model. The key input parameters for the PBPK model of MBQ-167 are summarized in **Table 1**.

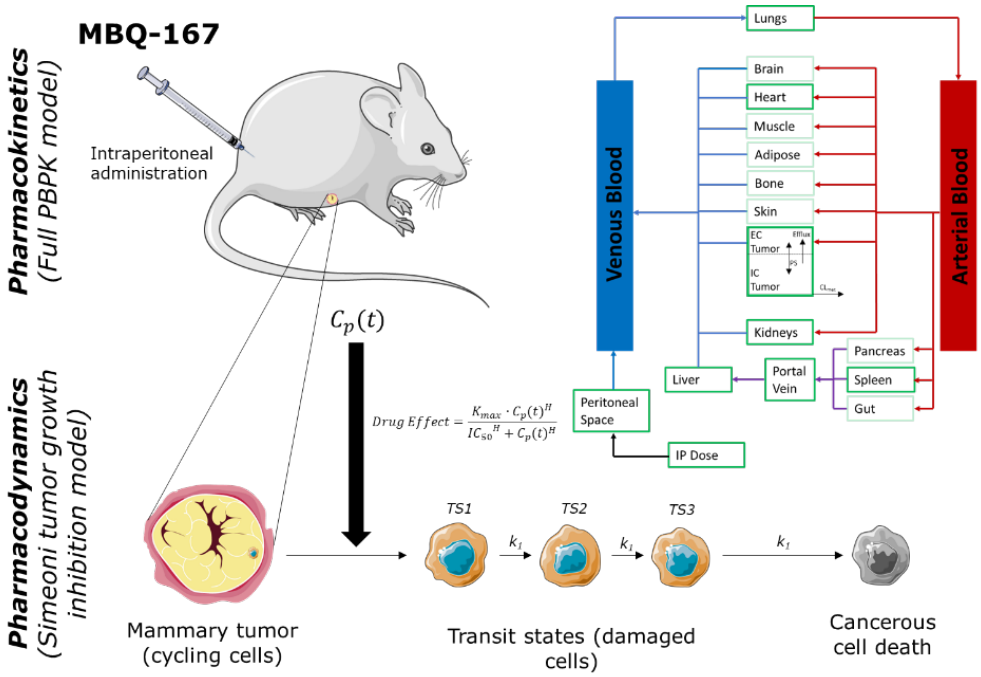

Figure 1. MBQ-167 PBPK-PD model structure. Light green compartments were included in the full PBPK distribution model but not evaluated in the present work. For the Triple Negative cell line, the number of transit compartments for the damaged cell resulted in 4 (see Table 2 for more details).

Physicochemical properties and plasma binding. The molecular weight of MBQ-167 is 338.414 g/mol, and the water partition coefficient ($logP_{octanol:water}$) ratio is 4.944. MBQ-167 is a monoprotic base compound with a pK_a of 0.27. The f_u in plasma was estimated to 0.02. B/P ratio was initially estimated in the base PBPK model development phase and then optimized using local sensitivity analysis (LSA) with a final value of 1.8.

Absorption. Since Simcyp V19 Animal Simulator lacks an explicitly implemented IP route of administration, the IP absorption was described through a first-order process, which included an absorption rate constant (k_a) that regulated the absorption to the venous blood, assuming an IP bioavailability of 100%, avoiding

gut and liver first-pass effect and pre-systemic degradation. In this sense, k_a value was optimized to 3 h^{-1} to characterize maximum plasma concentration (C_{max}) and time to maximum plasma concentration (T_{max}). Lag time (0.17 h) was incorporated to best reproduce the absorption process.

Distribution. Rodger and Rowland's method (method 2) within a full PBPK model distribution was used. Kp_t parameters of the heart, kidney, liver, lungs, and spleen were optimized based on the observed data from each tissue. The final values are provided in **Table 1**. A Kp_t scalar of 0.29 predicted a volume of distribution at steady state (V_{ss}) of 20.21 L/kg, which is in good agreement with that reported in the literature of 400 mL [26] for a mice population of 20 g of body weight.

Elimination. Due to the limited information of any active process in MBQ-167 renal excretion and/or tubular reabsorption, it was assumed that renal excretion was only mediated by glomerular filtration. For this reason, renal clearance (CL_R) was set as the mean basal glomerular filtration rate for mice (12-18 mL/min) [26]. The metabolism of MBQ-167 in the liver includes up to nine metabolites when incubated in liver microsomes, and that inhibits CYP3A4, 2C9, 2C19, and 1A2, but it is unknown through which isoenzyme this metabolism occurs. In this sense, liver metabolism was estimated based on the intrinsic clearance from in vitro hepatocytes (79 μL/min/10^6 cells) and optimizing the incubation unbound fraction of the drug (f_{u_inc}) to best predict the reported systemic plasmatic clearance value (2.15 mL/min).

Tumor disposition. Initial parameter estimation of the passive permeability clearance between intra- and extracellular water (PS) and the intrinsic clearance of an efflux transporter was performed, followed by an optimization of these values to best fit the observed data. Final values were set as 1.2 mL/min/mL tumor volume and 7 mL/min/mL tumor volume for PS and intrinsic clearance of the efflux transporter, respectively. MBQ-167 tumor intrinsic clearance (CL_{tumour}) was implemented to improve exposure predictions with a value of 2.2 mL/min/mL tumor volume. Vascularization was set as 16% of the tumor volume.

Population. Physiological parameters of the typical mouse were modified to reproduce the mice population used in the experimental procedure. In this sense, body weight, tissue volumes, blood flows, cardiac output, and liver and tumor density were adapted to the studied population.

Simulation Trials. Typical mouse predictions were generated, and individual simulations in the fed state were performed after a single MBQ-167 IP dose of 10 mg/kg of body weight for 12 h (plasma and tissues) and 24 h (tumor) duration.

Table 1. Parameters of the PBPK model for MBQ-167.

	Parameter (Units)	Value	Source / Reference / Comments
	Molecular Weight (g/mol)	338.414	
	$logP_{o:w}$	4.944	
	Compound Type	Monoprotic Base	
	pK_a	0.27	
	B/P	1.8	Optimized
	f_u plasma	0.02	Estimated
Distribution Model	Full PBPK		
	V_{ss} (L/kg)	20.21	Simcyp predicted (Method 2)
	Kp_t Heart	1	Optimized
	Kp_t Kidney	13.94	Optimized
	Kp_t Liver	14.66	Optimized
	Kp_t Lung	1.9	Optimized
	Kp_t Spleen	2.1	Optimized
	Kp_t Scalar	0.29	Optimized
Tumor	Permeability Limited Model		
	PS (mL/min/mL tumor volume)	1.2	Optimized
	Efflux transporter (µL/min/mL tumour)	7	Estimated
Elimination			
	Hep intrinsic CL (µL/min/10^6 cells)	79	In vitro determined
	f_{u_inc}	0.07	Optimized
	Typical Renal CL (mL/min)	0.3	Assumed based on maximum glomerular filtration rate for mice. [26]
	Tumour CL (mL/min/mL tumour volume)	2.2	Optimized
Administration Route	Other site		
	Dose (mg)	0.2	
	Condition	Fed	
	Input site	Venous Blood	Optimized
	Input model	First order	Optimized
	Lag time (h)	0.17	Optimized
	f_a	1	
	k_a (h^{-1})	3	Optimized

CL: clearance. **PS:** Passive permeability clearance between intra- and extracellular water. **Hep:** Hepatocytes. **f_{u_inc}:** fraction of unbound drug into the *in vitro* incubation. **k_a:** absorption rate constant. **f_a:** fraction of dose absorbed.

MBQ-167 PBPK model verification

The final MBQ-167 PBPK model was verified through both graphical and numerical analysis. Experimental and predicted longitudinal plasma concentration- (Cp) and tissue concentration- (Ct) profiles were generated, including the 95% Confidence Intervals (95% CI) of the observations at each sampling time and the mean predicted concentrations. LSA was performed to evaluate the relative impact of B/P, f_u, CL_R, $CL_{tumour,}$ and PS in the plasma PK exposure parameters (AUC_{0-t} and C_{max}). The performance of the MBQ-167 PBPK model was assessed by the fold error at each tissue, which referred to the ratio of the predicted AUC_{0-t} or C_{max} to the observed AUC_{0-t} or C_{max}, respectively (**Equation 1**). AUC_{0-t} was calculated by the trapezoidal rule. Both graphical and numerical analyses were performed in RStudio version 1.2.5019 with R version 3.5.1.

$$Fold\ ERROR\ PK\ parameter = \frac{Predicted\ PK\ parameter}{Observed\ PK\ parameter}$$ Equation 1

MBQ-167 tumor growth inhibition model development

An unperturbed and perturbed Simeoni tumour growth models [10] were developed within the Simcyp V19 Animal Simulator for two breast cancer (BC) cell lines, e.g., HER2+ and Triple Negative (**Supplementary Material Figure 1**. *Pharmacodynamics*). First, the parameters governing tumour growth, e.g., exponential growth rate (λ_0), linear growth rate (λ_1), and shape factor (Ψ), were estimated from *in vivo* experiments of tumor growth volume from the control group of HER2+ and Triple Negative cell lines, respectively (unperturbed model). Once characterized tumor growth, the inhibition model was developed. Linear and non-linear response models, as well as total plasma and whole tumor concentration as the input for the drug effect were tested. A parameter estimation including all dose levels (1 and 10 mg/kg for the HER2+ and for the Triple Negative cell lines) was performed to estimate the parameters governing this perturbed model: maximum inhibition (K_{max}), IC_{50} and transit rate of cell damage (k_1). The number of transit compartments was established regarding the promptness appearance of the tumor growth inhibition for each cell line. The initial tumour

volume was theoretically set as 0.1 mL for the HER2+ cell line. In the case of the Triple Negative cell line, initial tumour volume was estimated using MBQ-167 and vehicle-treated mice. Final tumour growth inhibition (TGI) model parameters are shown in **Table 2**.

Table 2. Parameters of the tumour growth (unperturbed and perturbed) model.

Parameter\Cell line	HER2+	Triple-Negative
System Related Parameters		
Tumour growth model	Simeoni	Simeoni
Initial tumour volume (mL)	0.1[c]	0.0384[b]
λ_0 (day^{-1})	0.2[a]	0.0393[b]
λ_1 (g/day)	0.12[a]	0.5457[b]
Ψ	0.7[a]	0.9985[b]
Number of transit compartments	3	4
Drug Related Parameters		
Response Model	E_{max}	E_{max}
Drug input	Total plasma concentration	Total plasma concentration
k_1 (day^{-1})	0.39[a]	0.0007[b]
IC_{50} (μM)	0.0187[b]	0.0001[b]
K_{max} (day^{-1})	0.3683[b]	0.0533[a]
H	0.5[a]	0.5[a]

[a]: optimized to best fit the observed data; [b]: estimated; [c]: assumed; λ_0: exponential growth rate; λ_1: linear growth rate; k_1: transit rate of cell damage; Ψ: shape factor; K_{max}: maximum inhibition; IC_{50}: concentration associated with K_{max}; H: Hill coefficient.

Model evaluation of tumor kinetics was performed by calculating the relative error (RE) (**Equation 2**).

$$RE(\%) = \frac{PRED\ Volume - \overline{OBS\ Volume}}{\overline{OBS\ Volume}} \cdot 100 \qquad \text{Equation 2}$$

RESULTS

MBQ-167 PBPK model

Model predictions after a single IP administration of 10 mg/kg of MBQ-167 are shown in **Figures 2 and 3**, showing that the PBPK model developed is able to capture the longitudinal MBQ-167 observations. C_{max} and T_{max} were adequately characterized in plasma and other organs (heart, lungs, liver, spleen, and kidneys), and slightly under-estimated the C_{max} and over-estimated the T_{max} in tumour tissue.

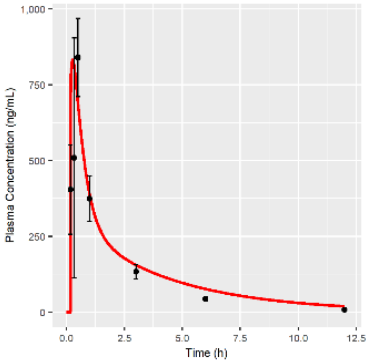

Figure 2. Plasma concentration-time profile after the intraperitoneal single dose administration of 10 mg/kg of MBQ-167 in mice. Red line represents the typical simulated individual. Black dots represent the mean of all observations at the sample time with the corresponding 95% Confidence Interval (vertical lines).

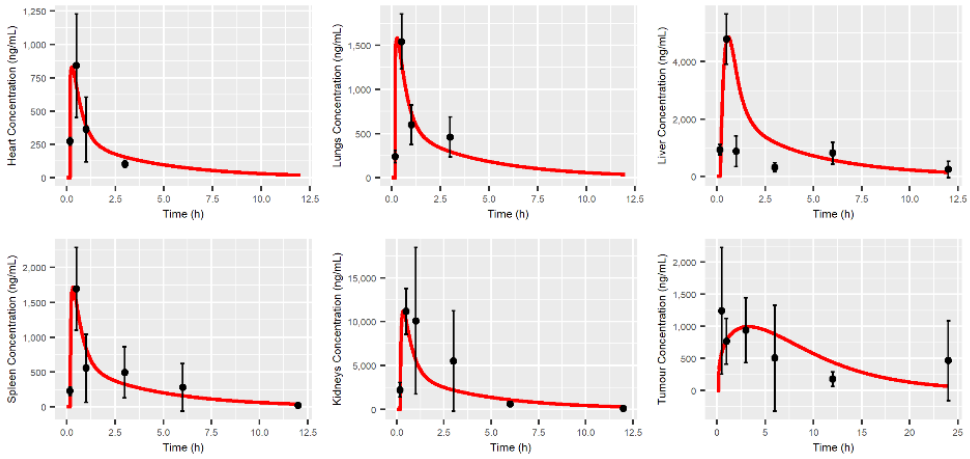

Figure 3. Tissue and tumor concentration-time profiles after the intraperitoneal single dose administration of 10 mg/kg of MBQ-167 in mice. Red line represents the typical simulated individual. Black dots represent the mean of all observations at the sample time with the corresponding 95% Confidence Interval (vertical lines).

These results agree with the numerical analysis (**Table 3**), as the fold error for C_{max} is close to the unity in all tissues except from tumour, where a value of 0.8 arises. AUC_{0-t} fold errors were within the 20% accepted range (0.8-1.2) for heart (1.02), lungs (0.97), spleen (0.81), and tumour (1.12). Liver AUC_{0-t} was slightly over-predicted, with an AUC_{0-t} fold error of 1.36, possibly due to the over-prediction of exposure between 1 and 5 hours after the administration of MBQ-167 (**Figure 3**). In order to balance the deviation caused by the PBPK model in the liver, the predictions in the kidney are under-estimated, leading to an AUC_{0-t}

fold error in kidneys equal to 0.63. However, it must be noted that the simulated typical profile matched the 95% CI of the observations in all sample times (**Figure 3**).

Table 3. AUC_{0-t} and C_{max} values of MBQ-167 with the corresponding fold error after IP single dose administration of 10 mg/kg in mice.

Tissue	AUC_{obs}	AUC_{pred}	AUC_{pred} / AUC_{obs}	$C_{max,obs}$	$C_{max,pred}$	$C_{max,pred}$ / $C_{max,obs}$
Plasma	1417.2	1549.1	1.09	839.9	833.31	0.99
Lung	1887.6	1838.2	0.97	1540.9	1583.3	1.03
Liver	8388.5	11444.3	1.36	4793.7	4865.6	1.01
Spleen	3983.9	3243.5	0.81	1693.4	1718.4	1.01
Kidneys	34279	21527.9	0.63	11160.4	11231.7	1.00
Heart	949.2	965.4	1.02	840.8	831.2	0.99
Tumour	10286.8	11492.8	1.12	1243.6	997.0	0.8

AUC_{0-t} (ng/mL·h); C_{max} (ng/mL). Observed and predicted PK parameters are calculated within the same time interval.

The PBPK model developed predicts a systemic plasma clearance of 2.13 mL/min with a clear dominance of liver metabolism (1.83 mL/min) over renal excretion (0.3 mL/min) of MBQ-167.

MBQ-167 tumour growth inhibition model

Figure 4 shows the PBPK-PD predictions of tumour growth for the HER2+ and Triple Negative cell lines in the absence of MBQ-167 (control group) and treated groups at 1 and 10 mg/kg dose levels. The unperturbed tumour growth models proposed by Simeoni *et al*. [10] (**Figure 4**) are capable of describing tumour growth with no antitumoral activity in both cell lines (control groups).

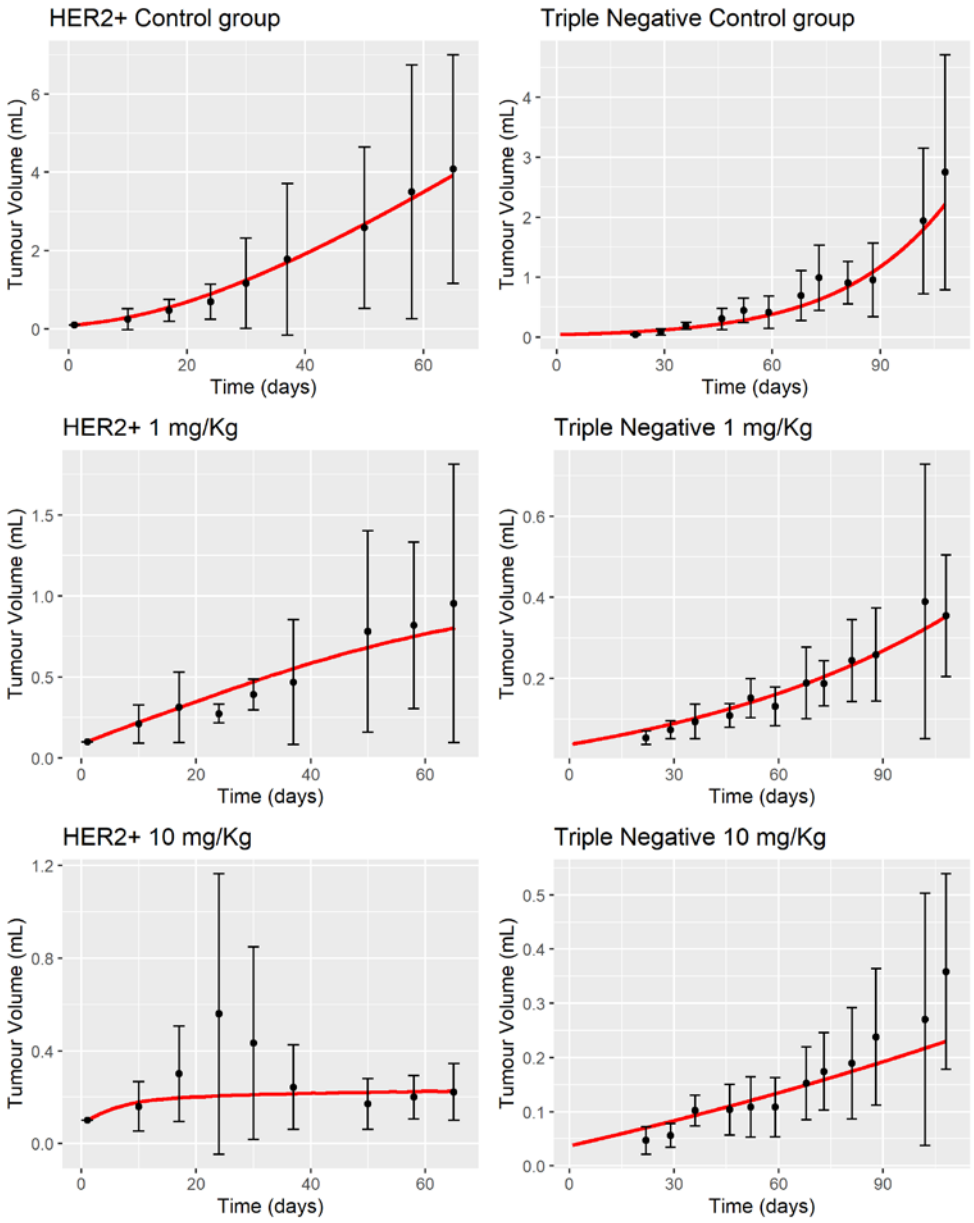

Figure 4. Tumor growth model (perturbed and unperturbed) for the HER2+ and Triple Negative cell lines. Red line represents the typical simulated individual. Black dots represent the mean of all observations at the sample time with the corresponding 95% Confidence Interval (vertical lines).

In addition, **Figure 4** depicts the predicted tumour growth dynamics in HER2+ and Triple Negative cell lines after the administration of MBQ-167 (perturbed model) at 1 and 10 mg/kg BW dose levels, respectively. The TGI models are in good agreement with observed data, with the predicted tumour growth profile within the 95% CI of all observations of the study. **Figure 5** represents the fold-error difference between the mean observed profile and model predictions. Based on the RE, the structural PBPK-PD is able to predict tumor kinetics of the control groups and the 1 mg/kg groups of HER2+ and Triple Negative cell lines, indicating that the mean tendency is adequately captured by the model. However, an under-prediction was observed in the tumor profile of Her2+ cell line at 10 mg/kg between days 10 and 30.

The parameters governing the exponential growth (λ_0) were 0.2 and 0.039 day^{-1}, which shows a more sustained and prolonged growth of the Triple Negative cell line in this phase. However, the zero-order process (λ_1) of Triple-Negative was higher (0.5457 g/day) compared to HER2+ cells (0.12 g/day). Different initial tumor volumes were assumed for the Her2+ cell line (0.1 mL) compared to Triple Negative (0.0384 mL) in order to properly capture the exponential growth in both cell lines. A different number of damaged cell compartments were considered in order to address the delay of death with respect to the drug treatment, assuming progressive damage of tumor cells. The different number of damaged compartments for each cell line has characterized, in a flexible manner, the different death rates of tumor cells for each cell line, allowing to a more sustained- and prolonged tumor growth inhibition in Triple-Negative cell line (n=4).

Different drug effect parameters (k_1 and K_{max}/IC_{50}) were considered for each cell line, showing a higher potency of MBQ-167 in Triple-Negative cells (IC_{50} = 0.0001 μM) compared to Her2+ cell line (IC_{50} = 0.0187 μM). The net effect, which results from the ration between $K_{max}/IC_{50,}$ was higher for the Triple Negative cell line (533 $mL/ng{\cdot}day^{-1}$) compared to the HER2+ cell line (19.7 $mL/ng{\cdot}day^{-1}$).

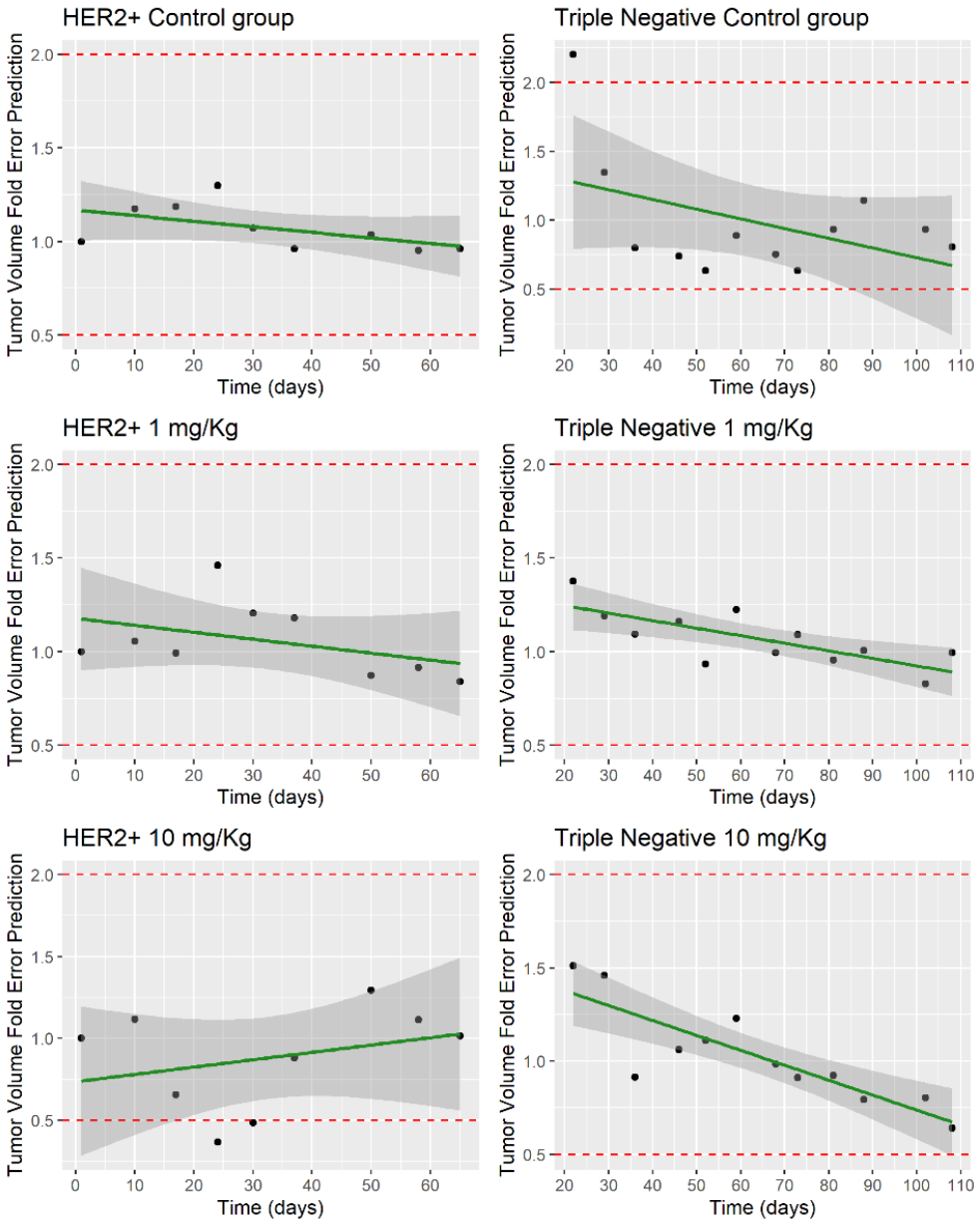

Figure 5. Evaluation of tumor volume predictions in unperturbed and perturbed (1 and 10 mg/kg) groups in Her2+ and Triple Negative cell lines. Red dashed lines represent the validation range (0.5 and 2-fold error). Green solid line represents the linear regression of the data. Black dots represent the fold-error with the mean profile for each group.

DISCUSSION

A PBPK-PD model in mice for the recently developed Rac/Cdc42 inhibitor MBQ-167 has been developed that is able to describe both the pharmacokinetic and pharmacodynamic properties of the drug. The PBPK-PD model properly describes the time course of MBQ-167 in plasma and other tissues (e.g., lungs, heart, liver, kidneys, spleen) and predicts tumor growth inhibition when administered to mice in two BC cell lines, HER2+ and Triple Negative. The model implements the IP administration of MBQ-167, full-body distribution, hepatic metabolism, and renal excretion. Furthermore, the model considers a permeability-limited tumor distribution and implements the Simeoni TGI model to assess the antitumoral effect.

MBQ-167 PBPK model

The developed PBPK framework is capable of adequately describing the time course of MBQ-167 in each of the mouse tissues. The relative error in AUC_{0-t} and C_{max} in each of the tissues is, in general, less than 20% for the typical profile, which shows that the PBPK model is capable of characterizing the average trend of behavior.

The time to reach maximum concentration (T_{max}) through IP route resulted in 0.26 h, showing a rapid absorption that is similar to other reported anticancer small molecules. [29–31] The model was able to fit all observations prior to 6 h, with a little overprediction from this time up to 12 h. Probably, the overprediction in the terminal phase of the Cp-time profile justifies the slight difference between predicted (2.13 mL/min) and observed (2.15 mL/min) systemic plasma clearance. The rapid elimination of MBQ-167 from plasma, with a predicted elimination half-life ($t_{1/2}$) of 2.98 h after IP administration of 10 mg/kg, is consistent with other reports of Rac inhibitors like EHop-016 or EHT1864, with $t_{1/2}$ values of 5.73 h [29] and 1.65 h [32] respectively. Predicted plasma exposition PK parameters AUC_{0-t} and C_{max} were remarkably close to that observed, with fold errors of 1.09 and 0.99, respectively, showing the optimal prediction performance of the model. The predicted V_{ss} (20.21 L/kg) reveals high distribution into peripheral tissues, with little remaining of MBQ-167 in the bloodstream. [26]

Tissue distribution of MBQ-167 was assessed plotting the corresponding concentration-time profiles in the liver, lungs, heart, kidneys, and spleen, verifying their fitting to the 95% CI of the observed values at each sample time and through the computing of the fold error for AUC_{0-t} and C_{max}. The highest concentration of MBQ-167 was found in the kidneys, with a C_{max} value of 11231.7 ng/mL, reflecting the important role of renal uptake and subsequent clearance in

drug disposition [26]. The predicted rank order of tissue drug exposure, determined by both AUC_{0-t} and C_{max} was kidneys > liver > spleen > lung > heart. Tumour concentration was adequately predicted by the model, with AUC_{0-t} and C_{max} fold errors in the desired range, and the predicted typical profile correctly fitting the observed data. However, a slight difference in the tumour disposition process is evident, with a predicted rate of distribution slower than that observed, as is determined by lower and longer C_{max} and T_{max}, respectively.

Regarding the elimination mechanisms, the PBPK-PD model predictions reveal liver metabolism as the major route of elimination, as it represents 86% of overall systemic clearance. However, these results must be handled with care as no additional information is known about renal excretion, and only glomerular filtration of unaltered MBQ-167 has been implemented in the model.

MBQ-167 tumour growth inhibition model

Tumour growth dynamics of two cell lines of breast cancer (HER2+ and Triple Negative) were modelled in the absence (unperturbed) or presence (perturbed) of MBQ-167 using the model proposed by Simeoni *et al*.[10]. There is vast scientific evidence regarding the ability of the model to quantitatively characterize the time-course of tumor dynamics in xenograft experiments and evaluate the efficacy of anticancer drugs early in discovery and development. [15,33–39] The mathematical framework allowed for an adequate prediction of the tumor dynamics under the different groups considered.

The PBPK-PD model is able to successfully predict tumor volume (RE<20%) in the unperturbed group of both cell lines. The TGI model accurately predicts tumor shrinkage (RE<20%) in HER2+ BC cell line after the administration of 1 and 10 mg/kg BW of MBQ-167 three times a week for 65 days in mice, with a relative tumor size reduction of 94.3% at the highest dose level. Model predictions in Triple-Negative cell lines agreed with the experimental data for the 1 mg/kg group, and a slightly under-prediction of final tumor volume was predicted in mice receiving 10 mg/kg three times a week for 108 days. The discrepancy could be explained by the fact that differences in λ_1 could appear between groups, but the overall time-course profile of tumour dynamics of each group is adequately captured by the model since mean predictions are within the 95% CI of the observed data and the predicted relative reduction in the final tumor size (89.6%) agrees with that observed (87.0%) at the 10 mg/kg BW dose level. It has been demonstrated that MBQ-167 reduces mammary fat pad tumor size starting approximately 3 weeks following treatment at a nontoxic concentration of 10 mg/kg BW, and resulting in total inhibition of metastases in mice [18]. These results could serve as an external validation of the PBPK-PD model due to the

accuracy in the prediction of the tumor size reduction, with a negligible difference in the final tumor volumes at the studied concentration of 10 mg/kg.

The use of quantitative structures for the optimal design of dosage regimens is one of the most relevant applications during the drug development process. In the Simeoni model, k_1 and k_2 represent the kinetics of cell death and the proportionality factor linking the plasma concentration to the effect (drug potency), respectively. [10] In this sense, deterministic simulations were performed in order to evaluate the influence of intensive dosing strategies on tumor dynamics (**Figure 6**). The results suggested a significant improvement of tumor reduction when once daily (QD) and/or twice daily (BID) schedules were considered, especially in the Her2+ cell line since tumor eradication is predicted at 1 mg/kg BID and 10 mg/kg BID or QD.

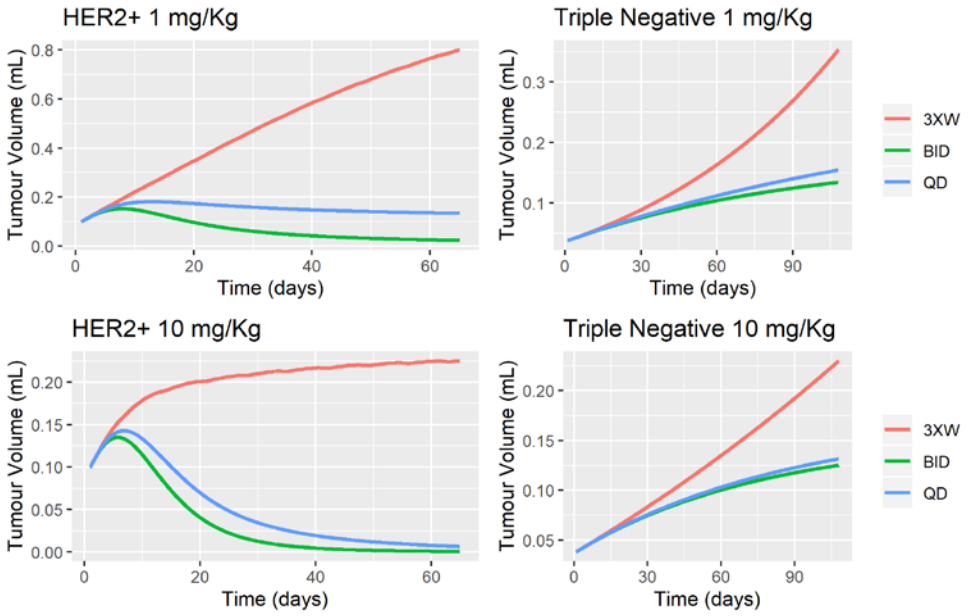

Figure 6. Deterministic simulations to evaluate the impact of intensive dosing strategies on tumor dynamics of HER2+ and Triple Negative cell lines in mice. 3XW: three times per week; BID: twice daily; QD: once daily.

The dose-dependent tumor shrinkage observed in the Her2+ cell line is negligible in the Triple Negative cell line, suggesting that maximal pharmacodynamic response is achieved at 1 mg/kg, but tumor stabilization is observed when BID or QD schedules are considered. The accumulation of MBQ-167 in plasma achieved with BID or QD schedule explains the net greater effect observed in tumor dynamics and the significant improvement in terms of tumor eradication (Her2+)

or tumor stabilization (Triple Negative). In this sense, the current PBPK-PD model allowed to quantitatively characterize system- (λ_0, λ_1, initial tumor volume, and Ψ), which regulate the exponential and linear tumor growth for each cell line, and drug-related (IC_{50}, $K_{max,}$ and k_1) parameters, which helped to guide optimal dosing regimens in future preclinical studies. These analyzes can serve as a basis for experimentally evaluating other dosing strategies that allow characterizing tumor dynamics with greater precision, achieving significant reductions in tumor size in both cell lines.

Among the most relevant limitations of the present work, we highlight the lack of an intravenous group, which would have allowed a more precise characterization of the disposition of MBQ-167. Secondly, the impossibility of characterizing the individual PBPK and PBPK-PD profile and, therefore, the inter-individual random components on the parameters of the model since Simcyp V19 Animal Simulator does not allow a population approximation of the data for mice. Furthermore, due to the study design, it is important to note that the typical PK profile was obtained from independent mice since it was not possible to gather the concentration in the tissues in the same animal over time. This necessarily increases the variability in the data and enhances parameter uncertainty. A major drawback of the current analysis was the inability to link concentrations in the tumor tissue as the driving force of the tumor dynamics and the negligible drug effect observed in the Triple-Negative cell line when 1 or 10 mg/kg dose regimens were considered, which resulted in an $IC_{50} = 10^{-4}$ μM. On the other hand, the current model is limited only to the experimental data available in mice without preclinical information in other animal models. Prospective analyses are encouraged to externally validate predictions of the current PBPK-PD model.

CONCLUSIONS

In summary, we have been able to successfully develop a PBPK-PD model of MBQ-167 in mice that accurately characterizes the pharmacokinetic properties of (i) MBQ-167 in different mouse tissues, (ii) the dynamics of tumor progression, and (iii) the anti-tumor effect of MBQ-167 in HER2+ and Triple Negative breast tumors following intraperitoneal administration. Moreover, the optimal dosing strategy analysis predicted tumor eradication in HER2+ and tumor stabilization in Triple-Negative cell lines when intensive schedules (BID and QD) were selected, despite the higher potency of MBQ-167 in Triple-Negative vs. Her2+ cell line. The findings of this study further support the development of MBQ-167 as a therapeutic for breast cancer treatment.

ACKNOWLEDGEMENTS

Funding: The *in vivo* data was generated with the support of UPR RCM NIH/NIMHHD R25GM061838 (to MdM) and NIH/NIGMS SC3GM084824, Susan Komen for the Cure OGI70023, and Puerto Rico Science, Technology, and Research Trust (PRSTRT) grants (to SD). Dr. Duconge's work is partly funded by grant #U54 MD007600-31 from the National Institute on Minority Health and Health Disparities (NIMHD) at the National Institutes of Health (NIH).

Certara UK (Simcyp Division) granted free access to the Simcyp Simulators through an academic license (subject to conditions).

AUTHOR CONTRIBUTIONS

Participated in research design: Javier Reig-López, Victor Mangas-Sanjuán, Maria del Mar Maldonado, Jorge Duconge, Suranganie Dharmawardhane.

Conducted experiments: Maria del Mar Maldonado, Ailed M. Cruz-Collazo, Jean F. Ruiz-Calderón.

Performed data analysis: Javier Reig-López, Matilde Merino-Sanjuan, Victor Mangas-Sanjuán, Jorge Duconge.

Wrote or contributed to the writing of the manuscript: Javier Reig-López, Maria del Mar Maldonado, Victor Mangas-Sanjuán, Jorge Duconge, Suranganie Dharmawardhane.

CONFLICT OF INTEREST: Authors declare no conflict of interest

REFERENCES

1. Mansinho, A.; Boni, V.; Miguel, M.; Calvo, E. New designs in early clinical drug development. Ann. Oncol. 2019, 30, 1460–1465, doi:10.1093/annonc/mdz191.

2. Moreno, L.; Pearson, A.D.J. How can attrition rates be reduced in cancer drug discovery? Expert Opin. Drug Discov. 2013, 8, 363–368, doi:10.1517/17460441.2013.768984.

3. Zhang, L.; Sinha, V.; Forgue, S.T.; Callies, S.; Ni, L.; Peck, R.; Allerheiligen, S.R.B. Model-Based Drug Development: The Road to Quantitative Pharmacology. J. Pharmacokinet. Pharmacodyn. 2006, 33, 369–393, doi:10.1007/s10928-006-9010-8.

4. Clewell, H.J.; Andersen, M.E. Physiologically-Based Pharmacokinetic Modeling and Bioactivation of Xenobiotics. Toxicol. Ind. Health 1994, 10, 1–24, doi:10.1177/074823379401000101.

5. Hines, R.N.; Simpson, P.M.; McCarver, D.G. Age-Dependent Human Hepatic Carboxylesterase 1 (CES1) and Carboxylesterase 2 (CES2) Postnatal Ontogeny. Drug Metab. Dispos. 2016, 44, 959–966, doi:10.1124/dmd.115.068957.

6. Yoon, M.; Clewell, H.J. Addressing Early Life Sensitivity Using Physiologically Based Pharmacokinetic Modeling and In Vitro to In Vivo Extrapolation. Toxicol. Res. 2016, 32, 15–20, doi:10.5487/TR.2016.32.1.015.

7. Gu, H.; Dutreix, C.; Rebello, S.; Ouatas, T.; Wang, L.; Chun, D.Y.; Einolf, H.J.; He, H. Simultaneous Physiologically Based Pharmacokinetic (PBPK) Modeling of Parent and Active Metabolites to Investigate Complex CYP3A4 Drug-Drug Interaction Potential: A Case Example of Midostaurin. Drug Metab. Dispos. 2018, 46, 109–121, doi:10.1124/dmd.117.078006.

8. European Medicines Agency Guideline on the reporting of physiologically based pharmacokinetic (PBPK) modelling and simulation Available online: https://www.ema.europa.eu/en/documents/scientific-guideline/guideline-reporting-physiologically-based-pharmacokinetic-pbpk-modelling-simulation_en.pdf (accessed on Aug 9, 2020).

9. US Food and Drug Administration Physiologically Based Pharmacokinetic Analyses — Format and Content Guidance for Industry Available online: https://www.fda.gov/media/101469/download (accessed on Aug 9, 2020).

10. Simeoni, M.; Magni, P.; Cammia, C.; De Nicolao, G.; Croci, V.; Pesenti, E.; Germani, M.; Poggesi, I.; Rocchetti, M. Predictive Pharmacokinetic-Pharmacodynamic Modeling of Tumor Growth Kinetics in Xenograft Models after Administration of Anticancer Agents. Cancer Res. 2004, 64, 1094–1101, doi:10.1158/0008-5472.CAN-03-2524.

11. Parra-Guillen, Z.P.; Berraondo, P.; Ribba, B.; Trocóniz, I.F. Modeling Tumor Response after Combined Administration of Different Immune-Stimulatory Agents. J. Pharmacol. Exp. Ther. 2013, 346, 432–442, doi:10.1124/jpet.113.206961.

12. Tate, S.C.; Burke, T.F.; Hartman, D.; Kulanthaivel, P.; Beckmann, R.P.; Cronier, D.M. Optimising the combination dosing strategy of abemaciclib and vemurafenib in BRAF-mutated melanoma xenograft tumours. Br. J. Cancer 2016, 114, 669–679, doi:10.1038/bjc.2016.40.

13. Tate, S.C.; Cai, S.; Ajamie, R.T.; Burke, T.; Beckmann, R.P.; Chan, E.M.; De Dios, A.; Wishart, G.N.; Gelbert, L.M.; Cronier, D.M. Semi-Mechanistic Pharmacokinetic/Pharmacodynamic Modeling of the Antitumor Activity of LY2835219, a New Cyclin-Dependent Kinase 4/6 Inhibitor, in Mice Bearing Human Tumor Xenografts. Clin. Cancer Res. 2014, 20, 3763–3774, doi:10.1158/1078-0432.CCR-13-2846.

14. Terranova, N.; Germani, M.; Del Bene, F.; Magni, P. A predictive pharmacokinetic–pharmacodynamic model of tumor growth kinetics in xenograft mice after administration of anticancer agents given in combination. Cancer Chemother. Pharmacol. 2013, 72, 471–482, doi:10.1007/s00280-013-2208-8.

15. Wang, S.; Zhu, X.; Han, M.; Hao, F.; Lu, W.; Zhou, T. Mechanistic Pharmacokinetic/Pharmacodynamic Model of Sunitinib and Dopamine in MCF-7/Adr Xenografts: Linking Cellular Heterogeneity to Tumour Burden. AAPS J. 2020, 22, 45, doi:10.1208/s12248-020-0428-5.

16. Yang, L.; Yong, L.; Zhu, X.; Feng, Y.; Fu, Y.; Kong, D.; Lu, W.; Zhou, T. Disease progression model of 4T1 metastatic breast cancer. J. Pharmacokinet. Pharmacodyn. 2020, 47, 105–116, doi:10.1007/s10928-020-09673-5.

17. Lestini, G.; Mentré, F.; Magni, P. Optimal Design for Informative Protocols in Xenograft Tumor Growth Inhibition Experiments in Mice. AAPS J. 2016, 18, 1233–1243, doi:10.1208/s12248-016-9924-z.

18. Humphries-Bickley, T.; Castillo-Pichardo, L.; Hernandez-O'Farrill, E.; Borrero-Garcia, L.D.; Forestier-Roman, I.; Gerena, Y.; Blanco, M.; Rivera-Robles, M.J.; Rodriguez-Medina, J.R.; Cubano, LA; et al. Characterization of a Dual Rac/Cdc42 Inhibitor MBQ-167 in Metastatic Cancer. Mol. Cancer Ther. 2017, 16, 805–818, doi:10.1158/1535-7163.MCT-16-0442.

19. Kazanietz, M.G.; Caloca, MJ The Rac GTPase in Cancer: From Old Concepts to New Paradigms. Cancer Res. 2017, 77, 5445–5451, doi:10.1158/0008-5472.CAN-17-1456.

20. Stengel, K.; Zheng, Y. Cdc42 in oncogenic transformation, invasion, and tumorigenesis. Cell Signal. 2011, 23, 1415–1423, doi:10.1016/j.jacc.2007.01.076.White.

21. Maldonado, M. del M.; Dharmawardhane, S. Targeting Rac and Cdc42 GTPases in Cancer. Cancer Res. 2018, 78, 3101 LP – 3111, doi:10.1158/0008-5472.CAN-18-0619.

22. Porter, A.P.; Papaioannou, A.; Malliri, A. Deregulation of Rho GTPases in cancer. Small GTPases 2016, 7, 123–138, doi:10.1080/21541248.2016.1173767.

23. De, P.; Aske, JC; Dey, N. RAC1 Takes the Lead in Solid Tumors. Cells 2019, 8, doi:10.3390/cells8050382.

24. Rivera-Robles, M.J.; Medina-Velazquez, J.; Asencio-Torres, G.M.; Gonzalez-Crespo, S.; Rymond, B.C.; Rodriguez-Medina, J.; Dharmawardhane, S. Targeting Cdc42 with the anticancer compound MBQ-167 inhibits cell polarity and growth in the budding yeast S. cerevisiae. Small GTPases 2018, 1–11, doi:10.1080/21541248.2018.1495008.

25. Al-abd, A.M.; Aljehani, Z.K.; Gazzaz, R.W.; Fakhri, SH; Jabbad, A.H.; Alahdal, A.M.; Torchilin, V.P. Pharmacokinetic strategies to improve drug penetration and entrapment within solid tumors. J. Control. Release 2015, doi:10.1016/j.jconrel.2015.08.055.

26. Maldonado, M. del M.; Rosado-González, G.; Bloom, J.; Duconge, J.; Ruiz-Calderón, J.F.; Hernández-O'Farrill, E.; Vlaar, C.; Rodríguez-Orengo, J.F.; Dharmawardhane, S. Pharmacokinetics of the Rac/Cdc42 Inhibitor MBQ-167 in Mice by Supercritical Fluid Chromatography-Tandem Mass Spectrometry. ACS Omega 2019, 4, 17981–17989, doi:10.1021/acsomega.9b01641.

27. The National Research Council Commitee for the Update of the Guide for the Care and Use of Laboratory Animals Guide for the Care and Use of Laboratory Animals; 8th ed.; National Academies Press: Washington DC, 2011; Vol. 46; ISBN 9780309154000.

28. Castillo-Pichardo, L.; Humphries-Bickley, T.; De La Parra, C.; Forestier-Roman, I.; Martinez-Ferrer, M.; Hernandez, E.; Vlaar, C.; Ferrer-Acosta, Y.; Washington, A. V.; Cubano, LA; et al. The Rac inhibitor EHop-016 inhibits mammary tumor growth and metastasis in a nude mouse model. Transl. Oncol. 2014, 7, 546–555, doi:10.1016/j.tranon.2014.07.004.

29. Humphries-Bickley, T.; Castillo-Pichardo, L.; Corujo-Carro, F.; Duconge, J.; Hernandez-O'Farrill, E.; Vlaar, C.; Rodriguez-Orengo, J.F.; Cubano, L.; Dharmawardhane, S. Pharmacokinetics of Rac inhibitor EHop-016 in mice by ultra-performance liquid chromatography tandem mass spectrometry. J. Chromatogr. B Anal. Technol. Biomed. Life Sci. 2015, 981–982, 19–26, doi:10.1016/j.jchromb.2014.12.021.

30. Jin, Y.; Li, J.; Rong, L.F.; Lü, XW; Huang, Y.; Xu, S.Y. Pharmacokinetics and tissue distribution of 5-fluorouracil encapsulated by galactosylceramide liposomes in mice. Acta Pharmacol. Sin. 2005, 26, 250–256, doi:10.1111/j.1745-7254.2005.00530.x.

31. Center for Drug Evaluation and Research. Pharmacology Review(s). Application Number: 22-059;

32. Hampsch, R.A.; Shee, K.; Bates, D.; Lewis, L.D.; Désiré, L.; Leblond, B.; Demidenko, E.; Stefan, K.; Huang, Y.H.; Miller, T.W. Therapeutic sensitivity to Rac GTPase inhibition requires consequential suppression of mTORC1, AKT, and MEK signaling in breast cancer. Oncotarget 2017, 8, 21806–21817, doi:10.18632/oncotarget.15586.

33. Schneider, B.K.; Boyer, A.; Ciccolini, J.; Barlesi, F.; Wang, K.; Benzekry, S.; Mochel, J.P. Optimal Scheduling of Bevacizumab and Pemetrexed/Cisplatin Dosing in Non-Small Cell Lung Cancer. CPT Pharmacometrics Syst. Pharmacol. 2019, 8, 577–586, doi:10.1002/psp4.12415.

34. Kobuchi, S.; Shimizu, R.; Ito, Y. Semi-Mechanism-Based Pharmacokinetic-Toxicodynamic Model of Oxaliplatin-Induced Acute and Chronic Neuropathy. Pharmaceutics 2020, 12, 125, doi:10.3390/pharmaceutics12020125.

35. Ma, Y.; Wang, S.; Ren, Y.; Li, J.; Guo, T.; Lu, W.; Zhou, T. Antitumor effect of axitinib combined with dopamine and PK-PD modeling in the treatment of human breast cancer xenograft. Acta Pharmacol. Sin. 2019, 40, 243–256, doi:10.1038/s41401-018-0006-x.

36. Li, J.; Chen, R.; Yao, Q.-Y.; Liu, S.-J.; Tian, X.-Y.; Hao, C.-Y.; Lu, W.; Zhou, T.-Y. Time-dependent pharmacokinetics of dexamethasone and its efficacy in human breast cancer xenograft mice: a semi-mechanism-based pharmacokinetic/pharmacodynamic model. Acta Pharmacol. Sin. 2018, 39, 472–481, doi:10.1038/aps.2017.153.

37. Ortega, J.L.; Cabanillas, F.; Rivera, N.; Tirado-Gomez, M.; Hallman, D.; Pardo, W.I.; Bruno, M. Results of Upfront Therapy for Marginal Zone Lymphoma. Clin. Lymphoma. Myeloma Leuk. 2017, 17, 879–883, doi:10.1016/j.clml.2017.09.014.

38. Yates, J.W.T.; Holt, S. V.; Logie, A.; Payne, K.; Woods, K.; Wilkinson, R.W.; Davies, B.R.; Guichard, S.M. A pharmacokinetic-pharmacodynamic model predicting tumour growth inhibition after intermittent administration with the mTOR kinase inhibitor AZD8055. Br. J. Pharmacol. 2017, 174, 2652–2661, doi:10.1111/bph.13886.

39. Hao, F.; Wang, S.; Zhu, X.; Xue, J.; Li, J.; Wang, L.; Li, J.; Lu, W.; Zhou, T. Pharmacokinetic-Pharmacodynamic Modeling of the Anti-Tumor Effect of Sunitinib Combined with Dopamine in the Human Non-Small Cell Lung Cancer Xenograft. Pharm. Res. 2017, 34, 408–418, doi:10.1007/s11095-016-2071-5.

Chapter 3

Current evidence, challenges, and opportunities of physiologically based pharmacokinetic models of atorvastatin for decision-making

Javier Reig-López[1], Alfredo García-Arieta[2], Víctor Mangas-Sanjuán[1,3], Matilde Merino-Sanjuan[1,3]

Affiliation: [1]Department of Pharmacy and Pharmaceutical Technology and Parasitology, University of Valencia. Valencia, Spain. [2]División de Farmacología y Evaluación Clínica, Departamento de Medicamentos de Uso Humano, Agencia Española de Medicamentos y Productos Sanitarios, Calle Campezo 1, Edificio 8, Madrid, 28022, Spain. [3]Interuniversity Research Institute for Molecular Recognition and Technological Development. Valencia, Spain.

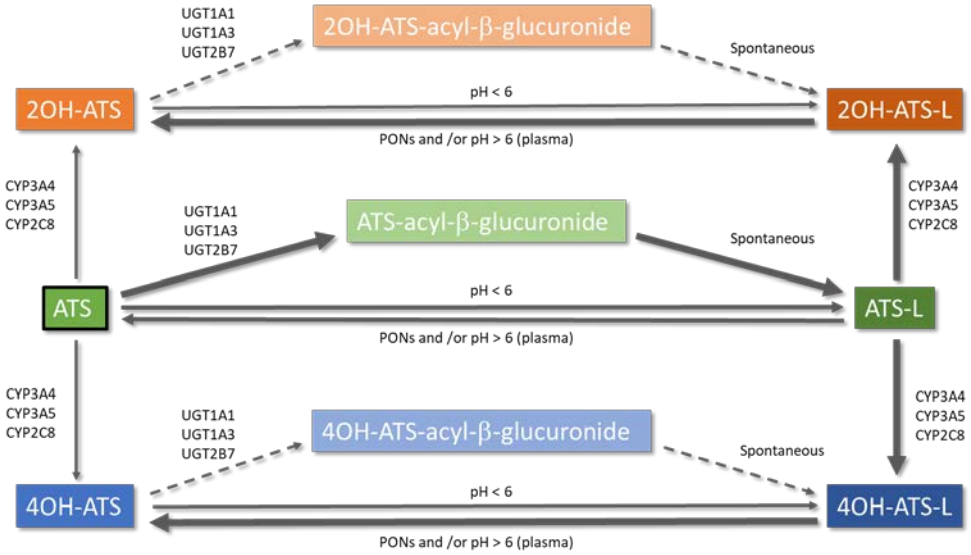

Pharmaceutics. 2021 May 13;13(5):709

INTRODUCTION

Statins are the first line treatment/treatment of choice/gold-standard in the pharmacological management of hypercholesterolemia [1] and they have been positioned as the most effective oral drugs for the treatment and prevention of cardiovascular diseases associated to dyslipidemia [2,3]. Statins are reversible inhibitors of the 3-hydroxy-3-methyl-glutharyl-coenzyme A (HMG-CoA) reductase, the enzyme responsible of de novo cholesterol biosynthesis. Statins can be administered in the active form (atorvastatin, fluvastatin, pitavastatin, pravastatin and rosuvastatin) or as inactive drugs (simvastatin and lovastatin), which require activation within the organism. Statins are, in general, safe and well tolerated [4,5]. In terms of safety concerns, the most frequent adverse events are myopathies (5-10%) [6], ranging from muscle pain to very rare cases of fatal rhabdomyolysis [7], and hepatotoxicity, which is present in 1 % of treated patients and resolves spontaneously after withdrawal of the drug [5].

Among the statins, atorvastatin (ATS) is one of the most prescribed [8] statin worldwide for the treatment of hypercholesterolemia in order to diminish the cardiovascular risk [9]. ATS is a second-generation synthetic statin that is administered as the calcium salt of the active hydroxy-acid form, although some generics have been developed with the magnesium salt to avoid the patent protection of the calcium salt. According to the desired reduction in low-density lipoprotein cholesterol (LDLc) levels, the clinical posology involves the use of 10-80 mg once daily at any time of the day. Despite of its wide, cost-effective use and pharmacological response, several factors undermine the clinical response of statins in the treatment of hypercholesterolemia, involving low adherence of patients, inadequate selection of the active ingredient, polymorphisms, adverse events (myopathies), drug-drug interactions (DDIs), etc. The use of model-based strategies able to properly characterize the time-course of the active entities are encouraged in order to optimize the dosing strategy in patients. Physiologically based pharmacokinetic (PBPK) modelling has emerged as a solid tool in the decision-making process during drug development, which has gained regulatory recognition in the last years [10,11]. The main applications of PBPK models range from drug-drug interactions (DDI), transporter evaluation, food-drug interactions, intrinsic factors evaluation, and extrapolation of drug exposure in special sub-groups of patients. Therefore, the aims of this review are (i) to summarize the physicochemical and pharmacokinetic (PK) characteristics involved in the time-course of ATS, and (ii) to evaluate the major highlights and limitations of the PBPK models of ATS published so far.

PHYSICOCHEMICAL PROPERTIES

Solubility

ATS (546 g/mol, pK_a 4.46) belongs to the class II of the Biopharmaceutical Classification System (BCS) due to its low solubility in the gastro-intestinal fluid, which contributes to its low bioavailability (12%) [12-14]. ATS solubility in deionized water is reported to be 0.0206 mg/mL at 37 °C [14]. A tri-hydrated calcium salt form of ATS (ATS-Ca) is included in the commercially available tablets of ATS. ATS-Ca has been isolated in amorphous and crystalline forms, but it is commercialized in its crystalline form due to the higher stability. ATS-Ca solubility increases with pH, being insoluble in acidic aqueous solutions of pH < 4 [15]. Solubility values in aqueous media for the amorphous and crystalline forms at 37 °C are 0.11-0.12 mg/mL in water, 0.01 mg/mL in HCl 0.1 N and 0.72 and 0.70 mg/mL in sodium phosphate 0.05 M pH 7.4, respectively [16]. Great efforts have been performed to improve ATS oral bioavailability trough formulation strategies to increase the solubility and/or dissolution rate of ATS-Ca such as micronization by antisolvent precipitation [15], microcapsulation [17], co-grinding techniques [18], co-amorphous formulations with nicotinamide [19], dry emulsions [13], inclusion complexes [20] and use of drug resinates [21]. Since ATS is administered mainly as the calcium salt, low solubility in the gastrointestinal (GI) tract should be considered in order to assess its PK characteristics.

Lipophilicity

Chemical structure of ATS (and of statins in general) can be divided into three parts: 1) the analogue of the target enzyme substrate (3-hydroxy-3-methyl-glutaril coenzyme A or HMG-CoA), 2) a complex hydrophobic ring structure covalently linked to the substrate analogue, and 3) side groups on the rings that define the solubility and PK properties [1]. While the analogue of the HMG-CoA (the mevalonate-like pharmacophore) is responsible for the reversible inhibition of the HMG-CoA reductase, the ring structure and its substituents lead to differences in lipophilicity, absorption properties, plasma protein binding and elimination [22]. Lipophilicity of ATS is determined by its logP of 4.1 [22] and its logD at pH 7.4 (1.52) [3].

ABSORPTION

A rapid oral absorption is expected after ATS administration, since the median T_{max} is reported to be 1 h, with a range of 0.5-3 h [3]. The oral fraction absorbed of ATS is 30% between 10-80 mg and its oral bioavailability is known to be low

(12%) [22-25] and dose-independent. Therefore, dissolution and pre-systemic metabolism (gut wall and liver first pass effect) are the key relevant processes affecting ATS bioavailability. The rate and extent of ATS absorption are influenced by the time of administration [26] and the presence of food [23]. A study with 16 healthy volunteers revealed that ATS maximum plasma concentration (C_{max}) and area under the plasma concentration-time curve (AUC) diminished by 47.9% and 12.7%, respectively, when a 80 mg dose was administered with food [27]. This reduction in ATS exposure has also been reported at the lowest dose level (10 mg) [28]. In this sense, the administration of ATS with food decreases its bioavailability by 13% [22,23]. Despite the administration of ATS in the evening is associated to a lower exposure compared when it is dosed in the morning (with mean C_{max} and AUC values 31% and 57% lower, respectively) and a food effect has been determined, no difference in the clinical response is observed [26,28]. For this reason, ATS can be administered at any time of the day and without regard to food. Gender is another covariate influencing ATS exposure, but it lacks of any clinical relevance, despite the 10% lower AUC and 20% higher C_{max} in females compared to males [12].

The intestinal absorption of ATS is a complex process as the net transport of this drug through the gut wall involves multiple mechanisms, being not only restricted to passive diffusion. *In vitro* experiments in Caco-2 cell monolayers revealed an apparent permeability (P_{app}) in the basolateral-to-apical direction 7-fold higher than in the apical-to-basolateral direction, showing the role of P-glycoprotein (P-gp) efflux (K_m and J_{max} values of 115±19 μM and 141±11 pmol/cm^2/min, respectively [29]). The interaction of ATS and P-gp has also been demonstrated in Madin-Darby canine kidney cells (MDCK) expressing human P-gp [30]. In this cell line, the efflux ratio after correcting with parental MDCKII cells resulted in 4.46 for ATS acid, suggesting ATS acid as a moderate substrate of P-gp. Moreover, monocarboxylic acid co-transporter (MCT) has been identified as a relevant transporter in the ATS absorption from the gut lumen with a K_m value in the mM range. As clinically relevant maximal concentrations in the intestinal lumen are estimated to be within the 70-550 μM range after doses of 10 to 80 mg [3], ATS MCT-mediated absorption may be a linear process at this concentrations, which is consistent with the proportional increase in the extent (AUC) of ATS absorption in the 10 to 80 mg dose range.

DISTRIBUTION

The passive membrane permeability of statins increases along with their lipophilicity and, consequently, lipophilic statins are distributed into peripheral

tissues [31]. ATS has a volume of distribution of 5.4 L/kg [24] and exhibits high degree of plasma protein binding (>98 %) [32]. Statins accumulation in the liver is mediated by hepatic uptake through the organic anion transporting polypeptide (OATP) family, sodium-dependent taurocholate co-transporting polypeptide (NTCP), and by efflux transporters of the ATP-binding cassette (ABC) family, located on the basolateral and canalicular membranes of the liver, respectively [33]. *In vitro* kinetic studies on ATS hepatic uptake revealed that OATP1B1 and OATP1B3 were the major ATS uptake transporters, while NTCP was found to be of minor importance in ATS disposition. The average contribution to ATS uptake resulted OATP1B1 > OATP1B3 >> OATP2B1 > NTCP and their respective K_m (μM) and V_{max} (pmol/min/mg protein) values are 0.77, 0.73, 2.84 and 185 and 6.61, 2.29, 24.27 and 2260, respectively [34]. An ATS intrinsic uptake clearance of 2030 mL/min (95% CI: 1140-2620 mL/min) was predicted and, assuming the same passive diffusion across the cell membrane of hepatocytes and HEK293 cells (120 μL/min/g of liver), transporter-mediated active uptake of ATS dominates overall ATS hepatic uptake [34]. Moreover, polymorphisms in transporters genes have been reported to affect the PK of statins and their therapeutic effects [35,36]. It has been demonstrated that liver-to-plasma concentration ratio of ATS is 2.7-fold higher (p = 0.002) in wild-type when compared to *Slco1b2-/-* mice after 1 mg/kg ATS tail vein injection [33]. In humans, it has been observed that ATS and its metabolites are sensitive to polymorphisms in *SLCO1B1*, as plasma concentrations were higher in subjects carrying the reduced function *SLCO1B1* 521C allele (T/C genotype) compared with the wild-type subjects (521 T/T) [37]. Another example comes from a fixed-order crossover study in 660 Finnish healthy volunteers [35], which concluded that individuals carrying the *ABCG2* c.421C>A single-nucleotide polymorphism (SNP) had a 72% higher ATS $AUC_{0\text{-}inf}$ than individuals with the c.421CC genotype (p = 0.049), suggesting that the *ABCG2* polymorphisms affect the PK of ATS. As the elimination half-life was not influenced by *ABCG2* polymorphism, it allowed the authors to conclude that ABCG2 influences mostly during the absorption phase, enhancing ATS absorption and bioavailability [35].

METABOLISM

Metabolism of ATS is an intricated pathway of different reactions that include glucuronidation [7,8,38], lactonization [39], and cytochrome P450-mediated oxidation [40,41]. A simplified scheme with the different metabolic pathways of ATS is depicted in Figure 1. ATS is administered as the hydroxy acid form (calcium salt) and its active metabolites (*ortho*-hydroxy atorvastatin (2OH-ATS) and *para*-hydroxy atorvastatin (4OH-ATS)) are equipotent to the parent compound, being

responsible of 70% of the HMG-CoA reductase inhibitory activity of ATS [42]. The *in vitro* HMG-CoA reductase inhibitory activity (IC_{50}) values for ATS, 2OH-ATS and 4OH-ATS are 3.71, 5.54 and 3.29 nM, respectively [43]. Both metabolites, as the parent compound, are equilibrated with the corresponding lactone forms (ATS-L, 2OH-ATS-L and 4OH-ATS-L) [38,39,41]. It has been demonstrated that lactonization might occur non-enzymatically at pH<6 [44] or enzymatically, being the former pathway negligible at pH>6. The formation of an acyl-glucuronide prior to lactonization is expected to be the major pathway for the enzymatic lactonization of ATS in humans, which is catalyzed by UDP-glucuronosyltransferases (UGTs) UGT1A1, UGT1A3 and UGT2B7. The isoenzyme UGT1A3 is the major contributor to this process with 200 times more activity than UGT2B7 [7]. The mechanism proposed for the lactonization is the formation of an acyl-β-D-glucuronide conjugate of the ATS acid (parent), elimination of the glucuronic moiety and final spontaneous cyclization to the corresponding lactone [38]. ATS glucuronidation, and thus lactonization, follows a non-linear kinetics with K_m and V_{max} values of 4 and 20 μM and 2280 and 120 pmol/min/mg for UGT1A3 and UGT2B7, respectively [7]. ATS lactonization is affected by polymorphisms in the *UGT1A* locus and has been demonstrated both, *in vitro* and *in vivo* in healthy volunteers [8]. On the other hand, the hydrolysis of the lactone forms of ATS and its metabolites to the corresponding carboxylates takes place non-enzymatically at pH>6 [44] or can be catalyzed by plasmatic esterases or paraoxonases (PONs) [38]. PONs are a family of esterase/lactonase enzymes whose encoding genes are located in tandem in the long arm of human chromosome 7 (7q 21-22) [45], being PON1, PON2 and PON3 highly involved in ATS metabolism. In addition, ATS increases the expression of PON2 [46]. A 3.8-fold higher ATS-L hydrolysis rate through PON1 and PON3 has been demonstrated *in vitro* when compared to spontaneous hydrolysis in a pooled microsomal fraction [47]. Additionally, results from incubation experiments in human liver microsomes (HLM) show a median ATS formation rate through hydrolysis of the corresponding lactone of 309.70 pmol/min/mg protein [47]. Hydrolysis of lactone forms has been demonstrated to occur in plasma [48]. Therefore, this process must be considered when modelling ATS and its metabolites to better assess its pharmacokinetics.

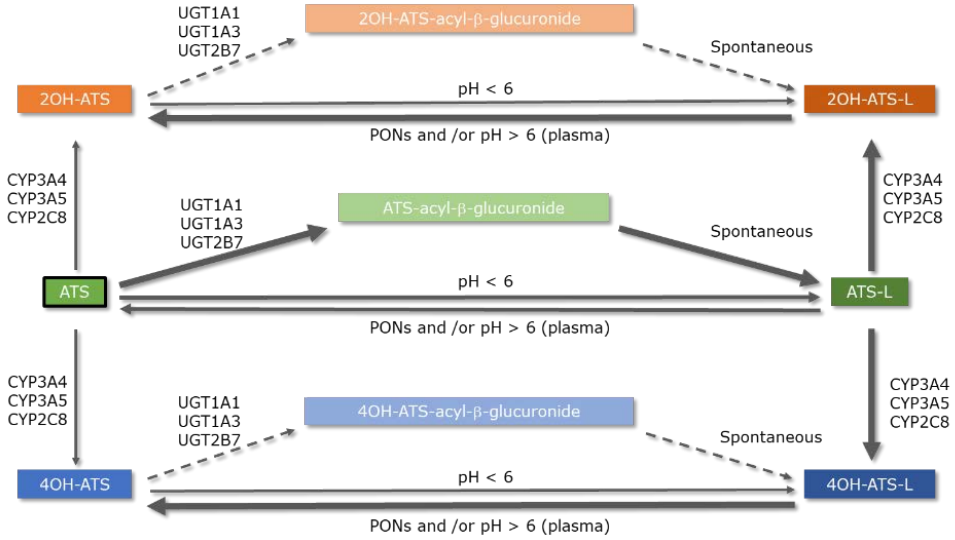

Figure 1: Metabolic pathways of atorvastatin. Arrows' thickness informs directly about the relevance of the reaction and the sense of the equilibrium. Dashed arrows represent a theoretically possible lactonization of 2OH-ATS and 4OH-ATS via an acyl-β-glucuronide. ATS: atorvastatin open acid form; ATS-L: atorvastatin lactone form.

Cytochrome P450-mediated oxidative metabolism has been described as a major pathway of biotransformation for statins in humans [38], where CYP3A4 is the major enzyme involved in the formation of the two hydroxy-metabolites of ATS [39,41]. The CYP3A4-mediated oxidation is clearly polarized to the lactone forms, with K_m and V_{max} values of 3.9 and 1.4 μM, and 4235 and 14312 pmol/min/mg for the *ortho*- and *para*- hydroxylated metabolites, respectively [39]. Differences in K_m and V_{max} values between the acid and lactone form of ATS result in an intrinsic clearance ratio lactone/acid equal to 73 [40] and in an specific metabolite clearance ratio for ortho-hydroxylation and para-hydroxylation of 20.2 and 83.1, respectively [39]. Quantum mechanics/molecular mechanics (QM/MM) have revealed that the acid form of ATS must pay a desolvation penalty of 5 Kcal/mol to enter in the more hydrophobic active site of the enzyme [39]. Moreover, the higher V_{max} value for the para-hydroxylation of ATS-L has been attributed to a shorter distance to the heme oxygen atom of the CYP3A4 [39]. Inhibition studies have demonstrated that ATS-L could be an inhibitor of the metabolism of the acid form [39]. It could be concluded that ATS lactonization change its affinity to the CYP3A, affect the preferred hydroxylation positions and may be responsible for DDIs at this level.

EXCRETION

Mass balance studies with [^{14}C]-ATS have revealed the biliary route as the major route of elimination of ATS and its metabolites, with a minor contribution of the renal excretion (1-2%) to the overall elimination of the drug [3,22]. In fact, renal impairment has no significant effect on the PK parameters of ATS [42], which helps the management of complex dyslipidemia in hypercholesterolemic hemodialysis patients, since no dose adjustment is required [49]. It has been demonstrated that ATS can be reabsorbed from the bile, thus suggesting biliary recycling as an important component in ATS metabolism and excretion and may contribute to the prolonged duration of ATS effect [43].

The involvement of P-gp in the absorption of ATS has been demonstrated *in vivo* due to the influence of polymorphisms in *ABCB1* genotypes [50]. However, the activity of P-gp affects the PK during the elimination phase more than in the absorption phase, as AUC and half-life ($t_{1/2}$) show greater differences ($p<0.05$), rather than C_{max} values, between genotypes [50]. These results suggest that P-gp affects the enterohepatic circulation of ATS.

PHYSIOLOGYCALLY BASED PHARMACOKINETIC MODELS OF ATORVASTATIN

The PK characteristics of ATS have led to the development of PBPK models that can better explain the complexity of each of the LADME processes of this drug. The PBPK models of ATS published until now are described below.

Zhang. 2015

This is the first PBPK model of ATS that assess not only the parent drug, but also the two main metabolites of the open acid form, ATS-L and 2OH-ATS [51]. This model is intended to evaluate DDIs between ATS and its metabolites at multiple scenarios (e.g., concomitant administration of enzyme inhibitors or inducers such as itraconazole, clarithromycin, cimetidine, rifampicin and phenytoin). The PBPK model incorporates the Advanced Dissolution, Absorption and Metabolism (ADAM) model to characterize the absorption process and a full PBPK distribution model for predicting volume of distribution at steady state (V_{ss}) and tissue-to-plasma partition coefficients ($K_{p,t}$). The intestinal efflux process is implemented using *in vitro* determined maximum rate of transporter-mediated efflux (J_{max}) and K_m of P-gp. The elimination of the open acid form occurs minimally through renal excretion (CL_R = 0.47 L/h), being the metabolic pathway the most important for ATS clearance. Enzymatic processes are mediated by CYP3A4 (*ortho*- and *para*-

hydroxylation) and CYP2C8 (*para*-hydroxylation) processes and glucuronidation reactions mediated by UGT1A1 and UGT1A3. It must be noted that, ATS hydroxylation by CYP3A4 incorporated *ortho*- and *para*-hydroxylation and the resulting metabolite for the *ortho*-hydroxylation was its active metabolite (2OH-ATS). However, an important issue here raises as the *in vitro* assays of ATS metabolism reveal lactonization as the critical first step in ATS disposition and suggest that ATS-hydroxylated metabolites would be mostly formed after hydrolysis of the corresponding lactone products (2OH-ATS-L and 4OH-ATS-L) due to the higher affinity of the lactone form of ATS for the active site of CYP450 isoforms [39]. In this sense, the ATS *ortho*-hydroxylation may be overestimated (Inter System Extrapolation Factors (ISEF) of 7) to reproduce 2OH-ATS levels and the resulting predicted CL of 51 L/h largely exceeds the observed after IV administration (37.5 L/h), with the corresponding lower predicted bioavailability (7% vs 14%). Additionally, 2OH-ATS product is not assessed by the model, but the corresponding formation pathway parameters are remarkably close to that of the *ortho*-hydroxylation route (ISEF of 7). This issue will produce higher amounts of 4OH-ATS than observed and probably causing an over-prediction of ATS systemic clearance. Permeability-limited liver model was used to assess hepatic OATP1B1-mediated active uptake and incorporated passive diffusion clearance in hepatocytes membrane. Different ISEFs were applied to best reproduce the observed data, a well-known approach for *in vitro-in vivo* extrapolations (IVIVE) in enzymatic and transporter-mediated processes. CYP3A4-mediated *ortho*-hydroxylation and UGT1A3-mediated glucuronidation generate the primary metabolites 2OH-ATS and ATS-L, respectively, which are modelled through minimal PBPK distribution models using a Single Adjusting Compartment (SAC). As expected, the predicted V_{ss} of ATS-L was higher than the V_{ss} of ATS and 2OH-ATS. Despite the octanol:water partitions coefficients are not different enough to justify this difference, the absence of the carboxylic acid functional group of the lactone form and the closed ring of its structure (neutral compound) may increase the permeability through cell membranes thus increasing its volume of distribution. As there were some physicochemical properties that were not available for these metabolites (e.g., B/P and f_u), ATS corresponding parameter values were assumed. Elimination of both metabolites were parameterized through enzyme kinetics, determining CYP3A4-intrinsic clearance with the retrograde model after assigning 40% and 30% contribution of CYP3A4 to the overall clearance of 2OH-ATS and ATS-L, respectively. The metabolized fractions of both metabolites were assigned to reproduce observed clinical DDIs, so they can be considered when assessing their elimination. However, in the case of ATS-L a value of 1892 μL/min/mg protein for its intrinsic clearance by HLMs has been published [40] that could have been used and optimized if necessary, in a more mechanistic manner.

Model performance was evaluated using 13 independent clinical trials (data from literature) after oral doses of 20 and 40 mg of ATS (Table 1). The prediction ability of the PBPK model was validated using DDIs clinical data with enzyme inhibitors and inducers.

Table 1. Study design and population characteristics of the physiologically based pharmacokinetic models of atorvastatin.

	Zhang. 2015	**Duan et al. 2017**	**Li et al. 2019**	**Morse et al. 2019**
Number of independent clinical studies	13[a]	7[b]	6[c]	5[d]
Dosing regimen (Number of trials)	SD (12) MD (2)	SD (6) MD (2)	SD (5) MD (1)	SD (5)
Number of subjects (total)	386	166	180	145
Clinical status (number of subjects)	HV (386)	HV (145) RTP (21)	HV (162) RTP (18)	HV (145)
Dose level (mg) (number of subjects)	20 (83) 40 (303)	10 (33) 20 (60) 40 (73)	10 (36) 20 (55) 40 (89)	10 (12) 40 (133)

[a]: [62-74]; [b]: [62,70,71,75-78]; [c]: [69,70,79-82]; [d]: [69,70,82-84]; SD: single dose schedule; MD: multiple dose schedule; HV: healthy volunteers; RTP: renal transplant patients.

There are some aspects that need further consideration regarding the involvement of P-gp and hepatic transporters. The authors stated that ATS exhibits high solubility and high permeability, considering the contribution of P-gp to the total exposure to be marginal. However, the involvement of P-gp in ATS PK has been demonstrated in humans due to the polymorphisms in ABCB1 genotypes, thus suggesting that P-gp affects the enterohepatic recirculation of ATS [50]. Additionally, ATS is currently considered as a BCS class II (low solubility, high permeability) and many efforts have been made to increase its bioavailability enhancing its solubility [14,17,20,52,53]. For these reasons, solubility and P-gp activity become essential in ATS absorption and disposition. Furthermore, the contribution of hepatic transporters to ATS disposition cannot be minimal as stated because it has been demonstrated *in vitro* that transporter-mediated hepatic uptake clearly dominates overall ATS hepatic uptake with 90% ± 2% contribution [34]. This implication in ATS exposure has been demonstrated *in vivo* [35,37]. Despite of this, the PBPK model of Zhang accurately described the time course of ATS, 2OH-ATS and ATS-L after the oral administration of 40 mg of ATS in more than 10 independent clinical studies as well as DDIs with enzyme inhibitors and inducers, being the model more accurate to reproduce changes in AUC than in C_{max}. Some of the limitations assumed by the authors are the lack of parameterization of the hydrolysis process of the lactone forms to the corresponding open acids and the optimization of the OATP1B1 kinetic parameters with only data from single dose studies with rifampicin.

Duan et al. 2017

In this work [54], Duan et al developed an ATS PBPK model to assess the role of OATP1B1 in ATS disposition evaluating *SLCO1B1* polymorphisms and the impact of DDIs on ATS exposure when co-administrated with known CYP and/or transporters inhibitors such as rifampicin, cyclosporine, gemfibrozil, itraconazole and erythromycin. The authors used different data sets to develop and evaluate the model using data from the literature. The absorption process was modelled using the ADAM model, predicting human effective permeability ($P_{eff,man}$) from Caco-2 cells. A full PBPK approach was considered as the distribution model, using Rodgers and Rowland method [55,56] to predict $K_{p,t}$ and V_{ss}. Metabolism was only modelled via CYP3A4 oxidation, calculating $CL_{int,CYP3A4}$ by means of two approaches: the first one, used the retrograde methodology with the reported IV ATS clearance of 37.5 L/h and assuming 100% contribution of CYP3A4 to overall metabolic clearance, resulting in an intrinsic clearance of 8 μL/min/pmol recombinant CYP; the second one, directly used intrinsic clearance from *in vitro* assays and accounted for *ortho*- and *para*-hydroxylation pathways. The $CL_{int,T}$ for OATP1B1 obtained with both approaches were optimized starting from the reported *in vivo* $CL_{int,T}$ of 910 mL/min/kg or 360 μL/min/million cells (based on SimCYP Simulator extrapolation algorithms), which was further decomposed in J_{max} and K_m. Both approaches provided similar simulated ATS profiles and required the optimization of $CL_{int,OATP1B1}$ with an scaling factor of 4 to best reproduce C_{max} and AUC of the training dataset. These results led to the consideration that hepatic uptake seems to be the rate limiting step in ATS elimination, which constitutes an important conclusion of this work. No other CYP (CYP2C8 nor CYP3A5) were considered to contribute to ATS metabolism, despite the well-known metabolic profile previously described. In addition, no lactonization process was implemented in the model which constitutes and important limitation (assumed by the authors) due to the relevance of the lactone forms of ATS and its metabolites, not only in the metabolic process [39], but also in terms of safety and toxicity [2,57]. The absence of these processes could explain the slight deficiency to accurately reproduce the terminal phase of the 20 and 40 mg oral dose of ATS. Regarding to the distribution model, a V_{ss} of 0.226 L/kg is predicted by the model, which is notably lower compared to previously reported values of 381 L [3], 5.4 L/kg [24] and 8.7 L/kg [51]. Therefore, model parameter optimizations with observed PK parameters that are largely influenced by volume of distribution (e.g., C_{max}) should be considered with caution. This PBPK model accounts for the first time for Breast Cancer Resistance Protein (BCRP) contribution to ATS disposition and it is in line with the available data published by Keskitalo et al [35] (subjects with the *ABCG2* c.421AA genotype showed a 72% and 46% increase in ATS AUC and C_{max}, respectively when compared to subjects

with the c.421CC genotype). These results, as well as the unchanged $t_{1/2}$ in both genotypes, suggested that the main role of BCRP is linked to the absorption phase. For this reason, intestinal BCRP activity was manually optimized to best fit C_{max} and T_{max} of the training dataset. BCRP canalicular efflux activity was also incorporated into the model, thus contributing to the biliary excretion of ATS, directly adopting the reported *in vitro* value of 1.4 μL/min/mg protein. A small contribution to overall elimination of ATS through the kidneys was also implemented. Model performance was determined assessing the ratio of simulated ($AUCR_{sim}$) and observed ($AUCR_{obs}$) results of AUC with and without the perpetrator drug of the DDI ($AUCR_{sim}/AUCR_{obs}$) according to the two-fold range (0.5-2) due to the known inter-study variability.

The PBPK model developed by Duan et al accurately described the time course of single oral doses of 20 mg and 40 mg of ATS in healthy volunteers. The PBPK model was able to capture the AUCRs in *SCLO1B1* polymorphism (c.521CC vs c.521TT) and in the presence of CYP3A4 or OATP1B1 inhibitors reasonably well (ratios within 2-fold of the observed value).

Li et al. 2019

Li et al. refined the published ATS and ATS-L PBPK models by Zhang (2015) incorporating biliary excretion of ATS and OATP1B3-mediated hepatic active uptake [58]. The aim of the work was to assess *in silico* the potential of severe and life-threating myopathies such as rhabdomyolysis when ATS is concomitantly administered with CYP3A4 and/or OATP inhibitors. Absorption and distribution processes were modelled using ADAM and full PBPK models, respectively, incorporating a permeability-limited liver model to deal with hepatic transporters. Enterohepatic recirculation of ATS was allowed, but the fraction available to be reabsorbed was not reported. Metabolism of both ATS and ATS-L was enzymatically modelled using V_{max} and K_m values of CYP3A4 *ortho*- and *para*-hydroxylation. Another important feature of this model is that renal excretion was not implemented and thus ATS elimination was restricted to the liver. Passive diffusion (CL_{PD}) of ATS in the membrane of hepatocytes was assumed to be consistent with *in vitro* results, while $CL_{int,T}$ was estimated through the Parameter Estimation module and each of the transporters involved in hepatic active uptake were assigned to contribute almost equally to the total intrinsic clearance (53% and 47% contribution for OATP1B1 and OATP1B3, respectively). It is true that OATP1B1 and OATP1B3 are the main transporters in ATS hepatic active uptake [34], but the protein expression levels are quite different (23.2 vs 3.2 fmol/μg membrane protein for OATP1B1 and OATP1B3, respectively), as well as V_{max} (OATP1B1 V_{max} is 3-fold higher than OATP1B3 V_{max}). So, the assigned role of each of these transporters should be considered with caution. The PBPK model did not

incorporate other transporters responsible of ATS hepatic active uptake (e.g., NTCP and OATP2B7) that had also demonstrated *in vitro* activity [34]. On the other hand, the ATS-L model needed the incorporation of empirical scaling factors to the metabolic pathways and an additional liver microsomal clearance to best fit the observed data. Sensitivity analysis on this additional clearance mechanism is lacking.

Model verification was performed by comparing simulated PK parameters AUC and C_{max} with observed data at different dose levels (10, 20 and 40 mg). Despite all simulations were within the desired 2-fold error range, AUC predictions were, in general, overpredicted, while C_{max} was less variable and closer to the observed values. This situation could be explained due to the absence of implementation of other metabolic pathways in the elimination of both ATS and ATS-L, such as CYP3A5 and CYP2C8-mediated hydroxylation. Model validation was performed using DDIs studies with ATS (and ATS-L) as victim drug and inhibitors (perpetrators) of CYP3A4 (itraconazole and clarithromycin), OATP1B1 and OATP1B3 (rifampicin) or both (cyclosporine). Results revealed an important feature of ATS PK: ATS lactonization must not be an immediate process and the intermediate of the acid-to-lactone conversion, e.g. acyl-β-D-glucuronide, should be present in the bloodstream sufficient enough to be victim of OATP-mediated transporter inhibition to increase ATS-L exposure more than 3 times when co-administered with rifampicin and cyclosporine. Thus, UGT-mediated glucuronidation is the main route of ATS lactonization and this metabolic pathway should be considered when developing ATS PBPK models. Finally, model application to predict ATS and ATS-L exposure in muscle tissues revealed that ATS-L levels are 18-fold higher than in plasma and 10- or 14-fold higher than ATS exposure in muscles tissues after single or multiple doses of 40 mg. These results are consistent with the high V_{ss} of ATS-L predicted by the model (141.3 L/kg).

However, the model has some limitations that are recognised by the authors and are summarized as follows: i) the lack of other recognised transporters implicated in ATS disposition such as MDR1 (P-gp) and BCRP; ii) the absence of pre-systemic non-enzymatic ATS lactonization at initial segments of the GI tract; iii) the impossibility to describe the kinetics of the glucuronide intermediate in the acid-to-lactone conversion.

Morse et al. 2019

This is the first PBPK model that considers pre-systemic degradation of ATS [59]. The model developed by Morse et al. states that ATS-L is mostly formed non-enzymatically in the stomach due to the low pH of this region of the GI tract. Taking this premise in mind, the authors developed a PBPK model to assess the

impact of increasing gastric emptying time after glucagon-like peptide-1 receptor agonists (GLP1RAs) administration. Due to the limitation of considering two active drugs as substrates in Simcyp v17, two PBPK models were simultaneously developed: one considering ATS as substrate and a second model considering ATS-L as substrate. This is made by dividing the oral dose of ATS as a function of the fraction absorbed (f_a) of ATS, since complete absorption of ATS has been suggested [3]. The pre-systemic degradation is performed optimising a stomach degradation rate constant to reproduce the dose-dependent change in C_{max}, which is observed in clinical studies. The fraction absorbed of ATS derived from the best scenario is considered to determine ATS-L f_a. This strategy allowed to manage a fraction of the dose administered directly as ATS-L and generating the corresponding substrate model file, thus assessing its ADME properties more mechanistically. To better characterize ATS pre-systemic degradation, pH-dependent solubility was added to the model, taking a dissolution profile directly from the literature [44]. However, it must be noted that this pH-dependent dissolution profile has been characterized for the sodium salt of ATS and at present ATS is administered as the tri-hydrated calcium salt of the carboxylic acid, which could lead to differences in the dissolution profile when comparing to clinical data. ADAM model is used for assessing the absorption of both substrates predicting $P_{eff,man}$ from Caco-2 cells and MDCK for ATS and ATS-L, respectively.

The model structure considers 2OH-ATS as a direct metabolite of ATS and a secondary metabolite of ATS-L due to plasmatic hydrolysis of 2OH-ATS-L after CYP-mediated hydroxylation. ATS is also considered in the ATS-L model as a direct metabolite after plasmatic esterases-mediated hydrolysis. ATS and ATS-L metabolism are parameterized by enzyme kinetics mainly through CYP3A4, although an additional non-CYP microsomal intrinsic clearance was optimized to best reproduce the *in vivo* interaction with itraconazole. Additionally, UGT1A3-mediated metabolism is also implemented for ATS, but it does not generate the corresponding lactone product. No other CYPs nor UGTs are considered. Plasmatic hydrolysis of lactone forms (ATS-L and 2OH-ATS-L) to the corresponding acid products (ATS and 2OH-ATS) are included in the model in terms of half-life (minutes) for ATS-L and through an esterase intrinsic clearance (μL/min/mg) for 2OH-ATS-L to best fit the observed data after an oral dose of 40 mg and verified with DDIs studies with itraconazole and dulaglutide. Additionally, sensitivity analyses on optimized parameters such as esterase activity and non-CYP mediated hepatic metabolism were performed. An important feature of this work is that some PBPK model parameters were determined *in vitro*, such as $CL_{int,OATP1B3}$ (μL/min/10^6 cells) for ATS and 2OH-ATS (31.5 and 25, respectively), P_{app} (10^{-6} cm/s) for ATS-L in MDCK cells (33) and CL_{PD} (no units provided) for ATS and 2OH-

ATS (13 and 5, respectively), thus avoiding some assumptions and optimizations, and increasing model identifiability [60].

Different distribution models are selected for each moiety and a K_p scalar is applied to best reproduce C_{max} (ATS) or $t_{1/2}$ (ATS-L and 2OH-ATS-L) at 40 mg dose level. ATS model predicted V_{ss} is, as in the PBPK model developed by Duan et al., quite lower (0.69 L/kg) than those previously published [51,58], so caution must be paid to the values of the model parameters optimised with observed PK parameters largely influenced by the volume of distribution. ATS-L exhibits a higher V_{ss} (18.182 L/kg), which is in line with its higher lipophilicity and neutral acid-base properties. Permeability-limited liver model is only used for ATS and 2OH-ATS, which incorporates a hepatic OATP1B3-mediated active uptake process optimized through a scaling factor. Biliary excretion, as well as sinusoidal efflux, of 2OH-ATS is added to the model with the corresponding optimized intrinsic clearance values. Model performance was finally verified comparing simulated PK parameters AUC, C_{max} and T_{max} with those obtained in clinical DDI studies with itraconazole and the GLP1RA dulaglutide.

The model developed by Morse et al. fills an important gap of the above PBPK models of ATS as it accounts for a non-enzymatic lactonization process due to the low pH of the stomach that takes place pre-systemically and is responsible of the rapid appearance of ATS-L in plasma (T_{max} range 2-3 h). In this line, a potential novel DDI with proton pump inhibitors (PPI) has been robustly identified and associated with increased plasma concentrations of ATS, 2OH-ATS, ATS-L and 2OH-ATS-L [61]. Despite some PPI like omeprazole and lansoprazole are known CYP substrates and enzyme inhibitors, the increase in the exposure was explained through an increase in ATS bioavailability secondary to an increase in ATS solubility and a decrease in the pre-systemic lactonization due to the PPI-induced rise in gastric pH.

DISCUSSION

The development of PBPK models, commonly known as “bottom-up approach”, largely rely on previously gather *in vitro* and/or *in vivo* information to build-up the mechanisms able to reproduce the experimental evidence from clinical trials. Minimal parameter estimation/optimization is, therefore, required to characterize the time-course of the analyte(s). In this sense, adequate external experimental evidence is needed in order to properly assess the mechanisms implemented in order to use the PBPK as a predictive tool for dose optimization in patients and/or special sub-groups of populations. The published PBPK models of ATS were

developed using an ATS dose range between 10 and 40 mg, but no information was incorporated into the models of the highest dose strength (80 mg). Additionally, clinical trials incorporated mainly healthy volunteers (n= 434) with no information regarding patients with hypercholesterolemia. Moreover, most of the clinical trials were conducted after single dose regimens (n= 17), whereas limited evidence was gathered after multiple dose regimens (n= 3). The multiple PK pathways affecting ATS could be partially influenced due to disease status and chronic administration of ATS. This limitation could impact the simulation-based dose selection in patients.

The low solubility of ATS is a major drawback affecting its absorption, and consequently, its bioavailability. The lack of adequate reported information regarding the solubility profile of ATS-Ca represents a limitation in the development of mechanistic models of ATS dissolution throughout the GI tract. Available information on the solubility profile of ATS-Na [44] could be used as a provisional input during model development, but additional efforts should be performed to properly provide experimental evidence about ATS-Ca on this regard. Due to the multiple processes affecting ATS-Ca within the GI lumen (lactonization, hydrolysis, drug dissolution), a detailed characterization of its solubility would enhance the prediction of its bioavailability and, therefore, the evaluation of new oral formulations of ATS incorporating mechanisms improving the solubility of ATS-Ca.

A relevant aspect that Li et al. incorporated into the PBPK model is the assumption that ATS lactonization might be a non-immediate process within the bloodstream, which was observed when OATP-mediated transporters inhibitors were co-administered with ATS. Acyl-β-D-glucuronide is an intermediate compound during the lactonization process, and it is a substrate of OATP transporters for hepatic uptake, which is inhibited in the presence of compounds with higher affinity to OATP transporters (i.e. rifampicin and cyclosporine). The kinetic equilibrium in plasma is, therefore, displaced to the more lipophilic form (ATS-L), affecting the distribution into low-perfused tissues. On the other hand, the PBPK model developed by Morse et al. incorporates the alternative lactonization pathway that occurs at low pH values (stomach). This process explains the rapid appearance of ATS-L in plasma due to pre-systemic lactonization. The higher permeability of ATS-L because of its higher lipophilicity compared to ATS enables to shorter T_{max} in plasma. In this sense, the incorporation of the lactonization process (UGT-mediated) is clearly required to properly characterize the disposition of ATS and ATS-L in plasma and other tissues.

Simcyp simulator represents one of the most used PBPK software currently available with scientific [85-87] and regulatory [60,88-90] agreement for the

establishment of quantitative PBPK frameworks allowing dose selection in special sub-groups of populations, DDI and transporter evaluation and biopharmaceutical specifications characterization. Nevertheless, the development of a PBPK model able to simultaneously predict the PK profile of the 6 analytes (ATS, 2OH-ATS, 4OH-ATS, ATS-L, 2OH-ATS-L, and 4OH-ATS-L) with the current version of Simcyp (v20) represents a major challenge, since it only allows to consider simultaneously one parent drug (substrate), two primary metabolites and a secondary metabolite. Considering the lactonization/hydrolysis equilibrium and the parallel formation of metabolites from ATS and ATS-L, the prediction ability of the PBPK model is clearly affected when more than 4 analytes are considered.

To the best of our knowledge, these are the four PBPK models of ATS published (Table 2). All of them consider ATS as a lipophilic monoprotic acid of 559 g/mol with a pK_a of about 4.4. The ADAM model is used to characterize the absorption of the drug and predict the human permeability from Caco-2 cells experiments. Full PBPK distribution models for ATS are used in all of them, being the Rodgers and Rowland method (#2) the most used to predict V_{ss} and $K_{p,t}$. This selection agrees with the physicochemical properties of ATS because of its degree of ionization at physiological pH (pKa ≈ 4.4), as this method can deal with the different fractions of the drug (ionized or non-ionized). Metabolism is modelled through enzyme kinetics in all cases and mainly by means of CYP3A4. However, some models use another CYP isoform (CYP2C8 in Zhang. 2015) or an unspecific metabolism through HLM (Morse et al. 2019). Lactonization is modelled enzymatically through UGT1A1 and UGT1A3 in the models of Zhang and Li et al., while it is considered to occur non-enzymatically in the stomach in Morse et al. As both processes have been demonstrated to contribute to ATS-L formation, any PBPK model of ATS should consider them to best reproduce the PK of ATS. Regarding to transport processes, it must be noted that all the models use the Permeability Limited Liver Model to account for active transport added to the passive diffusion through the cell membranes of the hepatocytes. OATP1A1 is incorporated in all the models, while OATP1B3 is only considered in the models of Li et al. and Morse et al. Efflux processes are implemented in the gut wall through P-gp and BCRP only in the model of Zhang and a canalicular efflux process mediated by BCRP is assessed only in the model of Duan et al. As stated previously, the role of P-gp [50] and BCRP [35] in the PK of ATS have been demonstrated *in vivo* so, the PBPK models of ATS should incorporate them to best characterize its absorption and enterohepatic recirculation. Renal excretion of ATS contributes to the overall elimination of the drug to a lesser extent so, its presence in PBPK models is not mandatory. For this reason, only 2 of the 4 models implemented it. However, as enterohepatic recirculation has been suggested (and demonstrated in pre-clinical species [43]), bile excretion is a route that could be

considered to best characterize this process as it occurs with the models of Duan et al. and Li et al.

Table 2. Parameters of each physiologically based pharmacokinetic model of atorvastatin.

Model parameter	Zhang. 2015	Duan et al. 2017	Li et al. 2019	Morse et al. 2019
Physicochemical properties				
Molecular weight (g/mol)	558.66	558.64	558.64	559.00
log$P_{o:w}$	5.7	4.07	4.434	5.39
Compound type	Monoprotic Acid	Monoprotic Acid	Monoprotic Acid	Monoprotic Acid
pK_a	4.46	4.46	4.46	4.33
B/P	0.61	0.61	0.61	0.55
f_u	0.051	0.024	0.050	0.022
Absorption				
Model	ADAM	ADAM	ADAM	ADAM
$P_{eff,man}$ (10^{-4} cm/s)	2.05	NR	1.05	4.49
In vitro assay	Caco-2	Caco-2	Caco-2	Caco-2
pH_{apical}:$pH_{basolateral}$	7.4:7.4	7.4:7.4	7.4:7.4	6.5:7.4
P_{app} (10^{-6} cm/s)	8.6	7.9	4.9	28.4
Refference compound	Propranolol	NR	NR	NR
$P_{app\ refference}$ (10^{-6} cm/s)	20	NR	NR	NR
Distribution				
Model	Full PBPK	Full PBPK	Full PBPK	Full PBPK
Method	1 and 2	2	2	2
V_{ss} (L/kg)	8.7	0.226	2.67	0.690
Kp scalar (model)	2(1) and 4.6(2)	NR	NR	2
Lipid Binding Scalar	NR	NR	4.15	NR
Metabolism				
Model	Enzyme kinetics	Enzyme kinetics	Enzyme kinetics	Enzyme kinetics
CYP3A4				
Metabolite	2OH-ATS			2OH-ATS
K_m (µM)	29.7		34.8	34.8
V_{max} (pmol/min/pmol isoform)	29.3		1048	1048
$f_{u,mic}$	1		NR	NR
Scaling Factor	7 (ISEF)		NR	NR
K_m (µM)	25.6		33	33
V_{max} (pmol/min/pmol isoform)	29.8		1353	1353
f_{umic}	1		NR	NR
CL_{int} (µL/min/pmol isoform)		8	NR	NR
Scaling Factor	7 (ISEF)			

Table 2. cont.

Model parameter	Zhang. 2015	Duan et al. 2017	Li et al. 2019	Morse et al. 2019
CYP2C8				
K_m (µM)	35.9			
V_{max} (pmol/min/pmol isoform)	0.29			
$f_{u,mic}$	1			
Scaling Factor	4 (ISEF)			
UGT1A1				
Metabolite	ATS-L		ATS-L	
K_m (µM)	11		2	
V_{max} (pmol/min/pmol isoform)	72		2	
$f_{u,mic}$	1		NR	
Scaling Factor	2 (ISEF)		NR	
UGT1A3				
Metabolite	ATS-L		ATS-L	
K_m (µM)	11		4	
V_{max} (pmol/min/pmol isoform)	72		38	
$f_{u,mic}$	1		NR	
Scaling Factor	2 (ISEF)		NR	
CL_{int} (µL/min/mg protein)				6.2
Other HLM				
CL_{int} (µL/min/mg protein)				65
Transport				
Intestine				
P-gp	Efflux (gut wall)			
K_m (µM)	115			
J_{max} (pmol/cm²/min)	141			
Scaling Factor	1 (RAF/REF)			
BCRP	Efflux (gut wall)			
$CL_{int,T}$ (µL/min)	6			
Liver				
CL_{PD} (mL/min/10^6 cells)	0.023	0.017	0.023	0.013
$f_{u,IW}$	0.324			
$f_{u,EW}$	0.038			
OATP1B1	Uptake (sinusoidal)			
CL_{int} (µL/min/10^6 cells)			1000	31.5
$CL_{int,T}$ (µL/min)	55			
K_m (µM)		0.77		
J_{max} (pmol/min/10^6 cells)		277.2		
Scaling Factor	10 (RAF/REF)	4		30

Table 2. cont.

Model parameter	Zhang. 2015	Duan et al. 2017	Li et al. 2019	Morse et al. 2019
OATP1B3	Uptake (sinusoidal)			
CL_{int} (µL / min / 10^6 cells)			900	31.5
Scaling Factor				30
BCRP	Efflux (canalicular)			
$CL_{int,T}$ (µL / min / 10^6 cells)		1.4		
Excretion				
CL_R (L / h)	0.47	0.375		
$CL_{int,bile}$ (µL / min / 10^6 cells)			10	

Green: data from literature; Blue: *in situ* determined value; Yellow: predicted value; Orange: optimized value according to observations; Red: assumed value; B/P: blood-to-plasma ratio; f_u: fraction unbound in plasma; ADAM: Advanced Dissolution, Absorption and Metabolism model; $P_{eff,man}$: human effective permeability; NR: not reported; P_{app}: apparent permeability; Method 1: Poulin and Theil method [91]; Method 2: Rodgers and Rowland method [55,56]; V_{ss}: volume of distribution at steady state; K_m: Michaelis-Menten constant; V_{max}: maximum rate of the enzymatic process; $f_{u,mic}$: fraction unbound in the microsomal incubation; CL_{int}: intrinsic clearance; HLM: human liver microsomes; P-gp: P-glycoprotein; J_{max}: maximum transport rate of the transporter; BCRP: breast cancer resistance protein; $CL_{int,T}$: total intrinsic clearance of the transporters; CL_{PD}: passive diffusion clearance through cell membranes; $f_{u,IW}$: fraction unbound in the intracellular water; $f_{u,EW}$: fraction unbound in the extracellular water; CL_R: renal clearance; $CL_{int,bile}$: biliary intrinsic clearance.

According to Table 2, there is no consensus between models regarding physicochemical parameters such as $logP_{o:w}$ (ranging from 4.07 to 5.7) and f_u (values from 2.2 to 5.1%). As a result, different V_{ss} values raise, ranging from 0.226 to 8.7 L/kg, despite using the same method for its prediction. Therefore, both parameters ($logP_{o:w}$ and f_u) influence the V_{ss} obtained. However, in the case of V_{ss} predicted by the model of Li et al. and Morse et al., the Lipid Binding Scalar overweights the $logP_{o:w}$ and enhances the distribution of ATS. B/P is homogeneous in all models with the exception of that of Morse et al., in which a default value of 0.55 and no distribution into red blood cells is assumed. $P_{eff,man}$ is another parameter highly variable between models depending on the value of the P_{app} introduced in the platform and the conditions of the *in vitro* experiment.

P-gp activity is only assessed in the model of Zhang, suggesting little confidence on the relevance of this transporter in ATS PK. Several studies with *in vitro* models have demonstrated that ATS is an inhibitor of P-gp and may be a substrate of this transporter [92]. Additionally, concomitant administration of 80 mg of ATS with digoxin increased digoxin AUC_{0-24} and C_{max} by 15% and 20%, respectively [93]. As neither digoxin T_{max} nor renal clearance were affected, it has been suggested that the mechanism of this DDI is the inhibition of the P-gp mediated intestinal efflux of digoxin by ATS. So, modelling of P-gp-mediated transport processes in

ATS PBPK is important to better characterize potential DDIs at this level not only as a perpetrator, but also as a victim drug, to avoid high exposures that could lead to the development of adverse events like myopathies. The model of Duan et al. confirms that ATS hepatic uptake by members of the OATP family is the rate limiting step in ATS elimination, as previously described. However, lactonization is not implemented in this model, which constitutes an important limitation to better characterize ATS metabolism.

The relative contribution of the hepatic uptake transporters OATP1B1 and OATP1B3 is assigned almost equally (53% and 47%, respectively) in the model of Li et al. after estimating total intrinsic uptake clearance instead of using enzymatic or intrinsic clearance values determined *in vitro* as Zhang, Duan et al. and Morse et al. did. Because protein expression levels and V_{max} of these transporters are quite different, this statement should be managed with caution when developing a PBPK model of ATS.

CONCLUSION

The development of solid physiologically based pharmacokinetic models clearly enhances the decision-making process, helping to understand and infer how PK processes may affect the optimal posology in the target population. Several aspects have been highlighted as critical elements in the complex pharmacokinetics of atorvastatin that could compromise its efficacy/safety in patients with hypercholesterolemia: (i) the integration of the lactonization process, which occurs within the GI lumen and plasma and represents a major kinetic process that affects the formation of additional active moieties (2OH-ATS and 4OH-ATS); (ii) the contribution of P-gp has been undermined in most of the PBPK models developed so far, limiting the evaluation of DDI effects; (iii) the varying effect of ATS-Ca solubility within the GI tract; (iv) the inclusion of additional experimental evidence in patients and multiple regimen schedules; and, (v) the simultaneous management of multiple analytes within the PBPK platforms in order to optimize the benefit/risk balance of ATS.

Author Contributions: c*onceptualization*, J.R.L., V.M.S., and M.M.S.; *investigation*, J.R.L., V.M.S., and M.M.S.; *writing original draft preparation*, J.R.L., V.M.S., and M.M.S.; *writing review and editing*, J.R.L., A.G.A., V.M.S., and M.M.S.; *supervision*, A.G.A., V.M.S., and M.M.S.
All authors have read and agreed to the published version of the manuscript.
Funding: This research received no external funding.
Institutional Review Board Statement: Not applicable.
Informed Consent Statement: Not applicable.

Data Availability Statement: Not applicable.
Conflicts of Interest: Authors declare no conflict of interest.

References:

[1] Michael Schachter. Chemical, Pharmacokinetic and Pharmacodynamic Properties of Statins: An Update.

[2] du Souich, P.; Roederer, G.; Dufour, R. Myotoxicity of Statins: Mechanism of Action. Pharmacology & therapeutics (Oxford) 2017, 175, 1-16.

[3] Lennernas, H. Clinical Pharmacokinetics of Atorvastatin. Clin. Pharmacokinet. 2003, 42, 1141-1160.

[4] Jiang, J.; Tang, Q.; Feng, J.; Dai, R.; Wang, Y.; Yang, Y.; Tang, X.; Deng, C.; Zeng, H.; Zhao, Y. et al. Association between SLCO1B1 −521T>C and −388A>G Polymorphisms and Risk of Statin-Induced Adverse Drug Reactions: A Meta-Analysis. SpringerPlus 2016, 5, 1-16.

[5] Christians, U.; Jacobsen, W.; Floren, L.C. Metabolism and Drug Interactions of 3-Hydroxy-3-Methylglutaryl Coenzyme A Reductase Inhibitors in Transplant Patients: Are the Statins Mechanistically Similar? Pharmacology & therapeutics (Oxford) 1998, 80, 1-34.

[6] Taha, D.A.; De Moor, C.H.; Barrett, D.A.; Gershkovich, P. Translational Insight into Statin-Induced Muscle Toxicity: From Cell Culture to Clinical Studies. Translational research : the journal of laboratory and clinical medicine 2014, 164, 85-109.

[7] Schirris, T.J.J.; Ritschel, T.; Bilos, A.; Smeitink, J.A.M.; Russel, F.G.M. Statin Lactonization by Uridine 5′-Diphospho-Glucuronosyltransferases (UGTs). Molecular pharmaceutics 2015, 12, 4048-4055.

[8] Riedmaier, S.; Klein, K.; Hofmann, U.; Keskitalo, J.E.; Neuvonen, P.J.; Schwab, M.; Niemi, M.; Zanger, U.M. UDP-Glucuronosyltransferase (UGT) Polymorphisms Affect Atorvastatin Lactonization in Vitro and in Vivo. Clin Pharmacol Ther 2009, 87, 65.

[9] Athyros, V.G.; Tziomalos, K.; Karagiannis, A.; Mikhailidis, D.P. Atorvastatin: Safety and Tolerability. Expert opinion on drug safety 2010, 9, 667-674.

[10] Physiologically Based Pharmacokinetic Analyses - Format and Content Guidance for Industry. US Official News 2018.

[11] Guideline on the Reporting of Physiologically Based Pharmacokinetic (PBPK) Modelling and Simulation. European Union News 2019.

[12] European Medicines Agency Referrals. Lipitor. Annex III Summary of Product Characteristics, Labelling and Package Leaflet. Available online: https://www.ema.europa.eu/en/medicines/human/referrals/lipitor (accessed on 5 March 2021).

[13] Yin, Y.; Cui, F.; Kim, J.S.; Choi, M.; Choi, B.C.; Chung, S.; Shim, C.; Kim, D. Preparation, Characterization and in Vitro Intestinal Absorption of a Dry Emulsion Formulation Containing Atorvastatin Calcium. Drug delivery 2009, 16, 30-36.

[14] Shaker, M.A.; Elbadawy, H.M.; Shaker, M.A. Improved Solubility, Dissolution, and Oral Bioavailability for Atorvastatin-Pluronic(R) Solid Dispersions. Int. J. Pharm. 2020, 574, 118891.

[15] Zhang, H.; Wang, J.; Zhang, Z.; Le, Y.; Shen, Z.; Chen, J. Micronization of Atorvastatin Calcium by Antisolvent Precipitation Process. International journal of pharmaceutics 2009, 374, 106-113.

[16] Drugs@FDA: FDA-Approved Drugs. Lipitor. Available online: https://www.accessdata.fda.gov (accessed on 3 March 2021).

[17] Khan, F.N.; Dehghan, M.H.G. Enhanced Bioavailability and Dissolution of Atorvastatin Calcium from Floating Microcapsules using Minimum Additives. Scientia pharmaceutica 2012, 80, 215-228.

[18] Prabhu, P.; Prabhu, P.; Patravale, V.; Patravale, V. Dissolution Enhancement of Atorvastatin Calcium by Co-Grinding Technique. Drug Deliv. and Transl. Res 2016, 6, 380-391.

[19] Shayanfar, A.; Ghavimi, H.; Hamishekar, H.; Jouyban, A. Coamorphous Atorvastatin Calcium to Improve its Physicochemical and Pharmacokinetic Properties. Journal of pharmacy & pharmaceutical sciences 2013, 16, 577-587.

[20] Kong, R.; Zhu, X.; Meteleva, E.S.; Polyakov, N.E.; Khvostov, M.V.; Baev, D.S.; Tolstikova, T.G.; Dushkin, A.V.; Su, W. Atorvastatin Calcium Inclusion Complexation with Polysaccharide Arabinogalactan and Saponin Disodium Glycyrrhizate for Increasing of Solubility and Bioavailability. Drug Deliv. Transl. Res. 2018, 8, 1200-1213.

[21] Kulthe, V.V.; Chaudhari, P.D. Drug Resinates an Attractive Approach of Solubility Enhancement of Atorvastatin Calcium. Indian. J. Pharm. Sci. 2013, 75, 523-532.

[22] Poli, A. Atorvastatin: Pharmacological Characteristics and Lipid-Lowering Effects. Drugs 2007, 67, 3-15.

[23] Corsini, A.; Bellosta, S.; Baetta, R.; Fumagalli, R.; Paoletti, R.; Bernini, F. New Insights into the Pharmacodynamic and Pharmacokinetic Properties of Statins. Pharmacology and Therapeutics 1999, 84, 413-428.

[24] Sirtori, C.R. The Pharmacology of Statins. Pharmacological research 2014, 88, 3-11.

[25] Shitara, Y.; Sugiyama, Y. Pharmacokinetic and Pharmacodynamic Alterations of 3-Hydroxy-3-Methylglutaryl Coenzyme A (HMG-CoA) Reductase Inhibitors: Drug-Drug Interactions and Interindividual Differences in Transporter and Metabolic Enzyme Functions. Pharmacology & therapeutics (Oxford) 2006, 112, 71-105.

[26] Cilla, D.D.; Gibson, D.M.; Whitfield, L.R.; Sedman, A.J. Pharmacodynamic Effects and Pharmacokinetics of Atorvastatin After Administration to Normocholesterolemic Subjects in the Morning and Evening. Journal of clinical pharmacology 1996, 36, 604-609.

[27] Radulovic, L.L.; Cilla, D.D.; Posvar, E.L.; Sedman, A.J.; Whitfield, L.R. Effect of Food on the Bioavailability of Atorvastatin, an HMG-CoA Reductase Inhibitor. J. Clin. Pharmacol. 1995, 35, 990-994.

[28] Whitfield, L.R.; Stern, R.H.; Sedman, A.J.; Abel, R.; Gibson, D.M. Effect of Food on the Pharmacodynamics and Pharmacokinetics of Atorvastatin, an Inhibitor of HMG-CoA Reductase. European journal of drug metabolism and pharmacokinetics 2000, 25, 97-101.

[29] Wu, X.; Whitfield, L.R.; Stewart, B.H. Atorvastatin Transport in the Caco-2 Cell Model: Contributions of P-Glycoprotein and the Proton-Monocarboxylic Acid Co-Transporter. Pharm. Res. 2000, 17, 209-215.

[30] Cuiping Chen; Rouchelle J. Mireles; Scott D. Campbell; Jian Lin; Jessica B. Mills; Jinghai J. Xu; Teresa A. Smolarek. Differential Interaction of 3-Hydroxy-3-Methylglutaryl-Coa Reductase Inhibitors with Abcb1, Abcc2, and Oatp1b1. Drug metabolism and disposition 2005, 33, 537-546.

[31] Neuvonen, P.J.; Niemi, M.; Backman, J.T. Drug Interactions with Lipid-Lowering Drugs: Mechanisms and Clinical Relevance. Clinical pharmacology and therapeutics 2006, 80, 565-581.

[32] Igel, M.; Sudhop, T.; von Bergmann, K. Metabolism and Drug Interactions of 3-Hydroxy-3-Methylglutaryl Coenzyme A-Reductase Inhibitors (Statins). Eur J Clin Pharmacol 2001, 57, 357-364.

[33] DeGorter, M.K.; Urquhart, B.L.; Gradhand, U.; Tirona, R.G.; Kim, R.B. Disposition of Atorvastatin, Rosuvastatin, and Simvastatin in Oatp1b2−/− Mice and Intraindividual Variability in Human Subjects. Journal of clinical pharmacology 2012, 52, 1689-1697.

[34] Vildhede, A.; Karlgren, M.; Svedberg, E.K.; Wisniewski, J.R.; Lai, Y.; Norén, A.; Artursson, P. Hepatic Uptake of Atorvastatin: Influence of Variability in Transporter Expression on Uptake Clearance and Drug-Drug Interactions. Drug metabolism and disposition 2014, 42, 1210-1218.

[35] Keskitalo, J.; Zolk, O.; Fromm, M.; Kurkinen, K.; Neuvonen, P.; Niemi, M. ABCG2 Polymorphism Markedly Affects the Pharmacokinetics of Atorvastatin and Rosuvastatin. Clinical pharmacology and therapeutics 2009, 86, 197-203.

[36] Prado, Y.; Zambrano, T.; Salazar, L.A. Transporter Genes ABCG2 rs2231142 and ABCB1 rs1128503 Polymorphisms and Atorvastatin Response in Chilean Subjects. Journal of clinical pharmacy and therapeutics 2018, 43, 87-91.

[37] Birmingham, B.K.; Bujac, S.R.; Elsby, R.; Azumaya, C.T.; Wei, C.; Chen, Y.; Mosqueda-Garcia, R.; Ambrose, H.J. Impact of ABCG2 and SLCO1B1 Polymorphisms on Pharmacokinetics of Rosuvastatin, Atorvastatin and Simvastatin Acid in Caucasian and Asian Subjects: A Class Effect? .

[38] Thomayant Prueksaritanont; Raju Subramanian; Xiaojun Fang; Bennett Ma; Yue Qiu; Jiunn H. Lin; Paul G. Pearson; Thomas A. Baillie. Glucuronidation of Statins in Animals and Humans: A Novel Mechanism of Statin Lactonization. Drug metabolism and disposition 2002, 30, 505-512.

[39] Jacobsen, W.; Kuhn, B.; Soldner, A.; Kirchner, G.; Sewing, K.; Kollman, P.A.; Benet, L.Z.; Christians, U. Lactonization is the Critical First Step in the Disposition of the 3-Hydroxy-3-Methylglutaryl-Coa Reductase Inhibitor Atorvastatin. Drug Metab. Dispos. 2000, 28, 1369-1378.

[40] Fujino, H.; Saito, T.; Tsunenari, Y.; Kojima, J.; Sakaeda, T. Metabolic Properties of the Acid and Lactone Forms of HMG-CoA Reductase Inhibitors. Xenobiotica 2004, 34, 961-971.

[41] Park, J.-.; Kim, K.-.; Bae, S.K.; Moon, B.-.; Liu, K.-.; Shin, J.-. Contribution of Cytochrome P450 3A4 and 3A5 to the Metabolism of Atorvastatin. Xenobiotica 2008, 38, 1240-1251.

[42] Malhotra, H.S.; Goa, K.L. Atorvastatin: An Updated Review of its Pharmacological Properties and use in Dyslipidaemia. Drugs 2001, 61, 1835-1881.

[43] Ann E. Black; Roger N. Hayes; Bruce D. Roth; Peter Woo; Thomas F. Woolf. Metabolism and Excretion of Atorvastatin in Rats and Dogs. Drug Metabolism and Disposition 1999, 27, 916-923.

[44] Kearney, A.S.; Crawford, L.F.; Mehta, S.C.; Radebaugh, G.W. The Interconversion Kinetics, Equilibrium, and Solubilities of the Lactone and Hydroxyacid Forms of the HMG-CoA Reductase Inhibitor, CI-981. Pharm. Res. 1993, 10, 1461-1465.

[45] Draganov, D.I.; Teiber, J.F.; Speelman, A.; Osawa, Y.; Sunahara, R.; La Du, B.N. Human Paraoxonases (PON1, PON2, and PON3) are Lactonases with Overlapping and Distinct Substrate Specificities. Journal of Lipid Research 2005, 46, 1239-1247.

[46] Furlong, C.E.; Marsillach, J.; Jarvik, G.P.; Costa, L.G. Paraoxonases-1, -2 and -3: What are their Functions? Chemico-biological interactions 2016, 259, 51-62.

[47] Riedmaier, S.; Klein, K.; Winter, S.; Hofmann, U.; Schwab, M.; Zanger, U.M. Paraoxonase (PON1 and PON3) Polymorphisms: Impact on Liver Expression and Atorvastatin-Lactone Hydrolysis. Frontiers in pharmacology 2011, 2, 41.

[48] Pankaj Partani S. Manaswita Verma Sanjay Gurule Arshad Khuroo Tausif Monif. Simultaneous Quantitation of Atorvastatin and its Two Active Metabolites in Human Plasma by Liquid Chromatography/ (-) Electrospray Tandem Mass Spectrometry. Journal of pharmaceutical analysis 2014, 4, 26-36.

[49] Lins, R.L.; Matthys, K.E.; Verpooten, G.A.; Peeters, P.C.; Dratwa, M.; Stolear, J.; Lameire, N.H. Pharmacokinetics of Atorvastatin and its Metabolites After Single and Multiple Dosing in Hypercholesterolaemic Haemodialysis Patients. Nephrology, dialysis, transplantation 2003, 18, 967-976.

[50] Keskitalo, J.; Kurkinen, K.; Neuvonen, P.; Niemi, M. ABCB1 Haplotypes Differentially Affect the Pharmacokinetics of the Acid and Lactone Forms of Simvastatin and Atorvastatin. Clinical pharmacology and therapeutics 2008, 84, 457-461.

[51] Zhang, T. Physiologically Based Pharmacokinetic Modeling of Disposition and Drug–drug Interactions for Atorvastatin and its Metabolites. European Journal of Pharmaceutical Sciences 2015, 77, 216-229.

[52] Rodde, M.S.; Divase, G.T.; Devkar, T.B.; Tekade, A.R. Solubility and Bioavailability Enhancement of Poorly Aqueous Soluble Atorvastatin: In Vitro, Ex Vivo, and in Vivo Studies. Biomed. Res. Int. 2014, 2014, 463895.

[53] Salmani, J.M.; Lv, H.; Asghar, S.; Zhou, J. Amorphous Solid Dispersion with Increased Gastric Solubility in Tandem with Oral Disintegrating Tablets: A Successful Approach to Improve the Bioavailability of Atorvastatin. Pharm. Dev. Technol. 2015, 20, 465-472.

[54] Duan, P.; Duan, P.; Zhao, P.; Zhao, P.; Zhang, L.; Zhang, L. Physiologically Based Pharmacokinetic (PBPK) Modeling of Pitavastatin and Atorvastatin to Predict Drug-Drug Interactions (DDIs). Eur J Drug Metab Pharmacokinet 2017, 42, 689-705.

[55] Rodgers, T.; Leahy, D.; Rowland, M. Physiologically Based Pharmacokinetic Modeling 1: Predicting the Tissue Distribution of Moderate-to-Strong Bases. J. Pharm. Sci. 2005, 94, 1259-1276.

[56] Rodgers, T.; Rowland, M. Physiologically Based Pharmacokinetic Modelling 2: Predicting the Tissue Distribution of Acids, very Weak Bases, Neutrals and Zwitterions. J. Pharm. Sci. 2006, 95, 1238-1257.

[57] Hermann, M.; Bogsrud, M.; Molden, E.; Asberg, A.; Mohebi, B.; Ose, L.; Retterstol, K. Exposure of Atorvastatin is Unchanged but Lactone and Acid Metabolites are Increased several-Fold in Patients with Atorvastatin-Induced Myopathy. Clinical pharmacology and therapeutics 2006, 79, 532-539.

[58] Li, S.; Yu, Y.; Jin, Z.; Dai, Y.; Lin, H.; Jiao, Z.; Ma, G.; Cai, W.; Han, B.; Xiang, X. Prediction of Pharmacokinetic Drug-Drug Interactions Causing Atorvastatin-Induced Rhabdomyolysis using Physiologically Based Pharmacokinetic Modelling. Biomedicine & Pharmacotherapy 2019, 119, 109416.

[59] Morse, B.L.; Alberts, J.J.; Posada, M.M.; Rehmel, J.; Kolur, A.; Tham, L.S.; Loghin, C.; Hillgren, K.M.; Hall, S.D.; Dickinson, G.L. Physiologically-Based Pharmacokinetic Modeling of Atorvastatin Incorporating Delayed Gastric Emptying and Acid-to-Lactone Conversion. CPT: Pharmacometrics & Systems Pharmacology 2019, 8, 664-675.

[60] Shebley, M.; Sandhu, P.; Emami Riedmaier, A.; Jamei, M.; Narayanan, R.; Patel, A.; Peters, S.A.; Reddy, V.P.; Zheng, M.; de Zwart, L. et al. Physiologically Based Pharmacokinetic Model Qualification and Reporting Procedures for Regulatory Submissions: A Consortium Perspective. Clinical pharmacology and therapeutics 2018, 104, 88-110.

[61] Turner, R.M.; Fontana, V.; FitzGerald, R.; Morris, A.P.; Pirmohamed, M. Investigating the Clinical Factors and Comedications Associated with Circulating Levels of Atorvastatin and its Major Metabolites in Secondary Prevention. British journal of clinical pharmacology 2020, 86, 62-74.

[62] Backman, J.T.; Luurila, H.; Neuvonen, M.; Neuvonen, P.J. Rifampin Markedly Decreases and Gemfibrozil Increases the Plasma Concentrations of Atorvastatin and its Metabolites. Clinical pharmacology and therapeutics 2005, 78, 154-167.

[63] Bullman, J.; Nicholls, A.; Van Landingham, K.; Fleck, R.; Vuong, A.; Miller, J.; Alexander, S.; Messenheimer, J. Effects of Lamotrigine and Phenytoin on the Pharmacokinetics of Atorvastatin in Healthy Volunteers. Epilepsia (Copenhagen) 2011, 52, 1351-1358.

[64] Derks, M.; Abt, M.; Parr, G.; Meneses-Lorente, G.; Young, A.; Phelan, M. No Clinically Relevant Drug-Drug Interactions when Dalcetrapib is Co-Administered with Atorvastatin. Expert opinion on investigational drugs 2010, 19, 1135-1145.

[65] Dingemanse, J.; Nicolas, L.; van Bortel, L. Investigation of Combined CYP3A4 Inductive/Inhibitory Properties by Studying Statin Interactions: A Model Study with the Renin Inhibitor ACT-178882. Eur J Clin Pharmacol 2014, 70, 675-684.

[66] Guo, C.; Pei, Q.; Yin, J.; Peng, X.; Zhou, B.; Zhao, Y.; Wu, L.; Meng, X.; Wang, G.; Li, Q. et al. Effects ofGinkgo Bilobaextracts on Pharmacokinetics and Efficacy of Atorvastatin Based on Plasma Indices. Xenobiotica 2012, 42, 784-790.

[67] Hoch, M.; Hoever, P.; Theodor, R.; Dingemanse, J. Almorexant Effects on CYP3A4 Activity Studied by its Simultaneous and Time-Separated Administration with Simvastatin and Atorvastatin. Eur J Clin Pharmacol 2013, 69, 1235-1245.

[68] Hulskotte, E.G.; Feng, H.P.; Xuan, F.; Gupta, S.; van Zutven, M.G.; O'Mara, E.; Wagner, J.A.; Butterton, J.R. Pharmacokinetic Evaluation of the Interaction between Hepatitis C Virus Protease Inhibitor Boceprevir and 3-Hydroxy-3-Methylglutaryl Coenzyme A Reductase Inhibitors Atorvastatin and Pravastatin. Antimicrob. Agents Chemother. 2013, 57, 2582-2588.

[69] Kantola, T.; Kivistö, K.T.; Neuvonen, P.J. Effect of Itraconazole on the Pharmacokinetics of Atorvastatin. Clinical pharmacology and therapeutics 1998, 64, 58-65.

[70] Lau, Y.Y.; Huang, Y.; Frassetto, L.; Benet, L.Z. Effect of OATP1B Transporter Inhibition on the Pharmacokinetics of Atorvastatin in Healthy Volunteers. Clinical pharmacology and therapeutics 2007, 81, 194-204.

[71] Mazzu, A. Itraconazole Alters the Pharmacokinetics of Atorvastatin to a Greater Extent than either Cerivastatin Or Pravastatin. Clinical Pharmacology & Therapeutics 2000, 68, 391.

[72] P. A. Pham; C. J. L. la Porte; L. S. Lee; R. van Heeswijk; J. P. Sabo; M. M. Elgadi; P. J. Piliero; P. Barditch-Crovo; E. Fuchs; C. Flexner et al. Differential Effects of Tipranavir Plus Ritonavir on Atorvastatin Or Rosuvastatin Pharmacokinetics in Healthy Volunteers. Antimicrobial Agents and Chemotherapy 2009, 53, 4385-4392.

[73] Rao, N.; Dvorchik, B.; Sussman, N.; Wang, H.; Yamamoto, K.; Mori, A.; Uchimura, T.; Chaikin, P. A Study of the Pharmacokinetic Interaction of Istradefylline, a Novel Therapeutic for Parkinson's Disease, and Atorvastatin. Journal of clinical pharmacology 2008, 48, 1092-1098.

[74] Shin, J.; Pauly, D.F.; Pacanowski, M.A.; Langaee, T.; Frye, R.F.; Johnson, J.A. Effect of Cytochrome P450 3A5 Genotype on Atorvastatin Pharmacokinetics and its Interaction with Clarithromycin. Pharmacotherapy 2011, 31, 942-950.

[75] Asberg, A.; Hartmann, A.; Fjeldsa, E.; Bergan, S.; Holdaas, H. Bilateral Pharmacokinetic Interaction between Cyclosporine A and Atorvastatin in Renal Transplant Recipients. American journal of transplantation 2001, 1, 382-386.

[76] Derks, M.; Abt, M.; Parr, G.; Meneses-Lorente, G.; Young, A.M.; Phelan, M. No Clinically Relevant Drug-Drug Interactions when Dalcetrapib is Co-Administered with Atorvastatin. Expert Opin. Investig. Drugs 2010, 19, 1135-1145.

[77] Pasanen, M.K.; Fredrikson, H.; Neuvonen, P.J.; Niemi, M. Different Effects of SLCO1B1 Polymorphism on the Pharmacokinetics of Atorvastatin and Rosuvastatin. Clinical pharmacology and therapeutics 2007, 82, 726-733.

[78] Siedlik, P.H.; Olson, S.C.; Yang, B.; Stern, R.H. Erythromycin Coadministration Increases Plasma Atorvastatin Concentrations. Journal of clinical pharmacology 1999, 39, 501-504.

[79] Hermann, M.; Åsberg, A.; Christensen, H.; Holdaas, H.; Hartmann, A.; Reubsaet, J.L.E. Substantially Elevated Levels of Atorvastatin and Metabolites in Cyclosporine-Treated Renal Transplant Recipients. Clinical Pharmacology & Therapeutics 2004, 76, 388-391.

[80] Keskitalo, J.; Zolk, O.; Fromm, M.; Kurkinen, K.; Neuvonen, P.; Niemi, M. ABCG2 Polymorphism Markedly Affects the Pharmacokinetics of Atorvastatin and Rosuvastatin. Clinical pharmacology and therapeutics 2009, 86, 197-203.

[81] Shin, J.; Pauly, D.F.; Pacanowski, M.A.; Langaee, T.; Frye, R.F.; Johnson, J.A. Effect of Cytochrome P450 3A5 Genotype on Atorvastatin Pharmacokinetics and its Interaction with Clarithromycin. Pharmacotherapy 2011, 31, 942-950.

[82] Whitfield, L.R.; Porcari, A.R.; Alvey, C.; Abel, R.; Bullen, W.; Hartman, D. Effect of Gemfibrozil and Fenofibrate on the Pharmacokinetics of Atorvastatin. Journal of clinical pharmacology 2011, 51, 378-388.

[83] de la Peña, A.; Cui, X.; Geiser, J.; Loghin, C. No Dose Adjustment is Recommended for Digoxin, Warfarin, Atorvastatin Or a Combination Oral Contraceptive when Coadministered with Dulaglutide. Clin Pharmacokinet 2017, 56, 1415-1427.

[84] Siedlik, P.H.; Olson, S.C.; Yang, B.; Stern, R.H. Erythromycin Coadministration Increases Plasma Atorvastatin Concentrations. Journal of clinical pharmacology 1999, 39, 501-504.

[85] Rostami-Hodjegan, A.; Tucker, G.T. Simulation and Prediction of in Vivo Drug Metabolism in Human Populations from in Vitro Data. Nature reviews. Drug discovery 2007, 6, 140-148.

[86] Rostami-Hodjegan, A. Physiologically Based Pharmacokinetics Joined with in Vitro-in Vivo Extrapolation of ADME: A Marriage Under the Arch of Systems Pharmacology. Clin. Pharmacol. Ther. 2012, 92, 50-61.

[87] Jamei, M.; Marciniak, S.; Edwards, D.; Wragg, K.; Feng, K.; Barnett, A.; Rostami-Hodjegan, A. The Simcyp Population Based Simulator: Architecture, Implementation, and Quality Assurance. In. Silico Pharmacol. 2013, 1, 9-9. eCollection 2013.

[88] Huang, S.M.; Rowland, M. The Role of Physiologically Based Pharmacokinetic Modeling in Regulatory Review. Clin. Pharmacol. Ther. 2012, 91, 542-549.

[89] Zhao, P.; Zhang, L.; Grillo, J.A.; Liu, Q.; Bullock, J.M.; Moon, Y.J.; Song, P.; Brar, S.S.; Madabushi, R.; Wu, T.C. et al. Applications of Physiologically Based Pharmacokinetic (PBPK) Modeling and Simulation during Regulatory Review. Clin. Pharmacol. Ther. 2011, 89, 259-267.

[90] Zhao, P.; Rowland, M.; Huang, S.M. Best Practice in the use of Physiologically Based Pharmacokinetic Modeling and Simulation to Address Clinical Pharmacology Regulatory Questions. Clin. Pharmacol. Ther. 2012, 92, 17-20.

[91] Poulin, P.; Theil, F.P. Prediction of Pharmacokinetics Prior to in Vivo Studies. 1. Mechanism-Based Prediction of Volume of Distribution. J. Pharm. Sci. 2002, 91, 129-156.

[92] Holtzman, C.W.; Wiggins, B.S.; Spinler, S.A. Role of P-Glycoprotein in Statin Drug Interactions. Pharmacotherapy 2006, 26, 1601-1607.

[93] Boyd, R.A.; Stern, R.H.; Stewart, B.H.; Wu, X.; Reyner, E.L.; Zegarac, E.A.; Randinitis, E.J.; Whitfield, L. Atorvastatin Coadministration may Increase Digoxin Concentrations by Inhibition of Intestinal P-Glycoprotein-Mediated Secretion. J. Clin. Pharmacol. 2000, 40, 91-98.

Chapter 4

A Physiologically Based Pharmacokinetic model for open acid and lactone forms of Atorvastatin and metabolites to Assess the Drug-Gene Interaction with SLCO1B1 Polymorphisms

Javier Reig-López[a,b], Matilde Merino-Sanjuan[a,b], Alfredo García-Arieta[c], Victor Mangas-Sanjuán[a,b]

Affiliation: [a]Department of Pharmacy and Pharmaceutical Technology and Parasitology, University of Valencia. Valencia, Spain. [b]Interuniversity Research Institute for Molecular Recognition and Technological Development, Valencia, Spain. [c]División de Farmacología y Evaluación Clínica, Departamento de Medicamentos de Uso Humano, Agencia Española de Medicamentos y Productos Sanitarios, Calle Campezo 1, Edificio 8, 28022 Madrid, Spain

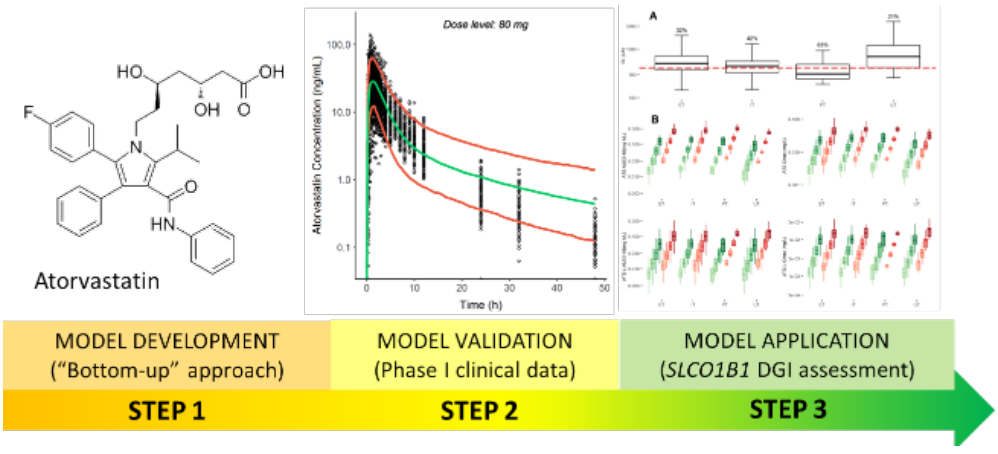

Biomedicine and Pharmacotherapy, 2022 Dec;156:113914

1. INTRODUCTION

Atorvastatin (ATS) is one of the most worldwide prescribed 3-hydroxy-3-methylglutaryl-coenzyme A (HMG-CoA) reductase reversible inhibitors for the treatment of hypercholesterolemia and lowering the cardiovascular risk [1]. ATS chemical characteristics [2], as well as pharmacological [3-5], pharmacokinetics (PK) [6,7], and safety and tolerability [8,9], have been extensively reviewed in the last years. Most common side effects are statin-induced myopathies (SIM), which constitute a heterogeneous clinical manifestation such as muscle weakness, muscle pain (myalgia), muscle tenderness, cramps, and arthralgia, with or without an elevation in serum creatine kinase (CK). The most severe form is rhabdomyolysis, a fatal and life-threating adverse effect that occurs in a very low percentage of treated patients (0.1–8.4/100,000 patients-year) [10]. It has been reported that patients with SIM have increased levels of atorvastatin lactone (ATS-L) ($p < 0.01$) and a 2.3-fold prolonged ATS half-life ($t_{1/2}$) ($p < 0.01$), when compared with patients without muscle related side effects [8].

Physiologically-based pharmacokinetic (PBPK) models integrate experimental (*in vitro* and/or *in vivo*) information together with a scientifically well-founded mechanistic framework of physiological and biological processes using implicit and explicit assumptions by incorporating drug-, system- and trial design-related parameters [11]. The intended use of PBPK models range from first-in-humans (FIH) dose selection and assessment of drug-drug interaction (DDI) to dose extrapolation in special populations (paediatrics, pregnancy, obese, ethnicities, etc.), formulation-related, drug product quality attributes, and food effects [12-14]. More recently, the evaluation of drug-gene interactions (DGIs) and drug-drug-gene interactions (DDGIs) has become a new research field and utility of PBPK models [15]. The exponential growth of PBPK models could be related to its mechanistic conceptualization, the prediction of drug concentrations in multiple unobserved physiological compartments and the more reliable implications of the forward projections of *what-if* or experimentally untested scenarios [11,16,17], which has led to a rapid adoption for drug development applications [13,18] and its recognition by the FDA [19,20] and EMA [21] regulatory authorities.

Recently, several PBPK models of ATS have been published, assessing the PK properties of ATS [22] and its main circulating metabolites 2-hydroxy-atorvastatin (2OH-ATS) and ATS-L [23]. Morse et al. proposed an innovative strategy developing a two-file PBPK model that included ATS and 2OH-ATS (model 1) and ATS-L, ATS, 2-hydrosy-atorvastatin lactone (2OH-ATS-L) and 2OH-ATS (model 2) [24] to account for the time-course of parent and metabolites. However, none of these PBPK models have assessed both ATS-L metabolites (i.e., 2OH-ATS-L and 4-hydroxy-atorvastatin lactone (4OH-ATS-L)) nor considered the administration

of a solid oral dosage form to reproduce its solubility-limited absorption, clinical trial design and real-life administration schedules.

The aims of this work are (i) to develop a full PBPK model for ATS and its metabolites in both, open acid and lactone forms able to predict the observed exposure from Phase I clinical trials and (ii) to quantitatively assess the impact of polymorphisms in *SLCO1B1* on ATS exposure.

2. MATERIALS AND METHODS

The ATS PBPK model was developed in the platform Simcyp® Simulator V19 [25] following a "bottom-up" approach and the "predict, confirm, learn and refine" rationale [13]. *In vitro* and *in vivo* properties of ATS and its metabolites together with the ADME properties of each compound have been extensively characterized in the literature [7], which serve as a scientific basis for the development of the PBPK model. The modelling workflow implemented in the current analysis is depicted in Figure 1. Firstly, a PBPK model of ATS was developed and its prediction ability was assessed with clinical observations after single oral dose administration of 20 mg ATS [26]. Secondly, we developed the ATS-L, 2OH-ATS, 2OH-ATS-L and 4OH-ATS-L model files sequentially and verified model performance globally in each step with observed clinical data by Riedmaier et al [26]. As this observed dataset for model development did not include the metabolite 4-hydroxy atorvastatin (4OH-ATS), this compound was not further assessed. A diagram including the description of the metabolic pathways of ATS, ATS-L and their pharmacologically active metabolites can be found elsewhere [7]. Simulations were conducted using the healthy volunteer population file available in Simcyp® Simulator V19. Model performance was assessed by the prediction error ($Parameter_{predicted}/Parameter_{observed}$) in exposure PK parameters (AUC and C_{max}). Internal model validation was conducted with clinical data from Phase I studies at 40 and 80 mg dose level after single oral dose administration of the calcium salt form of ATS (ATS-Ca) and external validation was performed using steady-state data after one week of daily administrations of 10 mg ATS-Ca in healthy volunteers. The model was also validated through the simulation of clinically relevant DDIs with known cytochrome P450 (CYP) and organic anion-transporting polypeptides (OATPs) inhibitors that have been observed *in vivo*. Finally, the full PBPK model was used to investigate the different ATS exposure regarding the activity of OATP1B1 to quantitatively assess the drug-gene interaction (DGI) between *SLCO1B1* polymorphisms and ATS. The development of each model file as well as their validation and application processes are described in more detail below.

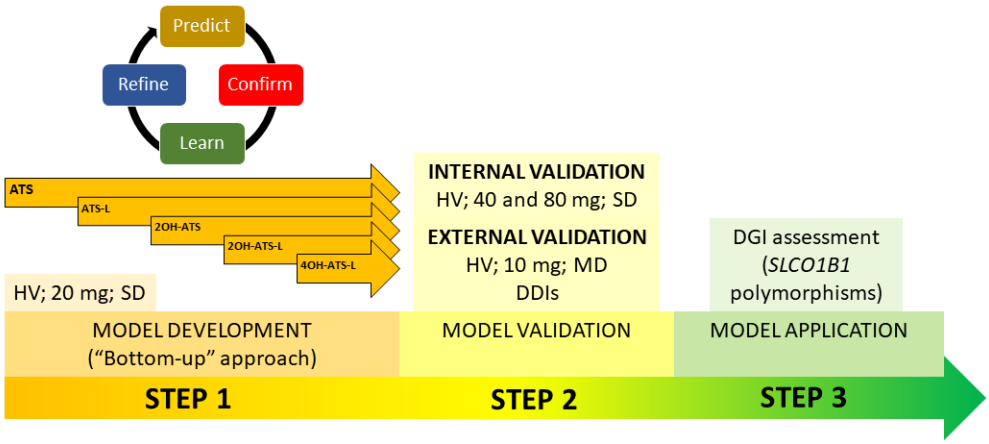

Figure 1. Workflow for the development of the atorvastatin full PBPK model. HV: healthy volunteers; SD: single dose; MD: multiple dose; DDI: drug-drug interaction; DGI: drug-gene interaction.

2.1. Development of ATS model file

The modelling parameters of the ATS model file are listed in Table 1. The model file represents the immediate release solid oral dosage form of ATS-Ca, which is the actual salt included in the commercially available medicines. *In vitro* ATS-Ca dissolution profiles at pH 1 and 6.8 were incorporated to better account for dissolution in the stomach and small intestine, respectively. The Advanced Dissolution, Absorption and Metabolism (ADAM) model already available in Simcyp® was used and the effective permeability in humans ($P_{eff,man}$ = 2.046·10^{-4} cm/s) was predicted from the apparent permeability (P_{app}) determined in Caco-2 cells [27]. Absorption was restricted to the upper part of the gastrointestinal (GI) tract [28], with an extremely low absorption rate at the colon. Efflux processes to the intestinal lumen through breast cancer resistant protein (BCRP) and P-glycoprotein (P-gp), both expressed at the apical side of enterocytes, were also included. A full PBPK distribution model was selected to better assess ATS disposition *in vivo*. Additionally, the permeability limited liver model was used to account for active uptake through OATPs in hepatocytes, which is known to be the rate determining step for ATS elimination [29]. Sodium-taurocholate transporting polypeptide (NTCP) activity was not included as its contribution to the overall active uptake of ATS has been reported to be negligible when compared to that of OATPs [30].

Elimination was assessed enzymatically, involving different CYPs- and UDP-glucuronosyl transferases (UGT)-mediated pathways. CYP-mediated metabolic reactions of ATS included hydroxylation in position 2 (*ortho*-hydroxylation) and 4

(*para*-hydroxylation). However, only 2OH-ATS was tracked as a metabolite as the model development dataset did not contain information about 4OH-ATS. So, development of the 4OH-ATS compound file was no further performed. Inter System Extrapolation Factors (ISEFs) for CYPs pathways were set depending on the *in vitro* system where the determinations were performed, with no parameter optimisation at this point and, thus, increasing model identifiability. Recombinant-expressed human UGT (rUGT) scalars were kept with default values with the exception of UGT1A3 in the liver, which was diminished by 50% to best reproduce observed ATS-L $AUC_{0\text{-}inf}$ at 20 mg. Excretion was incorporated into the model mainly through the bile with an optimized biliary clearance (CL_{bile}) of 50 $\mu L/min/10^6$ cells to reproduce observed $AUC_{0\text{-}inf}$ at 20 mg. Enterohepatic recirculation was allowed with all the biliary excreted ATS being available for reabsorption, as the extent of ATS absorption from the bile remains unknown [31]. Renal excretion contributed minimally to the systemic clearance with a 2% of the reference value of 37.5 L/h [6].

Table 1. Atorvastatin model file parameters.

Parameter	Value	Source
	Physicochemical Properties	
MW (g/mol)	558.64	Drugbank
Compound type	Monoprotic Acid	
logP	5.39	Drugbank
pK_a	4.33	Drugbank
	System-Drug Parameters	
f_u	0.022	[24]
B/P	0.61	[29]
	Absorption	
Model	ADAM	
P_{app} (Caco-2) (10^{-6} cm/s)	8.6	[32]
Reference compound	Propranolol	[32]
Ref. Comp. P_{app} (10^{-6} cm/s)	20.0	[32]
$P_{eff,man}$	2.046	Simcyp predicted
Formulation	Immediate Release	
Dissolution Type	Dissolution profile	
Absorption Scalars	SI Regional	
Absorption Scalar Duodenum	1.000	Default
Absorption Scalar Jejunum I	1.000	Default
Absorption Scalar Jejunum II	1.000	Default
Absorption Scalar Ileum I	1.000	Default
Absorption Scalar Ileum II	1.000	Default
Absorption Scalar Ileum III	1.000	Default
Absorption Scalar Ileum IV	1.000	Default
Absorption Scalar Colon	0.001	Assumed
	Distribution	
Model	Full PBPK	

Table 1. cont.

Parameter	Value	Source
$V_{d,ss}$ (L/kg)	2.945	Simcyp Predicted
Prediction Method	2 (Rodgers and Rowland)	
Kp scalar	1.00	Default
Lipid Binding Scalar	10.476	Simcyp Predicted
	Transport	
Intestine (efflux)		
P-gp J_{max} (pmol/min)	141.00	[33]
P-gp K_m (µM)	115.00	[33]
System	Caco-2	[33]
RAF/REF	0.99	Default
BCRP CL_{int} (µL/min)	6.00	[22]
Liver (passive difussion) (mL/min/10^6 cells)	0.013	Simcyp Predicted
Drug concentration available	Unbound and unionised	
Liver (active uptake; sinusoidal)		
OATP1B1 CL_{int} (µL/min/10^6 cells)	1011.00	Optimized as explained in Section 2.1
OATP1B3 CL_{int} (µL/min/10^6 cells)	718.00	Optimized as explained in Section 2.1
OATP2B7 CL_{int} (µL/min/10^6 cells)	171.00	Optimized as explained in Section 2.1
	Metabolism	
CYP-mediated pathways (Recombinant)		
CYP3A4 V_{max} (pmol/min/pmol) (*ortho*-hydroxylation)	29.30	[34]
CYP3A4 Km (µM) (*ortho*-hydroxylation)	29.70	[34]
System	Baculovirus	
$f_{u,mic}$	1.00	Default
ISEF	0.98	Default
CYP3A4 V_{max} (pmol/min/pmol) (*para*-hydroxylation)	29.80	[34]
CYP3A4 K_m (µM) (*para*-hydroxylation)	25.60	[34]
System	Baculovirus	
$f_{u,mic}$	1.00	Default
ISEF	0.98	Default
CYP3A5 V_{max} (pmol/min/pmol) (*ortho*-hydroxylation)	7.20	[35]
CYP3A5 K_m (µM) (*ortho*-hydroxylation)	54.90	[35]
System	BD SUP	
$f_{u,mic}$	1.00	Default
ISEF	0.24	Default

Table 1. cont.

Parameter	Value	Source
CYP3A5 V_{max} (pmol/min/pmol) (*para*-hydroxylation)	10.40	[35]
CYP3A5 K_m (μM) (*para*-hydroxylation)	42.60	[35]
System	BD SUP	
$f_{u,mic}$	1.00	Default
ISEF	0.24	Default
CYP2C8 V_{max} (pmol/min/pmol) (*para*-hydroxylation)	0.29	[34]
CYP2C8 K_m (μM) (*para*-hydroxylation)	35.90	[34]
System	Baculovirus	
$f_{u,mic}$	1.00	Default
ISEF	0.98	Default
UGT-mediated pathways (Recombinant)		
UGT1A1 V_{max} (pmol/min/mg protein)	120.00	[36]
UGT1A1 K_m (μM)	2.00	[36]
rUGT Scalars (Liver:Intestine:Renal)	1:1:1	Default
UGT1A3 V_{max} (pmol/min/mg protein)	2280.00	[36]
UGT1A1 K_m (μM)	4.00	[36]
rUGT Scalars (Liver:Intestine:Renal)	0.5:1:1	Optimized as explained in Section 2.1
UGT2B7 V_{max} (pmol/min/mg protein)	222.00	[36]
UGT2B7 K_m (μM)	20.00	[36]
rUGT Scalars (Liver:Intestine:Renal)	1:1:1	Default
	Excretion	
$CL_{biliary}$ (μL/min/10^6 cells)	50.00	Optimized as explained in Section 2.1
CL_R (L/h)	0.75	[6]

2.2. Development of ATS-L model file

The ATS-L model file consisted of a refinement of those previously published by Morse et al [24] and Li et al [23]. Physicochemical properties were derived from Morse's model. Enzymatic lactonization via UGTs was implemented within the enterocyte to account for the formation of ATS-L from ATS. The distribution process was modelled with a full PBPK model, setting the Kp scalar to 5 to best predict the reported $V_{d,ss}$ value (141.3 L/kg) [23]. ATS-L elimination was assessed enzymatically through CYP3A4 to form the corresponding hydroxylated forms, i.e.

2OH-ATS-L and 4OH-ATS-L. Additionally, lactone hydrolysis in plasma was implemented optimizing the half-life of this process to best predict ATS-L $AUC_{0\text{-}inf}$ at 20 mg. The final value of 3 min of this process agrees with previously published values [24]. Renal excretion of ATS-L was not implemented because of its lower hydrophilicity when comparing to ATS, which already has a minimal renal clearance. Final model parameters are listed in Table 2.

Table 2. Atorvastatin-lactone model file parameters.

Parameter	Value	Source
	Physicochemical Properties	
MW (g/mol)	540.62	Drugbank
Compound type	Neutral	
logP	6.05	[24]
	System-Drug Parameters	
f_u	0.012	[24]
B/P	1.00	[24]
	Distribution	
Model	Full PBPK	
$V_{d,ss}$ (L/kg)	129.90	Simcyp Predicted
Prediction Method	2 (Rodgers and Rowland)	
Kp scalar	5.00	Optimized as explained in Section 2.2
Lipid Binding Scalar	0.029	Simcyp Predicted
	Metabolism	
CYP-mediated pathways (HLM)		
CYP3A4 V_{max} (pmol/min/mg protein) (*ortho*-hydroxylation)	1397.00	[34]
CYP3A4 K_m (µM) (*ortho*-hydroxylation)	1.60	[34]
$f_{u,mic}$	1.00	Default
CYP3A4 V_{max} (pmol/min/mg protein) (*para*-hydroxylation)	3229.00	[34]
CYP3A4 K_m (µM) (*para*-hydroxylation)	1.80	[34]
$f_{u,mic}$	1.00	Default
ES $t_{1/2}$ (min)	3.00	Optimized as explained in Section 2.2

2.3. Development of 2OH-ATS model file

Model parameterisation of 2OH-ATS is shown in Table 3. Regarding red blood cells and plasma protein binding, we assumed the same values than those assigned to ATS, as no direct determination of these parameters has been found in the literature. The distribution model selected was a minimal PBPK model with a single

adjusting compartment (SAC) volume (V_{sac}) of 0.0032 L/kg. CYP3A4-mediated metabolism of 2OH-ATS was implemented, assuming a CL_{int} of 3.22 μL/min/pmol and an unspecific HLM CL_{int} of 663 μL/min/mg protein [27]. Additionally, biliary and renal excretion of this metabolite was incorporated, assuming equal CL_{bile} and CL_R as for ATS, since preclinical information of this metabolite was available [31] and renal excretion is a possible elimination pathway due to its higher hydrophilicity compared to ATS.

Table 3. 2-hydroxy-atorvastatin model file parameters.

Parameter	Value	Source
Physicochemical Properties		
MW (g/mol)	574.64	[27]
Compound type	Monoprotic Acid	
pK_a	4.33	[27]
logP	5.080	[27]
System-Drug Parameters		
f_u	0.022	Assumed
B/P	0.55	Assumed
Distribution		
Model	Minimal PBPK	
V_{sac} (L/kg)	0.0032	[27]
SAC k_{in} (1/h)	0.0016	[27]
SAC k_{out} (1/h)	2.78	[27]
$V_{d,ss}$ (L/kg)	4.036	Simcyp Predicted
Prediction Method	Method 1 (Poulin)	
Kp scalar	1.00	Default
Metabolism		
CYP-mediated pathways (Recombinant)		
CYP3A4 CL_{int} (mL/min/pmol)	3.22	[27]
$f_{u,mic}$	1.00	Default
Additional HLM CL_{int} (μL/min/mg protein)	663.00	[27]
Excretion		
$CL_{biliary}$ (μL/min/10^6 cells)	50.00	Assumed
CL_R (L/h)	0.75	Assumed

2.4. Development of 2OH-ATS-L model file

The physicochemical properties of 2OH-ATS-L were adapted to the values previously published by Morse et al [24]. A full PBPK model for distribution was selected and a $V_{d,ss}$ of 52 L/kg was predicted when setting the Kp scalar to 2, to best reproduce 2OH-ATS-L C_{max} at 20 mg dose level. As no CYP-mediated metabolism has been determined for this metabolite, elimination was defined through plasma estherases (assuming equal half-life as for ATS-L) and biliary clearance. 2OH-ATS-glucuronide conjugate is an intermediate reaction product of

lactonization as spontaneous cyclization occurs after elimination of the glucuronic moiety [7] and it has been determined in dog bile after oral administration of ATS [31]. For that reason, a CL_{bile} of 10 μL/min/10^6 cells was optimized to best predict its $AUC_{0\text{-}inf}$ at 20 mg dose level. Following the same rationale as with the development of the ATS-L file, no renal clearance was considered for this metabolite. 2OH-ATS-L model file parameters are listed in Table 4.

Table 4. 2-hydroxy-atorvastatin-lactone model file parameters.

Parameter	Value	Source
Physicochemical Properties		
MW (g/mol)	556.64	Drugbank
Compound type	Neutral	
logP	6.05	Assumed
System-Drug Parameters		
f_u	0.012	Assumed
B/P	1.00	Assumed
Distribution		
Model	Full PBPK	
$V_{d,ss}$ (L/kg)	52.002	Simcyp Predicted
Prediction Method	2 (Rodgers and Rowland)	
Kp scalar	2.00	Optimized as explained in Section 2.4
Lipid Binding Scalar	0.029	Simcyp Predicted
Metabolism		
ES $t_{1/2}$ (min)	3.00	Assumed
Excretion		
$CL_{biliary}$ (μL/min/10^6 cells)	10.00	Optimized as explained in Section 2.4

2.5. Development of 4OH-ATS-L model file

The 4OH-ATS-L model file was developed from 2OH-ATS-L, assuming the same physicochemical properties, plasma protein and red blood cell binding. A minimal PBPK distribution model was selected with V_{sac} of 10 L/kg and SAC intercompartment clearance (Q) of 1 L/h to best fit the observed data at 20 mg dose level. 4OH-ATS is the less abundant metabolite of ATS and it is mainly formed after ATS-L *para*-hydroxylation through CYP3A4 and subsequent hydrolysis of the hydroxylated lactone. The rate of *para*-hydroxylation of ATS-L is faster than the *ortho*-hydroxylation of ATS-L [7], but systemic exposure to 2OH-ATS is higher. This prompted us to consider a higher elimination rate of 4OH-ATS-L rather than a deeper distribution of the metabolite to other tissues/organs. In this regard, an optimized unspecific HLM CL_{int} of 4000 μL/min/mg protein and a plasma esterases-mediated hydrolysis $t_{1/2}$ of 2 min reproduced the observed $AUC_{0\text{-}inf}$ at 20 mg dose level. Equal biliary clearance as for 2OH-ATS-L and no renal excretion were considered. Parameterisation of 4OH-ATS-L is listed in Table 5.

Table 5. 4-hydroxy-atorvastatin-lactone model file parameters.

Parameter	Value	Source
	Physicochemical Properties	
MW (g/mol)	556.64	Drugbank
Compound type	Neutral	
logP	6.05	Assumed
	System-Drug Parameters	
f_u	0.012	Assumed
B/P	1.00	Assumed
	Distribution	
Model	Minimal PBPK	
V_{sac} (L/kg)	10	Optimized as explained in Section 2.5
SAC k_{in} (1/h)	0.0003	Optimized as explained in Section 2.5
SAC k_{out} (1/h)	0.001	Optimized as explained in Section 2.5
$V_{d,ss}$ (L/kg)	52.002	Simcyp Predicted
Prediction Method	2 (Rodgers and Rowland)	
Kp scalar	2.00	Assumed
Lipid Binding Scalar	0.029	Simcyp Predicted
	Metabolism	
ES $t_{1/2}$ (min)	2.00	Optimized as explained in Section 2.5
Additional HLM CL_{int} (µL/min/mg protein)	4000.00	Optimized as explained in Section 2.5
	Excretion	
$CL_{biliary}$ (µL/min/10^6 cells)	10.00	Assumed

2.6. Verification of model performance

Single oral dose administration of 20 mg of ATS-Ca to healthy volunteers was tested during model development to assess model accuracy in predicting $AUC_{0\text{-}inf}$ and C_{max} for ATS, ATS-L, 2OH-ATS, 2OH-ATS-L and 4OH-ATS-L. Due to structural limitations of the Simcyp® Simulator, verification of hydroxylated forms of ATS-L (i.e. 2OH-ATS-L and 4OH-ATS-L) were performed independently (two separated, but structurally identical, simulations) as the PBPK platform could only work with one of them as secondary metabolites at a time.

2.7. Internal validation

Single oral dose administration of 40 and 80 mg of ATS-Ca to 500 healthy volunteers (20 trials of 25 individuals each) aged between 20 and 50 years old with a female proportion of 50% was tested to validate the PBPK model developed with clinical observations from Phase I studies. Prediction error in $AUC_{0\text{-}48}$ and C_{max}

was determined for ATS and 2OH-ATS, and simulated versus observed concentration-time profiles were graphically assessed.

2.8. External validation

2.8.1. Predicting the PK at steady state in healthy volunteers

Multiple oral dose (q.d.) administrations during 1 week of 10 mg ATS-Ca to 18 healthy volunteers aged between 30 and 60 years old with a female proportion of 50% were performed to assess model predictions at steady state conditions. Prediction errors in AUC_{last} and C_{max} were computed and compared with clinical observations [37].

2.8.2. Predicting the outcome of DDI clinical trials

To verify the ability of the PBPK model to predict clinically relevant DDIs, different simulations of administration of ATS-Ca with known CYP (itraconazole and clarithromycin) and OATP (rifampicin at a single dose) inhibitors were performed and compared with clinical observations. **Itraconazole** is a known CYP3A4 inhibitor and both ATS and ATS-L are substrates of CYP3A4. The itraconazole model file already available in Simcyp® Simulator was directly used to perform the simulation in 50 healthy volunteers (5 trials of 10 individuals each). The trial design and subject characteristics were kept consistent with clinical observations reported by Kantola et al [38]. To assess the impact of ATS-Ca co-administered with **clarithromycin** (CYP3A4 inhibitor) a simulation of 65 healthy volunteers (5 trials of 13 individuals each) was performed to reproduce clinical observations reported by Shin et al [39], taking the clarithromycin model file directly from the Simcyp® Simulator inhibitors library. Regarding OATP mediated DDI, a simulation of a single dose administration of **rifampicin** (OATP1B1, OATP1B3 and OATO2B1 inhibitor) followed by a single dose of ATS-Ca was simulated in 55 healthy volunteers (5 trials of 11 individuals each), keeping the trial design as well as population characteristics consistent with the paper by Lau et al [40]. No optimisation of K_i values was performed to run the simulations. Prediction errors in PK exposure parameters, AUC and C_{max}, in the presence and absence of the perpetrator ($PK_{paramInh}/PK_{param}$) were computed.

2.9. Application of the PBPK model to assess DGIs

The PBPK model was ultimately applied to quantitatively evaluate the impact of OATP1B1 activity in ATS exposure, as it has been reported that the *SLCO1B1* genotype influences patients' adherence to ATS therapy as well as increases the

risk of SIMs [41]. Since *SLCO1B1* genotyping is not implemented in the Simcyp® Simulator V19, OATP1B1 phenotypes were considered. In this regard, we stratified the ATS exposure for poor (PT), extensive (ET), intermediate (IT) and ultra-rapid (UT) transporters, assuming that the *SLCO1B1*5* variant represents a loss-of-function allele that codifies a low OATP1B1 activity (i.e., PT). This analysis was performed through the simulation of a single oral dose administration of 40 mg of ATS-Ca to 500 individuals (20 trials of 25 individuals each) in the internal validation step.

3. RESULTS

Table 6 shows the exposure PK parameters for all the metabolites in both PBPK model development (20 mg dose) and validation (10, 40 and 80 mg dose) steps. Prediction error of AUC and C_{max} of ATS, ATS-L, 2OH-ATS-L and 4OH-ATS-L fell within the 2-fold range in all cases. Simulated concentration-time profiles *versus* observations for ATS, ATS-L, 2OH-ATS-L and 4OH-ATS-L can be found in the Supplementary Material. Additionally, the model was able to properly describe ATS exposure at steady state conditions after the administration of 10 mg q.d. for one week. However, the exposure predictions for 2OH-ATS were lower than those observed after 20, 40 and 80 mg dose administration with mean fold errors of 0.6 for AUC and 0.3 for C_{max}. At steady state conditions, model accuracy in the prediction of 2OH-ATS C_{max} increased up to 0.72, while maintaining the prediction error of 0.6 for AUC.

Table 6. Predicted and observed AUC and C_{max} for ATS, ATS-L, 2OH-ATS, 2OH-ATS-L and 4OH-ATS-L in each model development step.

	Analyte	Dose	Regimen	AUC_{obs}	AUC_{pred}	PE	$C_{max,obs}$	$C_{max,pred}$	PE
Model development	**ATS**	*20*	*SD*	26.3[a]	34.9[b]	1.33	6.2[c]	5.4[d]	0.87
	ATS-L	*20*	*SD*	21.9[a]	19.6[b]	0.89	1.5[c]	2.5[d]	1.67
	2OH-ATS	*20*	*SD*	29.8[a]	17.1[b]	0.57	3.9[c]	1.3[d]	0.33
	2OH-ATS-L	*20*	*SD*	34.1[a]	37.2[b]	1.01	2.4[c]	1.9[d]	0.79
	4OH-ATS-L	*20*	*SD*	7.0[a]	10.1[b]	1.44	0.2[c]	0.2[d]	1.05
Internal validation	**ATS**	*40*	*SD*	50.0[e]	79.0[e]	1.58	14.0[f]	15.0[f]	1.07
	2OH-ATS	*40*	*SD*	62.0[e]	35.0[e]	0.56	10.0[f]	3.0[f]	0.30
	ATS	*80*	*SD*	130.0[e]	157.0[e]	1.21	34.0[f]	29.0[f]	0.85
	2OH-ATS	*80*	*SD*	157.0[e]	82.0[e]	0.52	27.0[f]	7.0[f]	0.26
External validation	**ATS**	*10*	*MD*	26.0[g]	22.5[g]	0.86	3.5[h]	4.1[h]	1.17
	2OH-ATS	*10*	*MD*	14.0[g]	9.0[g]	0.64	1.1[h]	0.8[h]	0.73

Dose (mg); AUC (ng·h/mL); C_{max} (ng/mL); PE: prediction error; [a]: $AUC_{0\text{-}inf}$ for the wild type *1/*1; [b]: $AU_{C0\text{-}inf}$ for a population representative; [c]: C_{max} for the wild type *1/*1; [d]: C_{max} for a population representative; e: $AUC_{0\text{-}48}$ geometric mean value; [f]: C_{max} geometric mean value; [g]: $AUC_{0\text{-}24}$ for the las dose mean value; [h]: C_{max} for the last dose mean value.

Figure 2 shows the simulated mean, 5th and 95th percentiles profiles as well as observed data from Phase I clinical trials at 40 and 80 mg dose levels.

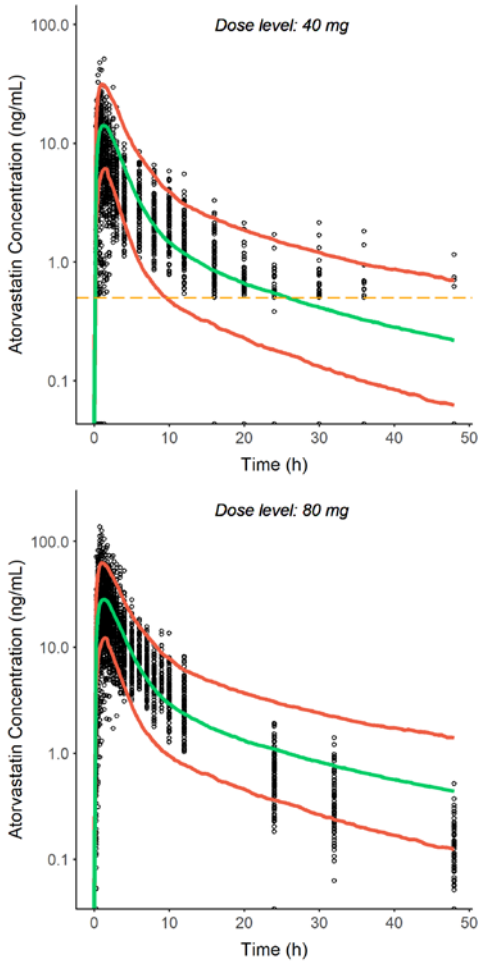

Figure 2. Plasma concentration-time profiles after the administration of ATS-Ca to healthy volunteers. Green line represents the median profile of all simulated individuals; red lines represent the 5th and 95th percentiles of the simulated individuals; circles represent observed data. The low limit of quantification of ATS was 0.5 ng/mL (orange dotted line).

The ATS PBPK model was able to properly describe clinically relevant DDIs with both CYP3A4 and OATPs inhibitors. Table 7 summarizes the observed and predicted ATS and ATS-L AUC and C_{max} ratios as well as the corresponding prediction error. According to these results, the mechanisms involved in the metabolic processes linked to CYP3A4 (perturbed by itraconazole and clarithromycin) are adequately characterized for both ATS and ATS-L, since the prediction errors are between 0.66 and 1.45. On the other hand, there is a slight underprediction of ATS exposure in the presence of OATP inhibitors (rifampicin),

although the results obtained are within the accepted range (0.61 and 0.79 for AUC and C_{max}, respectively). This outcome demonstrates the validity of the role played by this transporter as an uptake carrier in the elimination of ATS with the current PBPK framework. Simulation details of the DDI trials *in silico* performed, PK profiles of ATS alone and in the presence of these perpetrators and changes in the fraction metabolised through CYP3A4 are reported in the Supplementary Material of this publication.

Table 7. Predicted versus observed changes in AUC and C_{max} of ATS and ATS-L after concomitant administration of different perpetrators of DDIs.

***Perpetrator* / Victim**	**AUC ratio**			**C_{max} ratio**		
	Observed	Predicted	Ratio P/O	Observed	Predicted	Ratio P/O
Itraconazole						
ATS	3.31[a]	2.20[a]	0.66	1.2[c]	1.19[c]	0.99
	3.11[b]	2.08[b]	0.67			
ATS-L	3.98[a]	3.84[a]	0.96	2.26[c]	2.72[c]	1.20
	4.11[b]	3.85[b]	0.94			
Rifampicin						
ATS	7.25[a]	5.74[a]	0.79	10.46[c]	6.35[c]	0.61
Clarithromycin						
ATS	3.08[d]	2.90[d]	0.94	2.16[e]	1.89[e]	0.88
ATS-L	2.67[d]	3.86[d]	1.45	1.5[e]	2.04[e]	1.36

[a]: for $AUC_{0\text{-}inf}$ mean values; [b]: for $AUC_{0\text{-}72}$ mean values; [c]: for C_{max} mean values; [d]: for $AUC_{0\text{-}48}$ geometric mean values; [e]: for C_{max} geometric mean values

The impact of OATP1B1 activity on ATS CL, AUC and C_{max} is shown in Table 8. The analysis revealed a statistically significant difference in ATS CL ($p < 0.01$), as PT have a 30% lower clearance than ET individuals. Consequently, ATS AUC and C_{max} are increased by 40 and 33% ($p < 0.05$), respectively, in individuals carrying the *SLCO1B1*5* allele. Figure 3A shows the CL distribution values regarding OATP1B1 activity among the population simulated, showing that patients with lower CL than the CL threshold (414.67 L/h) estimated through a population PK analysis could be at higher risk of suffering muscle discomfort [1]. The clinical impact of OATP1B1 phenotypes on exposure endpoints (AUC and C_{max}) of ATS and ATS-L at 80 mg dose level is depicted in Figure 3B. The corresponding plots after single dose administration of 10, 20 and 40 mg ATS-Ca are provided in the Supplementary Material.

Table 8. Comparison of ATS exposure in extensive (ET) and poor (PT) transporters for OATP1B1 activity at 40 mg dose level.

PK param\Phenotype	ET (wild type)	PT (*SLCO1B1*5*)	Fold change[a]	p-value[b]
AUC_{0-48} (ng·h /mL)	86.77	121.60	1.40	< 0.05
C_{max} (ng/mL)	15.68	20.86	1.33	< 0.05
CL (L/h)	593.47	414.36	0.70	< 0.01
N (%)	304 (60.8)	16 (3.2)	-	-

[a]: fold change in AUC_{0-48}, C_{max} and CL was kept at 10, 20 and 80 mg dose levels; [b]: statistical significance in the differences was kept at 10, 20 and 80 mg dose levels. N: number of individuals with the corresponding phenotype.

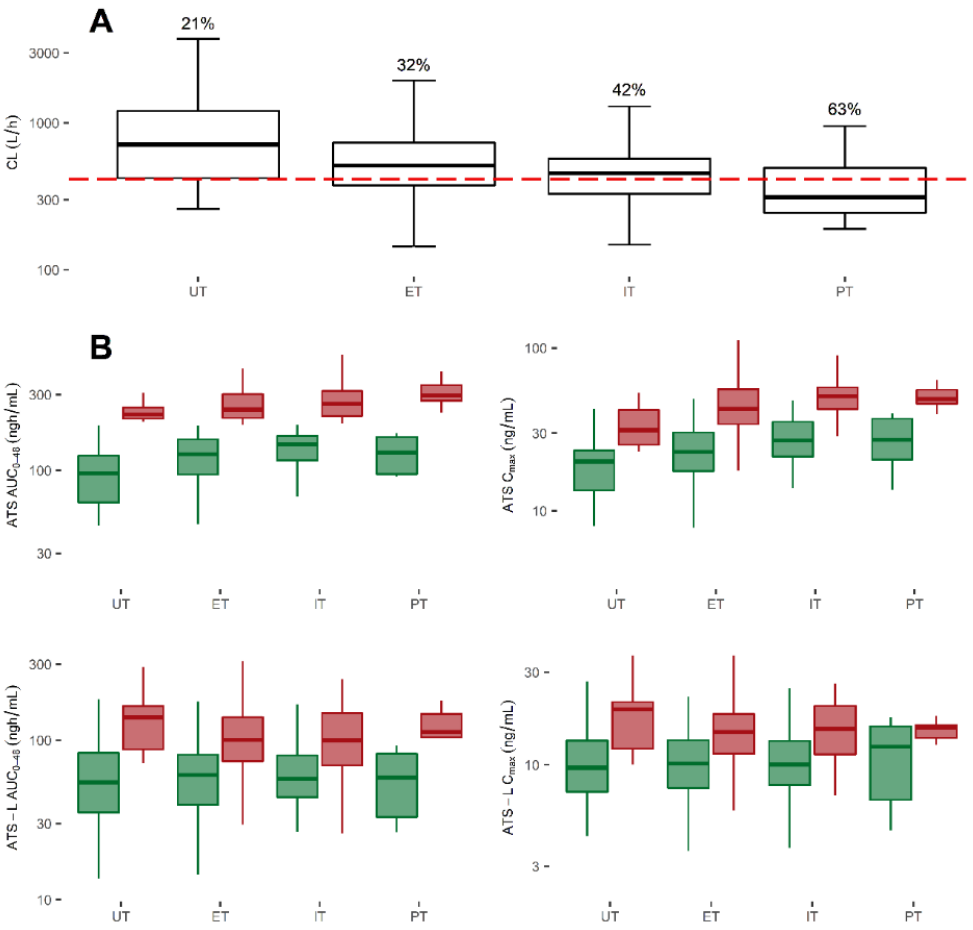

Figure 3. Clearance, AUC and C_{max} distribution values regarding OATP1B1 phenotype in the simulated population. A: Clearance distribution regarding OATP1B1 phenotype. Red dashed line indicates the CL threshold of 414.67 L/h. The percentage of patients at risk of suffering muscle discomfort is indicated

above each box; B: ATS and ATS-L AUC (left plots) and C_{max} (right plots) distribution values regarding OATP1B1 phenotype. Green boxes indicate patients with ATS CL above 414.67 L/h; red boxes indicate patients with ATS CL below 414.67 L/h; exposure shown for the 80 mg dose level. ET: Extensive transporter; IT: Intermediate transporter; PT: Poor transporter; UT: Ultra-rapid transporter.

4. DISCUSSION

The PBPK model here presented can describe within a 2-fold prediction error the exposure metrics, C_{max} and AUC, of ATS and its metabolites ATS-L, 2OH-ATS-L and 4OH-ATS-L, after single dose administration of 20, 40 and 80 mg and multiple administrations of 10 mg of ATS-Ca once daily for one week.

As AUC and C_{max} of ATS increase more than proportionally in the dose range from 0.5 to 80 mg/day [6], these results suggest good model performance, since AUC (1.33, 1.58 and 1.21) and C_{max} (0.87, 1.07 and 0.85) prediction errors at 20, 40 and 80 mg dose levels are randomly distributed within the accepted range (0.5-2).

The PBPK framework was able to characterize ATS-L observed data with prediction errors of 0.89 and 1.67 for AUC and C_{max}, respectively. It has to be noted that lactonization has only been assessed enzymatically through UGTs. Pre-systemic lactonization due to the low pH in the stomach has not been incorporated into the model due to structural limitations of the Simcyp® Simulator, as only one formation pathway can work at a time. For this reason, we did not account for ATS-L absorption in ATS-L model file. Hydroxylated ATS-L metabolites (i.e., 2OH-ATS-L and 4OH-ATS-L) were also well characterized by the model, with prediction errors of 1.01 and 1.44 for AUC and 0.79 and 1.05 for C_{max}, respectively. As they are directly formed after CYP-mediated hydroxylation of ATS-L, these results suggest that considering enzymatic lactonization as the main, but not the only, pathway of ATS-L formation is a good approximation to global ATS PK.

It had been previously suggested that the main formation pathway of hydroxylated metabolites of ATS (i.e., 2OH-ATS and 4OH-ATS) is the ATS lactonization, CYP-mediated hydroxylation and subsequent hydrolysis of the hydroxylated isomers of ATS-L [7]. Direct hydroxylation of ATS would run simultaneously to this metabolic route but playing a minor role in overall ATS elimination. In this sense, we directly used V_{max} values for CYP3A4-, CYP3A5- and CYP2C8-mediated hydroxylation after adjustment with the corresponding ISEF regarding the *in vitro* system used. It is not surprising, therefore, that exposure to 2OH-ATS is not accurately predicted by our model, with AUC and C_{max} prediction errors of 0.57 and 0.33, respectively, at 20 mg dose level. These results were also observed at higher dose levels in the same magnitude (see Table 6) and differed from those reported by Zhang et al [27]. However, it must be noted that these

authors increased CYP3A4 ISEF up to 7 and CYP2C8 ISEF up to 4 to reproduce the observed 2OH-ATS exposure. In our case, the PBPK model has not been optimized, and the validated ISEFs have been used directly for each CYP isoform.

Successful external validation of the PBPK model with observed data after daily administration of 10 mg ATS-Ca for one week was achieved, with ATS prediction errors of 0.87 and 1.17 for AUC and C_{max}, respectively. To the best of our knowledge, this is the first time that an ATS PBPK model can predict ATS exposure at steady state conditions, thus suggesting good model parameterization and performance. For 2OH-ATS, the PBPK model adequately predicted the exposure in the external validation step, with prediction errors for AUC and C_{max} of 0.64 and 0.72, respectively. The prediction error in AUC at 10 mg after a multiple dose regimen (0.64) is close to the prediction errors obtained after single dose regimen at 20 (0.57), 40 (0.56), and 80 mg (0.52), but the C_{max} prediction after 10 mg ATS daily improved (0.73) compared to single dose regimens (0.33, 0.30, and 0.26), which may be due to a combination of factors: (i) the less sensitivity of C_{max} steady-state observations to detect differences in the absorption process, and (ii) the lower amount of ATS within the enterocyte that favours linear conditions more than at higher dose levels, increasing the lactonization process over CYP-mediated hydroxylation, thus leading to lower C_{max} levels of 2OH-ATS.

As previously mentioned, ATS is a substrate CYP450 [31,35] and special care should be taken during the concomitant administration of substrates and/or inhibitors of this metabolic pathway [42]. Additionally, ATS is also a substrate of the OATPs family [30] and P-gp [33]. In this regard, many efforts had been made to assess the impact of concomitant medications on ATS exposure as a consequence of DDI at metabolic [38,43-45] and/or transporter levels [46-48]. Overall, the model can also predict increases in both, ATS and ATS-L exposures, when co-administered with CYP or OATP inhibitors, thus increasing its performance. Predicted ratios when co-administering ATS with itraconazole or clarithromycin (CYP3A4 inhibitors) suggest that increases in ATS exposure mainly originated from the plasma hydrolysis of the increased levels of circulating ATS-L due to the metabolism inhibition caused by the DDI. This back-conversion to the parent drug has been recommended when modelling ATS [7] and is consistent with the stability of the lactone in plasma [49].

It has been reported that ATS intrinsic uptake clearance is 1900 mL/min/10^6 cells [23] and that the relative contribution to overall uptake clearance is OATP1B1 (52.5%) > OATP1B3 (35%) >> OATP2B1 (8.75%) > NTCP (3.75%) [47]. However, NTCP contribution was negligible when compared to those OATPs. Consequently, OATPs relative contribution was set to 53.2, 37.8 and 9% for OATP1B1, OATP1B3 and OATP2B1, respectively, with no contribution of NTCP.

Good prediction of the DDI between ATS and rifampicin by this model structure justifies the assignment of the relative contribution of each OATP to overall uptake clearance.

The probability of suffering a drug-related adverse event increases as the number of medicines taken by patients does, as inhibition/induction of metabolic routes and/or transport processes can be altered by concomitant medications. Additionally, other factors such as age, renal function, comorbidities, and genetic variation also play a crucial role in the development of adverse effects. In this sense, the presence of polymorphisms in genes codifying transporters or metabolic enzymes involved in drug absorption or disposition processes may represent a relevant area of research in order to explain possible drug-related adverse effects. [50]. PBPK modelling merges system- and drug-related parameters with clinical trial designs, revealing itself as a powerful tool for assessing not only DDIs, but also DGIs [15]. In this work we have applied a full PBPK model of ATS to quantify the impact of different OATP1B1 phenotypes in ATS exposure and confirmed that poor transporter (carrying *SLCO1B1*5* allele) patients are at higher risk of suffering SIMs due to 30% lower clearance compared to extensive transporter patients, which is in line with the 2.3-fold longer ATS half-life observed in patients suffering SIMs [8]. This result is consistent with the reported hazard ratio of 1.4 (95% CI: 1.1-1.7, p = 0.02) for suffering SIMs and could explain the treatment discontinuation among these patients (odds ratio 1.67, p = 0.0001) observed in the context of routine clinical care [41]. Additionally, it has been reported that patients with ATS apparent clearance (CL/F) values below 414.67 L/h are at increased risk for suffering muscle discomfort [1] and that the prevalence of mild myalgia among patients taking statins ranges from 0.3-33% [10]. Our model predictions reveal that 34.8% of patients have an apparent clearance lower than 414.67 L/h and increased ATS and ATS-L exposure. Among these patients, the most affected are PT as 63% would be at risk of SIMs and the probability of muscle discomfort would decrease as OATP1B1 activity increases (IT, 42%; ET, 32%; UT, 21%) (Figure 3A). In this regard, patients at higher risk of suffering muscle discomfort (CL/F ≤ 414.67 L/h) would have 2.2- and 1.76-fold (p < 0.0001) higher ATS and ATS-L AUC, respectively (Figure 3B).

The PBPK model has some limitations that the authors realise and must be mentioned to avoid a misinterpretation of both, model parameterisation and results. In this regard, the PBPK framework does not account for all ATS active metabolites, as 4OH-ATS has not been modelled and 2OH-ATS model predictions are not accurately predicted due to a structural limitation in the PBPK platform, as only one second-generation metabolite can be modelled from the substrate and our proposal is to consider it as a third-generation metabolite mainly formed after

the hydrolysis of 2OH-ATS-L. Thus, extending the model to a PBPK/PD structure that could predict the lipid-lowering effect of ATS would not be feasible at the moment. Additionally, the model does not implement pre-systemic lactonization of ATS due to the low pH in the stomach because the Simcyp® Simulator V19 does not allow to track of a metabolite from an endogenous and exogenous pathway at a time. Notwithstanding, our work deepens in mechanistic processes that govern ATS PK, highlights the importance of enzymatic lactonization and predicts a higher probability of suffering muscle discomfort due to an approximately 2-fold increase in ATS and ATS-L exposure. The impact of *SLCO1B1* polymorphisms to predict muscle toxicity is highly dependent on the CL/F threshold considered (414.67 L/h) and, therefore, prospective analyses are encouraged to evaluate the relevance of PK endpoints on muscle toxicity. Clinical evidence would be highly appreciated to externally validate model predicted exposures in *SLCO1B1* polymorphisms after ATS administration.

5. CONCLUSIONS

The developed PBPK model was able to mechanistically characterize the exposure metrics of ATS, ATS-L, 2OH-ATS-L and 4OH-ATS-L at different dose levels and after single and multiple dose regimens after oral administration of ATS-Ca. The external validation through the successful prediction of the clinically relevant DDI between ATS and itraconazole, clarithromycin and rifampin endorses the role of the metabolic and transporters pathways here proposed. The model has been also applied to quantitatively assess the DGI between ATS and *SLCO1B1*5*, which originates a 30% decrease in mean ATS clearance when compared to the wild type. As a consequence of this interaction, 63% of patients with the PT phenotype (codified by *SLCO1B1*5*) could be at a higher risk of suffering muscle discomfort because of an apparent clearance below the previously reported value of 414.67 L/h. Using this cut-off we have been able to mechanistically predict the exposure change to ATS and ATS-L resulting in a 2.2- and 1.76-fold increase in AUC, respectively.

Despite more data are needed to validate model predictions in the different phenotypes for OATP1B1, the model here presented can anticipate an exposure-safety relationship between ATS and/or ATS-L and muscle-related adverse events from the mechanistical point of view of physiologically based pharmacokinetics.

Acknowledgements

The authors want to express their gratitude to Certara UK Limited (Simcyp Division) for granting free access to the Simcyp® Simulator through an academic

license agreement (subject to conditions). JRL wants to thank NS for providing language help and writing assistance.

References:

[1] G. Stillemans, A. Paquot, G. G. Muccioli, et al. Atorvastatin population pharmacokinetics in a real-life setting: Influence of genetic polymorphisms and association with clinical response. Clinical Translational Sci. 15 (2021) 667. https://doi.org/10.1111/cts.13185

[2] Michael Schachter. Chemical, pharmacokinetic and pharmacodynamic properties of statins: an update. https://doi.org/10.1111/j.1472-8206.2004.00299.x

[3] H. S. Malhotra and K. L. Goa. Atorvastatin: An Updated Review of its Pharmacological Properties and Use in Dyslipidaemia. Drugs. 61 (2001) 1835-81. https://doi.org/10.2165/00003495-200161120-00012

[4] C. R. Sirtori. The pharmacology of statins. Pharmacological research. 88 (2014) 3-11. https://doi.org/10.1016/j.phrs.2014.03.002

[5] A. Poli. Atorvastatin: Pharmacological Characteristics and Lipid-Lowering Effects. Drugs. 67 (2007) 3-15. https://doi.org/10.2165/00003495-200767001-00002

[6] H. Lennernas. Clinical pharmacokinetics of atorvastatin. Clin.Pharmacokinet. 42 (2003) 1141-60. https://doi.org/42135 [pii]

[7] J. Reig-López, A. García-Arieta, V. Mangas-Sanjuán and M. Merino-Sanjuán. Current Evidence, Challenges, and Opportunities of Physiologically Based Pharmacokinetic Models of Atorvastatin for Decision Making. Pharmaceutics. 13 (2021) 709. https://doi.org/10.3390/pharmaceutics13050709

[8] M. HERMANN, M. BOGSRUD, E. MOLDEN, et al. Exposure of atorvastatin is unchanged but lactone and acid metabolites are increased several-fold in patients with atorvastatin-induced myopathy. Clinical pharmacology and therapeutics. 79 (2006) 532-9. https://doi.org/10.1016/j.clpt.2006.02.014

[9] V. G. Athyros, K. Tziomalos, A. Karagiannis and D. P. Mikhailidis. Atorvastatin: safety and tolerability. Expert opinion on drug safety. 9 (2010) 667-74. https://doi.org/10.1517/14740338.2010.495385

[10] P. du Souich, G. Roederer and R. Dufour. Myotoxicity of statins: mechanism of action. Pharmacology & therapeutics (Oxford). 175 (2017) 1-16. https://doi.org/10.1016/j.pharmthera.2017.02.029

[11] S. Frechen and A. Rostami-Hodjegan. Quality Assurance of PBPK Modeling Platforms and Guidance on Building, Evaluating, Verifying and Applying PBPK Models Prudently under the Umbrella of Qualification: Why, When, What, How and By Whom? Pharm Res. 1 (123456789) https://doi.org/10.1007/s11095-022-03250-w

[12] P. J. Kilford, K. Chen, K. Crewe, et al. Prediction of CYP-mediated DDIs involving inhibition: Approaches to address the requirements for system qualification of the Simcyp Simulator. CPT: pharmacometrics and systems pharmacology. 00 (2022) 1. https://doi.org/10.1002/psp4.12794

[13] M. Shebley, P. Sandhu, A. Emami Riedmaier, et al. Physiologically Based Pharmacokinetic Model Qualification and Reporting Procedures for Regulatory Submissions: A Consortium Perspective. Clinical pharmacology and therapeutics. 104 (2018) 88-110. https://doi.org/10.1002/cpt.1013

[14] E. Tsakalozou, K. Alam, A. Babiskin and L. Zhao. Physiologically-Based Pharmacokinetic Modeling to Support Determination of Bioequivalence for Dermatological Drug Products: Scientific and Regulatory Considerations. Clin.Pharmacol.Ther. 111 (2022) 1036-49. https://doi.org/10.1002/cpt.2356 [doi]

[15] J. Wojtyniak, D. Selzer, M. Schwab and T. Lehr. Physiologically Based Precision Dosing Approach for Drug-Drug-Gene Interactions: A Simvastatin Network Analysis. Clin. Pharmacol. Ther. 109 (1201) 201. https://doi.org/10.1002/cpt.2111

[16] W. Lin, Y. Chen, J. D. Unadkat, X. Zhang, D. Wu and T. Heimbach. Applications, Challenges, and Outlook for PBPK Modeling and Simulation: A Regulatory, Industrial and Academic Perspective. Pharmaceutical research. 1 (2022) https://doi.org/10.1007/s11095-022-03274-2

[17] A. Rostami-Hodjegan. Physiologically based pharmacokinetics joined with in vitro-in vivo extrapolation of ADME: a marriage under the arch of systems pharmacology. Clin.Pharmacol.Ther. 92 (2012) 50-61. https://doi.org/10.1038/clpt.2012.65 [doi]

[18] E. El-khateeb, S. Burkhill, S. Murby, H. Amirat, A. Rostami-hodjegan and A. Ahmad. Physiological-based pharmacokinetic modeling trends in pharmaceutical drug development over the last 20-years; in-depth analysis of applications, organizations, and platforms. Biopharm Drug Dispos. 42 (2021) 107. https://doi.org/10.1002/bdd.2257

[19] Anonymous Physiologically Based Pharmacokinetic Analyses - Format and Content Guidance for Industry. US Official News. (2018)

[20] Anonymous The Use of Physiologically Based Pharmacokinetic Analyses--Biopharmaceutics Applications for Oral Drug Product Development, Manufacturing Changes, and Controls; Draft Guidance for Industry; Availability. The Federal Register / FIND. 85 (2020) 61953.

[21] Anonymous Guideline on the reporting of physiologically based pharmacokinetic (PBPK) modelling and simulation. European Union News. (2019)

[22] P. Duan, P. Duan, P. Zhao, P. Zhao, L. Zhang and L. Zhang. Physiologically Based Pharmacokinetic (PBPK) Modeling of Pitavastatin and Atorvastatin to Predict Drug-Drug Interactions (DDIs). Eur J Drug Metab Pharmacokinet. 42 (2017) 689-705. https://doi.org/10.1007/s13318-016-0383-9

[23] S. Li, Y. Yu, Z. Jin, et al. Prediction of pharmacokinetic drug-drug interactions causing atorvastatin-induced rhabdomyolysis using physiologically based pharmacokinetic modelling. Biomedicine & Pharmacotherapy. 119 (2019) 109416. https://doi.org/10.1016/j.biopha.2019.109416

[24] B. L. Morse, J. J. Alberts, M. M. Posada, et al. Physiologically-Based Pharmacokinetic Modeling of Atorvastatin Incorporating Delayed Gastric Emptying and Acid-to-Lactone Conversion. CPT: Pharmacometrics & Systems Pharmacology. 8 (2019) 664-75. https://doi.org/10.1002/psp4.12447

[25] Certara UK (Simcyp Division). Simcyp Simulator. v19 (2020)

[26] S. Riedmaier, K. Klein, U. Hofmann, et al. UDP-Glucuronosyltransferase (UGT) Polymorphisms Affect Atorvastatin Lactonization In Vitro and In Vivo. Clin Pharmacol Ther. 87 (2009) 65. https://doi.org/10.1038/clpt.2009.181

[27] T. Zhang. Physiologically based pharmacokinetic modeling of disposition and drug–drug interactions for atorvastatin and its metabolites. European Journal of Pharmaceutical Sciences. 77 (2015) 216-29. https://doi.org/10.1016/j.ejps.2015.06.019

[28] F. N. Khan and M. H. G. Dehghan. Enhanced Bioavailability and Dissolution of Atorvastatin Calcium from Floating Microcapsules using Minimum Additives. Scientia pharmaceutica. 80 (2012) 215-28. https://doi.org/10.3797/scipharm.1104-26

[29] T. WATANABE, H. KUSUHARA, K. MAEDA, et al. Investigation of the Rate-Determining Process in the Hepatic Elimination of HMG-CoA Reductase Inhibitors in Rats and Humans. Drug metabolism and disposition. 38 (2010) 215-22. https://doi.org/10.1124/dmd.109.030254

[30] A. Vildhede, M. Karlgren, E. K. Svedberg, et al. Hepatic uptake of atorvastatin: influence of variability in transporter expression on uptake clearance and drug-drug interactions. Drug metabolism and disposition. 42 (2014) 1210-8. https://doi.org/10.1124/dmd.113.056309

[31] Ann E. Black, Roger N. Hayes, Bruce D. Roth, Peter Woo and Thomas F. Woolf. Metabolism and Excretion of Atorvastatin in Rats And Dogs. Drug Metabolism and Disposition. 27 (1999) 916-23.

[32] J. Li, D. A. Volpe, Y. Wang, et al. Use of Transporter Knockdown Caco-2 Cells to Investigate the In Vitro Efflux of Statin Drugs. Drug Metab.Dispos. 39 (2011) 1196-202. https://doi.org/10.1124/dmd.111.038075

[33] X. Wu, L. R. Whitfield and B. H. Stewart. Atorvastatin transport in the Caco-2 cell model: contributions of P-glycoprotein and the proton-monocarboxylic acid co-transporter. Pharm.Res. 17 (2000) 209-15. https://doi.org/10.1023/a:1007525616017 [doi]

[34] W. Jacobsen, B. Kuhn, A. Soldner, et al. Lactonization Is the Critical First Step in the Disposition of the 3-Hydroxy-3-Methylglutaryl-Coa Reductase Inhibitor Atorvastatin. Drug Metab.Dispos. 28 (2000) 1369-78.

[35] J. -. Park, K. -. Kim, S. K. Bae, B. -. Moon, K. -. Liu and J. -. Shin. Contribution of cytochrome P450 3A4 and 3A5 to the metabolism of atorvastatin. Xenobiotica. 38 (2008) 1240-51. https://doi.org/10.1080/00498250802334391

[36] T. J. J. Schirris, T. Ritschel, A. Bilos, J. A. M. Smeitink and F. G. M. Russel. Statin Lactonization by Uridine 5′-Diphospho-glucuronosyltransferases (UGTs). Molecular pharmaceutics. 12 (2015) 4048-55. https://doi.org/10.1021/acs.molpharmaceut.5b00474

[37] M. Hermann, A. Åsberg, H. Christensen, H. Holdaas, A. Hartmann and J. L. E. Reubsaet. Substantially elevated levels of atorvastatin and metabolites in cyclosporine-treated renal transplant recipients. Clinical Pharmacology & Therapeutics. 76 (2004) 388-91. https://doi.org/https://doi.org/10.1016/j.clpt.2004.07.008

[38] T. Kantola, K. T. Kivistö and P. J. Neuvonen. Effect of itraconazole on the pharmacokinetics of atorvastatin. Clinical pharmacology and therapeutics. 64 (1998) 58-65. https://doi.org/10.1016/S0009-9236(98)90023-6

[39] J. Shin, D. F. Pauly, M. A. Pacanowski, T. Langaee, R. F. Frye and J. A. Johnson. Effect of Cytochrome P450 3A5 Genotype on Atorvastatin Pharmacokinetics and Its Interaction with Clarithromycin. Pharmacotherapy. 31 (2011) 942-50. https://doi.org/10.1592/phco.31.10.942

[40] Y. Y. Lau, Y. Huang, L. Frassetto and L. Z. Benet. Effect of OATP1B Transporter Inhibition on the Pharmacokinetics of Atorvastatin in Healthy Volunteers. Clinical pharmacology and therapeutics. 81 (2007) 194-204. https://doi.org/10.1038/sj.clpt.6100038

[41] D. Voora, J. Baye, A. Mcdermaid, et al. SLCO1B1*5 Allele is Associated with Atorvastatin Discontinuation and Adverse Muscle Symptoms in the Context of Routine Care. Clin Pharma and Therapeutics. (2022) https://doi.org/10.1002/cpt.2527

[42] M. Igel, T. Sudhop and K. von Bergmann. Metabolism and drug interactions of 3-hydroxy-3-methylglutaryl coenzyme A-reductase inhibitors (statins). Eur J Clin Pharmacol. 57 (2001) 357-64. https://doi.org/10.1007/s002280100329

[43] J. J. Lilja, K. T. Kivistö and P. J. Neuvonen. Grapefruit juice increases serum concentrations of atorvastatin and has no effect on pravastatin. Clin.Pharmacol.Ther. 66 (1999) 118-27. https://doi.org/S0009-9236(99)00102-2 [pii]

[44] J. Shin, D. F. Pauly, M. A. Pacanowski, T. Langaee, R. F. Frye and J. A. Johnson. Effect of Cytochrome P450 3A5 Genotype on Atorvastatin Pharmacokinetics and Its Interaction with Clarithromycin. Pharmacotherapy. 31 (2011) 942-50. https://doi.org/10.1592/phco.31.10.942

[45] I. G. Denisov, J. L. Baylon, Y. V. Grinkova, E. Tajkhorshid and S. G. Sligar. Drug–Drug Interactions between Atorvastatin and Dronedarone Mediated by Monomeric CYP3A4. Biochemistry (Easton). 57 (2018) 805-16. https://doi.org/10.1021/acs.biochem.7b01012

[46] R. A. Boyd, R. H. Stern, B. H. Stewart, et al. Atorvastatin coadministration may increase digoxin concentrations by inhibition of intestinal P-glycoprotein-mediated secretion. J.Clin.Pharmacol. 40 (2000) 91-8. https://doi.org/10.1177/00912700022008612 [doi]

[47] A. Vildhede, M. Karlgren, E. K. Svedberg, et al. Hepatic Uptake of Atorvastatin: Influence of Variability in Transporter Expression on Uptake Clearance and Drug-Drug Interactions. Drug metabolism and disposition. 42 (2014) 1210-8. https://doi.org/10.1124/dmd.113.056309

[48] R. M. Turner, V. Fontana, R. FitzGerald, A. P. Morris and M. Pirmohamed. Investigating the clinical factors and comedications associated with circulating levels of atorvastatin and its major metabolites in secondary prevention. British journal of clinical pharmacology. 86 (2020) 62-74. https://doi.org/10.1111/bcp.14133

[49] Pankaj Partani S. Manaswita Verma Sanjay Gurule Arshad Khuroo Tausif Monif. Simultaneous quantitation of atorvastatin and its two active metabolites in human plasma by liquid chromatography/ (-) electrospray tandem mass spectrometry. Journal of pharmaceutical analysis. 4 (2014) 26-36. https://doi.org/10.1016/j.jpha.2013.09.007

[50] M. A. Malki and E. R. Pearson. Drug-drug-gene interactions and adverse drug reactions. The pharmacogenomics journal. 20 (2020) 355-66. https://doi.org/10.1038/s41397-019-0122-0

Chapter 5

Application of population physiologically based pharmacokinetic modelling to optimize target expression and clearance mechanisms of therapeutic monoclonal antibodies

Javier Reig-Lopez[1,2], Weifeng Tang[3], Carlos Fernandez-Teruel[2], Matilde Merino-Sanjuan[1], Victor Mangas-Sanjuan[1], David W. Boulton[3] and Pradeep Sharma[2]

Affiliation: [1]Pharmacy and Pharmaceutical Technology and Parasitology Department, Faculty of Pharmacy, University of Valencia, Valencia, Spain; [2]Clinical Pharmacology and Quantitative Pharmacology, Clinical Pharmacology and Safety Sciences, R&D, AstraZeneca, Cambridge, UK; [3]Clinical Pharmacology and Quantitative Pharmacology, Clinical Pharmacology and Safety Sciences, R&D, AstraZeneca, Gaithersburg, Maryland, USA

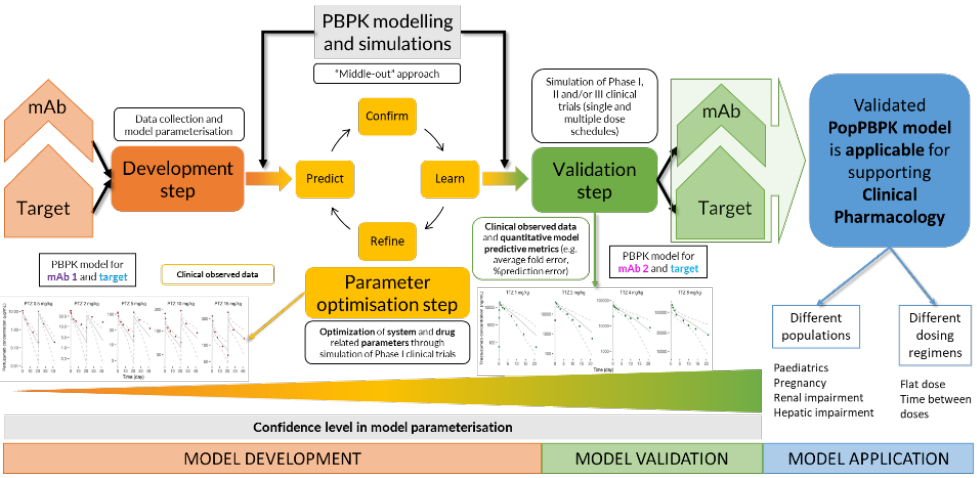

British Journal of Clinical Pharmacology. 2023; 1-12

INTRODUCTION

The activation of transmembrane tyrosine kinases receptors underlies the pathogenesis of many human malignancies [1]. Epidermal growth factor receptor (EGFR) family constitutes a group of four transmembrane receptors involved in signal transduction reactions that regulate cell growth and differentiation [2] and has developed in parallel with the evolution of complex organisms [3]. These four highly related receptors (i.e., HER1/ErbB-1/EGFR, HER2/ErbB-2/neu, HER3/ErbB-3 and HER4/ErbB-4) comprise a cysteine-rich extracellular ligand binding site, a transmembrane lipophilic segment, and an intracellular domain with tyrosine kinase catalytic activity [4]. The large extracellular domains (ECD) of theses receptors constitute an excellent opportunity to target biotherapeutics agents rationally designed to disrupt ligand-induced structural changes or dimerization as well as to selectively deliver cytotoxic drugs to malignant cells, making possible the concept of "magic bullet" proposed by Paul Ehrlich in the 19th century. The receptors are found in a variety of tissues as monomers and can associate with each other after ligand binding to form homodimers (i.e., HERx-HERx) or heterodimers (i.e., HERx-HERy) [2]. A range of growth factors serve as ligands, but none is specific for HER2 [2,3]. For this reason, HER2 is considered as a co-receptor able to heterodimerize (e.g., HER1-HER2) and participate in signal transduction in the absence of a specific ligand [2]. This heterodimerization does not occur randomly and there is a hierarchy that positions HER2 as the preferred dimerization partner [2,5].

Overexpression of EGFR and HER2 could result in reciprocal effects on the trafficking between both receptors [6] and has been associated with cell transformation and tumorigenesis [7]. Increased HER2 expression contributes to cell transformation, anchorage-independent cell growth, increased proliferation and mitogenic sensitivity, as well as tumour cell migration and invasiveness [6]. For example, breast cancers (BC) can have up to 40-100-fold increase in HER2 protein yielding in 2 million receptors expressed at the tumour cell surface [8]. The amplification of the expression of HER2 in BC has been associated with poor prognosis [9,10], shorter disease-free survival and overall survival [11] as well as more aggressive disease [12]. Despite HER2 is almost ubiquitously expressed [6], the difference in HER2 expression levels between normal tissues and tumours helps to target treatments to cancerous cells, thus minimising toxicity [8]. Increased levels of EGFR of an order of magnitude or greater have been found in many human malignancies including lung, head and neck, colorectal, prostate, breast and bladder cancers and correlate with poorer clinical outcome [4,13].

Trastuzumab (TTZ) is a humanized IgG1 monoclonal antibody (mAb) directed to the domain IV of the ECD of the HER2 receptor. TTZ mechanisms of action include

inhibition of HER2 shedding, inhibition of PI3K-AKT pathway, attenuation of cell signalling, antibody-dependent cellular cytotoxicity (ADCC) and inhibition of tumour angiogenesis [14]. Thus, binding of TTZ to HER2 blocks growth-stimulating intracellular signalling, decreases the cellular repair capacity, and possibly improves the apoptosis capacity [15].

Pertuzumab (PTZ), a recombinant humanized IgG1 mAb directed to the domain II of the ECD of HER2, inhibits the formation of HER2 homo- and heterodimers independently of HER2 expression levels without overlapping the binding site of TTZ [16]. Thus, minimising the formation of the most potent signalling HER dimer (i.e., HER2-HER3 heterodimer), PTZ affects key signalling pathways for cell growth and can also activate immune effectors functions such as ADCC because of its extracellular binding location [17].

Cetuximab (CTX) is a chimeric mouse-human mAb directed to the ECD of EGFR. After binding, CTX inhibits ligand-dependent activation of the EGFR thus inhibiting the downstream pathways that cause cell cycle progression, cell growth, and angiogenesis [13] . Additionally, CTX induces internalization and down-regulation of EGFR (leading to signal termination) [18] and initiates immunologic antitumor effects like ADCC [13].

Physiologically based pharmacokinetic (PBPK) modelling and simulation has positioned itself as a valuable tool in the model informed drug discovery and development paradigm in the last years. This modelling technique merges drug- and system-related parameters as well as clinical trial design and allows to virtually assess unexplored scenarios and answer “what-if” questions in the safest, fastest, and cheapest way. However, to get the highest confidence level in the PBPK model predictions that could impact clinical decisions, PBPK models need to be previously verified and subsequently validated, and this process is sometimes accomplished following multiple cycles of “predict, learn and confirm” and can be finally refined with available clinical data to improve model performance and prediction ability [19].

The aim of this work was to apply PBPK modelling and simulation to i) identify the most relevant system and/or drug related parameters in the disposition of EGFR family-directed mAbs and ii) optimise their values to best describe the observed clinical data in cancer patients.

METHODS

Simulations were performed in the PBPK platform Simcyp® Simulator V21R1 following a "middle-out" approach and the "predict, confirm, learn and refine" rationale [19]. Cancer population file already available in the simulator was used in all simulations to better characterise the physiologic changes in these patients. Data collection of physicochemical and pharmacokinetic parameters of PTZ, TTZ and CTX was performed searching in the literature values for molecular weight (MW), isoelectric point (*pI*), net charge, hydrodynamic radius, clearance, bioavailability, neonatal Fc receptor (FcRn) affinity, and binding kinetics to their corresponding targets (e.g., K_D, k_{on}, k_{off}, and k_{int}). In the same way, target abundance and synthesis and degradation rate constants were collected for HER2 and EGFR. Data from Phase I clinical trials were collected from literature to optimise target kinetics and/or mAb disposition processes after single-dose administration of PTZ and CTX to cancer patients overexpressing HER2 or EGFR, respectively. Finally, validation of the optimised biologic and/or target was performed with different datasets from Phase I, II or III clinical trials after single or multiple-dose administration schedules of PTZ, TTZ and CTX. Modelling strategies of PTZ/TTZ-HER2 and CTX-EGFR are described in more detail below.

PBPK modelling of HER2 directed monoclonal antibodies

HER2 target development and validation workflow are illustrated in Figure 1. Firstly, two locations of the receptor were added to the *Cancer* population file to better account for the distribution of this receptor over the body by creating two different targets, i.e., "HER2 tumour" and "HER2 normal tissues". Initial target concentrations (R_{max}) in tumor and normal tissues were set as 0.04 and 0.0016 μM, respectively [20]. Normal tissues expressing HER2 were adipose, bone, brain, gut, heart, kidney, liver, lung, pancreas, muscle, skin, and spleen. As no specific receptor concentration at each tissue has been reported, the concentration was assumed to be equally distributed among them. Then, a full PBPK model for PTZ was developed to describe the PK after single IV infusions of 0.5, 2, 5, 10 and 15 mg/kg to cancer patients overexpressing HER2 in a wide variety of tumour locations (e.g., breast, colorectal, lung, ovarian, pancreas and prostate) [21] with an FcRn-binding as a recycling pathway for PTZ non-specific catabolic clearance modelled in a 1:1 stoichiometry and governed by a K_D value of 0.57 μM [22]. A full TMDD model was incorporated to best describe the observed data (dose-dependent clearance) with k_{on} and k_{off} values of 403.2 $\mu M^{-1} \cdot h^{-1}$ and 3.42 h^{-1}, respectively [23]. A constant option for R_{max} in tumoral and normal tissues was selected. Manual optimisation of HER2 expression was preformed to better describe PTZ exposure after single-dose administration at different dose levels

[21]. Finally, a full PBPK model for TTZ was developed incorporating non-specific catabolic clearance as well as target-mediated clearance through a full TMDD model with k_{on} and k_{off} values of 740 $\mu M^{-1} \cdot h^{-1}$ and 4.07 h^{-1} [20] and a constant option for R_{max}. After optimising HER2 parameterisation in tumour and normal tissues with PTZ PBPK modelling, it was validated by running different simulations after single IV infusions of TTZ at 1, 2, 4, and 8 mg/kg dose levels. Additionally, simulations of multiple IV infusions of PTZ were compared with observed data in Phase I, II, and III clinical trials [24,25] and after sub-cutaneous (SC) single-dose administration to cancer patients [25] as well.

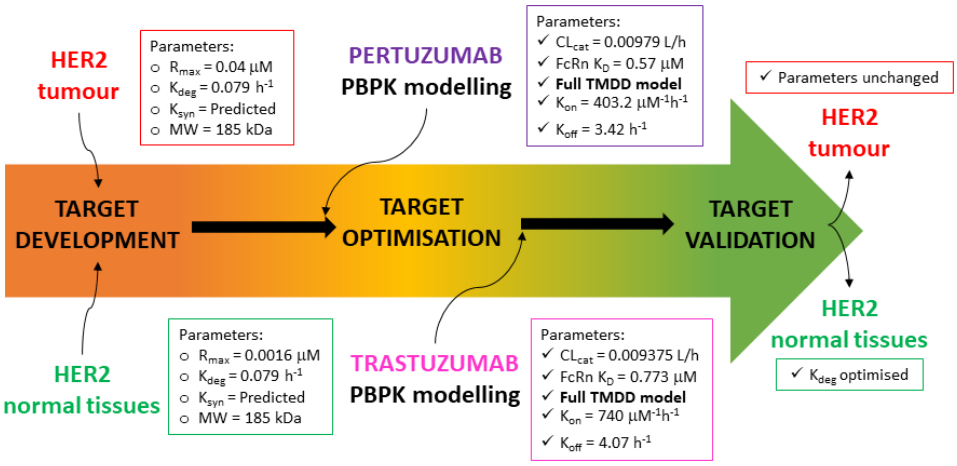

Figure 1: Workflow followed to validate HER2 target through PBPK modelling of PTZ and TTZ. R_{max}: abundance; k_{deg}: degradation rate constant for the target; k_{syn}: target synthesis rate constant ($k_{deg} \cdot R_{max}$); MW: molecular weight; CL_{cat}: non-specific catabolic clearance; FcRn K_D: equilibrium dissociation constant for FcRn-mAb 1:1 complex; TMDD: target-mediated drug disposition; k_{on}: rate constant for binding to the free target; k_{off}: rate constant for dissociation of mAb-target complex.

Numerical validation of PTZ PBPK model was also computed with data from another Phase Ib clinical study [26]. A first-order absorption model for PTZ SC administration was selected and parameterized with k_a and f_a. As no value for f_a has been found in the literature, estimated bioavailability (F) through this route of administration [25] was used instead. Final model parameters for PTZ/TTZ-HER2 PBPK framework are shown in Table 1.

Table 1. Final PBPK model parameters for PTZ/TTZ-HER2 framework.

	Monoclonal Antibody			
	Pertuzumab		Trastuzumab	
Parameter (units)	Value	Reference	Value	Reference
	Physicochemical Properties			
MW (KDa)	148.000	DrugBank	145.531	DrugBank
pI	8.48	[27]	8.39	[27]
Hydrodynamic Radius (nm)	-	Simcyp Predicted	-	Simcyp Predicted
f_u	1	Default	1	Default
B/P	0.55	Default	0.55	Default
	Absorption			
F_a	0.712	[25]	-	-
k_a (h^{-1})	0.0145	[25]	-	-
	Distribution			
Model	Full PBPK		Full PBPK	
K_{rc1}	16.7	Default	16.7	Default
K_D FcRn (μM)	0.57	[22]	0.773	[28]
	Elimination			
CL_{cat} (L/h)	0.00979	[24]	0.00938	[23]
	Target-Mediated Drug Disposition			
k_{on} ($\mu M^{-1}.h^{-1}$)	403.2	[23]	740.0	[20]
k_{off} (h^{-1})	3.42	[23]	4.07	[20]
	Target			
HER2	Tumour value	Reference	Normal tissues value	Reference
MW (KDa)	185.000	[3]	185.000	[3]
R_{max} (μM)	0.04	[20]	0.0016	[20]
k_{deg} (h^{-1})	0.079	[20]	0.398	Optimised (see Methods section)
k_{syn}	-	Simcyp Predicted	-	Simcyp Predicted

MW: molecular weight; *pI*: isoelectric point; f_u: fraction unbound in plasma; B/P: blood-to-plasma concentration ratio; F_a: fraction of the dose absorbed; k_a: first order absorption rate constant; K_{rc1}: recycling rate of FcRn-mAb 1:1 complex from endothelial space; K_D: equilibrium dissociation constant for FcRn-mAb 1:1 complex; CL_{cat}: catabolic non-specific clearance; k_{on}: rate constant for binding to free target; k_{off}: rate constant for dissociation of mAb-target complex; R_{max}: abundance; k_{deg}: degradation rate constant for the target; k_{syn}: target synthesis rate constant ($k_{deg} \cdot R_{max}$).

PBPK modelling of EGFR-directed monoclonal antibodies

CTX PBPK model development and validation was perform sequentially. We first created the EGFR target in the *Cancer* population file already available in the Simcyp® Simulator by characterising its abundance in tumour tissues as well as its synthesis and degradation kinetics. Data from literature estimating R_{max} and k_{deg} of EGFR through modelling the dynamics of CTX-EGFR binding in living tumours was taken [29] and set to $2 \cdot 10^{-6}$ μM and 0.013 h^{-1}, respectively. Then we developed a full PBPK model for CTX that accounted for non-specific and specific

elimination processes and a salvage pathway by binding to FcRn in the endosomal space with a K_D of 0.34 μM [22]. A full TMDD model characterised by k_{on} and k_{off} with an internalization process governed by k_{int} was added to the model. An additional systemic clearance (CL_{add}) value of 0.033 L/h was added to the CTX elimination processes to best describe the observed data in a Phase I clinical trial [30] in the optimisation step. No other changes were performed to the target. Finally, the model was validated numerically and through the simulation of a multiple-dose administration of CTX to cancer patients and compared with observations from Phase I/II clinical studies [31,32]. Model parameters for the CTX-EGFR PBPK model can be found in Table 2.

Table 2. Final PBPK model parameters for CTX-EGFR framework.

Monoclonal Antibody		
	Cetuximab	
Parameter (Units)	Value	Reference
Physicochemical Properties		
MW (KDa)	145.781	DrugBank
pI	8.48	DrugBank
Hydrodynamic Radius (nm)	-	Simcyp Predicted
f_u	1	Default
B/P	0.55	Default
Distribution		
Model	Full PBPK	
K_{rc1}	16.7	Default
K_D FcRn (μM)	0.34	[22]
Elimination		
CL_{cat} (L/h)	0.02375	[33]
CL_{add} (L/h)	0.033	Optimized (see Methods section)
Target-Mediated Drug Disposition		
k_{on} ($\mu M^{-1} \cdot h^{-1}$)	30	[29]
k_{off} (h^{-1})	0.0017	[29]
k_{int} (h^{-1})	0.14	[29]
Target		
EGFR	Value	Reference
MW (KDa)	134.276	DrugBank
R_{max} (μM)	0.000002	[29]
k_{deg} (h^{-1})	0.013	[29]
k_{syn}	-	Simcyp Predicted

MW: molecular weight; *pI*: isoelectric point; f_u: fraction unbound in plasma; B/P: blood-to-plasma concentration ratio; K_{rc1}: recycling rate of FcRn-mAb 1:1 complex from endothelial space; K_D: equilibrium dissociation constant for FcRn-mAb 1:1 complex; CL_{cat}: catabolic non-specific clearance; CL_{add}: additional systemic clearance; k_{on}: rate constant for binding to free target; k_{off}: rate constant for dissociation of mAb-target complex; k_{int}: rate constant for mAb-target complex internalisation; R_{max}: abundance; k_{deg}: degradation rate constant for the target; k_{syn}: target synthesis rate constant ($k_{deg} \cdot R_{max}$).

Simulations

All simulations included 100 cancer patients (10 trials of 10 subjects each) and matched trial design and population demographic characteristics of the corresponding clinical study. Initial tumour volume was set to 20 mL in all scenarios [34,35]. No lymph flow was considered to the tumour tissue because the lack of functional lymphatic vessels inside this neoplastic tissue [36]. Between-subject variability for optimised parameter values was set to 30% to reproduce the variability observed in the clinical setting [24,25,30]. More details about the simulations (age range, female proportion, dosing schedule, study duration, etc…) are provided in the Supplementary Material to allow reproducibility of the work here presented.

Model validation

Graphical assessment of simulated *versus* observed concentration-time profiles was performed to validate the optimised target expression or the mAb PBPK model. Simulations were considered satisfactory if observations fell within the 5th and 95th percentiles of the simulated concentration-time profiles. Additionally, following metrics (Equations 1-3) were computed to numerically assess the predictive power of the PBPK frameworks developed:

- Average Fold Error (AFE):

$$AFE = 10^{\frac{1}{n}\sum \log \frac{Pred_i}{Obs_i}} \quad (1)$$

- Absolute Average Fold Error (AAFE):

$$AAFE = 10^{\frac{1}{n}\sum \left|\log \frac{Pred_i}{Obs_i}\right|} \quad (2)$$

- Percent Prediction Error (PPE%):

$$PPE(\%) = Mean\left(\left|\frac{Pred_i - Obs_i}{Obs_i}\right| \times 100\right) \quad (3)$$

Where $Pred_i$ and Obs_i are the predicted and observed PK parameter been evaluated, respectively. In general, model predictions were considered satisfactory if 0.8≤AFE≤1.25, acceptable if 0.5≤AFE<0.8 or 1.25<AFE≤2 and poor if AFE<0.5 or AFE>2. Following the same rationale, AAFE≤1.25, 1.25<AFE≤2

and AAFE>2 were considered satisfactory, acceptable and poor, respectively. For PPE%, the lower the value, the better the prediction.

Nomenclature of Targets and Ligands

Key protein targets and ligands in this article are hyperlinked to corresponding entries in http://www.guidetopharmacology.org, and are permanently archived in the Concise Guide to PHARMACOLOGY 2019/20 [37].

RESULTS

PBPK modelling of HER2-directed monoclonal antibodies

Simulated *versus* observed concentration-time profiles of PTZ and TTZ at different dose levels, schedules and routes of administration are depicted in Figure 2. Optimisation of HER2 k_{deg} in normal tissues to a final value of 0.398 h^{-1} led to a PBPK model structure able to properly describe the time course of PTZ across different dose levels (Figure 2A). The model was validated through the simulation of four additional scenarios combining different dosing schedules (Figure 2B) and routes of administration (Figure 2C). Numerical assessment of the predictive power of the model further validated PTZ-HER2 PBPK framework as computed AFE and AAFE fell between the desired range of satisfactory results for PK exposure parameters AUC and C_{max} with PPE% below 15% (see Table 3).

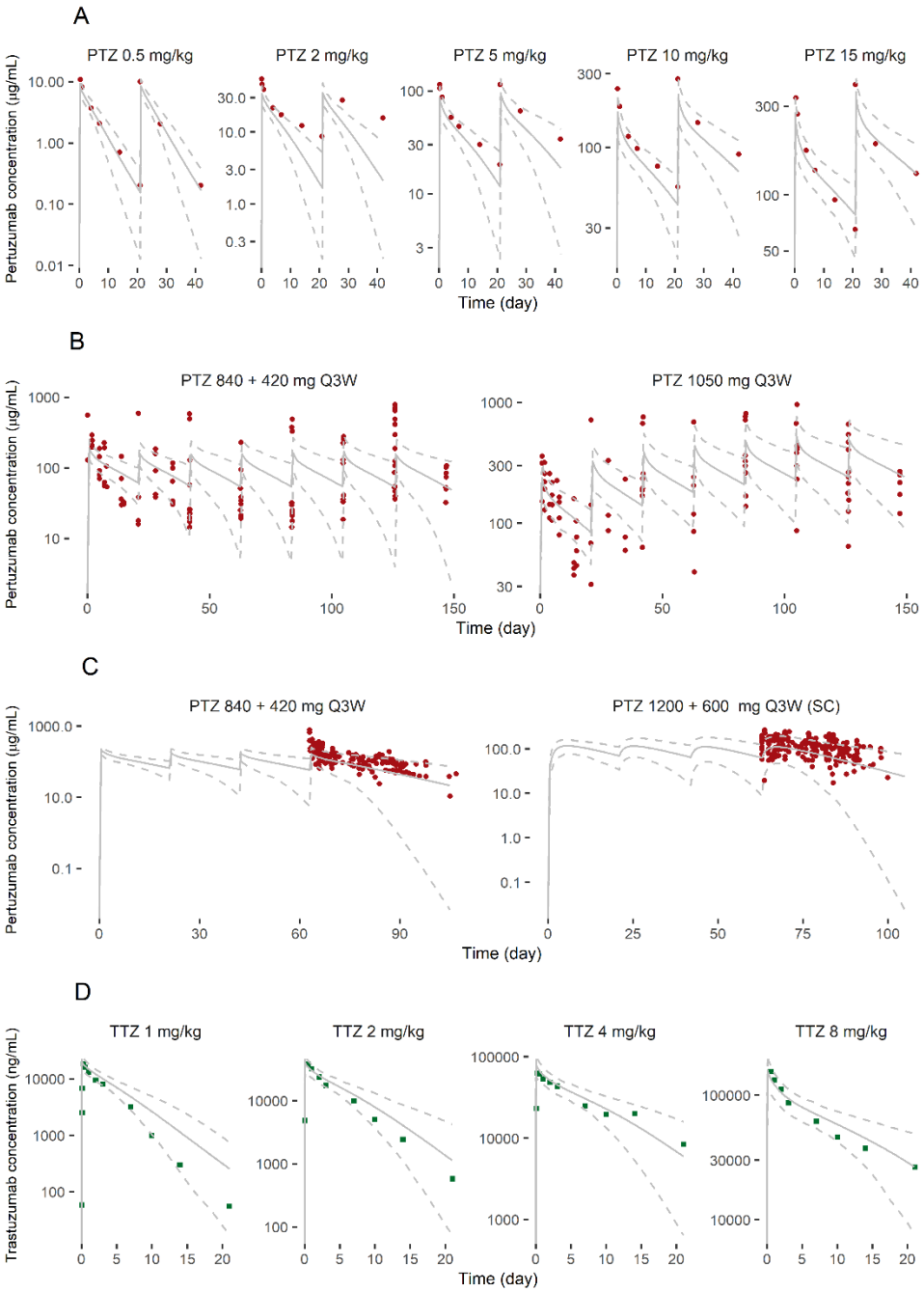

Figure 2. Graphical assessment of model performance: observed PTZ (dark red dots) and observed TTZ (dark green) *versus* median (continuous grey line) and 5th and 95th percentiles (dashed grey lines) of

predicted concentration-time profiles of PTZ and TTZ. PTZ: pertuzumab; TTZ: trastuzumab; Q3W. every three weeks; SC: sub-cutaneous.

HER2 final parameterisation from the PBPK modelling of PTZ was successfully cross validated through PBPK modelling of TTZ both graphically, with all observations at different dose levels after single IV infusion falling between 5th and 95th percentiles of the simulated profiles (Figure 2D), and numerically, with AFE, AAFE and PPE% values for AUC and C_{max} of 1.13, 1.16 and 16, and 1.01, 1.07 and 7, respectively (Table 3).

Table 3. Numerical validation of the PBPK models developed for PTZ, TTZ and CTX.

Monoclonal Antibody	**Pertuzumab**[a]		**Trastuzumab**[b]		**Cetuximab**[c]	
Metric/PK parameter	$AUC_{0\text{-}last}$ (mg·h/mL)	C_{max} (mg/mL)	$AUC_{0\text{-}inf}$ (ng·h/mL)	C_{max} (ng/mL)	$AUC_{0\text{-}last}$ (mg·h/mL)	C_{max} (mg/mL)
AFE	1.14	0.94	1.13	1.01	0.88	0.87
AAFE	1.14	1.12	1.16	1.07	1.16	1.15
PPE%	14	11	16	7	13	10

[a]: observed data from [26]; [b]: observed data from: [38]; [c]: observed data from [30]; AFE: average fold error; AAFE: absolute average fold error; PPE%: percent prediction error.

PBPK modelling of EGFR-directed monoclonal antibodies

Figure 3 shows observed *versus* predicted concentration-time profiles after single and multiple IV infusions of CTX at different dose levels. Graphical assessment of model performance after the incorporation of an additional systemic clearance of 0.033 L/h revealed good model parameterisation as observed data fell within the 5th and 95th percentiles of the simulated profiles regardless the dose level (Figure 3A). Additionally, numerical validation through the determination of AFE and AAFE showed a satisfactory predictive power of AUC and C_{max} of the PBPK model developed with PPE% 13% for AUC and 10% for C_{max} (see Table 3). Simulation of weekly IV infusions of CTX followed by a loading dose also described the observed data among multiple cycles of CTX treatment to squamous cell carcinoma of the head and neck patients alone (Figure 3B) [31] or in combination with radiation therapy (Figure 3C) [32], thus validating CTX PBPK model in a multiple dose administration schedule as well. The model properly described the elimination phase of CTX during all simulation time and accurately captured C_{max} and C_{trough} at steady state.

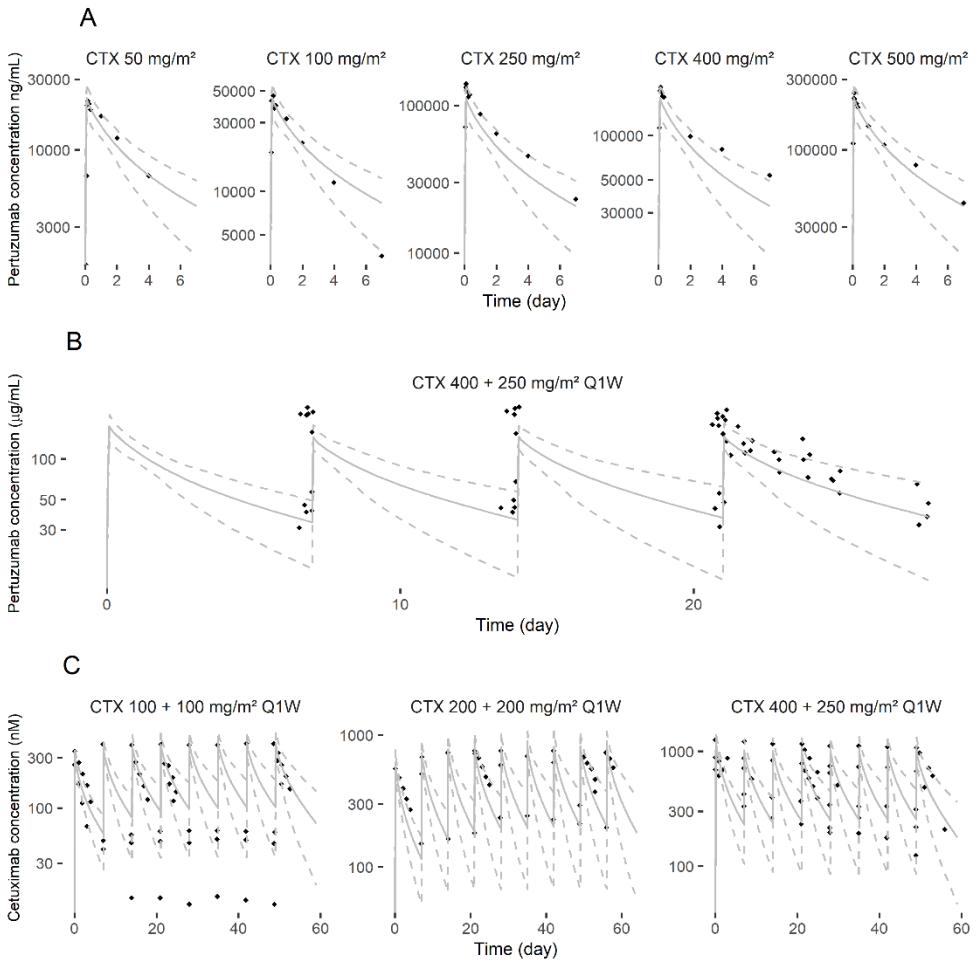

Figure 3. Graphical assessment of model performance: observed (black diamonds) *versus* median (continuous grey line) and 5th and 95th percentiles (dashed grey lines) of predicted concentration-time profiles of CTX; CTX: cetuximab; Q1W: every week.

DISCUSSION

A PBPK model for PTZ has been developed in cancer patients overexpressing HER2. Target parameterization has been optimized through PBPK modelling and simulation and cross-validated by PBPK modelling of TTZ in cancer patients. The PBPK framework developed can accurately reproduce the time course of both mAbs in cancer patients after single and multiple dose administrations and different dose levels. During model development, a 25-fold factor was applied to

HER2 concentration in normal tissues to calculate the concentration of the receptor in the cell membrane of malignant cells as median HER2 concentration in normal and cancerous tissues have been determined to be 1293.8 and 31656 pg/mg protein, respectively [11]. The TMDD model developed incorporates a constant option in R_{max} because neither TTZ nor PTZ binding to HER2 does increase the internalization or degradation rate of the receptor [5,7,39]. Additionally, it has been reported that treatment with a polyclonal anti-HER2 antibody induced rapid HER2 internalization probably due to multi-epitope interactions with the membrane receptor [40]. Following this rationale, anti-HER2 bispecific antibodies (anti-HER2-Bs) have been developed to target both domain II and IV in a non-overlapping manner to induce rapid internalization and efficient down-regulation of the receptor [41]. As this approach has been used in TTZ PBPK modelling previously [20,42], our decision of selecting a constant option for R_{max} is strongly supported.

Despite previously published PBPK models of HER2-directed mAbs, our TMDD model does not incorporate HER2 shedding because of the following reasons:

- The cleavage of the ECD of HER2 is slow and inefficient, even in the presence of activators [43]
- Baseline circulating HER2-ECD (cHER2-ECD) levels do not correlate with clinical response [10,12,44]
- Decreases in cHER2-ECD concentration because of treatment initiation are not sufficient to discriminate between patients with different clinical outcomes; measurable cHER2-ECD levels does not preclude clinical response [12,44]
- The role of cHER2-ECD as a predictor of response to TTZ therapy or tumour progression still unknown. The clinical utility of cHER2-ECD for predicting safety and efficacy is low [20]
- Serum HER2-ECD levels cannot be recommended to make TTZ decisions for individual patients [12]
- The effects of cHER2-ECD over time on TTZ exposure are overall small and the parameter most influencing TTZ clearance is the concentration of membrane bound HER2 [20]
- cHER2-ECD is unlikely to significantly affect TTZ pharmacokinetics as steady-state molar plasma concentration of TTZ are much higher than those of cHER2-ECD [12]

The role of cHER2-ECD on circulating levels of anti-HER2 mAbs is unclear due to incoherent reports [12,38,43,44]. Therefore, the shedding process was not included in the PBPK modelling of HER2-directed mAbs to increase model parsimony and structural and model parameters identifiability. Notwithstanding,

the impact of the cHER2-ECD on receptor occupancy (membrane-attached) and thus, on pharmacological effect, should be carefully evaluated to stablish an optimal dosing regimen in a case-by-case basis [45].

HER2 overexpression has been demonstrated to inhibit down-regulation of EGFR and of itself probably because the endocytic and endosomal sorting machinery can be impaired via saturation at high receptor levels, as the regulatory molecules involved in these processes have limited levels [6,7]. The optimised HER2 k_{deg} value in normal tissues of 0.398 h^{-1} is in good agreement with that reported by Hendriks et al (0.252 h^{-1}) [6]. In line with previous reports highlighting the impact of HER2 overexpression in disease on impairment of endocytic and endosomal sorting machinery, apparently because of limiting levels of the regulatory molecules involved in these processes [46-48], our model-based findings suggest that HER2 degradation rate constant in tumour tissue is likely to be 5-fold lower than in normal tissues. This is also in agreement with mathematical models on HER2 intracellular routing where overexpression of HER2 has been shown to shunt ligand-activated receptors to recycling fates [6], which is likely to lower the degradation rate.

The PBPK model developed for CTX in cancer patients with tumours overexpressing EGFR properly describes the observed data in a high variety of dosing schedules. Our model is able to predict reasonably well C_{trough} over time, what is clinically relevant as trough levels have been suggested to be important in response [30]. Understanding the biotransformation processes of therapeutic proteins (which must be clearly differentiated from specific or target-mediated and non-specific or catabolic elimination pathways) is of high value early on in drug discovery and development in order to detect vulnerable positions, re-engineer the molecule to replace the labile motive and ultimately design more stable drug candidates with better *in vivo* PK properties [49]. In this regard, the unexpected rapid clearance of CTX (with an unusually short half-life of 3-4 days) can be suggestive of alternative elimination processes not assessed by the mechanisms above mentioned.

In current CTX model, R_{max} expression from Tang et al [29] was used which is 1000-fold lower then Malik et al [20]. Sensitivity analysis conducted at CTX lowest dose clinically assessed (50 mg/m^2) revealed that there was no significant impact on PK profiles of CTX (Supplementary Material Table 2 and Figure 4). This is in agreement with fact that at clinically relevant therapeutic doses, TMDD of CTX is saturated [30]and hence it is unlikely that changes in R_{max} will influence CTX clearance.

The need for the additional systemic clearance of 0.033 L/h added to the PBPK model in the optimisation step could be related to: i) the efficient binding to FcgRIIIA receptor, ii) the binding to C1q subcomponent, and/or iii) the proteolytic cleavage of the lower hinge region by tumour-matrix metalloproteinases (MMPs) [50]. These non-specific non-catabolic elimination (biotransformation) pathways could also be related to the non-saturable, first-order elimination process that added to a zero-order and saturable clearance has been used to describe the population pharmacokinetics of CTX in head and neck cancer patients [33]. Additionally, it has been reported that polymorphisms in *FCGR2A* and *FCGR3A* are associated with clinical outcome in colorectal cancer patients treated with CTX as single agent thus suggesting these molecular markers could be useful to predict clinical outcome in metastatic colorectal cancer patients [51]. It is easily understood that an underlying mechanism not covered by catabolic clearance in the lysosomes nor specific target-mediated elimination processes contributes to CTX elimination *in vivo* and need to be accounted for when modelling its pharmacokinetics. Figure 4 illustrates our general proposal and the rationale followed to optimise biologic PK processes and/or target expression and kinetics through PBPK modelling and simulations. Initial data collection (or generation for *in house* data) and model parameterisation is verified and, if necessary, optimised by early modelling of Phase I clinical trials to assess the impact of different dose levels in biologic disposition processes, aimed to characterise non-linear kinetics of these large molecules. PBPK modelling easily allows it by differentiating target from biologic parameters, thus facilitating this optimisation step with a “middle-out” approach. Finally, the optimised framework is validated (or cross-validated in case a different biologic is used to confirm target parameterisation) using larger datasets coming from Phase II and III clinical trials and assessing different dosing schedules in the target population to increase the confidence in model parameterisation and predictions [52].

PopPBPK modelling strategy proposed had two major applications in clinical pharmacology development of therapeutics mAbs. Firstly, this PBPK modelling strategy provides clinical validation of target expression data which is then useful in developing prospective PBPK models for mAbs targeting same receptors in preclinical stage or as ‘back-up’ lead molecules [53]. Secondly, validated PBPK models may be directly employed to predict PK in various clinical scenarios of interest (e.g. different dosage regimens to mitigate safety related issues) and to predict local concentrations of mAb in local tissues or at target tissues [54]. Finally, these mechanistic frameworks are useful to explore the level of receptor occupancy (RO) achieved with a particular dosing schedule. Simulations at clinically relevant doses using optimised PBPK models of PTZ, TTZ or CTX, reveal persistently high (≥89%) of mean RO at steady state PK (see Supplementary

Material, Figures 1-3). Other indirect areas of application may warrant further research on feasibility to perform scaling to other populations groups e.g. from adults to paediatrics [55], or patient populations with comorbidities e.g. renal/hepatic impaired populations.

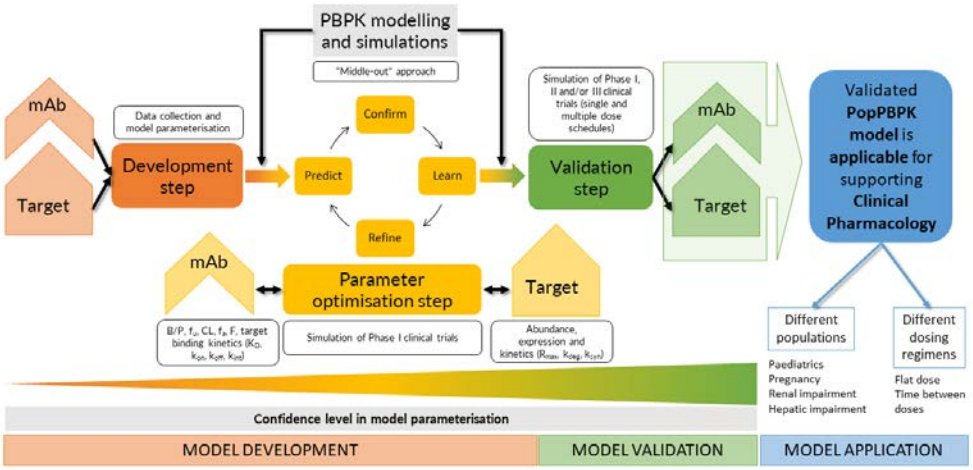

Figure 4. Optimisation of drug and system-related parameters through PBPK modelling and simulations. mAb: monoclonal antibody.

In **conclusion**, full PBPK models for PTZ, TTZ and CTX have been developed that are able to describe the time course of these biologics in a different set of scenarios. TMDD processes have also been added to model structures to account for non-linear PK. Optimisation of both system- and drug-related parameters have been performed through PBPK modelling and simulation to improve model performance and identifiability, highlighting the potential of this modelling technique in model informed drug discovery and development.

Acknowledgments

J.R.L. acknowledges AstraZeneca's support for the Research Stay to conduct this work.

Conflict of interest statement

J.R.L. was on PhD Research Stay with AstraZeneca during conduct of work. W.T., D.W.B., C.F.T. and P.S. are shareholders and/or employees of AstraZeneca. M.M.S and V.M.S have no conflict of interest.

Funding Information

Funding for a Summer Internship for J.R.L. was provided by AstraZeneca.

Data availability statement

All data generated and analysed during this study are included in this published article. All the original clinical PK data for this study can be accessed using the listed references.

Author contributions

Conceptualization and design: J.R.L., P.S. and V.M.S.; *data acquisition, modelling work and analysis*: J.R.L.; *data interpretation*: J.R.L., P.S. and V.M.S.; *drafting and revising manuscript*: J.R.L., P.S., V.M.S., M.M.S., C.F.T., D.W.B. and W.T. All authors have given final approval of the version of the manuscript to be published.

References

(1) Campbell MR, Ruiz-Saenz A, Zhang Y, Peterson E, Steri V, Oeffinger J, Sampang M, Jura N, Moasser MM. Extensive conformational and physical plasticity protects HER2-HER3 tumorigenic signaling. Cell Rep 2022; 40: 111338.
(2) Yarden Y. Biology of HER2 and its importance in breast cancer. Oncology 2001; 61 Suppl 2: 1-13.
(3) Rubin I, Yarden Y. The basic biology of HER2. Ann Oncol 2001; 12 Suppl 1: 3.
(4) Mendelsohn J, Baselga J. Status of epidermal growth factor receptor antagonists in the biology and treatment of cancer. J Clin Oncol 2003; 21: 2787-99.
(5) Austin CD, De Maziere AM, Pisacane PI, van Dijk SM, Eigenbrot C, Sliwkowski MX, Klumperman J, Scheller RH. Endocytosis and sorting of ErbB2 and the site of action of cancer therapeutics trastuzumab and geldanamycin. Mol Biol Cell 2004; 15: 5268-82.
(6) Hendriks BS, Opresko LK, Wiley HS, Lauffenburger D. Coregulation of epidermal growth factor receptor/human epidermal growth factor receptor 2 (HER2) levels and locations: quantitative analysis of HER2 overexpression effects. Cancer Res 2003; 63: 1130-7.
(7) Hendriks BS, Opresko LK, Wiley HS, Lauffenburger D. Quantitative analysis of HER2-mediated effects on HER2 and epidermal growth factor receptor endocytosis: distribution of homo- and heterodimers depends on relative HER2 levels. J Biol Chem 2003; 278: 23343-51.
(8) Gutierrez C, Schiff R. HER2: biology, detection, and clinical implications. Arch Pathol Lab Med 2011; 135: 55-62.
(9) Larson JS, Goodman LJ, Tan Y, Defazio-Eli L, Paquet AC, Cook JW, Rivera A, Frankson K, Bose J, Chen L, Cheung J, Shi Y, Irwin S, Kiss LDB, Huang W, Utter S, Sherwood T, Bates M, Weidler J, Parry G, Winslow J, Petropoulos CJ, Whitcomb JM. Analytical Validation of a Highly Quantitative, Sensitive, Accurate, and Reproducible Assay (HERmark) for the Measurement of HER2 Total Protein and HER2 Homodimers in FFPE Breast Cancer Tumor Specimens. Patholog Res Int 2010; 2010: 814176.
(10) Mazouni C, Hall A, Broglio K, Fritsche H, Andre F, Esteva FJ, Hortobagyi GN, Buzdar AU, Pusztai L, Cristofanilli M. Kinetics of serum HER-2/neu changes in patients with HER-2-positive primary breast cancer after initiation of primary chemotherapy. Cancer 2007; 109: 496-501.
(11) Olsen DA, Ostergaard B, Bokmand S, Wamberg PA, Jakobsen EH, Jakobsen A, Brandslund I. HER1-4 protein concentrations in normal breast tissue from breast cancer patients are expressed by the same profile as in the malignant tissue. Clin Chem Lab Med 2009; 47: 977-84.
(12) Lennon S, Barton C, Banken L, Gianni L, Marty M, Baselga J, Leyland-Jones B. Utility of serum HER2 extracellular domain assessment in clinical decision making: pooled analysis of four trials of trastuzumab in metastatic breast cancer. J Clin Oncol 2009; 27: 1685-93.
(13) Kurai J, Chikumi H, Hashimoto K, Takata M, Sako T, Yamaguchi K, Kinoshita N, Watanabe M, Touge H, Makino H, Igishi T, Hamada H, Yano S, Shimizu E. Therapeutic antitumor efficacy of anti-epidermal growth factor receptor antibody, cetuximab, against malignant pleural mesothelioma. Int J Oncol 2012; 41: 1610-8.
(14) Iqbal N, Iqbal N. Human Epidermal Growth Factor Receptor 2 (HER2) in Cancers: Overexpression and Therapeutic Implications. Mol Biol Int 2014; 2014: 852748.
(15) Carlsson J, Nordgren H, Sjostrom J, Wester K, Villman K, Bengtsson NO, Ostenstad B, Lundqvist H, Blomqvist C. HER2 expression in breast cancer primary tumours and corresponding metastases. Original data and literature review. Br J Cancer 2004; 90: 2344-8.

(16) Yamamoto N, Yamada Y, Fujiwara Y, Yamada K, Fujisaka Y, Shimizu T, Tamura T. Phase I and pharmacokinetic study of HER2-targeted rhuMAb 2C4 (Pertuzumab, RO4368451) in Japanese patients with solid tumors. Jpn J Clin Oncol 2009; 39: 260-6.
(17) Harbeck N, Beckmann MW, Rody A, Schneeweiss A, Muller V, Fehm T, Marschner N, Gluz O, Schrader I, Heinrich G, Untch M, Jackisch C. HER2 Dimerization Inhibitor Pertuzumab - Mode of Action and Clinical Data in Breast Cancer. Breast Care (Basel) 2013; 8: 49-55.
(18) Ogungbenro K, Patel A, Saunders M, Clark J, Duncombe R. An evaluation of cetuximab dosing strategies using pharmacokinetics and cost analysis. J Pharm Pharmacol 2019; 71: 1222-30.
(19) Shebley M, Sandhu P, Emami Riedmaier A, Jamei M, Narayanan R, Patel A, Peters SA, Reddy VP, Zheng M, de Zwart L, Beneton M, Bouzom F, Chen J, Chen Y, Cleary Y, Collins C, Dickinson GL, Djebli N, Einolf HJ, Gardner I, Huth F, Kazmi F, Khalil F, Lin J, Odinecs A, Patel C, Rong H, Schuck E, Sharma P, Wu S, Xu Y, Yamazaki S, Yoshida K, Rowland M. Physiologically Based Pharmacokinetic Model Qualification and Reporting Procedures for Regulatory Submissions: A Consortium Perspective. Clinical pharmacology and therapeutics 2018; 104: 88-110.
(20) Malik PRV, Hamadeh A, Phipps C, Edginton AN. Population PBPK modelling of trastuzumab: a framework for quantifying and predicting inter-individual variability. J Pharmacokinet Pharmacodyn 2017; 44: 277-90.
(21) Agus DB, Gordon MS, Taylor C, Natale RB, Karlan B, Mendelson DS, Press MF, Allison DE, Sliwkowski MX, Lieberman G, Kelsey SM, Fyfe G. Phase I clinical study of pertuzumab, a novel HER dimerization inhibitor, in patients with advanced cancer. J Clin Oncol 2005; 23: 2534-43.
(22) Chung S, Nguyen V, Lin YL, Lafrance-Vanasse J, Scales SJ, Lin K, Deng R, Williams K, Sperinde G, Li JJ, Zheng K, Sukumaran S, Tesar D, Ernst JA, Fischer S, Lazar GA, Prabhu S, Song A. An in vitro FcRn- dependent transcytosis assay as a screening tool for predictive assessment of nonspecific clearance of antibody therapeutics in humans. MAbs 2019; 11: 942-55.
(23) Adams CW, Allison DE, Flagella K, Presta L, Clarke J, Dybdal N, McKeever K, Sliwkowski MX. Humanization of a recombinant monoclonal antibody to produce a therapeutic HER dimerization inhibitor, pertuzumab. Cancer Immunol Immunother 2006; 55: 717-27.
(24) Garg A, Quartino A, Li J, Jin J, Wada DR, Li H, Cortes J, McNally V, Ross G, Visich J, Lum B. Population pharmacokinetic and covariate analysis of pertuzumab, a HER2-targeted monoclonal antibody, and evaluation of a fixed, non-weight-based dose in patients with a variety of solid tumors. Cancer Chemother Pharmacol 2014; 74: 819-29.
(25) Wang B, Deng R, Hennig S, Badovinac Crnjevic T, Kaewphluk M, Kagedal M, Quartino AL, Girish S, Li C, Kirschbrown WP. Population pharmacokinetic and exploratory exposure-response analysis of the fixed-dose combination of pertuzumab and trastuzumab for subcutaneous injection in patients with HER2-positive early breast cancer in the FeDeriCa study. Cancer Chemother Pharmacol 2021; 88: 499-512.
(26) Attard G, Kitzen J, Blagden SP, Fong PC, Pronk LC, Zhi J, Zugmaier G, Verweij J, de Bono JS, de Jonge M. A phase Ib study of pertuzumab, a recombinant humanised antibody to HER2, and docetaxel in patients with advanced solid tumours. Br J Cancer 2007; 97: 1338-43.
(27) Glover ZWK, Gennaro L, Yadav S, Demeule B, Wong PY, Sreedhara A. Compatibility and stability of pertuzumab and trastuzumab admixtures in i.v. infusion bags for coadministration. J Pharm Sci 2013; 102: 794-812.
(28) Suzuki T, Ishii-Watabe A, Tada M, Kobayashi T, Kanayasu-Toyoda T, Kawanishi T, Yamaguchi T. Importance of neonatal FcR in regulating the serum half-life of therapeutic proteins containing the Fc domain of human IgG1: a comparative study of the affinity of monoclonal antibodies and Fc-fusion proteins to human neonatal FcR. J Immunol 2010; 184: 1968-76.
(29) Tang Y, Cao Y. Modeling the dynamics of antibody-target binding in living tumors. Sci Rep 2020; 10: 16764-y.
(30) Fracasso PM, Burris H3, Arquette MA, Govindan R, Gao F, Wright LP, Goodner SA, Greco FA, Jones SF, Willcut N, Chodkiewicz C, Pathak A, Springett GM, Simon GR, Sullivan DM, Marcelpoil R, Mayfield SD, Mauro D, Garrett CR. A phase 1 escalating single-dose and weekly fixed-dose study of cetuximab: pharmacokinetic and pharmacodynamic rationale for dosing. Clin Cancer Res 2007; 13: 986-93.
(31) Dirks NL, Nolting A, Kovar A, Meibohm B. Population pharmacokinetics of cetuximab in patients with squamous cell carcinoma of the head and neck. J Clin Pharmacol 2008; 48: 267-78.
(32) Robert F, Ezekiel MP, Spencer SA, Meredith RF, Bonner JA, Khazaeli MB, Saleh MN, Carey D, LoBuglio AF, Wheeler RH, Cooper MR, Waksal HW. Phase I study of anti--epidermal growth factor receptor antibody cetuximab in combination with radiation therapy in patients with advanced head and neck cancer. J Clin Oncol 2001; 19: 3234-43.
(33) Pointreau Y, Azzopardi N, Ternant D, Calais G, Paintaud G. Cetuximab Pharmacokinetics Influences Overall Survival in Patients With Head and Neck Cancer. Ther Drug Monit 2016; 38: 567-72.
(34) Baxter LT, Zhu H, Mackensen DG, Butler WF, Jain RK. Biodistribution of monoclonal antibodies: scale-up from mouse to human using a physiologically based pharmacokinetic model. Cancer Res 1995; 55: 4611-22.
(35) Glassman PM, Balthasar JP. Physiologically-based pharmacokinetic modeling to predict the clinical pharmacokinetics of monoclonal antibodies. J Pharmacokinet Pharmacodyn 2016; 43: 427-46.
(36) Padera TP, Meijer EFJ, Munn LL. The Lymphatic System in Disease Processes and Cancer Progression. Annu Rev Biomed Eng 2016; 18: 125-58.
(37) Alexander SPH, Fabbro D, Kelly E, Mathie A, Peters JA, Veale EL, Armstrong JF, Faccenda E, Harding SD, Pawson AJ, Sharman JL, Southan C, Davies JA, CGTP Collaborators. THE CONCISE GUIDE TO PHARMACOLOGY 2019/20: Enzymes. Br J Pharmacol 2019; 176 Suppl 1: S297-396.

(38) Tokuda Y, Watanabe T, Omuro Y, Ando M, Katsumata N, Okumura A, Ohta M, Fujii H, Sasaki Y, Niwa T, Tajima T. Dose escalation and pharmacokinetic study of a humanized anti-HER2 monoclonal antibody in patients with HER2/neu-overexpressing metastatic breast cancer. Br J Cancer 1999; 81: 1419-25.
(39) Longva KE, Pedersen NM, Haslekas C, Stang E, Madshus IH. Herceptin-induced inhibition of ErbB2 signaling involves reduced phosphorylation of Akt but not endocytic down-regulation of ErbB2. Int J Cancer 2005; 116: 359-67.
(40) Ren X, Wei J, Lei G, Wang J, Lu J, Xia W, Spector N, Barak LS, Clay TM, Osada T, Hamilton E, Blackwell K, Hobeika AC, Morse MA, Lyerly HK, Chen W. Polyclonal HER2-specific antibodies induced by vaccination mediate receptor internalization and degradation in tumor cells. Breast Cancer Res 2012; 14: R89.
(41) Cheng J, Liang M, Carvalho MF, Tigue N, Faggioni R, Roskos LK, Vainshtein I. Molecular Mechanism of HER2 Rapid Internalization and Redirected Trafficking Induced by Anti-HER2 Biparatopic Antibody. Antibodies (Basel) 2020; 9: 49. doi: 10.3390/antib9030049.
(42) Li L, Gardner I, Rose R, Jamei M. Incorporating Target Shedding Into a Minimal PBPK-TMDD Model for Monoclonal Antibodies. CPT Pharmacometrics Syst Pharmacol 2014; 3: e96.
(43) Codony-Servat J, Albanell J, Lopez-Talavera JC, Arribas J, Baselga J. Cleavage of the HER2 ectodomain is a pervanadate-activable process that is inhibited by the tissue inhibitor of metalloproteases-1 in breast cancer cells. Cancer Res 1999; 59: 1196-201.
(44) Pegram MD, Lipton A, Hayes DF, Weber BL, Baselga JM, Tripathy D, Baly D, Baughman SA, Twaddell T, Glaspy JA, Slamon DJ. Phase II study of receptor-enhanced chemosensitivity using recombinant humanized anti-p185HER2/neu monoclonal antibody plus cisplatin in patients with HER2/neu-overexpressing metastatic breast cancer refractory to chemotherapy treatment. J Clin Oncol 1998; 16: 2659-71.
(45) Pressly MA, Peletier LA, Zheng S, Sharma VD, Lien YTK, Wang W, Zhou H, Schmidt S. The quest for balance between capturing data and model complexity: a quantitative clinical pharmacology approach applied to monoclonal antibodies. CPT Pharmacometrics Syst Pharmacol 2023.
(46) Wiley HS. Anomalous binding of epidermal growth factor to A431 cells is due to the effect of high receptor densities and a saturable endocytic system. J Cell Biol 1988; 107: 801-10.
(47) Kurten RC, Cadena DL, Gill GN. Enhanced degradation of EGF receptors by a sorting nexin, SNX1. Science 1996; 272: 1008-10.
(48) French AR, Sudlow GP, Wiley HS, Lauffenburger DA. Postendocytic trafficking of epidermal growth factor-receptor complexes is mediated through saturable and specific endosomal interactions. J Biol Chem 1994; 269: 15749-55.
(49) Schadt S, Hauri S, Lopes F, Edelmann MR, Staack RF, Villasenor R, Kettenberger H, Roth AB, Schuler F, Richter WF, Funk C. Are Biotransformation Studies of Therapeutic Proteins Needed? Scientific Considerations and Technical Challenges. Drug Metab Dispos 2019; 47: 1443-56.
(50) Deveuve Q, Lajoie L, Barrault B, Thibault G. The Proteolytic Cleavage of Therapeutic Monoclonal Antibody Hinge Region: More Than a Matter of Subclass. Front Immunol 2020; 11: 168.
(51) Zhang W, Gordon M, Schultheis AM, Yang DY, Nagashima F, Azuma M, Chang H, Borucka E, Lurje G, Sherrod AE, Iqbal S, Groshen S, Lenz H. FCGR2A and FCGR3A polymorphisms associated with clinical outcome of epidermal growth factor receptor expressing metastatic colorectal cancer patients treated with single-agent cetuximab. J Clin Oncol 2007; 25: 3712-8.
(52) Rostami-Hodjegan A. Reverse Translation in PBPK and QSP: Going Backwards in Order to Go Forward With Confidence. Clin Pharmacol Ther 2018; 103: 224-32.
(53) Jones HM, Zhang Z, Jasper P, Luo H, Avery LB, King LE, Neubert H, Barton HA, Betts AM, Webster R. A Physiologically-Based Pharmacokinetic Model for the Prediction of Monoclonal Antibody Pharmacokinetics From In Vitro Data. CPT Pharmacometrics Syst Pharmacol 2019; 8: 738-47.
(54) Chigutsa E, Jordie E, Riggs M, Nirula A, Elmokadem A, Knab T, Chien JY. A Quantitative Modeling and Simulation Framework to Support Candidate and Dose Selection of Anti-SARS-CoV-2 Monoclonal Antibodies to Advance Bamlanivimab Into a First-in-Human Clinical Trial. Clin Pharmacol Ther 2022; 111: 595-604.
(55) Gill KL, Jones HM. Opportunities and Challenges for PBPK Model of mAbs in Paediatrics and Pregnancy. AAPS J 2022; 24: 72-0.

Results and discussion

Part 1: methodological aspects of PBPK platforms.

This part summarizes the main findings of the research work previously described in Chapter 1.

A theoretical model previously published [38] incorporating complex absorption processes, intestinal transit, dissolution limited by solubility, variable expression of efflux transporter along the gut, and linear and non-linear metabolism in gut and liver was taken as reference. The model considered oral administration of the parent drug (PD) as an immediate release formulation, metabolism of PD to two metabolites (i.e., primary metabolite [PM] and secondary metabolite [SM]) and renal excretion of the metabolites.

Different approximations to the theoretical model were developed:

- **vNM**: semi-mechanistic version of the theoretical model with extraction-based metabolism of PD. ODE system was implemented and solved in NONMEM.
- **vPSEM**: model version with the same mathematical approximation that vNM but implemented in PhysPK Biosimulation Software (PhysPK). Accordingly, it was based on the same ODE system that vNM.
- **vPSIM**: semi-mechanistic version of the theoretical model with intrinsic clearance-based metabolism of PD implemented in PhysPK. This model version substitutes extraction based metabolic equations by intrinsic clearance functions.
- **vPPK**: physiological multilevel version of the theoretical model implemented in PhysPK. vPPK uses an acausal object-oriented modelling approach.

A set of 32 different scenarios (2 dose levels, BCS drug types II and IV, 4 metabolic scenarios and linear and non-linear P glycoprotein (P-gp) activity) were generated and analysed.

Validation of PhysPK Biosimulation Software

Graphical analysis of the correlations of plasma concentration levels of PD, PM and SM from the vPSEM *vs* vNM comparison after single dose administration in each of the scenarios generated demonstrated the ability of PhysPK to simulate almost equivalent concentration levels of PD, regardless of the scenario considered. PM and SM levels were also in good agreement between both software at low-medium concentration values, but small discrepancies were observed at high concentrations (C_{max}) in scenarios corresponding to low permeability and linear activity in P-gp. Nonetheless, linear correlation coefficient (R^2) was higher than 0.96 in all cases.

Mean relative error (RE) for AUC_{0-48} and C_{max} of vPSEM and vNM comparison were 3.96, 6.61 and 5.81% and 0.16, 2.92 and 1.53% for PD, PM, and SM, respectively. Based on these results good agreement between both software was demonstrated.

Metabolism Evaluation

This stage involved the comparison of two mathematical approximations of the theoretical model that can be selected in PhysPK (vPSIM *vs* vPSEM), which only differed from each other in their parametrization of metabolism.

As expected, results revealed PD to be the most sensitive analyte to changes in metabolism. In fact, individual RE for both PD AUC_{0-48} and C_{max} reached up to -50% in scenarios corresponding to non-linear kinetics in the metabolism of PD in gut and liver. Thus, the saturation of liver metabolism leads to a reduction in the rate of the metabolic process, increasing the differences in AUC_{0-48} and C_{max} due to the different parametrization between the two approaches (hepatic blood flow).

Modelling Approach Comparison: algorithmic *vs* acausal modelling

Individual AUC_{0-48} and C_{max} successfully matched between vPPK and vPSIM for PD, with mean RE for AUC_{0-48} and C_{max} of -0.02 and -0.04%, respectively. This outcome was independent of the absorption properties, dose level, P-gp activity, and gut and liver metabolic kinetics. Mean absolute error (MAE) and root mean squared error (RMSE) of PD AUC_{0-48} and C_{max} also improved in this comparison

and agreed with the negligible RE detected. Individual RE for AUC_{0-48} and C_{max} of PM and SM were greater than 10 % in some scenarios, with mean RE for PM and SM for AUC_{0-48} and C_{max} of 11.52 and 7.52%, and 10.01 and 6.64%, respectively.

The equivalence of the mathematical approximations in vPSIM and vPPK for PD compound was confirmed by comparing the vPPK *vs* vPSIM mean RE of AUC_{0-48} and C_{max}. Those values dramatically diminished and MAE and RMSE significantly improved. In the case of metabolites, the existence of exposure differences between vPPK and vPSIM point to the lack of a physiological blood perfusion in vPSIM, since in this model version metabolites are directly generated in their respective compartments. This explains the higher mean plasmatic concentrations in vPPK, as in this case, PM and SM are incorporated into the bloodstream before being excreted by kidneys, in contrast of what happens in vPSIM where they immediately start to be excreted once they are formed.

Part 2: PBPK modelling in the preclinical setting

This part summarizes the main findings of the research work previously described in Chapter 2.

Drug discovery and development represents an increasing economic and temporal cost for the pharmaceutical industry, which does not translate into significant increases in the number of approved active ingredients, especially in the oncology area [39,40]. One alternative is to develop mathematical models at the preclinical stages of the drug development process capable of better predicting efficacy or safety outcomes in order to efficiently design clinical trials [41]. Tumour growth inhibition (TGI) models [42] constitute a highly valuable preclinical methodology in oncology for the selection of therapeutic candidates and the design of optimal clinical evaluation strategies for the *in vivo* assessment of antitumor effect [43-48].

The anti-cancerous drug candidate MBQ-167 has been characterized as a potent inhibitor of the Rho GTPases Rac and Cdc42 [49]. These GTPases are overactive in different cancer types and promote cancer cell migration, invasion, proliferation, and oncogenic transformation [50-54]. MBQ-167 dually inhibits the activation of both GTPases, with half-maximal inhibitory concentrations (IC_{50}) of 0.1 μM and 0.08 μM for Rac and Cdc42, respectively. Preclinical studies have shown that MBQ-167 inhibits breast cancer (BC) cell migration, viability, tumour growth (91% reduction in tumour size is achieved in 2 months of treatment, with

the drug effect starting as early as 3 weeks of the first dose), and metastasis *in vivo* without apparent toxicity [49,55].

MBQ-167 PBPK/PD modelling strategy designed is illustrated in Figure 6 and briefly described as follows. First, physiological parameters of the typical mouse already available in Simcyp® Animal Simulator V19 were modified to reproduce the mice population used in the experimental procedure, physiochemical properties of MBQ-167 were introduced into the PBPK platform and the intraperitoneal (IP) route of administration was defined as a first order absorption process to the venous blood with a lag time of 0.17 h. Disposition processes were then modelled to generate an advanced PBPK model. Modelling of tumour tissue PK provided the final MBQ-167 PBPK model.

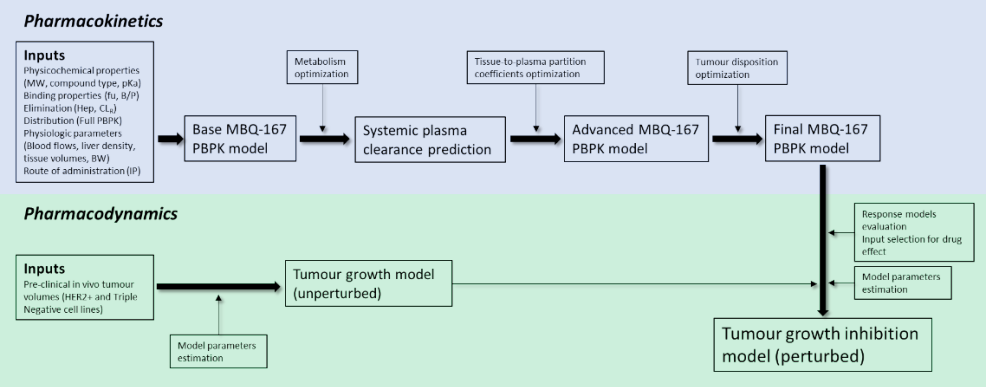

Figure 6. Modelling strategy followed to develop the PBPK/PD framework. MW: molecular weight; f_u: fraction unbound in plasma; B/P: blood-to-plasma concentration ratio; Hep: *in vitro* determined hepatocytes intrinsic clearance; CL_R: renal clearance; BW: body weight; IP: intraperitoneal

Pharmacodynamics of MBQ-167 was assessed with the Simeoni TGI model [42], developing first an unperturbed model for the BC cell lines HER2+ and Triple Negative describing tumour growth in control groups, and finally characterizing the inhibition properties through the estimation of maximum inhibition (K_{max}), IC_{50} and transit rate of cell damage (k_1). The number of transit compartments was established regarding the promptness appearance of the tumour growth inhibition for each cell line and resulted in 3 and 4 for HER2+ and Triple Negative cell lines, respectively.

Model predictions after a single IP administration of 10 mg/kg of MBQ-167 showed that the PBPK model developed was able to capture the longitudinal MBQ-167 observations. C_{max} and T_{max} were adequately characterized in plasma and other organs (heart, lungs, liver, spleen, and kidneys), and slightly biased in tumour tissue. These results agreed with the numerical analysis, as the fold error for C_{max}

was close to the unity in all tissues except in the tumour, where a value of 0.8 arised. Additionally, the RE in AUC_{0-t} and C_{max} in each tissue was, in general, less than 20% for the typical profile, showing that the PBPK model was able to characterize the average PK of MBQ-167.

The unperturbed model proposed by Simeoni *et al*. [42] was able to adequately describe tumour growth in both cell lines (control groups). The TGI model accurately predicted tumor shrinkage (RE<20%) in HER2+ cell line after the administration of 1 and 10 mg/kg of MBQ-167 three times a week for 65 days, with a relative tumor size reduction of 94.3% at the highest dose level. Model predictions in the Triple-Negative cell line agreed with the experimental data for the 1 mg/Kg group, and a slightly under-prediction of final tumor volume was predicted in mice receiving 10 mg/kg three times a week for 108 days. The discrepancy could be explained by the fact that differences in linear growth rate constant (λ_1) could appear between groups, but the overall time-course profile of tumour dynamics of each group was adequately captured by the model since mean predictions were within the 95% CI of the observed data and the predicted relative reduction in the final tumor size (89.6%) agreed with that observed (87.0%) at the 10 mg/kg dose level.

Different simulations were performed in order to evaluate the influence of more intensive dosing regimens on tumor size reduction. The results anticipated a significant improvement in tumor reduction when once daily (QD) and/or twice daily (BID) schedules were considered, especially in the HER2+ cell line since tumor eradication is predicted at 1 mg/kg BID and 10 mg/kg BID or QD. In the Triple Negative cell line, maximal pharmacodynamic effect is already achieved at 1 mg/kg, predicting tumour growth stabilization when BID or QD schedules are considered.

Part 3: PBPK modelling in the clinical setting

Assessing potential drug-gene interactions (DGI): a case-study with atorvastatin

This section summarizes the main findings of the research work previously described in Chapter 3 and Chapter 4.

Atorvastatin (ATS) is a second-generation synthetic statin that is administered as the calcium salt (ATS-Ca) of the active hydroxy-acid form and is one of the most

prescribed statins for the treatment of dyslipemia in order to diminish the cardiovascular risk.

Statins accumulation in the liver is mediated by hepatic active uptake through the organic anion transporting polypeptide (OATP) family, sodium-dependent taurocholate co-transporting polypeptide (NTCP), and by efflux transporters of the ATP-binding cassette (ABC) family, located on the basolateral and canalicular membranes of the liver, respectively [56]. *In vitro* kinetic studies on ATS hepatic uptake revealed that OATP1B1 and OATP1B3 are the major ATS uptake transporters, while NTCP was found to be of minor importance in ATS disposition. The average contribution to ATS uptake resulted OATP1B1 > OATP1B3 >> OATP2B1 > NTCP [57]. An ATS intrinsic uptake clearance of 2030 mL/min (95% CI: 1140-2620 mL/min) was predicted and, assuming the same passive diffusion across the cell membrane of hepatocytes and HEK293 cells (120 μL/min/g of liver), transporter-mediated active uptake of ATS was concluded to dominate overall ATS hepatic uptake [57]. Moreover, polymorphisms in transporters genes have been reported to affect the PK of statins and their therapeutic effects [58,59]. It has been demonstrated, for example, that $K_{pt,liver}$ of ATS is 2.7-fold higher ($p = 0.002$) in wild-type when compared to *Slco1b2-/-* mice after 1 mg/kg ATS tail vein injection [56]. In humans, it has been observed that ATS and its metabolites are sensitive to polymorphisms in *SLCO1B1*, as plasma concentrations were higher in subjects carrying the reduced function *SLCO1B1 521C* allele (T/C genotype) compared with the wild-type subjects (*521 T/T*) [60].

Metabolism of ATS is an intricated pathway of different reactions that include glucuronidation [61-63], lactonization [64], and CYP450-mediated oxidation [65,66]. ATS is administered as the hydroxy acid form and has equipotent active metabolites (*ortho*-hydroxy atorvastatin (2OH-ATS) and *para*-hydroxy atorvastatin (4OH-ATS)) that are responsible of 70% of the 3-hydroxy-3-methylglutaryl coenzyme A (HMG-CoA) reductase inhibitory activity [67]. Both metabolites, as well as the parent compound, are equilibrated with the corresponding lactone forms (ATS-L, 2OH-ATS-L and 4OH-ATS-L) [63,64,66]. It has been demonstrated that lactonization might occur non-enzymatically at pH<6 [68] or enzymatically, being the former pathway negligible at pH>6. The formation of a glucuronide prior to lactonization is expected to be the major pathway for the enzymatic lactonization of ATS in humans, which is catalyzed by UDP-glucuronosyltransferases (UGTs) 1A1, 1A3 and 2B7. The isoenzyme UGT1A3 is the major contributor to this process with 200 times more activity than UGT2B7 [61]. The mechanism proposed for the lactonization is the formation of an acyl-β-D-glucuronide of ATS acid, elimination of the glucuronic moiety and final spontaneous cyclization to the corresponding lactone [63]. ATS lactonization is

affected by polymorphisms in the *UGT1A* locus and has been demonstrated both, *in vitro* and *in vivo* [62]. On the other hand, the hydrolysis of the lactone forms of ATS and its metabolites to the corresponding carboxylates takes place non-enzymatically at pH>6 [68] or can be catalyzed by plasmatic esterases or paraoxonases (PONs) [63]. Hydrolysis of lactone forms has been demonstrated to occur in plasma [69]. Therefore, this process must be considered when modelling ATS and its metabolites to better assess their PK.

CYP450-mediated oxidative metabolism has been proposed as the main pathway of biotransformation for statins in humans [63], where CYP3A4 is the major enzyme involved in the formation of the hydroxy-metabolites of ATS [64,66]. The CYP3A4-mediated oxidation is clearly polarized to the lactone forms, with significant differences in maximum rates (V_{max}) and concentration associated with half-V_{max} (K_M) between open acid and lactone forms that result in an intrinsic clearance ratio lactone/acid equal to 73 [65]. Additionally, quantum mechanics/molecular mechanics have revealed that the acid form of ATS must pay a desolvation penalty of 5 Kcal/mol to enter in the more hydrophobic active site of the enzyme [64]. Moreover, the higher V_{max} value for the *para*-hydroxylation of ATS-L has been attributed to a shorter distance to the *heme* oxygen atom of the CYP3A4 [64]. Thus, ATS lactonization changes its affinity to the CYP450 and affects the preferred hydroxylation positions.

The PBPK model developed in Simcyp® Simulator V19 described within a 2-fold prediction error (PE) the exposure metrics, C_{max} and AUC, of ATS and its metabolites ATS-L, 2OH-ATS-L and 4OH-ATS-L, after single dose administration of 20, 40 and 80 mg and multiple administrations of 10 mg of ATS-Ca QD over one week.

The PBPK framework was able to characterize ATS-L observed data with prediction errors of 0.89 and 1.67 for AUC and C_{max}, respectively. It has to be noted that, in our model, lactonization has only been assessed enzymatically through UGTs. Pre-systemic lactonization due to the low pH in the stomach had not been incorporated into the PBPK model due to structural limitations of the Simcyp® Simulator, as only one formation pathway can work at a time. Hydroxylated ATS-L metabolites (i.e., 2OH-ATS-L and 4OH-ATS-L) were also well characterized, with PE of 1.01 and 1.44 for AUC and 0.79 and 1.05 for C_{max}, respectively. As these metabolites are directly formed after CYP450-mediated hydroxylation of ATS-L, these results suggest that considering enzymatic lactonization as the main, but not the only, pathway of ATS-L formation is a good approximation to global ATS PK.

It had been previously suggested that the main formation pathway of hydroxylated metabolites of ATS (i.e., 2OH-ATS and 4OH-ATS) is the ATS

lactonization, CYP450-mediated hydroxylation and subsequent hydrolysis of the hydroxylated isomers of ATS-L [70]. Direct hydroxylation of ATS would run simultaneously to this metabolic route but playing a minor role in overall ATS elimination. Therefore, it is not surprising that exposure to 2OH-ATS was not accurately predicted by our model, with AUC and C_{max} PE of 0.57 and 0.33, respectively, at 20 mg dose level. In our PBPK model inter-system extrapolation factors (ISEF) for the IVIVE have not been optimised, and validated ISEFs for the corresponding *in vitro* system have been directly used.

The ATS PBPK model was able to properly describe clinically relevant DDIs with both CYP3A4 and OATPs inhibitors. According to these results, the mechanisms involved in the metabolic processes linked to CYP3A4 (perturbed by itraconazole and clarithromycin) were adequately characterized for both ATS and ATS-L, since the PE were between 0.66 and 1.45. On the other hand, there was a slight underprediction of ATS exposure in the presence of OATP inhibitors (rifampicin), although the results obtained were also within the accepted 2-fold error range (0.61 and 0.79 for AUC and C_{max}, respectively). Nonetheless, this outcome confirmed the validity of the relative contribution assigned to each OATP isoform to overall ATS hepatic uptake that was set to OATP1B1 (53.2%) > OATP1B3 (37.8%) >> OATP2B1 (9%).

As Simcyp® Simulator V19 lacked the different genotypes in *SLCO1B1*, phenotypes were considered to better assess the DGI with *SLCO1B1* polymorphisms. In this regard, we stratified the ATS PK for poor (PT), extensive (ET), intermediate (IT) and ultra-rapid (UT) transporters, assuming that the *SLCO1B1*5* variant represents a loss-of-function allele that codifies an OATP1B1 isoform with reduced activity (i.e., PT).

The simulations performed revealed a statistically significant difference in ATS CL ($p < 0.01$), as PT would have a 30% lower clearance than ET individuals. Consequently, ATS AUC and C_{max} would be increased by 40 and 33% ($p < 0.05$), respectively, in individuals carrying the *SLCO1B1*5* allele (PT).

Additionally, our model-based predictions revealed that up to 34.8% of patients would have an apparent clearance lower than 414.67 L/h (a threshold that has been determined to increase muscle-related adverse events [71]) and, consequently, increased ATS and ATS-L exposure. Among these patients, the most affected would be individuals carrying the *SLCO1B1*5* variant (i.e., PT), as 63% would be at risk of muscle-related adverse events. In this regard, patients at higher risk of suffering muscle discomfort ($CL/F \leq 414.67$ L/h) would have 2.2- and 1.76-fold ($p < 0.0001$) higher ATS and ATS-L AUC, respectively. These results are consistent with the reported hazard ratio of 1.4 (95% CI: 1.1-1.7, $p = 0.02$)

for suffering statin-induced myopathies (SIMs) and could explain the treatment discontinuation among these patients (odds ratio 1.67, p = 0.0001) observed in the context of routine clinical care [41]. Our predictions are also in agreement with the reported increased levels of ATS-L ($p < 0.01$) and the 2.3-fold prolonged ATS $t_{1/2}$ ($p < 0.01$) that patients with SIM have when compared with patients not suffering from muscle-related adverse events [72], thus being able to anticipate and mechanistically assess an exposure-safety relationship.

Optimising target expression and elimination mechanisms of therapeutic monoclonal antibodies in oncology indication: case-studies with pertuzumab, trastuzumab and cetuximab

This section summarizes the main findings of the research work previously described in Chapter 5.

The activation of transmembrane tyrosine kinases receptors underlies the pathogenesis of many human malignancies [73]. Epidermal growth factor receptor (EGFR) family constitutes a group of four transmembrane receptors involved in signal transduction reactions that regulate cell growth and differentiation [74] and has developed in parallel with the evolution of complex organisms [75]. These four highly related receptors (i.e., EGFR/HER1/ErbB-1, HER2/ErbB-2/neu, HER3/ErbB-3 and HER4/ErbB-4) comprise a cysteine-rich extracellular ligand binding site, a transmembrane lipophilic segment, and an intracellular domain with tyrosine kinase catalytic activity [76]. The large extracellular domains (ECD) of theses receptors constitute an excellent opportunity to target biotherapeutics agents rationally designed to disrupt ligand-induced structural changes or dimerization as well as to selectively deliver cytotoxic drugs to malignant cells, making possible the concept of “magic bullet” proposed by Paul Ehrlich in the 19th century. The receptors are found in a variety of tissues as monomers and can associate with each other after ligand binding to form homodimers (i.e., HERx-HERx) or heterodimers (i.e., HERx-HERy) [74].

PBPK modelling of HER2-directed monoclonal antibodies

HER2 overexpression in tumour tissue was implemented applying a 25-fold factor to HER2 concentration in normal tissues, as median HER2 concentration in normal and cancerous tissues have been determined to be 1293.8 and 31656 pg/mg

protein, respectively [77]. The target-mediated drug disposition (TMDD) model developed incorporates a constant option in receptor abundance (R_{max}) because neither pertuzumab (PTZ) nor trastuzumab (TTZ) binding to HER2 does increase the internalization or degradation rate of the receptor [78-80].

The role of circulating HER2-ECD (cHER2-ECD) on plasmatic levels of anti-HER2 monoclonal antibodies (mAbs) is unclear due to incoherent reports [81-84]. Therefore, the shedding process was not included in the PBPK modelling of HER2-directed mAbs to increase model parsimony and structural and model parameters identifiability.

Optimisation of HER2 degradation rate constant (k_{deg}) in normal tissues to a final value of 0.398 h^{-1} led to a PBPK model structure able to properly describe the time course of PTZ across different dose levels. In line with previous reports highlighting the impact of HER2 overexpression in disease on impairment of endocytic and endosomal sorting machinery, apparently because of limiting levels of the regulatory molecules involved in these processes [85-87], our model-based findings suggest that HER2 k_{deg} in tumour tissue is likely to be 5-fold lower than in normal tissues (i.e., 0.079 h^{-1}). This is also in agreement with mathematical models on HER2 intracellular routing, where overexpression of HER2 has been shown to shunt ligand-activated receptors to recycling fates [88], which is likely to lower the k_{deg}.

Numerical assessment of the predictive power of the model further verified PTZ-HER2 PBPK framework as computed average fold error (AFE) and absolute AFE (AAFE) fell between the desired range of satisfactory results for PK exposure parameters AUC and C_{max} and with PPE% below 15%. HER2 final parameterisation from the PBPK modelling of PTZ was successfully cross validated through PBPK modelling of TTZ, with AFE, AAFE and PPE% values for AUC and C_{max} of 1.13, 1.16 and 16%, and 1.01, 1.07 and 7%, respectively.

PBPK modelling of EGFR-directed monoclonal antibodies

Graphical assessment of cetuximab (CTX) model performance after the incorporation of an additional systemic clearance of 0.033 L/h revealed good model parameterisation as observed data fell within the 5th and 95th percentiles of the simulated profiles regardless the dose level. Additionally, numerical validation through the determination of AFE and AAFE showed a satisfactory predictive power of AUC and C_{max} of the PBPK model developed, with PPE% 13% for AUC and 10% for C_{max}.

The unexpected rapid clearance of CTX (with an unusually short $t_{1/2}$ of 3-4 days) can be suggestive of alternative elimination processes not assessed by the non-specific (catabolic clearance) nor specific (target-mediated) routes of elimination. So, the need for the non-specific non-catabolic systemic clearance of 0.033 L/h added to the above-mentioned elimination mechanisms could be related to: i) the efficient binding to FcγRIIIA receptor, ii) the binding to C1q subcomponent, and/or iii) the proteolytic cleavage of the lower hinge region by tumour-matrix metalloproteinases [89]. Understanding the biotransformation processes of therapeutic proteins (which must be clearly differentiated from specific or target-mediated and non-specific or catabolic elimination pathways) is of high value early on in drug discovery and development in order to detect vulnerable positions, re-engineer the molecule to replace the labile motive and ultimately design more stable drug candidates with better *in vivo* PK properties [90].

The PopPBPK modelling strategy proposed (see Figure 7 below) would have two major applications in the clinical pharmacology program of therapeutic mAbs development process. Firstly, this PBPK modelling strategy provides clinical validation of target expression data which is then useful in developing prospective PBPK models for mAbs targeting same receptors in preclinical stage or as "back-up" lead molecules [91]. Secondly, validated PBPK models may be directly employed to predict i) PK in various clinical scenarios of interest (e.g., different dosage regimens to mitigate safety related issues), ii) local concentrations of mAb in specific tissues or at target tissues, and iii) receptor occupancy achieved with a particular dosing regimen.

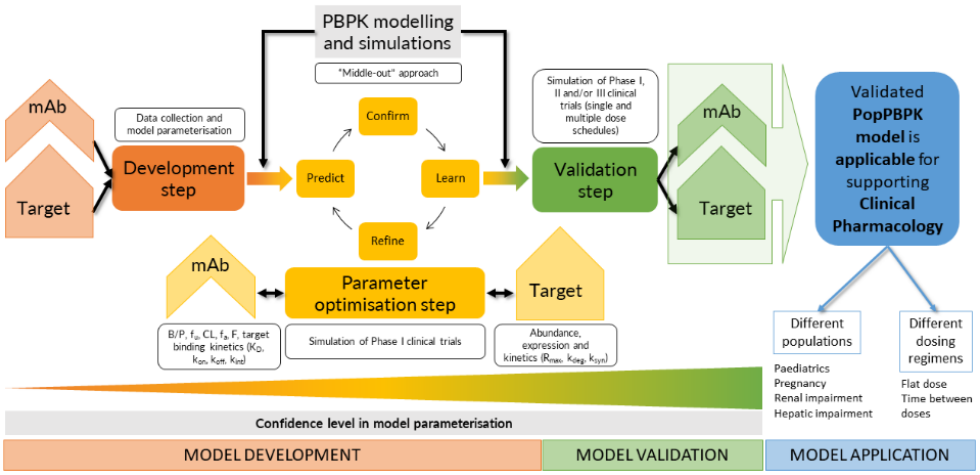

Figure 7. Optimisation of drug and system-related parameters through PBPK modelling and simulations. mAb: monoclonal antibody; B/P: blood-to-plasma concentration ratio; f_u: fraction unbound in plasma; CL: clearance; f_a: fraction of dose absorbed; F: bioavailability; K_D: mAb-target binding equilibrium

constant; k_{on}: second-order mAb-target association rate constant; k_{off}: first-order mAb-target dissociation rate constant; k_{int}: mAb-target internalization rate constant; R_{max}: target abundance; k_{deg}: first-order degradation rate constant of the target (target turnover); k_{syn}: zero-order production/synthesis rate constant of the target

Conclusions

1. Successful validation of PhysPK Biosimulation Software was achieved using NONMEM as the control basis for judging accuracy and precision of the results.
2. PBPK models with multilevel and acausal object-oriented modelling approaches allow for precise description of the time-course of the drug by independently considering simulation components from mathematical functions of the biological system.
3. A PBPK/PD model accurately describing the pharmacokinetic properties of MBQ-167 in different mouse tissues and its anti-tumour effect in HER2+ and Triple Negative breast cancer cell lines following intraperitoneal administration has been successfully developed.
4. Tumour eradication for HER2+ cell line and tumour stabilization for Triple Negative cell line are anticipated when MBQ-167 is administered at 10 mg/kg once or twice daily.
5. The atorvastatin PBPK model developed properly describes the time course of atorvastatin and its metabolites in both open acid and lactone forms. The external validation through the prediction of clinically relevant DDIs endorses the role of the metabolic and transporters pathways considered.
6. The quantitative assessment of the DGI between *SLCO1B1* polymorphisms and atorvastatin has revealed that up to 63% of patients carrying the *SLCO1B1*5* variant are at increased risk of suffering muscle-related adverse events.
7. Optimisation of target abundance and clearance mechanisms of biologic drugs through PBPK modelling and simulation highlights the potential of this modelling technique in model informed drug discovery and development

References

[1] O. J. Wouters, M. McKee and J. Luyten. Estimated Research and Development Investment Needed to Bring a New Medicine to Market, 2009-2018. JAMA. 323 (2020) 844-53. https://doi.org/10.1001/jama.2020.1166

[2] D. G. Brown, H. J. Wobst, A. Kapoor, L. A. Kenna and N. Southall. Clinical development times for innovative drugs. Nat.Rev.Drug Discov. 21 (2022) 793-4. https://doi.org/10.1038/d41573-021-00190-9

[3] R. Madabushi, P. Seo, L. Zhao, M. Tegenge and H. Zhu. Review: Role of Model-Informed Drug Development Approaches in the Lifecycle of Drug Development and Regulatory Decision-Making. Pharm.Res. 39 (2022) 1669-80. https://doi.org/10.1007/s11095-022-03288-w

[4] P. J. Williams and E. I. Ette. Pharmacometrics: Impacting Drug Development and Pharmacotherapy. Pharmacometrics. John Wiley & Sons, Inc.(2007) 1-21. https://doi.org/10.1002/9780470087978.ch1

[5] L. K. Paalzow. Torsten Teorell, the father of pharmacokinetics. Ups.J.Med.Sci. 100 (1995) 41-6. https://doi.org/10.3109/03009739509178895

[6] T. Teorell. Kinetics of distribution of substances administered to the body. I. The extravascular modes of administration. Archives Internationales de Pharmacodynamie et de Thérapie. 57 (1937) 205-25.

[7] L. Kuepfer, C. Niederalt, T. Wendl, et al. Applied Concepts in PBPK Modeling: How to Build a PBPK/PD Model. CPT Pharmacometrics Syst.Pharmacol. 5 (2016) 516-31. https://doi.org/10.1002/psp4.12134

[8] M. Jamei, S. Marciniak, K. Feng, A. Barnett, G. Tucker and A. Rostami-Hodjegan. The Simcyp population-based ADME simulator. Expert Opin.Drug Metab.Toxicol. 5 (2009) 211-23. https://doi.org/10.1517/17425250802691074

[9] M. Jamei. Recent Advances in Development and Application of Physiologically-Based Pharmacokinetic (PBPK) Models: a Transition from Academic Curiosity to Regulatory Acceptance. Curr.Pharmacol.Rep. 2 (2016) 161-9. https://doi.org/10.1007/s40495-016-0059-9

[10] H. M. Jones, I. B. Gardner and K. J. Watson. Modelling and PBPK simulation in drug discovery. AAPS J. 11 (2009) 155-66. https://doi.org/10.1208/s12248-009-9088-1

[11] A. Rostami-Hodjegan and G. T. Tucker. Simulation and prediction of in vivo drug metabolism in human populations from in vitro data. Nat.Rev.Drug Discov. 6 (2007) 140-8. https://doi.org/10.1038/nrd2173

[12] P. Poulin and F. P. Theil. Prediction of pharmacokinetics prior to in vivo studies. 1. Mechanism-based prediction of volume of distribution. J.Pharm.Sci. 91 (2002) 129-56. https://doi.org/S0022-3549(16)30889-9 [pii]

[13] T. Rodgers, D. Leahy and M. Rowland. Physiologically based pharmacokinetic modeling 1: predicting the tissue distribution of moderate-to-strong bases. J.Pharm.Sci. 94 (2005) 1259-76. https://doi.org/S0022-3549(16)31789-0 [pii]

[14] T. Rodgers and M. Rowland. Physiologically based pharmacokinetic modelling 2: predicting the tissue distribution of acids, very weak bases, neutrals and zwitterions. J.Pharm.Sci. 95 (2006) 1238-57. https://doi.org/10.1002/jps.20502

[15] M. V. Schmitt, A. Reichel, X. Liu, G. Fricker and P. Lienau. Extension of the Mechanistic Tissue Distribution Model of Rodgers and Rowland by Systematic Incorporation of Lysosomal Trapping: Impact on Unbound Partition Coefficient and Volume of Distribution Predictions in the Rat. Drug Metab.Dispos. 49 (2021) 53-61. https://doi.org/10.1124/dmd.120.000161

[16] P. Paixao, L. F. Gouveia and J. A. G. Morais. Prediction of drug distribution within blood. Eur.J.Pharm.Sci. 36 (2009) 544-54. https://doi.org/10.1016/j.ejps.2008.12.011

[17] T. Uchimura, M. Kato, T. Saito and H. Kinoshita. Prediction of human blood-to-plasma drug concentration ratio. Biopharm.Drug Dispos. 31 (2010) 286-97. https://doi.org/10.1002/bdd.711

[18] J. Yang, M. Jamei, K. R. Yeo, G. T. Tucker and A. Rostami-Hodjegan. Prediction of intestinal first-pass drug metabolism. Curr.Drug Metab. 8 (2007) 676-84. https://doi.org/10.2174/138920007782109733

[19] S. Frechen and A. Rostami-Hodjegan. Quality Assurance of PBPK Modeling Platforms and Guidance on Building, Evaluating, Verifying and Applying PBPK Models Prudently under the Umbrella of Qualification: Why, When, What, How and By Whom? Pharm.Res. 39 (2022) 1733-48. https://doi.org/10.1007/s11095-022-03250-w

[20] N. Tsamandouras, A. Rostami-Hodjegan and L. Aarons. Combining the 'bottom up' and 'top down' approaches in pharmacokinetic modelling: fitting PBPK models to observed clinical data. Br.J.Clin.Pharmacol. 79 (2015) 48-55. https://doi.org/10.1111/bcp.12234

[21] A. Rostami-Hodjegan. Reverse Translation in PBPK and QSP: Going Backwards in Order to Go Forward With Confidence. Clin.Pharmacol.Ther. 103 (2018) 224-32. https://doi.org/10.1002/cpt.904

[22] M. Shebley, P. Sandhu, A. Emami Riedmaier, et al. Physiologically Based Pharmacokinetic Model Qualification and Reporting Procedures for Regulatory Submissions: A Consortium Perspective. Clinical pharmacology and therapeutics. 104 (2018) 88-110. https://doi.org/10.1002/cpt.1013

[23] A. N. Edginton, F. Theil, W. Schmitt and S. Willmann. Whole body physiologically-based pharmacokinetic models: their use in clinical drug development. Expert Opin.Drug Metab.Toxicol. 4 (2008) 1143-52. https://doi.org/10.1517/17425255.4.9.1143

[24] P. Zhao, L. Zhang, J. A. Grillo, et al. Applications of physiologically based pharmacokinetic (PBPK) modeling and simulation during regulatory review. Clin.Pharmacol.Ther. 89 (2011) 259-67. https://doi.org/10.1038/clpt.2010.298 [doi]

[25] Sheila Annie Peters. OVERVIEW OF PBPK APPLICATIONS. Physiologically Based Pharmacokinetic (PBPK) Modeling and Simulations. John Wiley & Sons, Inc.(2022) 323-36. https://doi.org/10.1002/9781119497813.ch11

[26] P. Zhao, L. Zhang, J. A. Grillo, et al. Applications of physiologically based pharmacokinetic (PBPK) modeling and simulation during regulatory review. Clin.Pharmacol.Ther. 89 (2011) 259-67. https://doi.org/10.1038/clpt.2010.298

[27] (. European Medicines Agency. Reporting of physiologically based pharmacokinetic (PBPK) modelling and simulation - Scientific guideline. 2023 (2018)

[28] Food and Drugs Administration, (FDA). Physiologically Based Pharmacokinetic Analyses — Format and Content Guidance for Industry. 2023 (2018)

[29] M. Sato, Y. Ochiai, S. Kijima, et al. Quantitative Modeling and Simulation in PMDA: A Japanese Regulatory Perspective. CPT Pharmacometrics Syst.Pharmacol. 6 (2017) 413-5. https://doi.org/10.1002/psp4.12203

[30] M. Jamei. Recent Advances in Development and Application of Physiologically-Based Pharmacokinetic (PBPK) Models: a Transition from Academic Curiosity to Regulatory Acceptance. Curr.Pharmacol.Rep. 2 (2016) 161-9. https://doi.org/10.1007/s40495-016-0059-9

[31] X. Zhang, Y. Yang, M. Grimstein, et al. Application of PBPK Modeling and Simulation for Regulatory Decision Making and Its Impact on US Prescribing Information: An Update on the 2018-2019 Submissions to the US FDA's Office of Clinical Pharmacology. J.Clin.Pharmacol. 60 Suppl 1 (2020) S160-78. https://doi.org/10.1002/jcph.1767

[32] E. Manolis, F. T. Musuamba and K. E. Karlsson. The European Medicines Agency Experience With Pediatric Dose Selection. J.Clin.Pharmacol. 61 Suppl 1 (2021) S22-7. https://doi.org/10.1002/jcph.1863

[33] K. Umehara, F. Huth, Y. Jin, et al. Drug-drug interaction (DDI) assessments of ruxolitinib, a dual substrate of CYP3A4 and CYP2C9, using a verified physiologically based pharmacokinetic (PBPK) model to support regulatory submissions. Drug Metab.Pers.Ther. 34 (2019) /j/dmdi.2019.34.issue-0042. https://doi.org/10.1515/dmpt-2018-0042

[34] I. Loisios-Konstantinidis and J. Dressman. Physiologically Based Pharmacokinetic/Pharmacodynamic Modeling to Support Waivers of In Vivo Clinical Studies: Current Status, Challenges, and Opportunities. Mol.Pharmaceutics. 18 (2021) 1-17. https://doi.org/10.1021/acs.molpharmaceut.0c00903

[35] F. Bouzom, K. Ball, N. Perdaems and B. Walther. Physiologically based pharmacokinetic (PBPK) modelling tools: how to fit with our needs? Biopharm.Drug Dispos. 33 (2012) 55-71. https://doi.org/10.1002/bdd.1767

[36] A. Rostami-Hodjegan. Reverse Translation in PBPK and QSP: Going Backwards in Order to Go Forward With Confidence. Clin.Pharmacol.Ther. 103 (2018) 224-32. https://doi.org/10.1002/cpt.904

[37] C. Kuemmel, Y. Yang, X. Zhang, et al. Consideration of a Credibility Assessment Framework in Model-Informed Drug Development: Potential Application to Physiologically-Based Pharmacokinetic Modeling and Simulation. CPT Pharmacometrics Syst.Pharmacol. 9 (2020) 21-8. https://doi.org/10.1002/psp4.12479

[38] V. Mangas-Sanjuan, C. Navarro-Fontestad, A. Garcia-Arieta, I. F. Troconiz and M. Bermejo. Computer simulations for bioequivalence trials: Selection of analyte in BCS class II and IV drugs with first-pass metabolism, two metabolic

pathways and intestinal efflux transporter. Eur.J.Pharm.Sci. 117 (2018) 193-203. https://doi.org/10.1016/j.ejps.2018.02.014

[39] A. Mansinho, V. Boni, M. Miguel and E. Calvo. New designs in early clinical drug development. Ann.Oncol. 30 (2019) 1460-5. https://doi.org/10.1093/annonc/mdz191

[40] L. Moreno and A. D. J. Pearson. How can attrition rates be reduced in cancer drug discovery? Expert Opin.Drug Discov. 8 (2013) 363-8. https://doi.org/10.1517/17460441.2013.768984

[41] L. Zhang, V. Sinha, S. T. Forgue, et al. Model-based drug development: the road to quantitative pharmacology. J.Pharmacokinet.Pharmacodyn. 33 (2006) 369-93. https://doi.org/10.1007/s10928-006-9010-8

[42] M. Simeoni, P. Magni, C. Cammia, et al. Predictive pharmacokinetic-pharmacodynamic modeling of tumor growth kinetics in xenograft models after administration of anticancer agents. Cancer Res. 64 (2004) 1094-101. https://doi.org/10.1158/0008-5472.can-03-2524

[43] Z. P. Parra-Guillen, P. Berraondo, B. Ribba and I. F. Troconiz. Modeling tumor response after combined administration of different immune-stimulatory agents. J.Pharmacol.Exp.Ther. 346 (2013) 432-42. https://doi.org/10.1124/jpet.113.206961

[44] S. C. Tate, S. Cai, R. T. Ajamie, et al. Semi-mechanistic pharmacokinetic/pharmacodynamic modeling of the antitumor activity of LY2835219, a new cyclin-dependent kinase 4/6 inhibitor, in mice bearing human tumor xenografts. Clin.Cancer Res. 20 (2014) 3763-74. https://doi.org/10.1158/1078-0432.CCR-13-2846

[45] S. C. Tate, T. F. Burke, D. Hartman, P. Kulanthaivel, R. P. Beckmann and D. M. Cronier. Optimising the combination dosing strategy of abemaciclib and vemurafenib in BRAF-mutated melanoma xenograft tumours. Br.J.Cancer. 114 (2016) 669-79. https://doi.org/10.1038/bjc.2016.40

[46] N. Terranova, M. Germani, F. Del Bene and P. Magni. A predictive pharmacokinetic-pharmacodynamic model of tumor growth kinetics in xenograft mice after administration of anticancer agents given in combination. Cancer Chemother.Pharmacol. 72 (2013) 471-82. https://doi.org/10.1007/s00280-013-2208-8

[47] S. Wang, X. Zhu, M. Han, F. Hao, W. Lu and T. Zhou. Mechanistic Pharmacokinetic/Pharmacodynamic Model of Sunitinib and Dopamine in MCF-

7/Adr Xenografts: Linking Cellular Heterogeneity to Tumour Burden. AAPS J. 22 (2020) 45-5. https://doi.org/10.1208/s12248-020-0428-5

[48] L. Yang, L. Yong, X. Zhu, et al. Disease progression model of 4T1 metastatic breast cancer. J.Pharmacokinet.Pharmacodyn. 47 (2020) 105-16. https://doi.org/10.1007/s10928-020-09673-5

[49] T. Humphries-Bickley, L. Castillo-Pichardo, E. Hernandez-O'Farrill, et al. Characterization of a Dual Rac/Cdc42 Inhibitor MBQ-167 in Metastatic Cancer. Mol.Cancer.Ther. 16 (2017) 805-18. https://doi.org/10.1158/1535-7163.MCT-16-0442

[50] M. G. Kazanietz and M. J. Caloca. The Rac GTPase in Cancer: From Old Concepts to New Paradigms. Cancer Res. 77 (2017) 5445-51. https://doi.org/10.1158/0008-5472.CAN-17-1456

[51] K. Stengel and Y. Zheng. Cdc42 in oncogenic transformation, invasion, and tumorigenesis. Cell.Signal. 23 (2011) 1415-23. https://doi.org/10.1016/j.cellsig.2011.04.001

[52] M. D. M. Maldonado and S. Dharmawardhane. Targeting Rac and Cdc42 GTPases in Cancer. Cancer Res. 78 (2018) 3101-11. https://doi.org/10.1158/0008-5472.CAN-18-0619

[53] A. P. Porter, A. Papaioannou and A. Malliri. Deregulation of Rho GTPases in cancer. Small GTPases. 7 (2016) 123-38. https://doi.org/10.1080/21541248.2016.1173767

[54] P. De, J. C. Aske and N. Dey. RAC1 Takes the Lead in Solid Tumors. Cells. 8 (2019) 382. doi: 10.3390/cells8050382. https://doi.org/10.3390/cells8050382

[55] M. J. Rivera-Robles, J. Medina-Velazquez, G. M. Asencio-Torres, et al. Targeting Cdc42 with the anticancer compound MBQ-167 inhibits cell polarity and growth in the budding yeast S. cerevisiae. Small GTPases. 11 (2020) 430-40. https://doi.org/10.1080/21541248.2018.1495008

[56] M. K. DeGorter, B. L. Urquhart, U. Gradhand, R. G. Tirona and R. B. Kim. Disposition of Atorvastatin, Rosuvastatin, and Simvastatin in Oatp1b2−/− Mice and Intraindividual Variability in Human Subjects. Journal of clinical pharmacology. 52 (2012) 1689-97. https://doi.org/10.1177/0091270011422815

[57] A. Vildhede, M. Karlgren, E. K. Svedberg, et al. Hepatic uptake of atorvastatin: influence of variability in transporter expression on uptake clearance and drug-drug interactions. Drug metabolism and disposition. 42 (2014) 1210-8. https://doi.org/10.1124/dmd.113.056309

[58] J. Keskitalo, O. Zolk, M. Fromm, K. Kurkinen, P. Neuvonen and M. Niemi. ABCG2 Polymorphism Markedly Affects the Pharmacokinetics of Atorvastatin and Rosuvastatin. Clinical pharmacology and therapeutics. 86 (2009) 197-203. https://doi.org/10.1038/clpt.2009.79

[59] Y. Prado, T. Zambrano and L. A. Salazar. Transporter genes ABCG2 rs2231142 and ABCB1 rs1128503 polymorphisms and atorvastatin response in Chilean subjects. Journal of clinical pharmacy and therapeutics. 43 (2018) 87-91. https://doi.org/10.1111/jcpt.12607

[60] B. K. Birmingham, S. R. Bujac, R. Elsby, et al. Impact of ABCG2 and SLCO1B1 polymorphisms on pharmacokinetics of rosuvastatin, atorvastatin and simvastatin acid in Caucasian and Asian subjects: a class effect? https://doi.org/10.1007/s00228-014-1801-z

[61] T. J. J. Schirris, T. Ritschel, A. Bilos, J. A. M. Smeitink and F. G. M. Russel. Statin Lactonization by Uridine 5′-Diphospho-glucuronosyltransferases (UGTs). Molecular pharmaceutics. 12 (2015) 4048-55. https://doi.org/10.1021/acs.molpharmaceut.5b00474

[62] S. Riedmaier, K. Klein, U. Hofmann, et al. UDP-Glucuronosyltransferase (UGT) Polymorphisms Affect Atorvastatin Lactonization In Vitro and In Vivo. Clin Pharmacol Ther. 87 (2009) 65. https://doi.org/10.1038/clpt.2009.181

[63] Thomayant Prueksaritanont, Raju Subramanian, Xiaojun Fang, et al. Glucuronidation of Statins in Animals and Humans: A Novel Mechanism of Statin Lactonization. Drug metabolism and disposition. 30 (2002) 505-12. https://doi.org/10.1124/dmd.30.5.505

[64] W. Jacobsen, B. Kuhn, A. Soldner, et al. Lactonization Is the Critical First Step in the Disposition of the 3-Hydroxy-3-Methylglutaryl-Coa Reductase Inhibitor Atorvastatin. Drug Metab.Dispos. 28 (2000) 1369-78.

[65] H. Fujino, T. Saito, Y. Tsunenari, J. Kojima and T. Sakaeda. Metabolic properties of the acid and lactone forms of HMG-CoA reductase inhibitors. Xenobiotica. 34 (2004) 961-71. https://doi.org/10.1080/00498250400015319

[66] J. -. Park, K. -. Kim, S. K. Bae, B. -. Moon, K. -. Liu and J. -. Shin. Contribution of cytochrome P450 3A4 and 3A5 to the metabolism of atorvastatin. Xenobiotica. 38 (2008) 1240-51. https://doi.org/10.1080/00498250802334391

[67] H. S. Malhotra and K. L. Goa. Atorvastatin: An Updated Review of its Pharmacological Properties and Use in Dyslipidaemia. Drugs. 61 (2001) 1835-81. https://doi.org/10.2165/00003495-200161120-00012

[68] A. S. Kearney, L. F. Crawford, S. C. Mehta and G. W. Radebaugh. The interconversion kinetics, equilibrium, and solubilities of the lactone and hydroxyacid forms of the HMG-CoA reductase inhibitor, CI-981. Pharm.Res. 10 (1993) 1461-5. https://doi.org/10.1023/a:1018923325359 [doi]

[69] Pankaj Partani S. Manaswita Verma Sanjay Gurule Arshad Khuroo Tausif Monif. Simultaneous quantitation of atorvastatin and its two active metabolites in human plasma by liquid chromatography/ (-) electrospray tandem mass spectrometry. Journal of pharmaceutical analysis. 4 (2014) 26-36. https://doi.org/10.1016/j.jpha.2013.09.007

[70] J. Reig-López, A. García-Arieta, V. Mangas-Sanjuán and M. Merino-Sanjuán. Current Evidence, Challenges, and Opportunities of Physiologically Based Pharmacokinetic Models of Atorvastatin for Decision Making. Pharmaceutics. 13 (2021) 709. https://doi.org/10.3390/pharmaceutics13050709

[71] G. Stillemans, A. Paquot, G. G. Muccioli, et al. Atorvastatin population pharmacokinetics in a real-life setting: Influence of genetic polymorphisms and association with clinical response. Clinical Translational Sci. 15 (2021) 667. https://doi.org/10.1111/cts.13185

[72] M. HERMANN, M. BOGSRUD, E. MOLDEN, et al. Exposure of atorvastatin is unchanged but lactone and acid metabolites are increased several-fold in patients with atorvastatin-induced myopathy. Clinical pharmacology and therapeutics. 79 (2006) 532-9. https://doi.org/10.1016/j.clpt.2006.02.014

[73] M. R. Campbell, A. Ruiz-Saenz, Y. Zhang, et al. Extensive conformational and physical plasticity protects HER2-HER3 tumorigenic signaling. Cell.Rep. 40 (2022) 111338. https://doi.org/10.1016/j.celrep.2022.111338

[74] Y. Yarden. Biology of HER2 and its importance in breast cancer. Oncology. 61 Suppl 2 (2001) 1-13. https://doi.org/10.1159/000055396

[75] I. Rubin and Y. Yarden. The basic biology of HER2. Ann.Oncol. 12 Suppl 1 (2001) 3. https://doi.org/10.1093/annonc/12.suppl_1.s3

[76] J. Mendelsohn and J. Baselga. Status of epidermal growth factor receptor antagonists in the biology and treatment of cancer. J.Clin.Oncol. 21 (2003) 2787-99. https://doi.org/10.1200/JCO.2003.01.504

[77] D. A. Olsen, B. Ostergaard, S. Bokmand, et al. HER1-4 protein concentrations in normal breast tissue from breast cancer patients are expressed by the same profile as in the malignant tissue. Clin.Chem.Lab.Med. 47 (2009) 977-84. https://doi.org/10.1515/CCLM.2009.214

[78] C. D. Austin, A. M. De Maziere, P. I. Pisacane, et al. Endocytosis and sorting of ErbB2 and the site of action of cancer therapeutics trastuzumab and geldanamycin. Mol.Biol.Cell. 15 (2004) 5268-82. https://doi.org/10.1091/mbc.e04-07-0591

[79] B. S. Hendriks, L. K. Opresko, H. S. Wiley and D. Lauffenburger. Quantitative analysis of HER2-mediated effects on HER2 and epidermal growth factor receptor endocytosis: distribution of homo- and heterodimers depends on relative HER2 levels. J.Biol.Chem. 278 (2003) 23343-51. https://doi.org/10.1074/jbc.M300477200

[80] K. E. Longva, N. M. Pedersen, C. Haslekas, E. Stang and I. H. Madshus. Herceptin-induced inhibition of ErbB2 signaling involves reduced phosphorylation of Akt but not endocytic down-regulation of ErbB2. Int.J.Cancer. 116 (2005) 359-67. https://doi.org/10.1002/ijc.21015

[81] J. Codony-Servat, J. Albanell, J. C. Lopez-Talavera, J. Arribas and J. Baselga. Cleavage of the HER2 ectodomain is a pervanadate-activable process that is inhibited by the tissue inhibitor of metalloproteases-1 in breast cancer cells. Cancer Res. 59 (1999) 1196-201.

[82] Y. Tokuda, T. Watanabe, Y. Omuro, et al. Dose escalation and pharmacokinetic study of a humanized anti-HER2 monoclonal antibody in patients with HER2/neu-overexpressing metastatic breast cancer. Br.J.Cancer. 81 (1999) 1419-25. https://doi.org/10.1038/sj.bjc.6690343

[83] S. Lennon, C. Barton, L. Banken, et al. Utility of serum HER2 extracellular domain assessment in clinical decision making: pooled analysis of four trials of trastuzumab in metastatic breast cancer. J.Clin.Oncol. 27 (2009) 1685-93. https://doi.org/10.1200/JCO.2008.16.8351

[84] M. D. Pegram, A. Lipton, D. F. Hayes, et al. Phase II study of receptor-enhanced chemosensitivity using recombinant humanized anti-p185HER2/neu monoclonal antibody plus cisplatin in patients with HER2/neu-overexpressing metastatic breast cancer refractory to chemotherapy treatment. J.Clin.Oncol. 16 (1998) 2659-71. https://doi.org/10.1200/JCO.1998.16.8.2659

[85] H. S. Wiley. Anomalous binding of epidermal growth factor to A431 cells is due to the effect of high receptor densities and a saturable endocytic system. J.Cell Biol. 107 (1988) 801-10. https://doi.org/10.1083/jcb.107.2.801

[86] R. C. Kurten, D. L. Cadena and G. N. Gill. Enhanced degradation of EGF receptors by a sorting nexin, SNX1. Science. 272 (1996) 1008-10. https://doi.org/10.1126/science.272.5264.1008

[87] A. R. French, G. P. Sudlow, H. S. Wiley and D. A. Lauffenburger. Postendocytic trafficking of epidermal growth factor-receptor complexes is mediated through saturable and specific endosomal interactions. J.Biol.Chem. 269 (1994) 15749-55.

[88] B. S. Hendriks, L. K. Opresko, H. S. Wiley and D. Lauffenburger. Coregulation of epidermal growth factor receptor/human epidermal growth factor receptor 2 (HER2) levels and locations: quantitative analysis of HER2 overexpression effects. Cancer Res. 63 (2003) 1130-7.

[89] Q. Deveuve, L. Lajoie, B. Barrault and G. Thibault. The Proteolytic Cleavage of Therapeutic Monoclonal Antibody Hinge Region: More Than a Matter of Subclass. Front.Immunol. 11 (2020) 168. https://doi.org/10.3389/fimmu.2020.00168

[90] S. Schadt, S. Hauri, F. Lopes, et al. Are Biotransformation Studies of Therapeutic Proteins Needed? Scientific Considerations and Technical Challenges. Drug Metab.Dispos. 47 (2019) 1443-56. https://doi.org/10.1124/dmd.119.088997

[91] H. M. Jones, Z. Zhang, P. Jasper, et al. A Physiologically-Based Pharmacokinetic Model for the Prediction of Monoclonal Antibody Pharmacokinetics From In Vitro Data. CPT Pharmacometrics Syst.Pharmacol. 8 (2019) 738-47. https://doi.org/10.1002/psp4.12461

VNIVERSITAT DE VALÈNCIA